ISSN 2542-2049

Saint-Petersburg State University

18 International School-Conference

Magnetic resonance and its applications

proceedings

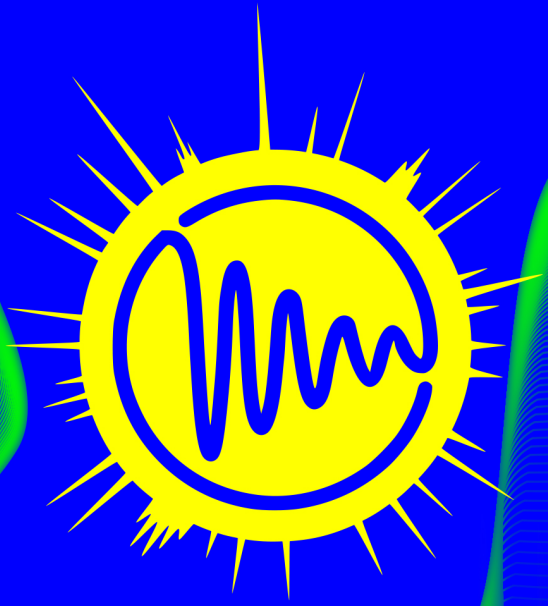

Spinus

29 March — 2 April 2021

Saint-Petersburg, Russia

SAINT PETERSBURG STATE UNIVERSITY
Department of Nuclear Physics Research Methods

18th International School-Conference

MAGNETIC RESONANCE AND ITS APPLICATIONS

Proceedings

an AMPERE event

March 29 — April 2, 2021
Saint Petersburg, Russia

Magnetic Resonance and its Applications. Spinus-2021.
Proceedings. Saint Petersburg State University, 2021. 282 pp.
ISSN 2542-2049

Schola **Spinus**

18th International School-Conference
MAGNETIC RESONANCE AND ITS APPLICATIONS
SPINUS-2021

ORGANIZING COMMITTEE

Chairman	Prof. Denis Markelov, SPSU
Vice-chairman	M. Sc. Alexander Ievlev, researcher, SPSU
Committee members	Prof. Marina Shelyapina, SPSU Dr. Andrey Egorov, associate professor, SPSU Dr. Andrey Komolkin, associate professor, SPSU Dr. Pavel Kupriyanov, assistant, SPSU Dr. Konstantin Tyutyukin, senior teacher, SPSU M. Sc. Timofey Popov, SPSU
Layout of proceedings	Aleksandr Levantovskii

CONTACTS

1, Ulyanovskay st., Peterhof, 198504, St. Petersburg, Russia
Department of Nuclear Physics Research Methods
St. Petersburg State University

Tel.	+7-953-350-0640
Fax	+7-812-428-7240
E-mail	spinus@spinus.spb.ru
Website	spinus.spb.ru

PROGRAM COMMITTEE

SCIENTIFIC ADVISER OF THE SCHOOL-CONFERENCE

Vladimir Chizhik	Honored Scientist of Russian Federation Honorary Professor of Saint Petersburg State University

ADVISORY BOARD

V. Balevicius	Professor, Vilnius University, Lithuania
C. Cabal	Professor, Havana University, Cuba
V. I. Chizhik	Professor, St. Petersburg State University, Russia
S. V. Dvinskikh	Professor, Royal Institute of Technology, Stockholm, Sweden
J. Fraissard	Professor, University Pierre and Marie Curie, Paris, France
L. Yu. Grunin	Associate Professor, CEO, Resonance Systems, Russia
E. Lahderanta	Professor, Lappeenranta Technical University, Finland
D. Michel	Professor, Leipzig University, Germany
B. Rameev	Professor, Gebze Technical University, Turkey
N. R. Skrynnikov	Professor, St. Petersburg University, Russia, Purdue University, USA
M. S. Tagirov	Professor, Kazan Federal University, Russia
L. M. Varela	Professor, University Santiago de Compostela, Spain
S. Vasiliev	Professor, University of Turku, Finland

Spinus

Saint Petersburg State University
spbu.ru

Resonance systems Ltd.
nmr-design.com

plscientific.se

Magicplot Systems, LLC
magicplot.com

MRRC "Spinus" SPbU, LLC
magres.ru

Contents

Schedule of Spinus-2021 (Moscow time!)

	29.03.21 Monday	30.03.21 Tuesday	31.03.21 Wednesday	01.04.21 Thursday	02.04.21 Friday
10:00 – 11:40	**Opening 20** **Levitt 40** **Salikhov 40**	**Vasiliev 40** **Bunkov 40** Koplak 20	**Koptyug 40** Mastova 15 Kononova 15 Skvortsova 15 Pichugina 15	**Price 40** **Stepišnik 40** Mozzhukhin 20	**Chizhik 40** Dvinskikh 30 Ubovich 15 Fedotova 15
11:40 – 12:00	**COFFEE BREAK**				
12:00 – 14:30	**Sato 40** **G. Papavassiliou 40** Gavrilenko 20 Alakshin 20 Andreev 15 Rakhimova 15	**Fraissard 40** **Kowalewski 40** Ferrauto 20 W. Papawassiliou 15 Chakalov 15 Khusnutdinov 20	**Pirogov 40** **Eichhoff 40** **Lurie 40** Kononenko 15 Koshman 15	**Grunin 40** Kulagina 20 Vasil'ev 20 Ivanova 15 Uguz 15 Gkoura 15 Khusnutdinova 15	**Tolstoy 40** Karpov 15 Koronatov 15 Antonova 15 Stanislavovas 15 Belov 15 Andronova 15 Tyurtyaeva 15
14:30 – 15:30	**LUNCH**				**MEETING OF AWARDING COMMISSION**
15:30 – 17:10	**Lapina 40** Tsyro 15 Ikeda 15 Nagmutdinova 15 Parfishina 15	**Bluemich 40** Oral blitz reports of young scientists (5min x 10)	**Meersmann 40** Lalli 20 Kusova 15 Cabal Mirabal I 20	Oral blitz reports of young scientists (5min x 14) Komolkin 20	**Awarding (16:00)** **Closing**
17:10 – 17:30	**COFFEE BREAK**				
17:30 – 18:50	**Jurga 40** **Charnaya 40**	**POSTER SESSION I**	Cabal Mirabal II 20 Tamayo Delgado 15 Dmitrenko 15 Kuzminova 15 Liamin 15	**POSTER SESSION II**	

Schedule

18-th International School-Conference

«Magnetic Resonance and its Applications. Spinus-2021»

March 29 - April 02, 2021

St. Petersburg

	MONDAY – 29 March 2021
Moscow time!	
10:00 – 10:20	**Opening**
10:20 – 11:00	**Malcolm Levitt (Southampton, UK)** **Lecture:** Navigating the space of spin operators
11:00 – 11:40	**Kev Salikhov (Kazan, Russia)** **Lecture:** On the importance of the paradigm in the development of science
11:40 – 12:00	**COFFEE BREAK**
12:00 – 12:40	**Kazunobu Sato (Osaka, Japan)** **Lecture:** Spin manipulation of organic radicals by advanced pulsed ESR spectroscopy

12:40 – 13:20	**Georgios Papavassiliou (Athens, Greece)** **Lecture:** Tracing the "invisible" Polarons in Ferromagnetic Manganites. A combined NMR and HRTEM study in the temperature range 3.2 - 1000K
13:20 – 13:40	**Andrey Gavrilenko (Kazan, Russia)** **Oral report:** Study of Doped Chalcopyrite Cu1-XPdXFeS2 Compounds by 63,65Cu NMR and EPR Methods
13:40 – 14:00	**Egor Alakshin (Kazan, Russia)** **Oral report:** Nanostructures research using nuclear magnetic resonance of helium-3
14:00 – 14:15	**Georgii Andreev (Kazan, Russia)** **Oral report:** Deviant behaviour of magnetization of microsized powder of Ising dipolar antiferromagnet LiDyF4 at temperatures T > TN
14:15 – 14:30	**Alina Rakhimova (Surgut, Russian)** **Oral report:** Electron spin resonance method data for core samples from the Tomsk region deposits
14:30 – 15:30	**LUNCH**
15:30 – 16:10	**Olga Lapina (Novosibirsk, Russia)** **Lecture:** Modern SSNMR for studing structure of functional materials
16:10 – 16:25	**Larisa Tsyro (Surgut, Russian)** **Oral report:** Spin properties of the water-Portland cement system
16:25 – 16:40	**Junko Ikeda (Chiba, Japan)** **Oral report:** The simple method of estimation of a retarder influence on the cement hardening process
16:40 – 16:55	**Anastasiia Nagmutdinova (Bologna, Italy)** **Oral report:** Time domain NMR Pake-Doublet analysis of sorption cycles experiments of cement materials
16:55 – 17:10	**Arina Parfishina (Kazan, Russia)** **Oral report:** The first observation of NMR in 169Tm in magnetically diluted Van Vleck paramagnet LiTm0.02Y0.98F4
17:10 – 17:30	**COFFEE BREAK**
17:30 – 18:10	**Stefan Jurga (Poznań, Poland)** **Lecture:** Copolymer systems studied by NMR and other complementary techniques
18:10 – 18:50	**Elena Charnaya (Saint-Petersburg, Russia)** **Lecture:** NMR studies of phase transitions in confined metals and alloys
	TUESDAY – 30 March 2021
Moscow time!	
10:00 – 10:40	**Sergey Vasiliev (Turku, Finland)** **Lecture:** Atomic hydrogen in solid molecular crystals. Magnetic Resonance and Quantum Diffusion

10:40 – 11:20	**Yury Bunkov (Moscow, Russia)** **Lecture:** Spin Superfluid Quantum Computing
11:20 – 11:40	**Oksana Koplak (Chernogolovka, Russia)** **Oral report:** Ferromagnetic resonance of magnetic multilayered structures
11:40 – 12:00	**COFFEE BREAK**
12:00 – 12:40	**Jacques Friassard (Paris, France)** **Lecture:** NMR Studies of metals and supported metal particles
12:40 – 13:20	**Jozef Kowalewski (Stockholm, Sweden)** **Lecture:** Paramagnetic relaxation in solution: an overview
13:20 – 13:40	**Giuseppe Ferrauto (Torino, Italy)** **Oral report:** Supramolecular interaction between macrocyclic Gd (III) complexes and polyaromatic systems as innovative way to enhance relaxivity
13:40 – 13:55	**Wassilios Papawassiliou (Stockholm, Sweden)** **Oral report:** Broadband High Resolution NMR Studies of Topological Matter
13:55 – 14:10	**Edem Chakalov (Saint-Petersburg, Russia)** **Oral report:** Using electronic criterion towards to the halogen bond for prediction 31P NMR chemical shift of phosphine oxides as probe acceptors
14:10 – 14:30	**Rustem Khusnutdinov (Kazan, Russia)** **Oral report:** Two-frequency flat gradiometer for searching explosives hidden under clothing – modeling and experiment
14:30 – 15:30	**LUNCH**
15:30 – 16:10	**Bernhard Bluemich (Aachen, Germany)** **Lecture:** Advances and Adventures with Compact Magnetic Resonance
16:10 – 17:10	Oral blitz reports of young scientists (5min × 10); see speakers below in the list of **POSTER SESSION I**
17:00 – 17:30	**COFFEE BREAK**
17:30 – 18:50	**POSTER SESSION I**

	WEDNESDAY – 31 March 2021
Moscow time!	
10:00 – 10:40	**Igor Koptyug (Novosibirsk, Russia)** **Lecture:** Parahydrogen-induced polarization: bridging the gap between homogeneous and heterogeneous catalysis

10:40– 10:55	**Anna Mastova (Novosibirsk, Russia)** **Oral report:** The 1H NMR and CIDNP study of the interaction of non-steroidal anti-inflammatory drug ketoprofen with L- and D-tryptophan
10:55 – 11:10	**Polina Kononova (Novosibirsk, Russia)** **Oral report:** The 1H NMR and MD study of the interaction of the antiviral agent glycyrrhizin with lipid membranes: an effect on lipid mobility and membrane fusion
11:10 – 11:25	**Polina Skvortsova (Kazan, Russia)** **Oral report:** Pillar[5]arene complexes with palindromic DNA decamer and plasmid DNA
11:25 – 11:40	**Alina Pichugina (Surgut, Russia)** **Oral report:** The role of radicals in the formation of pathogenic organomineral formations in the body
11:40 – 12:00	**COFFEE BREAK**
12:00 – 12:40	**Yuri Pirogov (Moscow, Russia)** **Lecture:** Multinuclear MRI investigations
12:40 – 13:20	**Uwe Eichhoff (Gaggenau, Germany)** **Lecture:** Advanced MRI-methods for evaluation of Parkinson`s disease
13:20 – 14:00	**David Lurie (Aberdeen, United Kingdom)** **Lecture:** Fast Field-Cycling Magnetic Resonance Imaging
14:00 – 14:15	**Elizaveta Kononenko (Novosibirsk, Russia)** **Oral report:** Operando 3D MRI visualization of complex heterogeneous catalytic system using parahydrogen
14:15 – 14:30	**Vladimir Koshman (Novosibirsk, Russia)** **Oral report:** The 1H NMR study of lipid peroxidation processes involving chelate complexes of thiosemicarbazone Dp44mT
14:30 – 15:30	**LUNCH**
15:30 – 16:10	**Thomas Meersmann (Nottingham, United Kingdom)** **Lecture:** Monoatomic spin systems as magnetic resonance probes for biomedical and engineering applications
16:10 – 16:30	**Daniela Lalli (Alessandria, Italy)** **Oral report:** Mn-Based Silica Nanoparticles as Potential MRI Probes
16:30 – 16:45	**Aleksandra Kusova (Kazan, Russia)** **Oral report:** Protein intermolecular interactions according to the translational diffusion by PFG NMR and DLS
16:45 – 17:00	**Carlos Cabal Mirabal (La Habana, Cuba)** **Oral report:** The sense of the development of MRI.
17:00 – 17:30	**COFFEE BREAK**
17:30 – 17:50	**Carlos Cabal Mirabal (La Habana, Cuba)** **Oral report:** Curie Spin relaxation contribution during the aggregation

	process of HbS Hemoglobin
17:50 – 18:05	**Fabian Tamayo Delgado (Santiago de Cuba, Cuba)** **Oral report:** Correlation times and water fractions distribution in HbA and HbS intracellular solutions
18:05 – 18:20	**Mariia Dmitrenko (Saint-Petersburg, Russia)** **Oral report:** Development and investigation of pervaporation green high-performance hydroxyethyl cellulose/sodium alginate membranes for dehydration
18:20 – 18:35	**Anna Kuzminova (Saint-Petersburg, Russia)** **Oral report:** The correlation of structure with transport properties of novel pervaporation sodium alginate membranes modified by Zr-MOFs
18:35 – 18:50	**Vladislav Liamin (Saint-Petersburg, Russia)** **Oral report:** Investigation of novel pervaporation membranes based on sodium alginate – fullerene derivative composites
	THURSDAY – 01 April 2021
Moscow time!	
10:00 – 10:40	**William Price (Sydney, Australia)** **Lecture:** NMR Diffusion Measurements and Time-Dependent Samples
10:40 – 11:20	**Janez Stepišnik (Ljubljana, Slovenia)** **Lecture:** Frequency selection of molecular translation dynamics with different NMR MGSE sequences
11:20 – 11:40	**Georgy Mozzhukhin (Gebze-Kocaeli, Turkey)** **Oral report:** Quadrupole coupling constants in compounds with amino-groups in liquids
11:40 – 12:00	**COFFEE BREAK**
12:00 – 12:40	**Leonid Grunin (Kirchheim/Teck, Germany)** **Lecture:** Review of Pulse Sequences Applicable in Time-Domain NMR.
12:40 – 13:00	**Tatiana Kulagina (Chernogolovka, Russia)** **Oral report:** Structure and Mobility of Elastomers Studied by the signals of primary and stimulated echoes
13:00 – 13:20	**Sergey Vasil'ev (Chernogolovka, Russia)** **Oral report:** Hambergite (Be2BO3OH) as a model of one-dimensional dipolar coupled 1H zig-zag spin chain.
13:20 – 13:35	**Maria Ivanova (Yoshkar-Ola, Russia)** **Oral report:** TD-NMR in study of fat melting
13: 35– 13: 50	**Sirvan Sultan Uguz (Ankara, Turkey)** **Oral report:** Use of TD NMR Approaches for Characterisation of Bovine and Porcine Gelatin Based Soft Candies

13: 50 – 14:05	**Lydia Gkoura (Athens, Greece)** **Oral report:** 2D NMR diffusion-relaxation (DT2) studies of water in hydrophobic carbon nanotubes
14:05 – 14:20	**Naira Khusnutdinova (Saint-Petersburg, Russia)** **Oral report:** Modeling the system of the melt of carbosilane dendrimers
14:20 – 15:30	**LUNCH**
15:30 – 16:50	Oral blitz reports of young scientists (5min × 14); see speakers below in the list of **POSTER SESSION II**
16:50 – 17:10	**Andrei Komolkin (Saint-Petersburg, Russia)** **Oral report:** Master programs in Physics at Saint Petersburg State University
17:10 – 17:30	**COFFEE BREAK**
17:30 – 19:00	**POSTER SESSION II**
	FRIDAY – 02April 2021
Moscow time!	
10:00 – 10:40	**Vladimir Chizhik (Saint-Petersburg, Russia)** **Lecture:** A new model of the microstructure of mixtures of ionic liquids with water: an alternative to " water pockets"
10:40 – 11: 10	**Sergey Dvinskikh (Stokholm, Sweden)** **Oral report:** Ionic liquid crystals studied by solid-state NMR spectroscopy
11: 10 – 11: 25	**Milosh Ubovich (Saint-Petersburg, Russia)** **Oral report:** Rotational motion of ions in alkylammonium nitrate ionic liquids by molecular dynamics simulation method
11: 25 – 11: 40	**Elisaveta Fedotova (Saint-Petersburg, Russia)** **Oral report:** Computer simulation of atactic polymers
11:40 – 12:00	**COFFEE BREAK**
12:00 – 12:40	**Peter Tolstoy (Saint-Petersburg, Russia)** **Lecture:** Self-assembly of small molecules by H-bonds: how to distinguish dimers, trimers, tetramers by NMR
12:40 – 12:55	**Valerii Karpov (Saint-Petersburg, Russia)** **Oral report:** Sensitivity of 77Se chemical shift to the selenium atom surroundings in water media
12:55 – 13:10	**Aleksandr Koronatov (Saint-Petersburg, Russia)** **Oral report:** 2D NMR Structure Determination of 3,4-Dihydro-1,2,4-triazine Intermediate in Novel Rh(II)-catalyzed Transannulation Reaction

13:10 – 13:25	**Nadezhda Antonova (Saint-Petersburg, Russia)** **Oral report:** Micelle formation in magnesium hexanoate solution in the presence of a peptide 1B03
13:25 – 13:40	**Andrey Stanislavovas (Kazan, Russia)** **Oral report:** Spin kinetics of gaseous 3He in oriented aerogels
13:40 – 13:55	**Konstantin Belov (Ivanovo, Russia)** **Oral report:** Comparison of the spatial structure of the mefenamic acid molecule in solution at normal and supercritical state
13:55 – 14:10	**Elizaveta Andronova (Saint-Petersburg, Russia)** **Oral report:** Proton mobility in Dion-Jacobson phase HCa2Nb3O10 studied by 1H NMR
14:10 – 14:25	**Anna Tyurtyaeva (Saint-Petersburg, Russia)** **Oral report:** Nanoconfined water in pillared zeolites probed by 1H NMR
14:25 – 16:00	**MEETING OF AWARDING COMMISSION**
16:00 – 17:00	**AWARDING and CLOSING**

POSTER SESSION I (Tuesday, 17:30 – 18:50)		
1	Dmitry Aleshin	Double step spin transition in binuclear Fe-Fe helicates with incapsulated anion by NMR spectroscopy
2	Aleksandra Andrzejowska	Molecular dynamic of bound water in Antarctic lichenized fungus Umbilicaria antarctica Frey & I.M. observed by sorption isotherm and 1H-NMR
3	Valerii Bezrodnyi	Computer simulation and NMR study of the temperature dependencies of the structural and dynamic characteristics of Lys2Arg peptide dendrimers
4	Dmitriy Blokhin	The spatial structure of SEM1(86-107) peptide in “protein–micelle of dodecylphosphocholine” complex by NMR spectroscopy
5	Agata Bogdał	The classification of residual bound water fractions in rehydrated phospholipid lyophilizates
6	Anna Butyugina	Computer simulation of ionic liquid [C12-Im-C12]+[BF4]– in smectic-A phase
7	Mariia Dmitrenko	The application of bulk and surface modifications for sodium alginate membranes for enhanced pervaporation dehydration
8	Emil Fatullaev	The Brownian dynamics and numerical self-consistent field simulations of the dendrigraft nanocontainers
9	Albina Gafarova	EPR Study and DFT-Assisted Identification of Radicals in γ-Irradiated Calcium Gluconate
10	Irina Golubeva	Primary echo signals in flexible polymers with isolated three-spin groups

11	Sofia Mikhtaniuk	The structural and dynamic characteristics of Lys2Gly and Lys2Lys peptide dendrimers. The molecular dynamics simulation and NMR relaxation at different temperatures
12	Alexander Selivanov	Optimization of parameters for molecular dynamics modeling of ionic liquid [BMIM][SCN].
13	Nina Djapic	Chiral carbon bearing the hydrogen: a porphyrin and the tetrapyrroles
14	Grigorii Karnaukh	Direct exchange of identical quantum objects with a finite number of eigenstates
15	Pavel Kupriyanov	Peculiarities of processing and analysis of NMR spectra of liquids with a low abundance of studied nuclei in the Earth magnetic field
16	Yury Neronov	Determination of the magnetic moments of the 6Li and 7Li nuclei using a spectrometer that registers simultaneous signals from two types of nuclei
17	Mikhail Rudavets	Mellin-Barnes Integral Approach for Exact Evaluation of Spin Echo Signals from Fluids with Magnetizible Grains.
18	Arseniy Slobodyuk	NMR spectra, structure and ionic motions in the new potassium fluoridooxalate zirconates
19	Murat Tagirov	Magnon quantisation in the magnetic field gradient

POSTER SESSION II (Thursday, 17:30 – 18:50)		
1	Olga Kokh	Investigation of the molecular mobility of the ionic liquid BmpyrrNTF2 by NMR methods
2	Mikhail Kostin	The study of non-covalent interactions in complexes of CH3Br by quantum-chemical calculations
3	Karol Kubat	Hydration properties of tadalafil preparations in the matrix of the soluplus polymer.
4	Anna Kuzminova	Development and characterization of novel pervaporation membranes based on sodium alginate modified by FeBTC
5	Anna Lavrova	The basic physics of ASL perfusion and its applications in neuroimaging: a review
6	Sultonazar Mamadazizov	14N Quadrupole Coupling Constants calculation in some compounds with amino groups
7	Yulianela Mengana	Evaluation of the dynamic viscosity in protein solutions applying Nuclear Magnetic Relaxation.
8	Anastasia Nikitina	Research and development of an information system for optimizing the contrast of a magnetic resonance image
9	Vasilii Pelipko	Nuclear Overhauser effect in determination the geometric configuration of the N'-substituted hydrazone methylpyruvate
10	Julia Popova	The Application of Nuclear Magnetic Resonance Spectroscopy to the Calculation of Lignin Structure Formulas

11	Mark Smirnov	1H High-resolution NMR spectrometry and relaxometry for soybean oil research
12	Viktoria Vasinovich	Peculiarities of microstructure in mixtures SLAS-DTAB-D2O according to NMR data
13	Irina Yefimova	Molecular Dynamics simulation of ethylenediamine-Cu2+ complex and copper-II chloride in aqueous solutions
14	Valerii Bezrodnyi	Novel lysine-based peptide dendrimers modeled by the self-consistent field approach
15	Sofia Mikhtaniuk	The self-assembly of the amphiphilc molecules consisting of polylysine dendrons with the single and double hydrophobic tails
16	Daniel Jakubiec	1H-NMR spectroscopy and relaxometry studies of hydration from gaseous phase of foliose lichenized fungi: Roccellina nigricans from Atacama Desert region Chañaral.
17	Dmitriy Kitanin	The distribution of electron density in orpiment. Crystalline and amorphous phases.
18	Alexandr Ievlev	Modern capabilities of NMR magnetometry.
19	Yury Neronov	NMR spectra of potassium-39 nuclei in aqueous solutions and determination of the magnetic moment of the 39K nucleus.
20	Arseniy Slobodyuk	NMR study of structure and inner motion types of ZnZrF6•6H2O and its dehydration products

Spinus

The School-Conference "Spinus" of Saint Petersburg State University

The St. Petersburg State University (SPbSU) holds International School-Conference "Magnetic resonance and its application" (Spinus) since 2004. "Spinus" is organized in according to the subjects of researches and Master Programs, which have been developed and implemented in the SPbSU. In modern physics, the term "magnetic resonance" refers to a set of phenomena accompanied with the emission or absorption of electromagnetic waves of the radiofrequency diapason by quantum systems (nuclei, electrons, atoms, molecules, etc.). These phenomena, the physical nature of which is of independent interest, provided the basis of radiospectroscopic methods for studying the structure of matter and physical-chemical processes in it. They are also used for the creation of quantum generators, amplifiers, and magnetometers. For the development of ideas and applications of magnetic resonance six Nobel Prizes were awarded in the areas of physics, chemistry, biology, physiology and medicine (the latter was in 2003).

Primarily, magnetic resonance methods are:

- Nuclear Magnetic Resonance (NMR)
- Electron Paramagnetic Resonance (EPR)
- Nuclear Quadrupole Resonance (NQR)

These methods, being contactless, do not destroy an object under a study, that makes them unique and in demand not only in physics and chemistry, but also in medicine, geology, biology, archeology. Now, any medical center with high reputation has a magnetic resonance imaging (MRI). In Russia, NMR is used in oil well logging, laboratory analysis of the productivity of oil-bearing reservoirs, analysis of oil content and moisture of seeds; EPR technique is used for geological research, non-destructive control of precious stones, as well as for the dating of paleontological artifacts; there are NQR applications for remote detection of solid explosives and narcotics. Magnetometry methods based on magnetic resonance are indispensable for carrying out archaeological researches.

Earlier the school organizers worked at the Department of quantum magnetic phenomena (QMPh) of the St. Petersburg State University, which was founded in 1993 on the initiative of Professor V. I. Chizhik on the basis of the laboratory, created in the 50s of the last century by F. I. Skripov at the Department of Radio Physics (the branch "Quantum Radiophysics"). On January 1, 2014, the Department of QMPh joined the united Department of nuclear-physics research methods (Head of the Department is Corresponding Member of the Russian Academy of Sciences, Professor Mikhail Kovalchuk). The QMPh collective has a number of priority works in the field of nuclear magnetic resonance. One of the most significant achievements was the first in the world implementation (in 1958) of the Fourier transform of a free induction signal in order to obtain a NMR spectrum (see the details in [1]). Concurrently with the research activity, the staff of the department are actively involved in the development of practical applications of magnetic resonance. The department graduates work not only in Russia and the CIS, but also in Sweden, USA, New Zealand, England, Cuba, Germany, France, Italy, occupying positions from a highly advanced operator of radiospectrometers to a professor.

The main research areas developing in the team of quantum magnetic phenomena:

- Nuclear magnetic relaxation in liquids;
- Nuclear magnetic resonance in solids, including magnetically ordered materials;
- NMR in liquid crystals;
- NMR in heterogeneous systems;
- MRI in weak magnetic fields;

- Electron paramagnetic resonance;
- Nuclear magnetic resonance in the magnetic field of the Earth;
- The quantum magnetometry in archeology.

It is evident from the above that the scope of our research interests is quite wide. We are always open for the collaboration with researchers from various fields of science.

Our team has published a series of monographs, textbooks and training manuals on Magnetic Resonance. For example:

1. Vladimir I. Chizhik, Yuri S. Chernyshev, Alexey V. Donets, Viatcheslav Frolov, Andrei Komolkin, Marina G. Shelyapina. Magnetic Resonance and Its Applications. 2014, Springer-Verlag. 782 pp. *(Now more than 33 000 chapter downloads).*
2. Квантовая радиофизика: магнитный резонанс и его приложения. Учеб. пособие. 2-е изд., перераб. Под ред. В. И. Чижика. – СПб.: Изд-во С.-Петерб. ун-та, 2009. 700 с.
3. В. И. Чижик. Ядерная магнитная релаксация. Учеб. пособие. 3-е изд. – СПб.: Изд-во С.-Петерб. ун-та, 2004. 388 с.
4. Практикум по магнитному резонансу. Учебное пособие. Под ред. В. И. Чижика. – СПб.: Изд-во С.-Петерб. ун-та, 2003. 184 с.

Due to the COVID-19 coronavirus pandemic and the prohibition to hold any public events, the Organizing Committee of “Spinus-2021” have decided to implement the School-Conference in the on-line format using ZOOM (not in a face-to-face format). We hope that the next “Spinus 2022” will be held the usual format! We will be very glad to see you at next conference! Welcome!

Dr. Sci., Professor, SPbSU, Denis A. Markelov
Chairman of Organizing committee of the 18th School-conference
“Magnetic resonance and its applications” Spinus-2021

References

1. V. I. Chizhik. On the history of the Fourier transform in NMR spectroscopy. 2018, Bulletin du groupement AMPERE, 67, № 4 (273), p 5-6.

Lectures

Advances and adventures with compact magnetic resonance

Bernhard Blümich

Retired from RWTH Aachen University, Germany

Making the NMR equipment small on the expense of magnetic field strength bears challenges and opportunities. The main challenge for spectroscopy is to make the magnetic field homogeneous in a large volume with small magnets. The challenge in stray-field relaxometry for nondestructive materials testing is to make the magnet light with a strong stray-field at large distance. This type of research equipment enables new research opportunities. Following an introduction to compact magnetic resonance [1-3] a spectroscopically resolved ODNP study is reported with in an open, compact magnet [4] as well as recent investigations [5] of master violins [6] antique Roman frescoes and biofilms in Yellowstone National Park with the NMR-MOUSE.

References

1. B. Blümich, S. Haber-Pohlmeier, W. Zia, Compact NMR, de Gruyter, Berlin, 2014
2. B. Blümich, K. Singh, Desktop NMR and Its Applications From Materials Science To Organic Chemistry, Angew. Chem. Int. Ed. 57 (2018) 6996 – 7010
3. B. Blümich, Low-field and benchtop NMR, J. Magn. Reson. 306 (2019) 27–35
4. T. Überrück, M. Adams, J. Granwehr, B. Blümich, A compact X-Band ODNP spectrometer towards hyperpolarized ^{1}H spectroscopy, J. Magn. Reson. 314 (2020) 106724 1-7
5. B. Blümich, D. Jaschtschuk, C. Rehorn, Advances and Adventures with Mobile NMR, in: S. Haber-Pohlmeier, L. Ciubanu, B. Blümich, eds., Magnetic Resonance Microscopy Instrumentation and Applications in Engineering, Life Science and Energy Research, Wiley-VCH, Weinheim, 2021, in preparation
6. B. Blümich, M. Baias, C. Rehorn, V. Gabrielli, D. Jaschtschuk, C. Harrison, C. Invernizzi, M. Malagodi, Comparison of historical violins by non-destructive MRI depth profiling, Microchemical Journal 158 (2020) 105219

Spin Superfluid Quantum Computing

Yu. M. Bunkov

Russian Quantum Center, Skolkovo, 143025 Moscow, Russia.
E-mail: y.bunkov@rqc.ru

The conventional magnon Bose-Einstein condensation (BEC of magnons with k = 0) has been observed in magnetically ordered materials with repulsive interaction between magnons. In particularly it was observed in Yttrium Iron Garnet (YIG) film, magnetized perpendicular to the surface. For YIG film the critical density of non-equilibrium magnons for BEC condensation is $N_{BEC} \simeq M - M_z = M\,(1-\cos\beta)$, and corresponds to a deflection of precessing magnetization on an angle $\beta \simeq 3^\circ$ [1]. Here M is the magnetization and M_z its projection on the magnetic field. In these conditions the eigen state of magnon BEC determines by its frequency and does not depend on the exciting RF power (Fig. 1) [2].

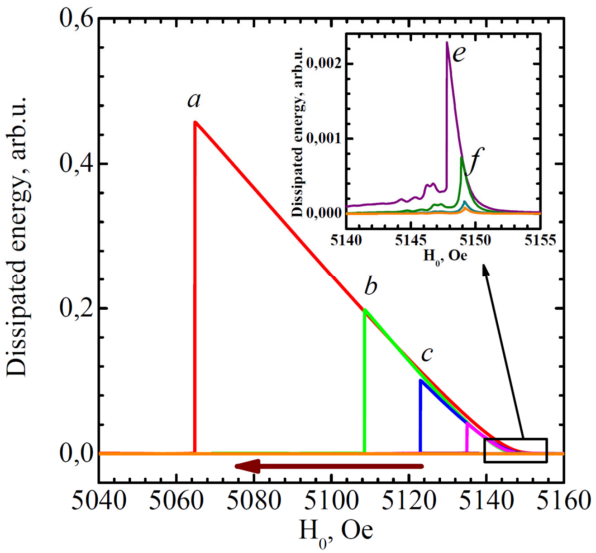

Figure 1. The energy dissipated by a magnon spin system at a magnetic field sweep at a different level of exciting RF power. The energy was calculated as a product of absorption signal on the amplitude of magnetic field. The dissipated energy depends on a frequency shift from the resonance and does not depend on the RF power!
The enlarged scale is shown in the inset

The BEC state persists permanently at the conditions, when the losses (evaporation) of quasiparticles are replenished by an excitation of new quasiparticles. This is the first permanent superfluid state, which exist at room temperature. The energy gap of magnon superfluid state can be adjusted by RF pumping frequency. Our discovery open the way for observation of coherent quantum transport phenomena at a room temperature, like magnetic Josephson effect, long distance spin transport, phase slippage, Goldstone modes (analog of second sound in superfluid ^{4}He) and others. This discovery may be applied for quantum computing. It may combine the spin type Q-bit and Josephson superfluid Q-bit at a combined systems.

Particularly, the qubit magnetic systems, analogous to a well-known superconducting qubits, can be considered: charge qubit (a), flux qubit (b) and phase qubit (c).

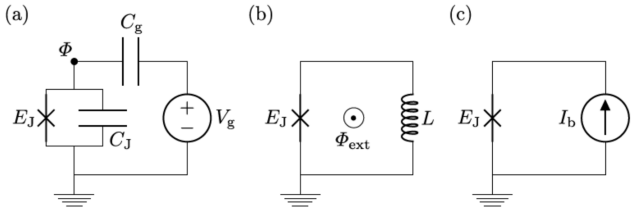

Figure 2. The types of circuits of Josephson junction superconducting qubit

Roughly speaking, the charge qubit is a box for charge, controlled by an external voltage V_g; the flux qubit is a loop controlled by an external magnetic flux F_{ext}; and the phase qubit is a Josephson junction biased by a current I_b. Using the analogy between electric superconductivity and spin superfluidity, we can suggest the next constructions of magnonic qubits. The charge qubit based on the repulsive interaction between magons, which realized by a frequency shift of the resonance frequency from the number of non-equilibrium magnons. For YIG film it reads:

$$\omega - \omega_0 = \gamma 4\pi M_S(1 - \cos\beta),$$

In the units of number of magnons n it roughly reads:

$$\Delta\omega(n) = \omega_0(1 + n/3N),$$

The pumping RF frequency plays a role of voltage for magnonic superfluid state. By choosing the frequency between the n and n + 1 state we can make a magnonic analog of charge qubit. The atomic density in the ferromagnetic sublattice of the YIG is of the order of $N = 10^{22}$ per cm^3. If a sample of a YIG film has dimensions of the order of 10^{-15} cm^3, each new non-equilibrium magnon shifts the resonance frequency on about 30 kHz at RF frequency about 10 GHz. By connect the sample with the source of magnons with a given chemical potential by a Josephson junction, we will be able to recognize the quantum states with n and n+1 magnon.

The analogy with a phase qubit is more complicate. The superconducting phase qubit based on Aharonov-Bohm effect. The phase of charged particle, moving along a path *L* changes by:

$$\Delta\alpha_{AB} = -e\int_L \vec{A}\cdot d\vec{r}.$$

For the close path it leads to a quantization of a phase on 2nπ. The similar effect exist for a magnetic particles (or quasiparticles) and names Aharonov- Casher effect:

$$\theta_{\text{A-C}} = \frac{g\mu_B}{\hbar c^2}\oint \mathrm{dl}\cdot(\mathbf{E}\times\mathbf{e}_z)$$

It leads to a similar effect of phase quantization for spin supercurrent. In this way, the phase difference at the Josephson junction can be controlled by applying the electric field. Furthermore, this phase can oscillate by application of AC electric voltage. This possibility makes a new way for dealing with phase qubit. As concerning the flax qubit, the situation is more complicate, since the magnetic flax does not quantized in a close magnonic loop. Indeed,

the real superconducting qubits are the superposition of a big number of a small samples connected by the Josephson junctions [3].

The similar system can be fabricated with the small samples of YIG films, as shown in Fig. 3. The magnonic superconducting system may have many advantages. First of all, they exist at room temperature, since the temperature of ferromagnetic transition in YIG is about 600K. Secondary, the magnonic precession interacts directly with the RF field. This simplifies the programing and read out the results of calculations. Furthermore, the dimensions of Josephson junction can be much large, then for a supercunducting quantum circuits. It can be adjusted by locally applying the magnetic field (3) or electric current (2) (See Fig. 3). The problem of relaxation of magnons can be solved by a permanent source of a new magnons with a controllable chemical potential throw the peripheral YIG strips (1). The read out of the information from each element can be performed by RF resonator (4) or Spin-Hall effect (5), as well by optical methods (6). The very important circumstance is the possibility of print circuits fabrication and scaling the construction. The last question is the temperature of real quantum processor. It's, possibly, necessary to cool down the processor to a sub-kelvin region of temperature for to avoid the thermal fluctuations of qubits. Indeed, question of noise of Bose condensate magnon gas is not so clear. Definitely, the magnon processor will be less sensitive to an external noise, since there is not an electric charged particle. In conclusion, the idea to use the magnonic superfluidity for quantum calculations is very new and has a great potential of its development. For review of spin superfluidity please see [4].

In conclusion it is useful to mention, that the spin superfluid phenomena is the result of repulsive interaction between non-equilibrium magnons in out of plain magnetized YIG film. There were published many experiments with in-plane magnetized film. The long distance spin waves propagating were demonstrated. The magnon BEC formation was also announced. Indeed, in these systems the magnonic interaction is attractive and, consequently, the critical superfluid velocity is zero and effect of magnon superfluidity does not exist. For review of spin superfluidity please see [4].

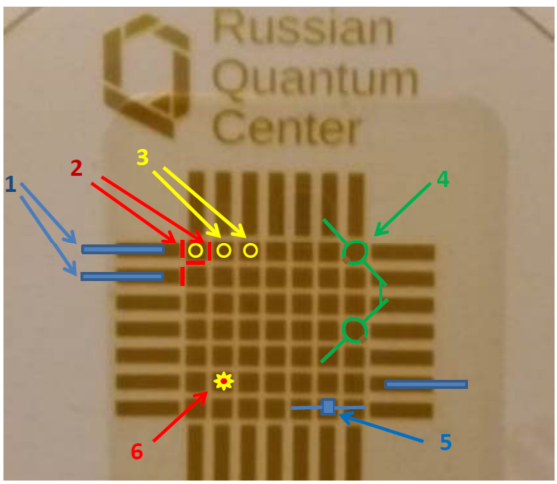

Figure 3. The prototype of magnonic quantum processor (from [5])

Financial support by the Russian Science Foundation within the Grant 19-12-00397 "Spin Superfluids" is gratefully acknowledged.

References

1. Yu. M. Bunkov and V. L. Safonov, J. Magnetism Magnetic Materials, **452**, 30–34 (2018).
2. Yu. M. Bunkov et al., https://arxiv.org/abs/1810.08051; https://arxiv.org/abs/1911.03708
3. F. Arute, et al., Nature, 574, 505 (2019).
4. Yu. M. Bunkov and G. E. Volovik, "Spin Superuidity and Magnon BEC" in Novel Superuids Ch.4, eds. Bennemann, K. H. & Ketterson, J. B. Oxford Univ. Press, Oxford, (2013), arXiv:1003.4889v3.
5. Yu. M. Bunkov, "Quantum Magnonics", JETP, 131, 18-28 (2020).

NMR studies of phase transitions in confined metals and alloys

Elena V. Charnaya, Denis Yu. Nefedov, Andrei V. Uskov, Dmitrii Yu. Podorozhkin

St. Peterburg State University, St. Peterburg 198504 Russia
E-mail: charnaya@mail.ru

Introduction

A concise review of the use of NMR as a probe for studying different kinds of phase transitions in liquid and solid metals and alloys embedded into nanoporous silica matrices is presented. The attention is focused on last studies of the liquid-liquid phase transitions in confined melts and structural modifications under nanoconfinement while the melting and freezing transitions are also discussed.

Liquid-liquid phase transitions under nanoconfinement

Structural transformations in liquids pose severe challenges to condensed matter physics. The nature of LLPT is poorly understood and even its occurrence in many substances is in doubt. It was suggested that LLPT at ambient pressure takes place under strong supercooling. Therefore, LLPT in bulk is disguised by crystallization or vitrification processes. In contrast, liquids confined to nanoporous matrices are easy to supercool to temperatures much lower than the melting temperatures. This raises expectations that LLPT can be found in liquids under nanoconfinement. For metallic substances NMR acts as a powerful experimental technique which gives valuable information about the internal structure of liquids through measurements of the Knight shift caused by coupling with conduction electrons. Here we review NMR measurements of the Knight shift, which were carried out to study LLPT in the nanostructured Ga and Ga-In-Sn and Ga-In alloys in the supercooled state. NMR studies revealed a step-like splitting of the gallium resonance line upon cooling. At warming the gradual change of the Knight shift was observed which could happen when the confined melts pass over the critical point of the LLPT line on the phase diagram.

Structural transformations under nanoconfinement

NMR was applied to studies of polymorphism in confined metals and alloys. It was shown that for metallic sodium within fine pores of porous glasses the temperature of the structural phase transition, which occurs in bulk below 40 K, rises remarkably up to more than 200 K. The emergence and stabilization of a solid phase with the structure of β-Ga was observed for gallium alloy confined to silica opal matrices. The temperature ranges of this phase occurrence and quadrupole constant temperature dependences were obtained.

Melting and freezing in confined nanoparticles

The melting and crystallization phase transitions for metallic components of nanocomposites were noticeably moved to lower temperatures and strongly diffused. For some metals as mercury and tin the occurrence of the liquid skin upon melting was suggested. The pronounced hysteresis between melting and freezing was ascribed to heterogeneous nucleation under confinement. The step-like freezing and melting of gallium within pores was found to occur due to the emergence of different crystalline phases.

Acknowledgements

This work is supported by RFBR (grant 19-07-00028). Part of measurements was done in SPbGU using the equipment of "Centre for Diagnostics of Functional Materials for Medicine, Pharmacology and Nanoelectronics".

A new model of the microstructure of mixtures of ionic liquids with water: an alternative to "water pockets"

V. I. Chizhik[1], S. S. Bystrov[1], V. V. Matveev[1], A. V. Egorov[1], and V. Balevičius[2]

[1]St. Peterburg State University, St. Peterburg 198504 Russia
[2]Vilnius University, Vilnius, Lithuania
E-mail: v.chizhik@spbu.ru

Unique physical and chemical properties of ionic liquids, ILs, (neat and in solutions) such as high thermal stability, low vapor pressure, high boiling point, and the ability to dissolve a wide range of chemical species, determine numerous applications in "green" chemistry and material science. Aqueous solutions of ILs play a large role in various practical applications.

The results of detailed investigation of the local and translational mobility in a set of imidazolium-based ionic liquids (1-butyl-3-methylimidazolium) in a wide temperature range and varying anions (BF_4^-, I^-, Cl^-, Br^-, NO_3^-, TfO^-) are presented. The measurements of temperature dependencies of the spin-lattice relaxation times of ^1H and ^{13}C nuclei are motivated, in particular, by the need to obtain a fundamental characterization of molecular mobility in the substances under study, namely, to estimate the correlation times for the motion of individual molecular groups. The study of translational diffusion is very important for deeper understanding the peculiarities of molecular motion of the components in objects under investigation, since it constitutes to the basic form of "transport" which reflects molecular interactions of molecules or ions with their environment. The correlation between local and translational mobility in pure ionic liquids of the [bmim][A] type was investigated using the data on NMR-relaxation rates and diffusion coefficients. It has been found that a sufficiently clear correlation is realized only in the case of ILs with relatively low viscosity and only at temperatures above room temperature. The mutual sequence of the values of diffusion coefficients (D) for different ILs corresponds qualitatively to the data on their viscosity η. It is shown here that for the $[bmim]^+$ cation the temperature dependencies of the product $D\eta$ do not follow the Stokes-Einstein relation for most systems studied, i.e. there realized so-called "diffusion-viscosity decoupling".

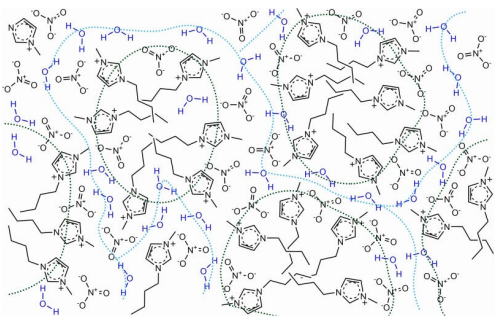

Figure 1. A simplified model of a mixture of IL and water (approximately 50 mol %). The black dotted lines indicate hydrophobic fragments, and the blue ones show the "facilitated" diffusion paths of water molecules and, possibly, anions

In terms of practical application, it is important to have an idea how the IL structure changes with the addition of water. There are a few points of view on this issue. In the past few years, the hypothesis about the existence of so-called "water pockets" in mixtures of water with a number of ionic liquids has been discussed in the literature. The concept of "water pockets"

was introduced by a group (groups) of Japanese researchers. The hypothesis is based on a certain set of experimental data (obtained by various methods: SANS/SAXS, Raman, NMR, ... etc.) about the heterogeneous structure of such mixtures at a nanometer level [1-4]. In the report the critical review of existing models of the microstructure of mixtures "IL – water" and the justification of a new hypothesis about the structure of systems such as "[bmim]A – H_2O" are given [5, 6].

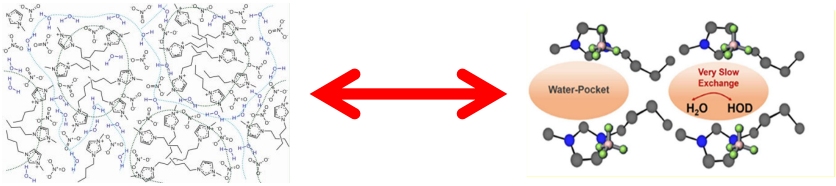

Acknowledgements

The NMR measurements have been carried out in the Center for Magnetic Resonance of Research park of Saint Petersburg State University.

This work was supported by Russian Foundation for Basic Research (RFBR) grant #17-03-00057a.

References

1. Abe, H.; Hatano, N.; Ima, Y.; Ohta, S.; Shimizu, A.; Yoshimura, Y. Peculiar Concentration Dependence of H/D Exchange Reaction in 1-Butyl-3-Methylimidazolium Tetrafluoroborate-D2O Mixtures. Open J. Phys. Chem. 2011, 01 (03), 70. https://doi.org/10.4236/ojpc.2011.13010.
2. Abe, H.; Takekiyo, T.; Shigemi, M.; Yoshimura, Y.; Tsuge, S.; Hanasaki, T.; Ohishi, K.; Takata, S.; Suzuki, J. Direct Evidence of Confined Water in Room-Temperature Ionic Liquids by Complementary Use of Small-Angle X-Ray and Neutron Scattering. J. Phys. Chem. Lett. 2014, 5 (7), 1175–1180. https://doi.org/10.1021/jz500299z.
3. Saihara, K.; Yoshimura, Y.; Ohta, S.; Shimizu, A. Properties of Water Confined in Ionic Liquids. Sci. Rep. 2015, 5, 10619. https://doi.org/10.1038/srep10619.
4. Abe, H.; Takekiyo, T.; Yoshimura, Y.; Saihara, K.; Shimizu, A. Anomalous Freezing of Nano-Confined Water in Room-Temperature Ionic Liquid 1-Butyl-3-Methylimidazolium Nitrate. ChemPhysChem 2016, 17 (8), 1136–1142. https://doi.org/10.1002/cphc.201501199.
5. Bystrov S. S., V. V. Matveev, Y. S. Chernyshev, V. Balevičius, V. I. Chizhik. Molecular Mobility in a Set of Imidazolium-Based Ionic Liquids [bmim] + A - by the NMR-Relaxation Method. Journal of Physical Chemistry B. 123, 10, 2362-2372. Doi: 10.1021/acs.jpcb.8b11250.
6. Bystrov S. S., Vladimir V. Matveev, Andrei V. Egorov, Yurii S. Chernyshev, Vladislav A. Konovalov, Vytautas Balevičius, and Vladimir I. Chizhik. Translational Diffusion in a Set of Imidazolium-Based Ionic Liquids [bmim]+A- and Their Mixtures with Water. J. Phys. Chem. B. DOI: 10.1021/acs.jpcb.9b06802.

Advanced MRI-methods for evaluation of Parkinson's disease

Uwe Eichhoff

Bruker BioSpin GmbH retired; D 76571 Gaggenau, Germany, Max Hildebrandt-Str.40
E-mail: barbara.uwe@t-online.de

Introduction

Parkinson's disease (PD) is a long-term degenerative disorder of the central nervous system. It initially affects the motor system per year in more than 6 million people and results in over 120.000 deaths. There is no cure for Parkinson`s disease and treatment can only improve the symptoms. In biopsies the only hint for PD is a reduction of the dark pigmented area in the substantia nigra, located deeply in the central brain. The pigmentation results from iron-containing nigrosomes, a small cluster of dopamine-releasing cells. Loss of these cells means less distribution of the neurotransmitter dopamine resulting in an impairment of the neuronal pathways. The nigrosomes contain paramagnetic iron and therefore can be selectively observed with MRI. During lifetime these cells die continously. In Parkinson's disease for unknown reasons this process is accelerated.

Susceptibility weighted Imaging

Imaging of nigrosomes can be accomplished by MRI-methods, which are sensitive to susceptibility changes produced by tissue iron content leading to a phase shift in gradient echo images. In NMR and MRI phase sensitive detection is applied delivering a real and imaginary part of the complex signal. Diagnostic MRI images are magnitude images, where the phase information is discarded. The raw phase image does not reflect anatomy and is clinically almost worthless. Applying a spatial high pass-filter allows to select the contribution from susceptibility changes. This brings back some anatomical details but the modified phase images cannot compete with the brilliant clinical magnitude images. Therefore phase must be reintroduced into the clinical magnitude images. From the phase image a phase mask is created and multiplied into the magnitude image leading to a susceptibility weighted image [1]. The calculation of a quantitative susceptibility map (QSM) from the susceptibility-induced small magnetic field variations is much more complicated. The tissue local magnetic field can be approximated as the convolution of a the dipole kernel with the susceptibility distribution, which is executed in the Fourier domain by multiplication. The calculation of the susceptibility distribution is an ill-posed inverse problem. In the Fourier domain the susceptibility appears to be undersampled at points where the dipole kernel is zero. Scanning the object under different orientations to the external magnetic field may be one solution, but often a modest amount of additional information may be sufficient for uniquely solving this problem [2].

Application to Parkinson's disease

SWI and QSM show clearly the susceptibility differences in brain structures allowing their segmentation, especially in the subcortical region [3]. Susceptibility images allow a clear differentiation between healthy controls and Parkinson's disease and show an increase of susceptibility with age [4] and its correlation with disease duration and severity characterized by a clinical score [5]. Besides SWI and QSM, other MRI methods can be employed to investigate Parkinson's disease. Diffusion tensor images reveals a reduction in the volume of the subthalamic nucleus and a decrease in the tissue fractional anisotropy [6]. If structural connections are impaired, this also implies impairment in functional connectivity. Resting state functional MRI (rs-fMRI) shows a disruption of Cortical and Subcortical Effective Connectivity in Early Parkinson's Disease [7]. Another application of MRI to Parkinson's disease is the control of electrode placement for surgery and deep brain stimulation.

References

1. E.M.Haacke, Y.Xu, N.Cheng, J.R.Reichenbach, Mag. Reson. Med. 52(3), 612 (2004)
2. J.Liu, T.Liu, L. de Rochefort, J.Ledoux, I.Khalidov, Neuroimage 59(3), 2560 (2012)
3. B.Yu,L. Li,X.Li ,N.He,H.Wei,C.Zuo, F.Yan, Y.Zhang, Proc. Intl. Soc. Mag. Reson. Med. 28(2020)1526
4. N. He, K. Ghass, P., Z. Cheng, Yan Li, M.Jokar, S.K.Sethi, W. Chen, Chen, F. Yan, E.M.Haacke, Proc. Intl. Soc. Mag. Reson. Med.(2020)0201
5. C.Liu, H.Wei, N.-J.Gong, M.Cronin, R.Dibb, K.Decker, Tomography 1(1) (2015) 3-17
6. R. Patriat, J. Kaplan, J. J. Niederer, S. A. Huffmaster, M. Petrucci, N. Harel, C. MacKinnon, Proc. Intl. Soc. Mag. Reson. Med. 26 (2018) 0425
7. K.R. Sreenivasan, E. Bayram, V.Mishra, Z.Yang, C. Bird, X. Zhuang, D. Cordes, B. Bluett, Proc. Intl. Soc. Mag. Reson. Med. 26 (2018) 0426

NMR Studies of metals and supported metal particles

Jacques Fraissard

Sorbonne Universite, UPMC, Paris
Ecole supérieure de Physique et Chimie Industrielle de Paris

The chemical and petroleum industries rely upon metal catalysts for the manufacture of a wide range of essential products. Metal clusters or crystallites in the catalysts are studied by several techniques: gas adsorption isotherms, electron microscopy, EXAFS, Mössbauer spectroscopy, etc., but their number proves that none of them is able to characterise these particles correctly.

The magnetic properties of these latter should depend on their size, at least when they are sufficiently small, whence the interest of NMR. There are, *a priori*, several ways of applying NMR to such a problem:

- Detection of the metal nucleus. However, this method cannot be generalised to all metal catalysts, since few metals can be detected by NMR. Moreover, the experimental conditions are particularly difficult and require very experienced physicists.
- The use of a probe which can be detected by NMR and adsorbed on the particles. This is an indirect measurement, much easier experimentally, which was developed using hydrogen and xenon adsorption and their detection by NMR.

These techniques make it possible to determine many properties of metal catalysts such as: particles size, dispersion on support, metal-support interaction, particle location in porous systems, distribution of chemisorbed phases, alloys.

Review of Pulse Sequences Applicable in Time-Domain NMR

Leonid Grunin[1,2]

[1]*Resonance Systems GmbH, Seestr. 28, Kirchheim u. Teck D-73230, Germany*
[2]*Volga State University of Technology, Lenin sq. 3, Yoshkar-Ola, 424000, Russian Federation*
E-mail: mobilenmr@hotmail.com
http://www.nmr-design.com

Introduction

Such experiments like Free Induction Decay (FID), Hahan Echo (HE), Curr-Purcell-Meiboom-Gill (CPMG), Inversion-Recovery (IR) and Saturation-Recovery (SR) became classic many years ago. They are normally well applicable in relatively low-field Time-Domain NMR (TD-NMR) area and they still serve as the mainstream basis for the most industrial and academic researches, that involve NMR relaxation.

As technology of measurement hardware revolutionary evolves, the new horizons for TD-NMR applications are arising, so many of techniques that have been attributed to conventional area of High Field High Resolution magnetic resonance are getting chances to be successfully used in table-top portable “low resolution” machines.

The lecture is designed both to describe standard measurements approaches of NMR relaxations times and amplitudes as well as to uncover the changes in TD-NMR that have happened in last decade and widened the classical list with such pulse sequences as

- Solid Echo
- Magic Sandwich Echo
- Goldman-Shen
- Double Quantum Filter
- Fast Inversion-Recovery

All listed techniques are supplied with real practical examples and experimental data.

Experiments with Pulsed Field Gradient for material diffusion measurements and imaging are also presented in the lecture.

Copolymer systems studied by NMR and other complementary techniques

Jacek Jenczyk, Stefan Jurga

NanoBioMedical Centre, Adam Mickiewicz University, Wszechnicy Piastowskiej 3, 61-614 Poznań, Poland
E-mail: stjurga@amu.edu.pl
http://www.cnbm.amu.edu.pl

Introduction

Block copolymers (BCPs) represent interesting group among synthetic materials since they are well known from their unique self-assembling properties [1]. Below critical temperature T_{ODT} (order-disorder transition temperature) two dissimilar blocks become immiscible and undergo reorganization leading to domain like structures formation. It has been confirmed that thermodynamic equilibrium conditions require minimalization of the contact surface across two different phases and hence various morphologies can develop depending on volume fraction of one block with respect to another. Theoretically calculated phase diagram predicts several fundamental morphologies namely, spheroidal with cubic arrangement, cylindrical with hexagonal arrangement, gyroidal bicontinuous and lamelar. BCPs self-assembly has drawn the attention of scientists and engineers working in a field of microelectronics and nanolithography due to both periodic nature and nanoscopic dimensions of observed domain structures. The ultimate goal is to develope bottom-up technology based on self-organized organic compounds which on the one hand would be a low cost alternative to the expensive top-down strategies and on the other hand would provide a high quality products comparable with those manufactured utilizing already established methods. It has been well documented that BCP patterning can easily compete with conventional photolithography giving access to sub-10-nanometric feature sizes. Therefore, BCPs based technology requires thorough assessment of domain architecture, domain dimensions and the size of interfacial region. The latter parameter appears to be particularly important in nanolithography however its accurate estimation remains challenging. Throughout the processing stages, quite often the BCPs matrix undergoes selective etching and hence the interface determines eventual feature size resolution and sharpnes of attained structural motifs. Although, microscopic and scattering techniques provide complete and reliable picture concerning the domain morphology and its periodicity, they both lack of quantitative data regarding the mentioned transition phase. Therefore, in order to thoroughly monitor the copolymer systems, complementary NMR methods are employed. Accordingly, when investigated spectrocopically, this seemingly simple, two phase BCPs model reveals additional interesting features and more complex structure than expected.

Methods

NMR spin diffusion method for determination of domain sizes in heterogeneous polymers, which is schematically illustrated in Fig. 1 was introduced by Clauss *et al.* [2]. The basic idea of the experiment relies on the fact that if there is any nonuniform distribution of magnetization present across the heterogeneous domains, there will be spontaneous magnetization transfer observed.

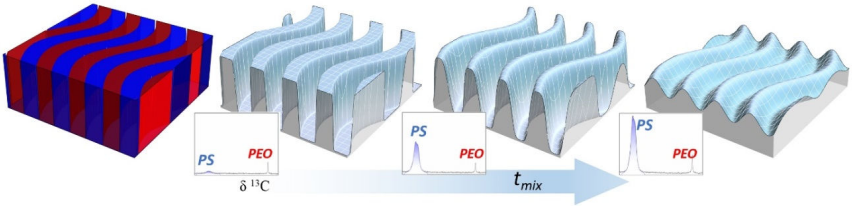

Figure 1. Schematically illustrated method of NMR spin-diffusion in the case of lamellar morphology BCP. Magnetization profiles evolve during mixing time to reach the state of evenly distributed magnetization across the domains

It has been shown that this magnetization transfer follows general diffusion equation and it is modulated by internuclear dipolar interactions via "flip-flop" mechanism. Therefore, different materials are characterized by different spin diffusion coefficients due to both inequivalent proton densities and inherently different molecular dynamics. NMR spin diffusion experiment involves acquisition of a set of NMR spectra, each recorded for one specified mixing time t_{mix}, to monitor their evolution due to magnetization transfer. Accordingly, provided the domain architecture (i.e. lamellar, cylindrical or other) and the spin diffusion coefficients are known, it is possible to estimate both the domain size and the interfacial region size. This apprach proved to be particularly usefull in the case of block copolymer structural studies where it is usually employed as a complementary method to support other techniques providing sufficient resolution such as SAXS, SANS, TEM or AFM. Mentioned here, standard scattering and microscopic techniques, applied in the case of organic materials studies, can be demanding and require either relatively strong sources, proper staining procedures or rigorous sample praparation protocols to gain satisfactory data. Whereas NMR spin-diffusion can be performed using standard pulse spectrometers and it does not require any sample modification prior experiment since the inherent features of the material, such as chemical structure and the molecular dynamics, determine the contrast used in this method. Moreover, it is worth again emphasizing that NMR spin-diffusion provides an insite into the interfacial regions which is unique in comparison to other methods. Our NMR results were confronted with AFM microscopic data.

Apart form structural studies we also monitored polymer chain dynamics using both, broadband dielectric spectroscopy and NMR relaxometry. Obtained data enabled assessment of: i) the polymer chain reorientations difference between neat polymers and their copolymers, ii) impact of nanoparticles inclusion on polymer dynamics, iii) observation of motions within rigid and mobile amorphous phase within semicrystalline polymers.

Results example

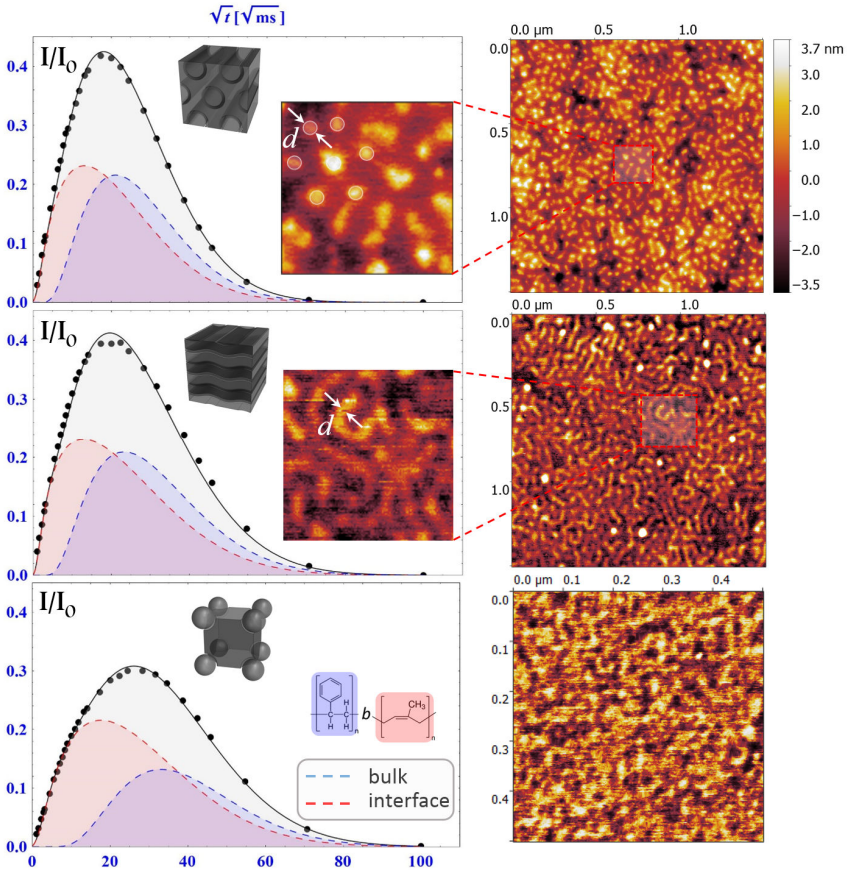

Figure 2. Left) NMR spin-diffusion profiles obtained for different poly(styrene-b-isoprene) block copolymers. Right) AFM graphs taken for thin BCP films

Acknowledgements

The research was supported by the H2020-INFRAIA-2016-2017 project under research grant "EUSMI – European infrastructure for spectroscopy, scattering and imaging of soft matter", contract number GA731019, funded under H2020-EU.1.4.1.2.–RIA.

References

1. Bates, C.M. and F.S. Bates, *50th Anniversary Perspective: Block Polymers—Pure Potential.* Macromolecules, 2017. **50**(1): p. 3-22.
2. Clauss, J., K. Schmidt-Rohr, and H.W. Spiess, *Determination of domain sizes in heterogeneous polymers by solid-state NMR.* Acta Polymerica, 1993. **44**(1): p. 1-17.

Parahydrogen-induced polarization: bridging the gap between homogeneous and heterogeneous catalysis

Igor V. Koptyug

International Tomography Center SB RAS. Institutskaya 3A, Novosibirsk. 630090, Russia
E-mail: koptyug@tomo.nsc.ru
http://www.tomo.nsc.ru/en/structure/lab/lmrm

Introduction

Hyperpolarization techniques that utilize parahydrogen (p-H_2) to enhance the sensitivity in NMR and MRI experiments by 3-4 orders of magnitude and more in various spectroscopic and imaging applications is a rapidly growing field of research. Such studies are very promising for the development of novel highly sensitive tools for medical diagnostics at the molecular and cellular level, and of advanced techniques for gaining a detailed understanding of the mechanisms of molecular transformations in modern industrial-scale catalysis. In particular, hydrogenation of unsaturated compounds with molecular hydrogen can lead to significant signal amplification in NMR and MRI if parahydrogen is used in the reaction instead of ordinary H_2. This provides important information on the existence and the nature of the active catalytic sites that can implement the pairwise addition of H_2 to a substrate, which is the key requirement for observing signal enhancement.

Parahydrogen-based NMR signal enhancement

We have established the fact that the centers of pairwise H_2 addition exist not only for heterogeneous catalysts comprising metal complexes immobilized on solid supports, but also for supported metal catalysts, which was rather unexpected since such a reaction mechanism is usually associated with homogeneous hydrogenation through the formation of a dihydride metal complex. We have demonstrated the pairwise addition of H_2 for other types of heterogeneous catalysts as well, including metal oxides, sulfides, carbides, etc. For all these catalysts, NMR signals of the hydrogenation products exhibit pronounced enhancements with respect to thermally equilibrated NMR spectra.

With the purpose of a deliberate design and synthesis of catalysts possessing centers of pairwise hydrogen addition to a substrate, we used isolated metal-based structures on the surface of a support, such as single-site/single-atom catalysts. Examples of such systems for which we were able to observe the pairwise addition of hydrogen and the associated NMR signal enhancement include isolated Co(II),O centers on SiO_2, Cr(III),O on SiO_2-Al_2O_3, oxo-vanadium complex on SiO_2, and others. The greatest activity in pairwise hydrogen addition was observed, in particular, with bimetallic catalysts. These include catalysts with the Au_{shell}-Pd_{core} nanoparticle structure deposited on pyrolytic graphite, as well as Pd-In/Al_2O_3 intermetallic catalysts - single-site systems in which the active metal atom is isolated by a group of atoms of an element which is inactive in the reaction.

The enhancement of the NMR signals using parahydrogen in catalytic hydrogenation reactions, in addition to important mechanistic information about these processes, makes it possible to perform MRI studies of operating reactors, as illustrated with the example of model systems with catalytically active metal nanoparticles supported on a TiO_2 layer deposited on glass tubes or plates. This approach allowed us to visualize the catalytically active regions of a model reactor during the hydrogenation of propene.

The field of parahydrogen-based NMR signal enhancement enjoys the fact that p-H_2, the nuclear spin isomer (NSIM) of H_2, is easily produced by magnetically assisted equilibration of H_2 at cryogenic temperatures. Indeed, the equilibrium ratio of the two spin isomers in “normal” H_2 shifts to an almost pure p-H_2 near liquid H_2 temperature (~20.3 K). Unfortunately, this approach does not work for larger and heavier symmetric molecules because of a much smaller

energy difference between the molecular rotational levels compared to H_2. This makes the NSIM enrichment by equilibration at low temperatures impractical for molecules other than H_2 and its isotopologue D_2 Some other approaches for NSIM enrichment are known, but unfortunately the quantities of NSIM-enriched material that they can produce are far below the amounts required for most scientific purposes. This is a significant obstacle for the studies of fundamental properties and behavior of NSIM as well as their various applications which require the facile availability of NSIM in sufficient quantities. This is particularly true for the development of their novel and advanced applications in NMR and MRI because, similar to p-H_2, NSIM of other molecules could provide very large NMR signal enhancements. NSIM-based approach for signal enhancement in NMR and MRI is thus currently based exclusively on the use of parahydrogen, and therefore at present it is suitable only for those reactions that involve H_2 as one of the reactants. Furthermore, facile dissociation of H_2 on metal-based catalysts combined with very high mobility of surface hydrogens often lead to significantly reduced signal enhancement levels in many heterogeneous catalytic processes involving H_2. Importantly, the possibility to use NSIM of molecules other than H_2 in such studies can potentially result in a broad range of novel hypersensitive NMR and MRI methods and their advanced applications. Therefore, the development of novel techniques for NSIM enrichment is highly desired. The results of the ongoing efforts in this direction will be presented as well.

Acknowledgements

This work was supported by the grants from RFBR (19-29-10003 and 19-53-12013).

References

1. K. V. Kovtunov, I. V. Koptyug, M. Fekete, S. B. Duckett, T. Theis, B. Joalland, E. Y. Chekmenev. – *Angew. Chem. Int. Ed.*, **59**, 17788-17797 (2020)
2. V. V. Zhivonitko, A. I. Svyatova, K. V. Kovtunov, I. V. Koptyug. – *Annu. Rep. NMR Spectrosc*., **95**, 83-145 (2018)
3. K. V. Kovtunov, D. B. Burueva, L. M. Kovtunova, V. I. Bukhtiyarov, I. V. Koptyug. – *Chem. Eur. J*., **25**, 1420-1431 (2019)
4. K. V. Kovtunov, O. G. Salnikov, I. V. Skovpin, N. V. Chukanov, D. B. Burueva, I. V. Koptyug. – *Pure & Appl. Chem*., **92**, 1029-1046 (2020)

Paramagnetic relaxation in solution: an overview

Jozef Kowalewski

Stockholm University, Stockholm, Sweden

Presence of paramagnetic species in solution has a profound effect on NMR properties, not least on nuclear spin relaxation which is strongly enhanced. The origin of the effect is the interaction between nuclear spins and the unpaired electron spins – the hyperfine interaction. The hyperfine interaction is commonly divided into a dipolar and scalar part, similar to the dipolar interactions between the nuclear spins and the J-coupling, respectively. The difference is that the hyperfine interaction is much stronger, because of the very large magnitude of the magnetic dipole associated with an unpaired electron, about 650 times larger than that of a proton. The electron spin is also subject to other strong interactions, among which the electron Zeeman and the zero-field splitting (ZFS) are most important. The strong interactions of the electron spin result also in very rapid electron spin relaxation.

The nuclear spin relaxation is usually described by second order perturbation theory, in a formulation known as Redfield theory. This approach can be applied to paramagnetic relaxation. However, the fact that the electron spin interacts so strongly with its surroundings sets limits to the validity and applicability of the Redfield theory. As a consequence, theoretical description of NMR relaxation in paramagnetic solutions becomes rather complicated and a decisive progress has first occurred during the last few decades.

The historical development of our understanding of paramagnetic relaxation effects will be presented. Experimental strategies, mainly nuclear magnetic relaxation dispersion (NMRD) measurements based on the fast field-cycling (FFC), will be described and illustrative examples – from the field of MRI contrast agents as well as from paramagnetic metalloproteins – will be provided.

Modern SSNMR spectroscopy for studying the structure of functional materials

Olga B. Lapina

Boreskov Institute of Catalysis, pr. Lavrentieva 5, 630090, Novosibirsk, Russia
E-mail: olga@catalysis.ru

Knowledge of the structure of the local environment of the nuclei is the key to determining the properties of functional materials. Due to the high sensitivity to the local environment of the nuclei, NMR has become one of the most informative methods in materials science and catalysis. Nevertheless, the existing limitations in the sensitivity of the NMR technique and necessity to solve problems standing at the boundaries of related disciplines suggest the development of new methodologies and new approaches. To overcome the Boltzmann limitation and significantly increase the sensitivity of NMR spectroscopy, methods of dynamic nuclear polarization, laser hyperpolarization methods, as well as measurements in high magnetic fields are used. In turn, increasing the sensitivity of the method became a powerful impulse for the development of multinuclear and multidimensional NMR spectroscopy in solids. In combination with modern quantum chemical calculations, a new direction was formed in the early 2000s – NMR crystallography.

NMR crystallography combines state-of-the-art high-resolution solid-state NMR experiments with modern quantum chemical calculations, which allow us to study the structural and dynamic characteristics of various systems.

Based on the literature data and the data obtained in our group, the current capabilities of multinuclear NMR crystallography in its application to various functional materials will be discussed.

High magnetic fields (now up to 35 T) significantly increase NMR sensitivity thus allowing to perform experiments on the so-called “difficult” nuclei, i.e. nuclei with low natural content or a low gyromagnetic ratio. For quadrupolar nuclei, nuclei with a large electric quadrupole moment also fall into the “difficult” category. In high magnetic fields, the line width decreases due to the second order of quadrupole interaction. Thus, in strong magnetic fields, it becomes possible to conduct NMR studies on the following quadrupolar nuclei: ^{17}O, ^{25}Mg, ^{39}K, ^{43}Ca, ^{47}Ti, ^{49}Ti, ^{67}Zn, ^{71}Ga, ^{73}Ge, ^{87}Sr, ^{91}Zr, ^{93}Nb, ^{95}Mo, ^{115}In, ^{137}Ba, ^{139}La, ^{185}Re, ^{187}Re, ^{209}Bi.

As an example, the results obtained by ^{93}Nb NMR crystallography will be demonstrated. The isotope niobium-93 has the maximum known spin (I=9/2), a large quadrupole moment, and, like all heavy nuclei, a significant amount of chemical shift anisotropy. Using the method of NMR crystallography, which in this case is a combination of NMR experiments in various magnetic fields (up to 21 T) with different rotational speeds (up to 70 kHz) with quantum chemical calculations and in situ XRD experiments, the polycondensation process that occurs with an increase in temperature in niobium oxalate was studied. This approach allowed us to establish the mechanism of polycondensation of niobium-oxygen polyhedra. These results proved to be base for determining the mechanism of formation of NbTiO nanosheets from layered KTiNbOx compounds, promising catalysts for the decomposition of biomass.

Acknowledgement

This work was supported by the Ministry of Science and Higher Education of the Russian Federation within the governmental order for Boreskov Institute of Catalysis (project AAAA-A21-121011390054-1).

Navigating the space of spin operators

Malcolm H. Levitt and Christian Bengs

Department of Chemistry, University of Southampton, SO17 1BJ
E-mail: mhl@soton.ac.uk

Magnetic resonance experiments may be thought of as journeys in the space of spin operators.

But what is this space? Does it have a boundary? If it does, what is the shape of that boundary? Is the boundary spherical? Or does it have straight edges?

If a boundary exists, is it possible to reach it?

Also: what is the equation of motion for our "space rocket"? Does the equation of motion used by scientists at the start of magnetic resonance (in the 1950's) remain valid today? Is the standard equation of motion still valid even if we travel very far from the launching pad?

I expect to explore these questions and hopefully give some answers. On the way there will be an opportunity to look at the scenery, perhaps with a novel perspective.

Fast field-cycling magnetic resonance imaging

David J. Lurie[1], Lionel M. Broche[1], Gareth R. Davies[1], Mary Joan Macleod[1], P. James Ross[1] and Robert Stormont[1,2]

[1]School of Medicine, Medical Sciences and Nutrition, University of Aberdeen, Foresterhill, Aberdeen, United Kingdom AB25 2ZD
[2]GE Healthcare, Waukesha, WI, USA
E-mail: d.lurie@abdn.ac.uk
https://www.abdn.ac.uk/research/ffc-mri/

Introduction

Most contrast in conventional MRI arises from differences in T_1 between normal and diseased tissues. Several studies on small tissue samples have shown that extra information could be obtained from T_1-dispersion measurements (plots of T_1 versus magnetic field), but this information is invisible to standard MRI scanners, which operate only at fixed magnetic field (e.g. 1.5 T, 3.0 T). We have developed Fast Field-Cycling Magnetic Resonance Imaging (FFC-MRI) to exploit T_1-dispersion as a potential biomarker, with the aim of increasing diagnostic potential [1].

Methods

T_1-dispersion is typically measured using FFC, by switching the magnetic field rapidly between levels during the pulse sequence [2]. In this way, a single instrument can be used to measure T_1 over a wide range of magnetic field strengths. FFC-MRI obtains spatially-resolved T_1-dispersion data, by collecting images at a range of evolution fields [3].

In our lab we have built a range of FFC-MRI equipment, including two whole-body human sized scanners, operating at detection fields of 0.06 T [4] and 0.2 T [5]. The 0.06 T device uses a double magnet, with field-cycling being accomplished by switching on and off a resistive magnet inside the bore of a permanent magnet; this has the benefit of inherently high field stability during the detection period. The 0.2 T FFC-MRI system (Fig. 1) uses a single resistive magnet which has the advantage of increased flexibility in pulse sequence programming, at the expense of lower field stability during the detection period, necessitating more complex instrumentation.

Figure 1. 0.2 T FFC-MRI scanner at the University of Aberdeen

Results

Our laboratory is investigating a range of applications of FFC relaxometry and FFC-MRI. We have demonstrated that FFC relaxometry can detect the formation of cross-linked fibrin protein from fibrinogen *in vitro*, via the measurement of ^{14}N-^{1}H cross-relaxation phenomena [6]. We have also shown that FFC-MRI can detect changes in human cartilage induced by osteoarthritis [7]. Experiments on resected tissues from breast cancer patients have demonstrated significant differences in the dispersion curves between normal and diseased tissues [8]. We have performed *in vivo* studies on patients with acute ischaemic stroke; FFC-MRI images exhibited increased intensity in stroke-affected regions, with maximum contrast typically at the lowest field used (0.2 mT) [9]. We have also begun studies on patients with brain cancer and patients with breast cancer. All human studies were conducted following approval of the relevant Research Ethics Committees and with the informed consent of patients.

Other work has focused on speeding up the collection of FFC-MRI images by incorporating rapid MRI scanning methods along with the use of improved pulse sequences and algorithms [10, 11]. Work to improve the hardware and software is ongoing, including the implementation of improved radiofrequency coils [12].

Conclusions

Our work has shown that FFC-MRI has significant potential for the generation and use of novel biomarkers arising from ultra-low field MRI contrast and from low- and ultra-low field T_1-dispersion phenomena.

Acknowledgements

This project received funding from the European Union's Horizon 2020 research and innovation programme under grant agreement No 668119 (project "IDentIFY").

References

1. D.J. Lurie et al. *Comptes Rendus Physique* 11, 136-148 (2010).
2. R. Kimmich and E. Anoardo *Prog.Nucl.Magn.Reson.Spectrosc*. 44, 257-320 (2004).
3. D.J. Lurie, P.J. Ross and L.M. Broche, in: "Field-cycling NMR Relaxometry: Instrumentation, Model Theories and Applications"; New Developments in NMR No. 18, Kimmich R., ed., Royal Society of Chemistry, UK, pp 358-384 (2018).
4. D.J. Lurie et al. *Phys.Med.Biol*. 43, 1877-1886 (1998).
5. L.M. Broche et al. *Scientific Reports* 9:10402 (2019).
6. L.M. Broche et al. *Magn.Reson.Med*. 67, 1453-1457 (2012).
7. L.M. Broche, G.P. Ashcroft and D.J. Lurie *Magn.Reson.Med*. 68, 358-362 (2012).
8. E. Masiewicz et al. *Scientific Reports* 10:14207 (2020).
9. L.M. Broche et al. *11th Conference on FFC NMR Relaxometry, Pisa, Italy*, p6 (2019).
10. P.J. Ross, L.M. Broche and D.J. Lurie *Magn.Reson.Med*. 73, 1120-1124 (2015).
11. L.M. Broche, P.J. Ross, K.J. Pine and D.J. Lurie *J.Magn.Reson*. 238, 44-51 (2014).
12. G.R. Davies et al. *ISMRM 27th Annual Meeting, Montreal, Canada*, p1570 (2019).

Monoatomic spin systems as magnetic resonance probes for biomedical and engineering applications

Thomas Meersmann

Sir Peter Mansfield Imaging Centre, Division of Respiratory Medicine, School of Medicine, University of Nottingham, Nottingham, NG7 2RD, United Kingdom.
Department of Electrical and Electronic Engineering, University of Nottingham, Ningbo, PR China.

Introduction

Compared to magnetic resonance with molecules, monoatomic spin systems appear, at a first glance, to be fairly limited. Perhaps one of the most prominent and best known exception is the xenon isotope ^{129}Xe with its large chemical shift range that has been used extensively in the past decades for NMR spectroscopy as a probe for porous materials [1-3]. Furthermore, unlike molecules that experience fast spin-rotational relaxation, the gas phase relaxation of this monoatomic noble gas is fairly slow and thus allows for many applications of hyperpolarized ^{129}Xe for NMR spectroscopy and MR imaging including lung functional MRI [4, 5]. Xenon's tissue solubility, large chemical shift range, and interaction with specific sensor molecules allows for a variety of biomedical hyperpolarized ^{129}Xe application [6].

However, there are other monoatomic spin systems that deserve attention, most prominently $^{23}Na^{+}$ ions that that is native to many organisms and causes the second strongest (non-hyperpolarized) MRI signal that arises from the human body. It has a spin I = 3/2 and therefore has a nuclear electric quadrupole moment but, because of the high symmetry of monoatomic systems, its quadrupolar relaxation and quadrupolar coupling is limited, leading to relatively narrow spectral lines. Quadrupolar interactions are nevertheless present and can be exploited as a probe for the local molecular environment of the sodium ions [7].

Furthermore, the quadrupole moment of noble gas isotopes with nuclear with spin I > ½ can also be utilized as probes for their respective environments, such as the surrounding surfaces. The relaxation of quadrupolar noble gases is much faster than that of I = ½ noble gas isotopes but it is long enough to enable hyperpolarization and to utilize the hyperpolarized state for NMR and MRI applications [8].

Hyperpolarized (hp) ^{129}Xe (nuclear spin I = ½)

Using spin exchange optical pumping (SEOP), high levels of spin polarization, P, can be produced for ^{129}Xe that improves the gas phase MR signal by 4 – 5 orders of magnitude. The polarization typically produced is similar to what one would obtain at high fields and very low temperature (< 0.1 K) but this spin temperature is not in thermal equilibrium with the gas phase atoms, hence this non-equilibrium polarization is called hyperpolarization [9, 10]. This laser-based technology can produce hp ^{129}Xe as MRI contrast agent for the gas phase but also for dissolved phase and this has found utilization for pulmonary MRI.

Together with the University of Sheffield and Oxford University, Nottingham is currently employing pulmonary hp ^{129}Xe MRI in a first multi-centre study with this technology to observe the long-term effects of Covid-19. We are also interested in engineering applications and have utilized paramagnetic relaxation of hp ^{129}Xe for the study surfaces, in particular for chemical engineering and materials science applications. Generally, MRI of fluid flow can probe the structure-transport relationship [3], and we use hp ^{129}Xe to study gas transport and reactive zones in diesel catalysts that consist of materials with hierarchical pore structure. The combustion and high temperature resistance of the hyperpolarized spin state allows usage of these novel contrast agents for in situ MRI of chemical reactors. The accessibility of catalytic and paramagnetic centers can be probed through ^{129}Xe relaxation measurements provide insights into catalytic activity in these systems [11]. Furthermore, the chemical shift can be

utilized as a temperature sensor in time resolved measurements of catalytic start up reactions [12].

Thermally polarized $^{23}Na^{+}$ (nuclear spin I = 3/2)

The high nuclear spin S = 3/2 of ^{23}Na, and its nuclear electric quadrupole moment, make it possible to distinguish between free and bound sodium in magnetic resonance (MR) measurements arises from. A triple quantum (TQ) coherence can be induced through specific MR protocols if the ^{23}Na is in its bound state and therefore in a slow motional molecular environment. As it is not possible to generate TQ coherence in fast moving free sodium ions, it is possible to use this difference in signal to 'tag' specifically bound sodium as illustrated in Fig. 1.

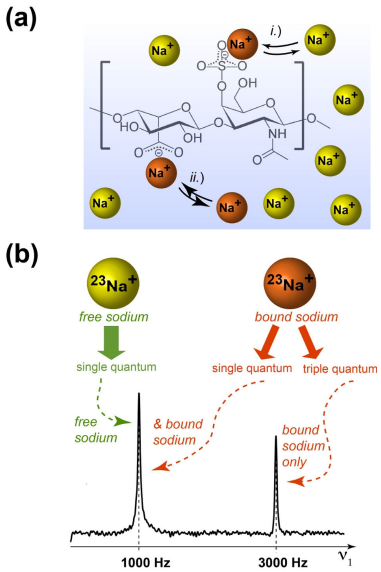

Figure 1. Concept of identification of bound-state sodium ions through triple quantum coherence filtered (TQF) ^{23}Na MRI and time proportional phase incrementation (TQ-TTPI) ^{23}Na MR Spectroscopy. (a) Possible interactions of sodium ions ($^{23}Na^{+}$) with electro-negative sites of a glycosaminoglycan (GAG), such as dermatan sulphate. Yellow indicates dissolved (i.e. free) sodium ions; Orange indicates $^{23}Na^{+}$ in a bound or temporary bound state with the macromolecule. (b) Analogous to clinical and pre-clinical ^{1}H MRI, ^{23}Na MRI generates and detects single quantum coherence. However, the physical property of the ^{23}Na nuclei also enables temporary generation of a triple quantum (TQ) coherence through specific MR protocols if the sodium is in a slow motional molecular environment. Both, TQ-TPPI spectroscopy (shown here) and TQF MRI utilize the different properties of SQ and TQ coherence for the differentiation between slowly moving bound sodium and rapidly moving free sodium ions.

Utilizing this concept, we have studied sodium storage in human skin and hypothesize the presence of a dynamic dermal 'Third Space Repository' for sodium within the dermis layer. The methodology was applied to explore how Type 2 Diabetes Mellitus (T2D) influences dermal sodium. Using a similar concept, we have previously shown that a modified double quantum filtered (DQF-MA) sequence, developed by Gil Navon and co-workers, allows for the probing of flow induced molecular alignment [13, 14].

Hyperpolarized ^{83}Kr (nuclear spin I = 9/2)

Our group has previously shown that quadrupolar T_1 relaxation of the hyperpolarized noble gas isotope ^{83}Kr allows for probing of surfaces that are in contact with the noble gas. We have shown that surface quadrupolar relaxation (SQUARE) T_1 maps of ^{83}Kr are indicative of an emphysema model in excised rodent lungs [15]. MRI at the very low resonance frequency ^{83}Kr (i.e. 11.5 MHz at 7 T) requires hyperpolarization through SEOP, similar in protocol to that used for the hp ^{129}Xe production. However, as a consequence of quadrupolar relaxation, hp ^{83}Kr cannot be concentrated from buffer gases of the laser pumping process through cryogenic separation or through membranes without depolarization. Therefore, a new production methodology was developed that uses molecular hydrogen as buffer gas during SEOP and its

subsequent removal through catalytic combustion [16]. We present novel, custom-made instrumentation that has been developed and constructed to make this approach feasible for clinical applications (Fig. 2).

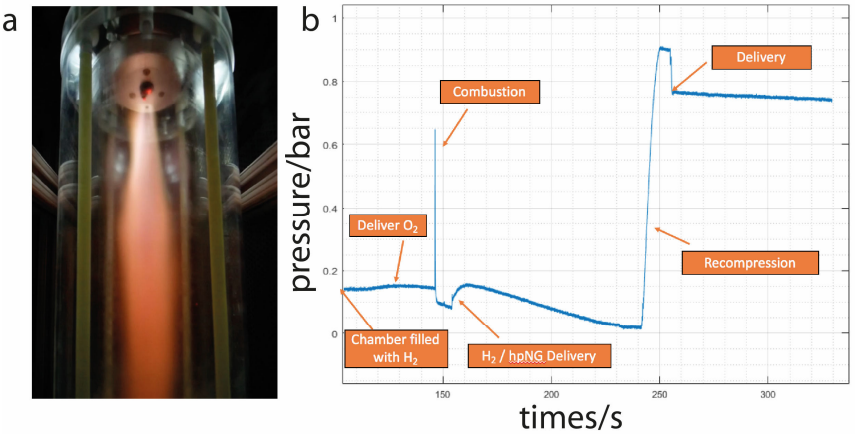

Figure 2. Combustion system to concentrate hyperpolarized noble gases. a) Combustion chamber with 4 L volume to remove H_2 through catalytically triggered combustion. The SEOP gas mixture only contains about 5% xenon or krypton for the laser pumping process and molecular hydrogen (95%) is used as buffer gas for the laser pumping process. b) Pressure curve of the purification process. Initially, the chamber is filled with pure hydrogen and O_2 is added to trigger the initial Knallgas reaction at about 150s. After this time the SEOP gas mixture is added to react the H_2 away (H_2O will condense out of the gas phase). After completed reaction, a pneumatically operated piston will pressurizer the remaining noble gas to for delivery to a breathing apparatus.

References

1. T. Ito, and J. Fraissard, J Chem Phys **76** (1982).
2. M. A. Springuel-Huet *et al*., Magnetic Resonance in Chemistry **37** (1999).
3. K. Bartik *et al*., Actualite Chimique (2005).
4. N. J. Stewart *et al.*, Magn Reson Med **74** (2015).
5. J. C. Woods *et al.*, J Magn Reson Imaging **52** (2020).
6. D. M. L. Lilburn, G. E. Pavlovskaya, and T. Meersmann, J Magn Reson **229** (2013).
7. G. Jaccard, S. Wimperis, and G. Bodenhausen, J Chem Phys **85** (1986).
8. G. E. Pavlovskaya *et al.*, P Natl Acad Sci USA **102** (2005).
9. D. Raftery *et al*., Phys Rev Lett **66** (1991).
10. J. W. Plummer *et al*., J Magn Reson **320** (2020).
11. D. B. Burueva *et al*., ACS Catal. **10** (2020).
12. F. Hill-Casey et al., Chemical Engineering Journal **405** (2021).
13. U. Eliav, H. Shinar, and G. Navon, J Magn Reson **98** (1992).
14. G. E. Pavlovskaya, and T. Meersmann, J Phys Chem Lett **5** (2014).
15. D. M. L. Lilburn *et al*., J R Soc Interface **12** (2015).
16. N. J. Rogers *et al*., P Natl Acad Sci USA **113** (2016).

Tracing the "invisible" Polarons in Ferromagnetic Manganites. A combined NMR and HRTEM study in the temperature range 3.2–1000 K

Georgios Papavassiliou[1], Nikolaos Panopoulos[1], Michael Fardis[1], Jamal Hassan[2], Saeed Alhassan[2], Hae Jin Kim[3]

[1]Institute of Nanoscience and Nanotechnology, NCSR Demokritos, 15310 Aghia Paraskevi, Attiki, Greece
[2]Khalifa University of Science and Technology, Abu Dhabi, United Arabic Emirates
[3]Korea Basic Science Institute,350-333, Daejeon, Republic of Korea
E-mail: g.papavassiliou@inn.demokritos.gr

The remarkable electronic properties of Colossal Magnetoresistive Manganites are widely believed to be caused by the competition between a ferromagnetic metallic state and an antiferromagnetic insulating state with complex spin, charge, and orbital ordering. However, the physics underlying their magnetotransport properties is still not clear, especially the role of correlated Jahn-Teller polarons, which depending on temperature and doping, might form a liquid, glass or stripe polaron state [1]. This question touches one of the most fundamental problems in the physics of doped Mott insulators, i.e. understanding the mechanism that chemical doping makes an insulator becoming superconductive as in the case of cuprates, or exhibiting the Colossal Magnetoresistance, as in the case of manganites. Here, by using ^{139}La NMR and high resolution transmission electron microscopy in the temperature range 3.2 K to 1000 K, we have monitored the formation and evolution of zig-zaged polarons (CE-type) in optimally doped $La_{0.67}Ca_{0.33}MnO_3$ [2]. While NMR experiments show that correlated polarons dominate electron spin dynamics in the ferromagnetic phase, at very low temperatures they appear to form a quantum liquid-crystal ferromagnetic phase, embedded into a ferromagnetic matrix with 3D polaron correlations [2]. This is evidence that similarly to high Tc cuprates, quantum soft phases underlie the exotic physical properties of Colossal Magnetoresistive Manganites.

References

1. D. Koumoulis, N. Panopoulos, A. Reyes, M. Fardis, M. Pissas, A. Douvalis, T. Bakas, D. Argyriou and G. Papavassiliou – *Phys. Rev. Letters **104**, 077204 (2010).*
2. N. Panopoulos, M. Pissas, H. J. Kim, Jin-Gyu Kim, S. J. Yoo, J. Hassan, Y. AlWahed, S. Alhassan, M. Fardis, N. Boukos, G. Papavassiliou – *npj Quantum Materials Nature **3***, 20 (2018).

Multinuclear MRI investigations

Yuri A. Pirogov

Faculty of Physics, Lomonosov Moscow State University, 119991, Moscow, Russia
E-mail: yupi937@gmail.com

New approaches to MRI on heavier than proton nuclei are considered. The aim of using heavy nuclei visualization is to find proton-less tissues and farm-preparations inside of organism in vivo. First of all, it is important to know where fluorine contenting preparations – blood substitute Perftoran®, contrasting gases in MRI pulmonology, etc., are localized. An analogical problem has place in discovering ^{23}Na, ^{13}C, ^{31}P, ^{2}H and other nuclei in content of tissues and preparations, especially ^{23}Na ones which influence onto blood tension level, kidney diseases, initiation of diabetes. It is interesting a production of hyperpolarized state of nuclei ^{129}Xe, ^{36}Kr, ^{3}He, ^{13}C, ^{29}Si allowing to enhance MRI signals until 4-5 orders and provide high contrasting MRI images.

Research has been supported by RFBR grants No.19-29-10015, 20-52-10004 and Interdisciplinary Scientific and Educational School of Moscow University "Photonic and Quantum Technologies. Digital Medicine".

NMR diffusion measurements and time-dependent samples

William S. Price

Nanoscale Organisation and Dynamics Group, Western Sydney University, Penrith, NSW, Australia
E-mail: w.price@westernsydney.edu.au
https://westernsydney.edu.au/nanoscale

In the last few decades NMR diffusometry (also known as Pulsed Gradient Spin-echo NMR, PGSE NMR, Diffusion Ordered Spectroscopy or DOSY) has gone from being a niche area to a mainstream NMR technique as well as being incorporated into MRI [1-4]. Amongst the NMR measurable quantities, translational diffusion is special as it confers enormous benefits – it allows molecular size and motion to be detected – very important for studying chemical reactions and probing the structure of solutions and materials (e.g., [5]). This increase in usage has also been accompanied by enormous technical and theoretical advances which make NMR a "sharper tool".

NMR diffusion measurements are typically performed by measuring the spin echo attenuation for ~15 different values of the diffusion sensing gradients (g). And, given the recycle delay and the number of scans (NS) used at each gradient value, a diffusion measurement typically takes from minutes to hours. In such measurements it is normally assumed that the concentration of the various species is time independent. Thus, in addition to increasing throughput, increasing the speed of NMR diffusion measurements extends the practical lower limit of detection that can be used as well as increasing the feasibility of applying the technique to the study of reacting systems [6-8].

In reality, many samples change with time due to various types of reactions (e.g., exchange, polymerisation). To properly interpret the NMR diffusion data from such systems requires improvements in theory (e.g., the Kärger equations [9]) and/or shorter measuring times. Numerous methods for increasing the measurement efficiency of NMR diffusion measurements have been proposed but most have significant limitations such as loss of chemical shift information or no longer having a defined diffusion measurement timescale Δ.

We have shown that measurement efficiency can be increased by running the experiment in a **steady state mode** [10, 11]. We have also explored a seemingly unutilised approach in which NS is varied through the array of g values in the measurement and the signal is normalised by the value of NS used at each iteration [12]. In contrast to conventionally performed measurements where the same NS is used at each iteration, this new **normalisation approach** requires far fewer total scans. Both the steady state and normalisation approaches can shorten the experimental time by more than 70% without any loss in accuracy and, unlike previous approaches, are totally general in their application. Systems that change rapidly can also be probed using **time resolved diffusion NMR measurements** [6-8]. We discuss and illustrate these three approaches in this presentation.

References

1. J. Kärger, H. Pfeifer, W. Heink. Principles and Applications of Self-Diffusion Measurements by Nuclear Magnetic Resonance. *Adv. Magn. Reson.,* **12,** 1-89 (1988).
2. W.S. Price, NMR Studies of Translational Motion: Principles and Applications 1st ed., Cambridge University Press, Cambridge, 2009.
3. P.T. Callaghan, Translational Dynamics & Magnetic Resonance 1st ed., Oxford University Press, Oxford, 2011.
4. A. Gupta, T. Stait-Gardner, W.S. Price. NMR Imaging and Diffusion. *Adsorption,* (2021) In press.

5. S.S. Bystrov, V.V. Matveev, A.V. Egorov, Y.S. Chernyshev, V.A. Konovalov, V. Balevičius, V.I. Chizhik. Translational Diffusion in a Set of Imidazolium-Based Ionic Liquids $[Bmim]^{+}A^{-}$ and Their Mixtures with Water. *J. Phys. Chem. B,* **123,** 9187-9197 (2019).
6. M. Urbańczyk, D. Bernin, A. Czuroń, K. Kazimierczuk. Monitoring Polydispersity by NMR Diffusometry with Tailored Norm Regularisation and Moving-Frame Processing. *Analyst,* **141,** 1745-1752 (2016).
7. T.S.C. MacDonald, W.S. Price, J.E. Beves. Time-Resolved Diffusion NMR Measurements for Transient Processes. *ChemPhysChem,* **20,** 926-930 (2019).
8. T.S.C. MacDonald, B.L. Feringa, W.S. Price, S.J. Wezenberg, J.E. Beves. Controlled Diffusion of Photoswitchable Receptors by Binding Anti-Electrostatic Hydrogen-Bonded Phosphate Oligomers. *J. Am. Chem. Soc.,* **142,** 20014-20020 (2020).
9. D. Wijesekera, T. Stait-Gardner, A. Gupta, J. Chen, G. Zheng, A.M. Torres, W.S. Price. A Complete Derivation of the Kärger Equations for Analyzing NMR Diffusion Measurements of Exchanging Systems. *Concepts Magn. Reson. A,* **47,** e21468 (2019).
10. T. Stait-Gardner, P.G. Anil Kumar, W.S. Price. Steady State Effects in PGSE NMR Diffusion Experiments. *Chem.Phys.Lett.,* **462,** 331-336 (2008).
11. M. Zubkov, T. Stait-Gardner, W.S. Price, P. Stilbs. Steady State Effects in a Two-Pulse Diffusion-Weighted Sequence. *J. Chem. Phys.,* **142,** 154201 (2015).
12. R. Masuda, A. Gupta, T. Stait-Gardner, G. Zheng, A.M. Torres, W.S. Price. Shortening NMR Experimental Times. *Magn. Reson. Chem.,* **56,** 847-851 (2018).

On the importance of the paradigm in the development of science

K. M. Salikhov

Zavoisky Physical-Technical Institute of the Federal Research Center «Kazan Scientific Center of the Russian Academy of Sciences»
Kazan, 420029, Sibirsky trakt, 10/7

A paradigm is a model that has been adopted by the scientific community for solving problems of fundamental and applied problems.

There are paradigms on a universal scale, like the standard big bang model.

There are paradigms in different sections, in certain areas of science. The paradigm offers a model that adequately reflects all the achievements of science at the moment. The scientific paradigm is not something given once and for all. Achievements appear that do not fit into the accepted paradigm. As such achievements accumulate, scientists revise the accepted paradigm, formulate a new paradigm. The development of science is an endless series of changing paradigms. We all know many examples of paradigm shifts. Paradigm shifts of universal significance are seen as scientific revolutions.

The paradigm helps the scientist to organize his work in such a way as to more purposefully storm the fortress of knowledge. The paradigm makes it possible to reveal truly qualitatively new knowledge. If the paradigm is not formulated, that is, the existing knowledge is not reduced to a clear model, then it is very difficult to decide whether a new observation is fundamentally new knowledge. Or is it just the replication of already known knowledge, an increase in the database, which in itself is also a very necessary thing.

In my report, I plan to share my experience of changing the scientific paradigm in one specific discipline: spin exchange and its manifestations in EPR spectroscopy.

It turned out like this. Two years ago, at the request of Springer, I began to prepare a new edition of a book on spin exchange. The first edition was published by Nauka in 1977 and published by Springer in 1980. That book was written jointly with Yury N. Molin and Kirill I. Zamaraev. I wrote the theory section of that book.

I started writing a new book. I raised all my work in this area and appreciated with a fresh eye what I had done. After reviewing everything that had been done in spin exchange and rethinking my theories, I suddenly realized that the totality of the new exceeded the critical mass. The generally accepted spin exchange paradigm is bursting at the seams and hindering the development of science.

As a result, it became obvious that there was a need to formulate a new spin exchange paradigm. Which I did. So in 2019 the book [1] was published.

From the new paradigm, the following moments can be singled out [1-4]:

1. I wrote down a new kinetic equation to describe the motion of the magnetization of electron spins, taking into account the spin exchange of paramagnetic particles in the course of bimolecular collisions and dipole-dipole spin-spin interaction.

2. Due to the transfer of spin coherence, collective modes of spin motion are formed in dilute solutions of paramagnetic particles.

3. Each resonant line of the collective mode has a mixed shape, is the sum of the absorption and dispersion lines.

4. Within the framework of a new paradigm, I predicted the existence of a new quasiparticle, which I called a spin polariton.

Working on a new paradigm opened up new degrees of freedom for me, broadened my horizons and gave a great impetus to my scientific research. I realized that the paradigm is practically an important tool for scientific knowledge and its effective development.

The paradigm serves as a basis for planning research, a tool for assessing the value of the result obtained in the course of research.

The paradigm accelerates the progress of scientific research. I have changed my personal paradigm for organizing my work. I have already shared with some of my colleagues and began to look closely at some other areas of science in which I plan to use the experience gained in formulating the paradigm.

Moreover, I am convinced that such work should be carried out in other fields of science, if we want to conduct our scientific work more effectively. If any of you are interested in this prospect, I will be very happy to interact with you.

References

1. M. Salikhov. Fundamentals of spin exchange. Story of a paradigm shift. Springer (2019).
2. K.M. Salikhov. State of the theory of spin exchange in dilute solution of paramagnetic particles. New paradigm of spin exchange and its manifestations in EPR spectroscopy. UFN, **189**, 1017-1043 (2019).
3. K.M. Salikhov. Interpretation of the Nature of the Mixed Form of Resonance Lines of the EPR Spectrum in a New Paradigm of Spin Exchange. Abnormal “Resonance” of Non-Resonant Spins. J. Phys. Chem. *B* , **124**, 30, 6628-6641 (2020).
4. K.M. Salikhov. New paradigm of spin exchange and its manifestations in EPR spectroscopy. Applied Magnetic Resonance, **51**, 297-325 (2020).

Spin manipulation of stable organic radicals by advanced pulse-ESR spectroscopy

Kazunobu Sato

Graduate School of Science, Osaka City University, Osaka 558-8585, Japan
E-mail: sato@sci.osaka-cu.ac.jp
https://qcqis.sci.osaka-cu.ac.jp/ms/

Molecular spin quantum control is one of the challenging issues for realizing quantum computing and quantum information processing. Pulsed NMR techniques have been applied to molecules to implement elementary quantum algorithms, demonstrating the usefulness of pulsed magnetic resonance techniques as quantum spin technology. We have applied pulsed ESR techniques to molecular spin systems to manipulate electron spin qubits in molecules [1-4]. A pulsed ESR spectrometer with an arbitrary waveform generator (AWG) has been introduced to sophisticated ESR measurements, expanding research fields in spin science and technology. We have implemented electron spin technology with AWG for the precise manipulation of molecular spins. Microwave pulses generated by AWG have been utilized for electron-spin excitation in molecular spin systems. In this paper, we describe the AWG-based spin technology which enables us to manipulate molecular spins. The AWG technology has been applied to typical spin systems for demonstrating the spin excitation underlying quantum control. We also show a GRAPE (GRadient Ascent Pulse Engineering) approach which is promising for global control of spins in molecular spin systems. The GRAPE technology has been proposed by Khaneja and coworkers in NMR spectroscopy in order to perform optimal control of coupled nuclear spins [5]. We have applied the AWG-based pulsed ESR technology with GRAPE pulses to stable molecular spin systems for precise quantum manipulation of electron spins [4].

Two typical *g*-engineered synthetic biradicals shown in Figure 1, which consist of trityl and nitroxide radicals, have been considered by the topological symmetry argument. Their magnetic properties were fully identified by multi-frequency ESR spectroscopy, illustrating that these biradicals serve as testing grounds for development in quantum spin manipulation techniques for magnetic electron resonance spectroscopy, which are based on novel AWG pulse microwave technology.

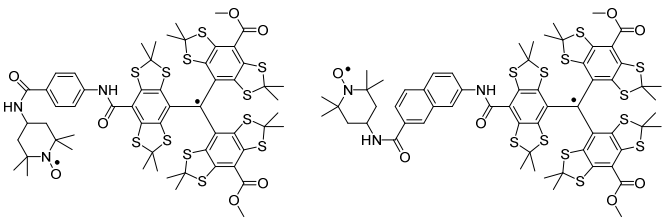

Figure 1. Weakly exchange-coupled organic biradicals

Pulsed ESR experiments using the arbitrary waveform pulses have been performed by using a customized pulse X-band ESR spectrometer based on Bruker ESP380E equipped with AWG's. The arbitrary waveform pulses were numerically optimized, attempting to make an enhancement of the signal intensities from the NO site. We have observed FT-ESR spectra of the biradicals by applying the arbitrary waveform pulses. In the observed FT-ESR spectra of the biradicals, the NO transitions due to the sublevels of $|M_I = +1\rangle$ and $|M_I = 0\rangle$ were relatively enhanced by the arbitrary waveform pulses rather than that of the conventional FT-ESR spectra.

The pulse AWG-ESR experiments show that the arbitrary waveform technology like the GRAPE MW pulses is capable of making spin manipulations based on the selective excitations.

Acknowledgements

This work was supported by JSPS and RFBR under the Japan–Russia Research Cooperative Program, JSPS KAKENHI Grant Numbers. JP17H03012 and JP19H05621. This work was also supported by the AOARD Scientific Project on "Molecular Spins for Quantum Technologies" (FA2386-17-1-4040, 4041), U.S.

References

1. K. Sato, Y. Morita, T. Takui et al, *J. Mater. Chem.* **2009**, *19*, 3739–3754.
2. S. Nakazawa, K. Sato, Y. Morita, T. Takui et al. *Angew. Chem. Int. Ed.* **2012**, *51*, 9860-9864.
3. S. Yamamoto, K. Sato, T. Takui et al. *Phys. Chem. Chem. Phys.* **2015**, *17*, 2742-2749.
4. K. Sato, E. Bagryanskaya, T. Takui et al. *J. Phys. Chem. A* **2019**, *123*, 7507–7517.
5. N. Khaneja, T. Reiss, C. Kehket et al. *J. Magn. Reson.* **2005**, *172*, 296-305.

Frequency selection of molecular translation dynamics with different NMR MGSE sequences

Janez Stepišnik

University of Ljubljana, Slovenia

The NMR modulated gradient spin echo (MGSE) method allows insight into molecular motion by measuring directly not only the molecular self-diffusion coefficient but also the low frequency part of the velocity autocorrelation function, which contains important details about the molecular translation dynamics. The MGSE sequence creates the spectrum of spatial spin phase discord with a single dominant peak that allows to pick up the value of the spectrum of correlation at the modulation frequency as demonstrated by numerous measurements in liquids. The MGSE method can uses also the inhomogeneous magnetic fields generated in porous media due to differences in magnetic susceptibility at solid/liquid interfaces and due to intrinsic or artificially doped magnetic impurities to gain insight into the molecular dynamics in the structure of a porous medium. In this paper, we will analyze spin phase modulations with different gradients spin echo sequences, for the best frequency selection of molecular translation dynamics.

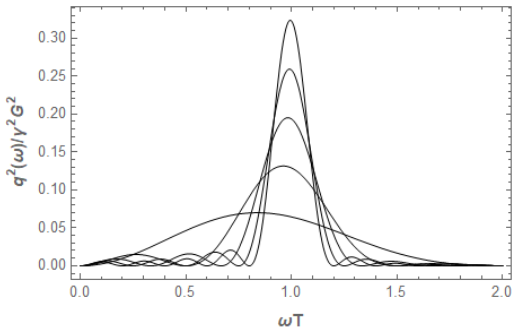

Figure 1. Spectral selection with the CPMG RF sequence in a fixed magnetic field gradient

Self-assembly of small molecules by H-bonds: how to distinguish dimers, trimers, tetramers by NMR

Peter M. Tolstoy[1], Valeriia V. Mulloyarova[1], Ivan S. Giba[2], Alexandra M. Puzyk[1]

[1]Institute of Chemistry, St. Petersburg State University
[2]Department of Physics, St. Peterburg State University
E-mail: peter.tolstoy@spbu.ru
http://en-chem.spbu.ru/index.php/research/research-groups/30-research/research-groups/184-research-group-of-associate-professor-tolstoy-p

Introduction

It is a common knowledge that RCOOH acids prefer to form cyclic dimers. In contrast, R_2POOH acids have a tendency to trimerize. The aggregation numbers for R_2AsOOH acids are mostly unknown. What causes this difference? Why some acids form only dimers, while others form trimers and even tetramers? Is it possible to determine stoichiometry using liquid-state NMR spectroscopy?

Main objects

The main molecular objects selected for this study are shown schematically in Figure 1. All of these molecules (-COOH, -AsOOH and -POOH acids) have both proton donating and proton accepting functionalities, thus being able to self-associate by forming multiple hydrogen bonds.

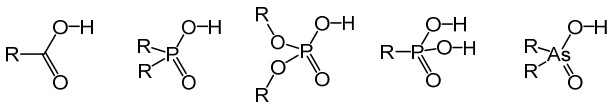

Figure 1. –XOOH (X = C, P, As) acids, studied in this work

Methodology

The observation of intrinsic (not averaged) NMR parameters of intermolecular complexes requires the proton and molecular exchanges to be slow in the NMR time scale. We have achieved the necessary increase of the complex's life time in solution by using the mixture of liquefied freonic gases CDF_3/CDF_2Cl as a solvent, which allowed us to lower the temperature of the sample down to 100 K. Such solvent exhibits relatively good solubility of organic compounds and remain non-viscous practically down to its freezing temperature.

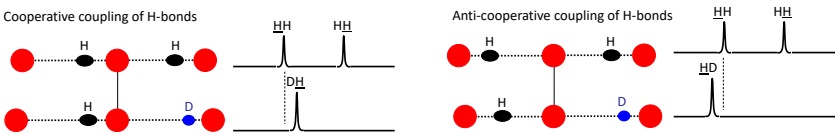

Figure 2. Cooperative and anti-cooperative couplings of H-bonds

Another important stratagem used for this investigation is the usage of partial H/D substitution in mobile proton sites. When the bridging proton is substituted by a deuteron, the bond lengthens, *i.e.* the heavy atom distance increases. For complexes with several mutually coupled hydrogen bonds this means that the neighboring (not deuterated) hydrogen bonds changes as well, which is observed as a change in corresponding ^1H NMR chemical shifts, the phenomenon which is called "vicinal H/D isotope effects". The two coupling schemes – cooperative or anti-cooperative coupling – manifest themselves by opposite signs of vicinal isotope effects, thus allowing one to elucidate the coupling scheme within a complex (Figure 2).

In turn, the number of vicinal H/D isotope effects allows one to count the number of interacting hydrogen bonds within the complex.

Example of the results

We demonstrate that in a polar aprotic medium, in contrast to the case of carboxylic acids (RCOOH), the rings of hydrogen bonds in cyclic self-associates of arsinic (R_2AsOOH), phosphinic (R_2POOH), phosphoric ($(RO)_2POOH$) and phosphonic ($RP(O)(OH)_2$) acids are non-planar. Cyclic trimers, tetramers and even cage-like structures are being formed, if the molecular geometry fits just right. As an example, in Figure 3 we showcase the 3D-tetramerization of a phosphonic acid.

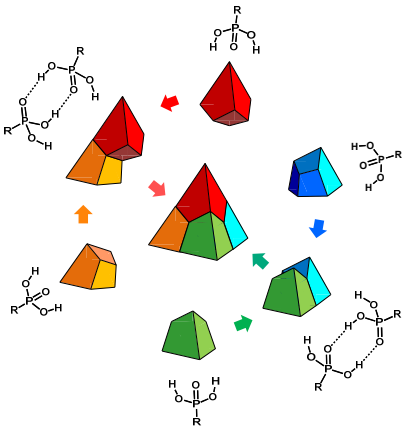

Figure 3. Cage-like tetramerization of phosphonic acids

Acknowledgements

This presentation is based on several publications prepared within the framework of the grants RSF 18-13-00050 and RFBR 19-33-90047.

References

1. V. Mulloyarova, I. Giba, M. Kostin, G. Denisov, I. Shenderovich, P. Tolstoy, *Phys. Chem. Chem. Phys.* **2018**, *20*, 4901.
2. V. Mulloyarova, I. Giba, G. Denisov, P. Tolstoy, *J. Phys. Chem A* **2019**, *123*, 6761.
3. V. Mulloyarova, D. Ustimchuk, A. Filarowski, P. Tolstoy, *Molecules* **2020**, *25*, 1907.
4. I. Giba, P. Tolstoy, *Symmetry* **2021**, *13*, 258.
5. V. Mulloyarova, A. Puzyk, A. Efimova, A. Antonov, R. Evarestov, I. Aliyarova, R. Asfin, P. Tolstoy, *J. Mol. Struct.* **2021**, *accepted*.

Atomic hydrogen in solid molecular crystals. Magnetic resonance and quantum diffusion

S. Vasiliev[1], S. Sheludiakov[2], J. Järvinen[1], J. Ahokas[1], D. M. Lee[2] and V. V. Khmelenko[2]

[1]Department of Physics and Astronomy, University of Turku, 20014, Turku, Finland,
[2]Department of Physics and Astronomy, Texas A&M University, College Station, TX, 77843, USA
E-mail: servas@utu.fi

Solid hydrogen isotopes represent a special class of so-called quantum crystals which are characterized by a weak intermolecular interactions and a large zero-point energy. These properties are most pronounced in the crystals with the lowest meting point: He, H_2, Ne, Ar, Kr. In chemistry, these crystals serve as a matrix for isolation of free radicals, which otherwise rapidly recombine being in a gas phase or liquid. Magnetic resonance studies of the radicals in molecular matrices formed a rich field of experimental research in physical chemistry. This research is pursued in our laboratory for nearly two decades, and I shall present a short review of the most interesting results.

Although, the goal of the matrix isolation is to isolate the radicals from each other and prevent recombination, for the lightest radicals: hydrogen and deuterium atoms, pronounced quantum effects occur at low temperatures. Hydrogen and deuterium atoms become delocalized in the lattice and diffuse in a series of exchange tunneling reactions: $H+H_2=H_2+H$ and $D+D_2=D_2+D$ [1]. Similar exchange reactions $D+H_2=HD+H$ and $D+HD=D_2+H$, involving both hydrogen isotopes may take place in D_2:H_2 (HD) mixtures and result in a spectacular conversion of atomic deuterium into hydrogen atoms, while T-to-H conversion can be expected in T_2-H_2 mixtures [2]. Impurity atoms are not stable and recombine into molecules if encounter each other in neighboring lattice sites.

The isotopic exchange reactions were studied in a temperature range 0.1-1.5K which appear to be the lowest temperature where chemical reactions have been observed in a solid phase so far. We measured the reaction rate of $D+HD=D_2+H$ in HD and D_2:0.23% HD matrices and found, that the rate of the reaction is nearly independent of temperature within this range [1]. Our results suggest that atoms remain mobile in the temperature range, even though both H and D recombination is strongly inhibited at temperatures below 1K.

We observed that Dynamic Nuclear Polarization (DNP) of H atoms in D_2:H_2 (HD) mixtures can be created by both the Overhauser and Solid effects efficiently. In addition to that, nuclear spins of hydrogen atoms can be polarized by saturating the center of the ESR spectrum resembling Overhauser effect in metals, the effect which is absent for H atoms in pure H_2 samples [3]. We suggested that a large number of H radical pairs formed during the course of the isotopic exchange reactions, coupled by strong exchange interaction. The radical pairs may possess an allowed transition at the center of the ESR spectrum while D atoms help to create a strong enough oscillating field at the position of ESR pumping.

In our recent study [4], we measured the rate of quantum diffusion of H atoms in solid H_2 crystals which turned out to be two orders of magnitude larger than the diffusion of atoms towards each other when they approach close enough to recombine back to molecules. In the latter case, interaction between atoms create energy levels mismatch in the neighboring lattice cites, and extra energy is required for hopping of the atoms.

References

1. S. Sheludiakov et al., Phys. Chem. Chem. Phys., 18, 29600 (2016).
2. S. Sheludiakov et al., Phys. Chem. Chem. Phys., 19, 2834 (2017).
3. S. Sheludiakov et al., Phys.Rev.Lett., 113, 265303 (2014).
4. S. Sheludiakov et al., accepted to Phys. Rev. Lett. (2021).

Electrophoretic NMR assembly

Extending the capability of conventional NMR instruments

P&L Scientific

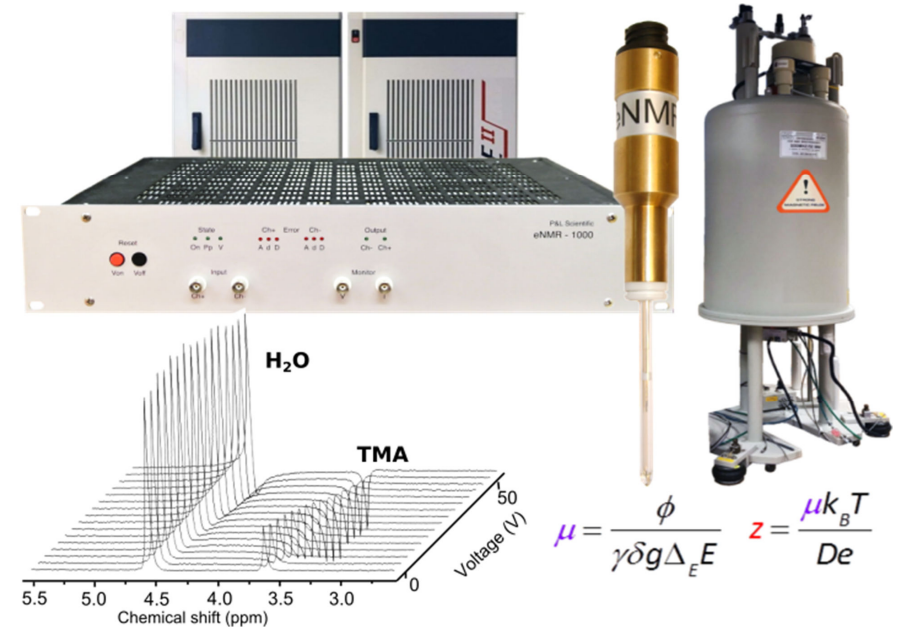

The electrophoretic mobility and the effective charge can be obtained by recording the variation of spectral phase by increasing electric field

Key features

- Well-established scientific background and proven technology
- Operates as add-on for any conventional NMR spectrometer and probe with gradient; requires no additional hardware or software
- Advanced sample cell and RF filter system
- Straightforward embedding of high voltage pulse generation in conventional NMR pulse programs
- Probe and user protection system

info@plscientific.se

Specifications

Output voltage:	0 to ±1000 V
Digital To Analogue converter size:	2×12 bit
Output current	
at ±1000 V:	0 to ±100 mA
at ±500 V:	0 to ±200 mA
Output power:	
Peak power	300 W
Mean power	30 W
Minimum/maximum pulse length:	500 µs / 1 s
Duty cycle:	30 %
Output pulse shapes:	Rectangular
Slew rate:	Greater then 25 V / µs
Settling time (to 2%):	Less than 200 µs for 2 kV step
Stability	
Drift with time	Less than 200 ppm/hr, noncumulative
Drift with temperature	Less than 300 ppm/°C
RF Filters	10 MHz low pass
Power consumption:	80 W for 220 V AC
Dimensions of the main unit:	430×340×90 (fits in standard 19'' rack); weight - 8 kg

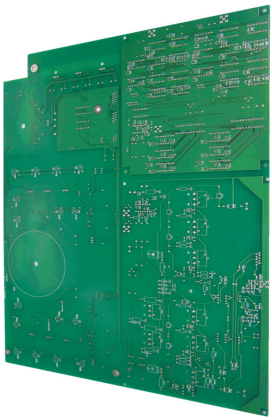

Selected applications

Physical chemistry – ion pairing and association in simple and complex (polyelectrolytes) ionic mixtures.

Batteries and fuel cells - chemically selective measurement of ionic migration.

Biochemistry – biomolecular charge and association.

Analytical chemistry – electrophoretic analysis of complex ionic mixtures

Pharmaceutical chemistry – release and association of charged drugs

Metallorganic chemistry – the structure of supramolecular complexes from the observed charge

info@plscientific.se

2D electrophoretic mobility spectroscopy (2D MOSY) based on eNMR

Extending the power of 2D NMR spectroscopy

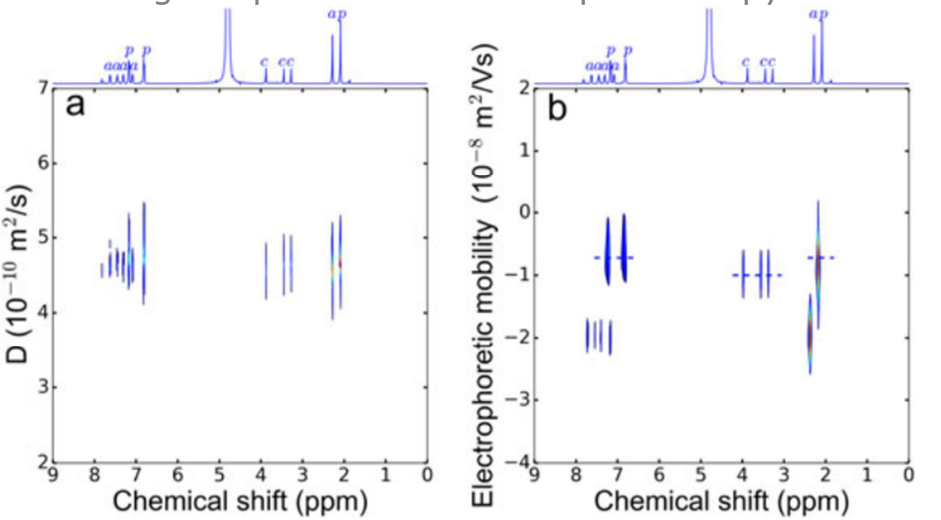

Direct comparison of 2D DOSY (a) and 2D MOSY (b) experiments for a dissolved Thomapyrin® tablet clearly illustrates the superior performance of the 2D MOSY in selection of the different species

Selected articles for eNMR applications

Y. Fang, P. V. Yushmanov, and I. Furó, Assessing 2D electrophoretic mobility spectroscopy (2D MOSY) for analytical applications, Magn. Reson. Chem. 55 DOI: 10.1002/mrc.4558 (2017).

E. Bialik, B. Stenqvist, Y. Fang, Å. Östlund, I. Furó, B. Lindman, M. Lund, and D. Bernin, Ionization of cellobiose in aqueous alkali and the mechanism of cellulose dissolution, J. Phys. Chem. Lett. 7 5044-5048 (2016).

M. Giesecke, F. Hallberg, Y. Fang, P. Stilbs, and I. Furó, Binding of monovalent and multivalent metal cations to polyethylene oxide in methanol probed by electrophoretic and diffusion NMR, J. Phys. Chem. B 120 10358−10366 (2016).

M. Bielejewski, M. Giesecke and I. Furó, On electrophoretic NMR. Exploring high conductivity samples, J. Magn. Reson. 243 17-24 (2014).

L. Patel, O. Mansour, M. Crossman, P. Griffiths, Electrophoretic NMR characterization of charged side chain cationic polyelectrolytes and their interaction with the anionic surfactant, sodium dodecyl sulfate, Langmuir 2019, 35, 28, 9233-9238

 info@plscientific.se

Our NMR services

Repair and modification of the NMR spectrometers and hardware components

- RF amplifiers
- Gradient units
- Synthesizer and SGU 400 - 1000 boards
- Power supplies and shim system
- Temperature and MAS controllers

Repair of the NMR probes:

- Solving arcing problems; bad sensitivity and RF tuning/matching
- Replacing broken glass and ceramics in the probe body
- Repairing certain gradient coils in diffusion and high-resolution probes
- Repair of MAS probes; arcing and spinning problem
- Repair of probe accessories for temperature control

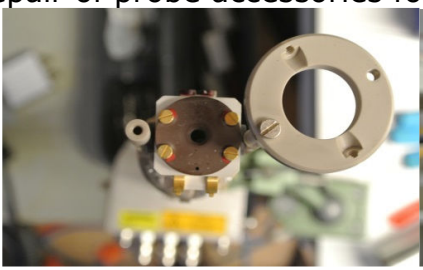

Modification of the NMR probes

- Adaptation of an existing NMR probe to a different spectrometer or NMR frequency.
- Change of RF coil position and configuration
- Adaptation of temperature control components and connectors
- Change of body geometry, dimensions and mounting
- Modification NMR inserts used in several diffusion NMR probes (like Bruker Diff30) to different frequency or double-tuned configuration

info@plscientific.se

Oral Reports

Nanostructures research using nuclear magnetic resonance of helium-3

E. M. Alakshin[1], G. A. Dolgorukov[1], A. V. Klochkov[1], E. I. Kondratyeva[1], V. V. Kuzmin[1], K. R. Safiullin[1,2], A. A. Stanislavovas[1], M. S. Tagirov[1,2]

[1]Kazan Federal University, 420008, Kazan, Russian Federation,
[2]Tatarstan Academy of Sciences, 420111, Kazan, Russian Federation
E-mail: alakshin@gmail.com

The study of the spin kinetics of helium-3 in contact with nanostructures will be presented. Three different groups of nanostructures such as trifluoride nanoparticles (LaF_3, PrF_3, DyF_3), aerogels (oriented Al_2O_3) and detonated nanodiamonds were studied.

Nanoparticles

The spin kinetics data of ^{3}He in contact with varios trifluoride nanosized powders will be presented. Results for LaF_3 nanopowder demonstrated that the nuclear magnetic relaxation of the adsorbed ^{3}He occurs due to the modulation of dipole-dipole interaction by the quantum motion in the adsorbed two-dimensional film. The analysis of obtained data for PrF_3 nanoparticles testifies in favor of cross-relaxation presence in the nuclear spin–lattice relaxation data, which takes place between ^{3}He and ^{141}Pr nuclei. The magnetic phase transition in DyF_3 is accompanied by a considerable change in the character of fluctuations of the magnetic moments of Dy^{3+} ions, which affect the spin kinetics of ^{3}He in contact with the substrate. Significant changes in the relaxations rates of the longitudinal and transverse magnetizations of liquid ^{3}He have been discovered in the region of magnetic ordering of the solid matrix.

Aerogels

Our group systematically studied the nuclear magnetic relaxation of ^{3}He in contact with aerogels. The determining role of the adsorbed layer in relaxation processes of gaseous and liquid ^{3}He was confrmed. It is known that aerogel acts as an impurity and affects phases of superfluid ^{3}He. Nowadays, it is of interest to study superfluid ^{3}He in contact with anisotropic aerogels (group of prof. Dmitriev V. V., Moscow). An additional mechanism of the ^{3}He relaxation in aerogels is found and it is shown that this relaxation mechanism is not associated with the adsorbed layer. A hypothesis about the influence of intrinsic paramagnetic centers on the relaxation of gaseous ^{3}He is proposed.

Nanodimonds

In recent years nanodiamonds have become a widely investigated material for quantum engineering, biological and electronic applications. The spin-lattice (T_1) and spin-spin (T_2) relaxation times of ^{3}He were measured in adsorbed, gas and liquid phases in a detonation nanodiamond sample. The observed T_1 and T_2 are much shorter in comparison with ^{3}He in similar experiments for samples with restricted geometry, thus we assume a strong impact of paramagnetic centers on nuclear magnetic relaxation. Experiments with nanodiamond surface preplated with N_2 or ^{4}He layers will be presented. The model of ^{3}He relaxation in contact with detonation nanodiamonds that describes our experimental results will be proposed.

This work was supported by the Russian Science Foundation (project no. 19-72-10061).

Deviant behaviour of magnetization of microsized powder of Ising dipolar antiferromagnet $LiDyF_4$ at temperatures $T > T_N$

G. Iu. Andreev[1], M. A. Cherosov[1], A. G. Kiiamov[1], S. L. Korableva[1], I. V. Romanova[1], A. S. Semakin[1], M. S. Tagirov[1,2]

[1]Kazan Federal University, Institute of Physics, Kremlevskaia str, 16a, Kazan, 420008, Russia
[3]Tatarstan Academy of Sciences, Institute of Applied Research, Levobulachnaia 36a, Kazan, 420111, Russia
E-mail: ujif28@mail.ru

Introduction

Lithium–rare-earth double fluorides attract interest as model objects in physics of dipolar magnets [1]. Crystal symmetry of concentrated $LiDyF_4$ is $I4_1/a$, unit cell contains two magnetically equivalent Dy^{3+} ions at sites with the S_4 point symmetry [1, 2, 3]. Single crystal is Ising dipolar planar antiferromagnet, $T_N = 0.610(15)$ K, magnetic moments are ordered normally to c axis [4].

Methods and Materials

Micropowder of $LiDyF_4$ is prepared by sintering powders of LiF and DyF_3 taken in proportions according to phase diagrams from [2]. Initial batches, 0.121 g of LiF and 0.642 g of DyF_3 are dried for 2 hours at 150°C and $4 \cdot 10^{-3}$ Pa in vitreous carbon crucible. Sintering is performed in the same crucible for 18 hours at 600^0C in Ar atmosphere. X-ray powder diffraction and optical microscopy are used for characterization of the samples. Size of particles is about 1 μm according to images of sample taken via optical microscopy.Magnetization of the sample is measured in the range of applied magnetic fields 0–90 kOe and in the temperature range 2–300 K on vibration magnetometer *VSM* at *Physical Property Measurement System* (*PPMS*®).

Theoretical analysis

The Hamiltonian of rare earth ion in crystal lattice and external magnetic field **H** is diagonalized in the basis of the first 146 levels of the full space of states of $4f^9$ electronic configuration. Considered form of the one-ion Hamiltonian H is

$$H = H^0 + H_{\text{Zee}} + H_{\text{cf}} + H^{(\text{P})}.$$

The first term is the free ion energy (the Hamiltonian H described in [5]), the second is the electron Zeeman energy

$$H_{\text{Zee}} = \mu_{\text{B}} \mathbf{H}_{\text{loc}} (2\mathbf{S} + \mathbf{L}).$$

$\mathbf{H}_{\text{loc}}$ is the local magnetic field that includes the applied field **H**, the molecular field $Q\mathbf{M}$ and the demagnetizing factor of sphere $N_{\text{m}} = 1$ [6]:

$$\mathbf{H}_{\text{loc}} = \mathbf{H} + \sum_{s`} \mathbf{M}(\text{s`}) \left(Q(\text{s},\text{s`}) - \frac{4\pi}{3v} N_{\text{m}} \right).$$

The third term is the crystal field on Dy^{3+} ion in S_4 point symmetry:

$$H_{\text{cf}} = B_0^2 O_0^2 + B_0^4 O_0^4 + B_4^4 O_4^4 + B_{-4}^4 O_{-4}^4 + B_0^6 O_0^6 + B_4^6 O_4^6 + B_{-4}^6 O_{-4}^6,$$

where set of parameters B^k_p is taken from [6].

The fourth term of Hamiltonian represents linear interaction of rare-earth ion with homogeneous macrodeformations $e_{\alpha\beta}$ [6]:

$$H^{(\text{P})} = \sum_{\alpha\beta} V_{\alpha\beta} e_{\alpha\beta}, \text{ where } V_{\alpha\beta} = \sum_{pk} B^k_{p,\alpha\beta} O^k_p.$$

Magnetization M for powder of spherical particles, distributed equiprobably respecting the direction of applied field **H** is calculated as follows ($1/\beta = k_B T$):

$$M = \frac{1}{4\pi}\int_0^{2\pi} d\varphi \int_0^{\pi} d\theta \sin\theta \frac{\mu_B g_L}{m} \frac{\mathrm{Sp}\left[\mathbf{J}\frac{\mathbf{H}}{|\mathbf{H}|}\exp(-H\beta)\right]}{\mathrm{Sp}\left[\exp(-H\beta)\right]}.$$

Results and discussion

Experimental and calculated field dependencies of magnetization are presented at Fig. 1. Qualitative agreement between them appears at at $T > 10$ K. At $T = 5$ K measurements of magnetization have a shape of loop: measurements in increasing and decreasing field do not converge. Full hysteresis forms two loops connecting at zero (Fig. 2). Temperature dependence of the area of hysteresis is presented at Fig. 3. As it may be seen, effect of magnetization loops appear at $T < 7$ K and area of loops grows with descending temperature.

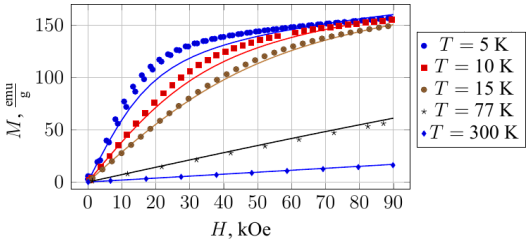

Figure 1. Field dependence of magnetization M at different temperature T
Symbols: experimental data. Lines: calculations

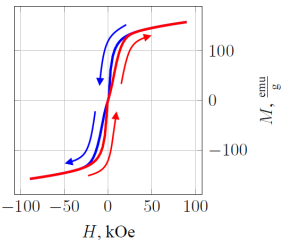

Figure 2. Full hysteresis at 2 K
Arrows represent direction of measurement

Magnetic longitudal relaxation time τ is measured by time-resolved investigation of magnetization. Applied field is changed from 0 kOe to 12 kOe or from 90 kOe to 12 kOe. Start of the measurements of magnetization is defined by the moment of establishment of the desired value of external field (12 kOe). Relaxation time τ is got via aproximation of time dependence by exponent function $M = A + B \cdot \exp(-t/\tau)$. Obtained values are about seconds and tens of seconds in the temperature range 2-7 K.

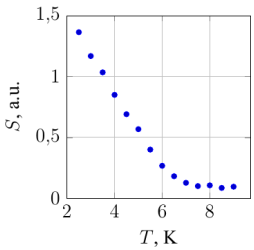

Figure 3. Temperature dependence of area S of hysteresis

Butterfly hysteresis and slow magnetic relaxation were already described in literature: for single-molecule magnets (SMM) [7] and for spin-phonon coupling [8]. Whether described case is related to one of these two or represents another phenomenon is a subject of following studies.

Acknowledgements

The financial support of the Russian Foundation for Basic Research and the Government of the Republic of Tatarstan (project 18-42-160012 p_a) is gratefully acknowledged.

The authors are grateful to Prof. B.Z. Malkin for helpful discussions.

References

1. L.K. Aminov et al. – *Handbook on the Physics and Chemistry of Rare Earths,* **22**, 295-506 (1996).
2. R.E. Thoma et al. – *Inorganic Chemistry,* **9**, 5, 1096-1101 (1970).
3. C. Keller, H. Schmutz. – *Journal of Inorganic and Nuclear Chemistry*, **27**, 4, 900-901 (1965).
4. G. Mennenga, et al. – *Journal of Magnetism and Magnetic Materials,* **44,** 48-58 (1984).
5. W.T. Carnall et al. – *The Journal of Chemical Physics,* **90**, 3443-3457 (1989).
6. I.V. Romanova, M.S. Tagirov. – *Magn. Reson. Solids,* **21**, 19412 (2019).
7. H.L.C. Feltham, S. Brooker. – *Coordination Chemistry Reviews*, **276**, 1-33 (2014).
8. R. Schenker et al. – *Physical Review B*, **72**, 184403 (2005).

Proton mobility in Dion-Jacobson phase $HCa_2Nb_3O_{10}$ studied by ^1H NMR

Elizaveta A. Andronova, Marina G. Shelyapina, Denis Y. Nefedov, Oleg I. Silyukov, Irina A. Zvereva

Saint Petersburg State University, Saint Petersburg 199034, Russia, E-mail: andronova.elizaveta@mail.ru

Introduction

Layered perovskite-type oxides are promising materials for photocatalytic water decomposition under sunlight irradiation for further hydrogen storage. Moreover, they exhibit rather high mobility of interlayer cations and ability to intercalate water and other molecules more spectacular for protonated materials [1]. Simultaneous presence of lattice protons and water molecules in a charged nanoconfinement (that is an interlayer space in layered perovskite-like oxides) may result in formation of more complex proton containing species. Moreover, their mobility should be affected by interaction with the inner charged layer. In this context, it is extremely important to identify proton containing species in the interlayer slabs and study their mobility and determine the localization of intercalated water molecules in the interlayer space. For these objectives we used Nuclear Magnetic Resonance (NMR) method that is a tool enabling to probe both localization and dynamics of protons in such compounds [2].

In this contribution we report on the results of the ^1H NMR study of proton mobility in three forms of the layered perovskite-like oxide $HCa_2Nb_3O_{10}$: alpha-, beta-, and gamma-phase.

Materials and methods

The studied compound belongs to the Dion-Jacobson phase and consists of three perovskite-like slabs and the H atoms between them (Fig. 1) [3]. Intercalation of water molecules into the interlayer space leads to expansion along the *c*-axis.

Here we studied three forms of $HCa_2Nb_3O_{10}$ which differ from each other by the content of intercalated water. According to the thermogravimetric analysis there are 2.13, 1.26, and 0.58 H_2O molecules per formula unit in the alpha-, beta-, and gamma-phase, respectively. These phases were investigated by ^1H NMR under Magic Angle Spinning (MAS).

^1H NMR experiments were conducted using a Bruker Avance IIITM 400 MHz solid-state NMR spectrometer with a double-resonance 4 mm low temperature MAS probe. The rotation frequency was equal to 12 kHz. The entire investigated temperature interval lies between 130 and 300 K, and the temperature change was controlled with accuracy 0.5 K.

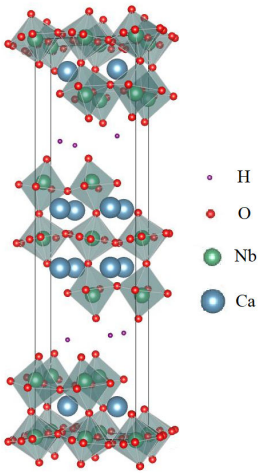

Figure 1. Formula unit of the layered perovskite-like oxide $HCa_2Nb_3O_{10}$

Results and discussion

^1H MAS NMR spectra of $HCa_2Nb_3O_{10}$ alpha-, beta-, and gamma-phase acquired at 259 K are shown in Figure 2. As one can see from the given illustration, the spectra for investigated phases are essentially different: the spectra of alpha- and gamma-phase represent more complex structure including several spectral lines, while the beta-form is characterized by the only one line. Moreover, it is evident that the individual ^1H spectral lines of different phases have

essentially different linewidth that reflects different mobilities of the corresponding species. With temperature decreasing spectra completely change: lines shift and broaden, their intensity redistributes. Described process is clearly demonstrated by Figure 3 in which the chemical shift δ, full width at half maximum $\Delta\nu_{1/2}$, and relative intensity of individual spectral lines of all phases were plotted as a function of temperature (to make these graphs clearer several alpha-form lines were excluded).

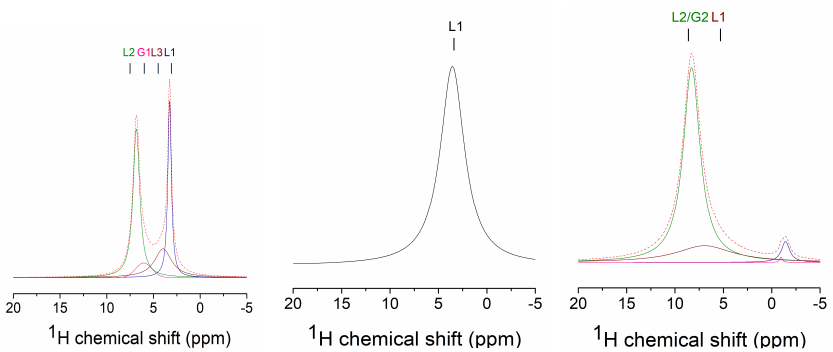

Figure 2. ^{1}H MAS NMR spectra of alpha- (a), beta (b), and gamma-phase (c) of $HCa_2Nb_3O_{10}$ at 259 K

As one can see from Fig. 2a, the alpha-form is characterized by two intense spectral lines at 3 and almost 7 ppm (L1 and L2) and two smaller lines at 4 and 6 ppm (L3 and G1). With temperature decreasing L1 and G1 rapidly disappear, and below 230 K only two lines, L2 and L3, can be seen clearly. Moreover, the intensity of L3 also declines, so at the end of the temperature interval we can observe just L2. In addition, through the entire temperature region from 274 K to 150 K a slight increase of the L2 linewidth can be observed, which is represented by Figure 3b.

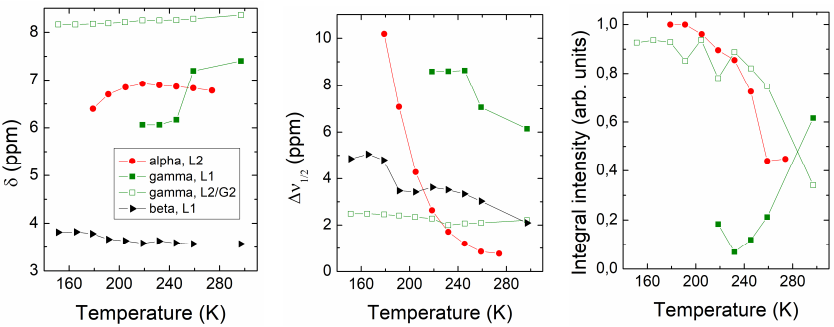

Figure 3. The chemical shift δ, linewidth at half maximum $\Delta\nu_{1/2}$, and relative intensity of some spectral lines as a function of temperature in the alpha-, beta-, and gamma-phase

For the beta-phase ^{1}H NMR MAS spectrum consists of a single line at about 3.6 ppm, the chemical shift of which gradually increases as temperature decreases (Fig. 2b and 3a). And

as in the previous case we can mention the linewidth increase tendency at lower temperatures (Fig. 3b) that reflects the slowdown of proton mobility.

For the gamma-phase $HCa_2Nb_3O_{10}$ we can observe two intense lines at about 7.5 and 8.5 ppm (L1 and L2) on ^{1}H NMR MAS spectra, see Fig. 2c. With temperature decreasing the first one becomes less intensive, and below 200 K only L2 is observed (Fig. 3c). It is interesting that the chemical shift and linewidth of the last one remain almost constant over the investigated temperature region (Fig. 3a and 3b). But from 220 K L2 becomes more and more asymmetric, namely its left tail becomes steeper, therefore, we conclude that L2 consists of two lines, one of which is gaussian.

Conclusion

The results of the ^{1}H MAS NMR study of the protons localization and their motional characteristics in three phases of $HCa_2Nb_3O_{10}$ can be summarized as follows:

- depending on water content different proton containing species in the interlayer space of $HCa_2Nb_3O_{10}$ are present, moreover, their variety, relative content, and mobility are affected by temperature;
- complex structure and temperature behavior of the ^{1}H MAS NMR spectrum for the alpha-phase reflect complicated interaction processes of different proton containing species in the charged nanoconfinement;
- for the beta-phase the only ^{1}H NMR line allows us to assume that there is a fast exchange between the lattice and water protons, accounting for a strong interaction of water molecules with perovskite layer;
- ^{1}H MAS NMR spectra of the gamma-phase suggest formation of the hydroxonium ion near room temperature (line at about 7.5 ppm), the line about 8.5 ppm can be assigned to the protons. With temperature decreasing the hydroxonium ion breaks apart.

Acknowledgement

The studies were carried out at Saint Petersburg State University: Centre for Diagnostics of Functional Materials for Medicine, Pharmacology and Nanoelectronics, Centre of Thermal Analysis and Calorimetry. The work was supported by Russian Scientific Foundation (Project No. 19-13-00184).

References

1. I. A. Rodionov, I. A. Zvereva, Chem. Rev. **85** (2016) 248.
2. M. G. Shelyapina, D. Y. Nefedov, A. V. Kostromin, O. I. Silyukov, I. A. Zvereva, Ceram. Interact. **45** (2019) 5788.
3. H. Fukuoka, T. Isami, S. Yamanaka, Journal of Solid State Chemistry **151** (2000) 40.

Micelle formation in magnesium hexanoate solution in the presence of a peptide 1B03

N. A. Antonova, A. V. Komolkin

St.Petersburg State University, 7-9 Universitetskaya Emb., 199034, St.Petersburg, Russia
E-mail: st054868@student.spbu.ru

Introduction

The OPLS-AA, CHARMM, AMBER [1-3] potentials are widely used for computer simulation. In all of them the charge of the divalent magnesium ion is +2e and the charge of the acid residue of hexanoic acid is −1e. Earlier it was published [4] that the electric charges of ions, specified in the standard file of potentials of atom-atom interactions OPLS-AA, are not acceptable for simulation of concentrated ionic systems. As a result of simulation of micelle formation in an aqueous solution of magnesium hexanoate, the charges calculated by the Mulliken method turned out to be the best suitable: +1.4e for the magnesium ion and −0.7e for the acid residue.

The purpose of this work was to investigate the structure and dynamics of aggregates in a concentrated solution of magnesium hexanoate depending on the model ion charges in the presence of the peptide 1B03 and compare the result with the results of previous work.

Model systems

1B03 is the abbreviated name of the solution structure of the antibody-bound HIV-1IIIB V3 peptide in the Protein Data Bank [5]. This peptide consists of 18 amino acid residues, among which there are several positively charged amino acid residues: 4 arginines and 1 lysine. The total charge of the molecule is +5e.

Magnesium hexanoate molecule was constructed in Jmol [6]. The model of water was chosen SPC/E [7]. The structure of the peptide 1B03 was taken from the Protein Data Bank. The parameters of simulation were taken from the OPLS-AA [1]. The process of micelle formation was carried out by the method of molecular dynamics.

Two systems were created. Each of them consisted of the peptide molecule, 150 magnesium ions, 305 ions of the acid residue of hexanoic acid, and 5944 water molecules. Each system was simulated during 15 ns. Charges of ions and molecules in systems are given in the Table 1. The charge of the peptide molecule +3.5e was obtained by scaling the partial charges of the peptide atoms, so that the total charge of each of the five positively charged amino acid residues (4 arginines and 1 lysine) was +0.7e instead of +1e.

Table 1. Charges of ions in the modeled systems

System	Charge of the peptide	Charge of magnesium ion	Charge of acid residue
I	+5	+2	−1
II	+3.5	+1.4	−0.7

The results of simulation of the systems in the presence of a peptide were compared with similar systems without a peptide, in which there are the same charges of corresponding particles.

Results analysis

To analyze the results it was necessary to calculate radial distribution functions (RDF). RDF shows probability of finding atoms at a certain distance. In the Figure 1 and the Figure 2 there are RDFs between magnesium ions for three systems without a peptide and two systems

in the presence of the peptide respectively. Black line in the Figure 1 shows RDF between magnesium ions in an aqueous solution of magnesium hexanoate when the charges of magnesium ions and acid residues are +2e and −1e respectively. In the presence of the peptide, a system with such charges was not simulated.

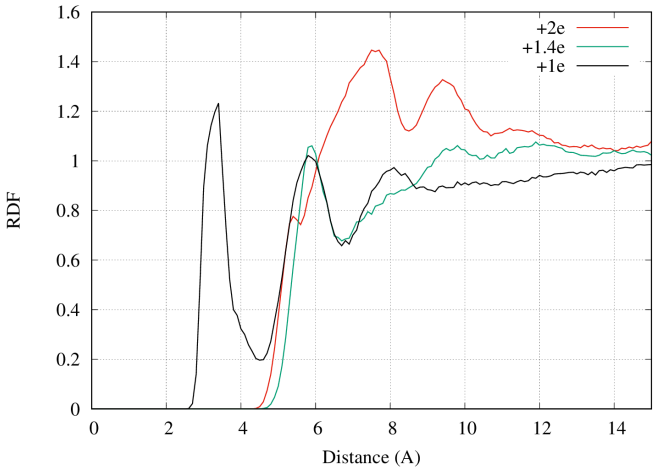

Figure 1. RDFs between magnesium ions in systems without a peptide

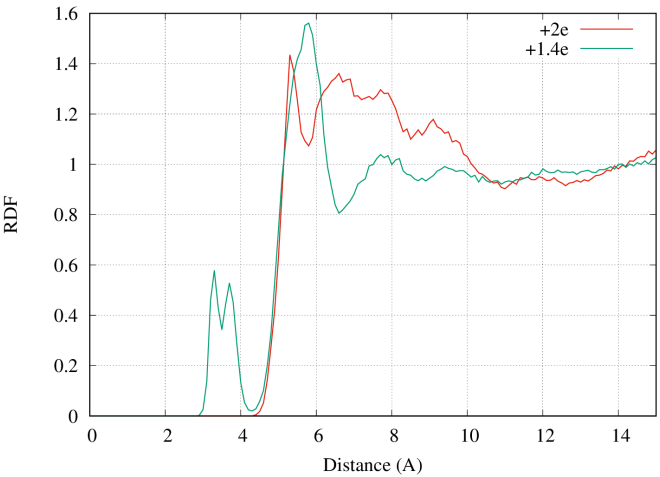

Figure 2. RDFs between magnesium ions in systems with a peptide

In the presence of the peptide molecule, contact pairs Mg-Mg appear in system II (green line in the Figure 2), as evidenced by a small peak at a distance of ~3.5 Å between magnesium ions (kinks in the graphs are associated with a lack of statistics due to the small amount of magnesium ions). Also in this graph, with the appearance of the peptide, the peak at a distance of ~5.8 Å becomes higher and wider than the same in the Fig. 1, i.e. more pairs of magnesium

ions now interact with each other through two water molecules. At the same time, practically nothing has changed in system I (red line) in the interaction of magnesium ions with each other.

RDFs between magnesium ion and acid residue were also analyzed.

Conclusion

In the presence of a peptide, the dissociation of magnesium hexanoate is little dependent on charge. This is in stark contrast to the results obtained for systems without a peptide. In addition to this, acid residues also form bonds with positively charged amino acid residues. The rest of the interactions of magnesium ions, acid residues and water molecules with each other almost did not change with the appearance of the peptide in the system. Micelles in systems with a peptide are formed more actively, and the sizes of micelles are approximately the same in both systems, while in systems without a peptide larger micelles are formed at a lower model charge.

Acknowledgements

Research was carried out using computational resources provided by Resource Center "Computer Center of SPbU" (http://cc.spbu.ru).

References

1. William L. Jorgensen Research Group — OPLS-AA. URL: http://zarbi.chem.yale.edu/oplsaam.html (accessed 01.03.2019)
2. CHARMM (Chemistry at HARvard Macromolecular Mechanics). URL: https://www.charmm.org (accessed 01.03.2019)
3. The Amber Home Page | Tools for molecular simulation. URL: http://ambermd.org/ (accessed 01.03.2019)
4. N.A. Antonova, A.M. Ryzhkov, A.V. Komolkin. Computer simulation of micelle formation in magnesium hexanoate solution // Magnetic resonance and its applications: Proceedings 16th International School-Conference, Saint-Petersburg, March 31–April 5, 2019. — Saint Petersburg, VVM Publisher, 2019. P. 130-132.
5. V. Tugarinov, A. Zvi, R. Levy, J. Anglister. A cis proline turn linking two beta-hairpin strands in the solution structure of an antibody-bound HIV-1IIIB V3 peptide. – *Nat. Struct. Mol. Biol.,* **1999**, v. 6, No. 4, 331-335
6. Jmol: an open-source browser-based HTML5 viewer and stand-alone Java viewer for chemical structures in 3D. URL: http://jmol.sourceforge.net/ (accessed 01.03.2019)
7. Berendsen H., Grigera J., Stratsmaa T. The missing term in effective pair potentials. – *J. Phys. Chem.* **1987**, v.191, No.24, 6269–6271

Comparison of the spatial structure of the mefenamic acid molecule in solution at normal and supercritical state

K. V. Belov[1], L. A. E. Batista de Carvalho[2], M. G. Kiselev[1], I. A. Khodov[1]

[1]G. A. Krestov Institute of Solutions Chemistry, Russian Academy of Sciences, Ivanovo, Russian Federation
[2]University of Coimbra, Coimbra, 3004-504, Portugal
E-mail: iakh@isc-ras.ru

Today, one of the most important problems of the pharmaceutical science is investigation and analysis of the new polymorphic forms of drugs. There are some methods for the dealing with problems of this kind not least of which is nuclear magnetic resonance (NMR) spectroscopy. The NMR spectroscopy is a powerful technique for the primary analysis of the characteristics of the structure of the studied biologically active compounds in the solutions. It is known that the spatial structure of small molecules of the drugs in saturated solutions to define their molecular configuration in the crystalline form (polymorphic form). Therefore, the analysis of conformational equilibrium is an important stage in the direction with the search for new polymorphic forms of drugs. The conformation preference is depended due to several factors such as temperature, pressure, solvent used, etc. The using supercritical fluids as media to determine conformational preference is one of the most perspective ways to determine the mechanisms of nucleation.

First the all, we are started our investigation with the conformational lability of the 2-(2,3-dimethylphenyl) aminobenzoic acid (mefenamic acid) molecule in a solution of the deuterated dimethyl sulfoxide (DMSO-d_6) and then we are measured in supercritical carbon dioxide ($scCO_2$) by the NMR spectroscopy.

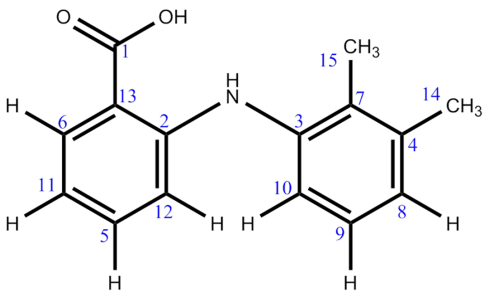

Figure 1. Chemical structure of molecule mefenamic acid

The chemical structure of mefenamic acid was determined by ^1H - ^{13}C HSQC, HMBC and ^1H -^1H TOCSY approaches. This techniques is make possible to assign the NMR signals in the ^1H and ^{13}C spectra to the molecular group of the mefenamic acid. The obtained data by analysis of conformational equilibria based on the method of nuclear Overhauser effect spectroscopy (NOESY). The NOESY cross-peaks provide information on internuclear distances were assumed to be 2–5 Å. The analysis of the NOESY spectral data allowed to reveal the specific characteristic of the conformational behavior in a solution of DMSO-d_6 and $scCO_2$.

Acknowledgements

This work was supported by the Ministry of Education and Science of the Russian Federation, Russia (contracts No. 01201260481 and No. 0120095082), by the Russian

Foundation for Basic Research (MK., grant No. 18-29-06008) and Council for Grants of the President of the Russian Federation, Russia (IK, project MK-662.2021.1.3). The NMR spectroscopy experiment was performed using the molecular fluid spectroscopy facility (http://www.ckp-rf.ru/usu/503933/) of G.A. Krestov Institute of Solution Chemistry of the Russian Academy of Sciences (ISC RAS) (Russia).

Hambergite (Be_2BO_3OH) as a model of one-dimensional dipolar coupled ^1H zig-zag spin chain

G. A. Bochkin[1], E. B. Fel'dman[1], E. I. Kuznetsova[1], I. D. Lazarev[1,2], S. G. Vasil'ev[1]

[1]Institute of Problems of Chemical Physics, Chernogolovka 142432, Moscow Oblast, Russia
[2]Faculty of Fundamental Physical-Chemical Engineering, Lomonosov Moscow State University, GSP-1, Moscow 119991, Russia
E-mail: viesssw@mail.ru

Introduction

NMR spectroscopy in solids serves as a fruitful source of structural information on the local surroundings of the resonating nuclei. Dipole-dipole interaction (DDI) between spins in a rigid lattice has been used in numerous studies to determine internuclear distances and to investigate the mobility of atoms and molecules. The resolved patterns due to the dipolar interaction offering rich structural information is generally restricted to the cases where these prevails within a small group of spins. This is a consequence of the long range character of the DDI. Nevertheless, the resolved dipolar spectra are not exceptionally inherent to the small spin systems as demonstrated by an example of the linear chain of uniformly spaced spins. Such an arrangement of ^1H and ^{19}F spins can be found in hydroxy- and fluorapatite crystals [1]. In the present work we consider another crystal, hambergite, as a model of one-dimensional chain of ^1H nuclei [2, 3] and compare it with a well-known apatite structures.

The structure of hambergite

Hambergite (Be_2BO_3OH) is an orthorhombic crystal belonging to the space group Pbca. The lattice parameters are $a \approx 9.8$ Å, $b \approx 12.2$ Å and $c \approx 4.4$ Å. Every unit cell comprises 8 formula units, thus contains 8 protons. These protons form 4 well-isolated chains. The distance between nearest neighbors is constant and equals to 2.312 Å. Every next nearest neighbor in the chain lies along a straight line, while the nearest neighbors form an angle $\psi = 16.7°$ or $\psi = (180° - 16.7°)$ with this line. Thus, the distinctive feature of the structure is the zig-zag arrangement of ^1H spins along a c-axis of the crystal (Fig. 1).

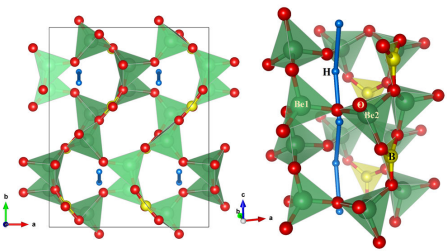

Figure 1. The structure of hambergite crystal: unit cell (left); ^1H chain and the surroundings. Oxygen is shown in red, boron in yellow, hydrogen in blue, BeO_4 are shown as green tetrahedra. The blue bonds connect neighboring protons in the chains

Results and discussion

The experiments were performed on a Bruker Avance III spectrometer equipped with the 9.4 T wide bore magnet (the resonance frequency on ^1H nuclei is 400.2 MHz). The natural crystals of hambergite were used for investigation. The crystal was mounted on the rotating glass rod to obtain the different orientations of the external magnetic field with respect to the chain axis. In the considered cases the rotation axis was set perpendicular to the chain axis. The

second moment for protons and other nuclei were calculated according to Van Vleck's formulas for 3 x 3 x 3 supercell and the results are shown in Fig. 2.

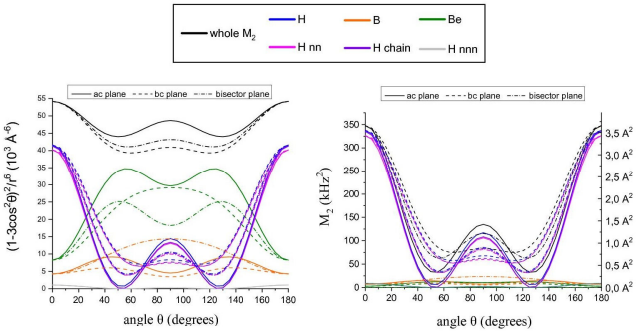

Figure 2. The second moment M_2 calculated as a function of the orientation in the external magnetic field (different line styles correspond to different rotation planes): only the spatial part (left); total M_2 (right)

The calculations of the second moment of ^{1}H NMR line taking into account the homo- and heteronuclear interactions provide a reasonable explanation of the experimental data. The calculations reveal dominating contribution of the ^{1}H spins lying along the c-axis of the crystal. These spins are arranged in well-isolated chains in a zig-zag manner along c-direction. The contribution due to the dipolar interactions with the spins in the same chain is more than 96% of the total second moment when the chain is oriented along the external magnetic field.

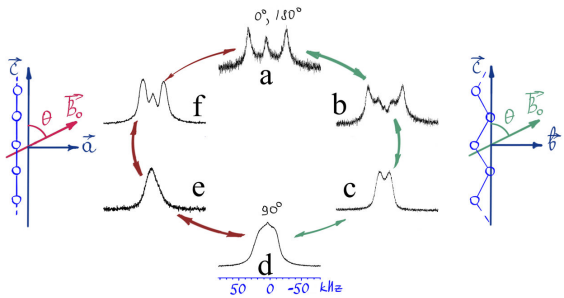

Figure 3 The schematic representation of the transformation of the ^{1}H NMR spectra due to the reorientation of the external magnetic field with respect to the chain axis

Besides the changes of the width of ^{1}H resonance hamberigite demonstrates interesting transformation of the lineshape when observed at different orientations. The scheme which captures the general features of the ^{1}H NMR spectra of hambergite crystal occurring at different orientations in the magnetic field is represented in Fig. 3. The line is strongly anisotropic. The position when the c-axis coincides with the magnetic field is easily identifiable as a broadest triplet (Fig. 3a), while it transforms into a flat-topped line when axis is oriented at 90 almost independent on the direction of the rotation (Fig. 3d). Depending on the direction of the rotation the lineshape transformation is typical for a linear chain (Fig. 3 e and f) or for a zig-zag chain (Fig. 3 b and c). The corresponding positions of the chain with respect to the magnetic field are schematically shown on the left and right sides of Fig. 3, respectively.

The obtained results show that the experimental shape of ^{1}H NMR line can be described by taking into account the interactions with relatively few nearest spins in the chain. The ^{1}H spins in hambergite crystals could serve a good model of the quasi-one-dimensional spin chain. A specific feature of a zigzag arrangement of spins in the chains is that, depending on the orientation, the dipolar coupling can be set equal for all pairs of nearest spins or alternating in strength between successive pairs of spins in the chain to a varying degree. Hambergite provides a new rich testbed to explore the dynamics of a many-body quantum spin system.

Acknowledgements

This work was performed as a part of a state task, State Registration no. 0089-2019-0002. This work was supported by the Russian Foundation for Basic Research, Grant no. 20-03-00147. I.L. acknowledges support from the Foundation for the Advancement of Theoretical Physics and Mathematics BASIS No. 19-1-5-130-1 URL: https://basis-foundation.ru/en/foundation/. The experiments were performed using the equipment of the Multi-User Analytical Center of IPCP RAS and Research Resource Center of Science Center RAS

References

1. G. A. Bochkin, E. B. Fel'dman, I. D. Lazarev, A. A. Samoilenko and S. G. Vasil'ev, Journal of Magnetic Resonance, 2019, 301, 10-18.
2. G. A. Bochkin, S. G. Vasil'ev, S. I. Doronin, E. I. Kuznetsova, I. D. Lazarev and E. B. Fel'dman, Applied Magnetic Resonance, 2020, 51, 667-678.
3. G. A. Bochkin, E. B. Fel'dman, E. I. Kuznetsova, I. D. Lazarev, S. G. Vasil'ev and V. I. Volkov, Journal of Magnetic Resonance, 2020, 319, 106816.

The sense of the development of MRI

Carlos Cabal Mirabal[1,2]

[1]*Physics Faculty Havana University, Cuba*
[2]*Medical Biophysics Center Oriente University*
E-mail: carlos.cabal@fisica.uh.cu; carlos.cabal@quimica.unlp.edu.ar

Magnetic Resonance (MR) has demonstrated its potential during the last decades in several Science and Technology fields. MR research, development and investment have significant importance in present and even the near future. A briefly synopsis of the reasons for this statement is presented. The connection between MR, specially the MR imaging, the ongoing revolutions, Biology in particular, is illustrate [2-6]. The main challenges in development of the new MR hardware are discused [7-9]. The physical, technological, biomedical and market reasons are presented. The greater emphasis on the development of the new technologies should promote superior and easier access to MRI studies and earlier diagnostic of the diseases and anomalies. The MRI physics and technological opportunities for the new development are mentioned. The needed networks to develop these technologies are remarked.

Cuban experiences concerning to the calculation, design, construction and validation Magnetic Resonance (MR) technology and introduction in the clinical practice and research are mentioned. Cuban MR Technology includes MR relaxometry, Magnetometers and MRI whole body machines worked in hospital for more than 15 years [10, 11]. Furthermore, a resume of Kinetics studies of Complex Biomedical Problems by Magnetic Resonance are presented.

References

1. Lammers T, Aime S, Hennink WE, Storm G, Kiessling F. Theranostic nanomedicine. *Acc Chem Res* 2011; 44: 1029-38.
2. C. Cabal**,** "Regularidades y tendencias de las tecnologías al servicio de la Medicina Moderna" *Revista Cubana de Salud Pública*, 2008, Vol. 34 No. 3 pp. 1-5.
3. C. Cabal, D. Darias, E. Gonzalez A. Musacchio, "The Theranostics and the molecular imaging. New concepts and technologies for the drug development", Biotecnología Aplicada, 2013, Vol.30,3,172-77
4. MIT Convergence: The Future of Health June 2016, Cambridge, Massachusetts, .June 2016, http://www.convergencerevolution.net/s/Convergence-The-Future-of-Health-2016-Report-55pf.pdf
5. Convergence. Facilitating Transdisciplinary Integration of Life of Sciences, Physical Sciences, and Engineering and Beyond, Committee on Key challenge Areas for Convergence and health Board on Life Sciences. Division on Earth and Life Studies. National Research council of National Academies, The National Academic Press, 2014, Washington DC, www.nap.edu http://ciret-transdisciplinarity.org/E06DA98B-6B14-49A7-A07D-6BA40CF99342/FinalDownload/DownloadId-3FFFBA8AB4E9123E2010902920E17AE0/E06DA98B-6B14-49A7-A07D-6BA40CF99342/quoideneuf/NSF_Report_on_TD.pdf
6. Quantum Manifesto A New Era of Technology, Draft - March 2016 https://time.tno.nl/media/7638/quantum_manifesto.pdf
7. S. Kathiravanand , J. Kanakaraj "A Review on Potential Issues and Challenges in MR Imaging" The Scientific World Journal Volume2013,ArticleID783715,10pages http://dx.doi.org/10.1155/2013/783715
8. A. Nowogrodzki, "The Strongest Scanners", Nature, 2018 VOL 563, p.24- 26
9. M. Sarracanie, N. Salameh "Low-Field MRI: How Low Can We Go? A Fresh View on an Old Debate" 2020, Front. Phys. 8:172. doi: 10.3389/fphy.2020.00172

10. C. Cabal Mirabal “Magnetic Resonance Project 35-26-7. A Cuban Case of Engineering Physics and Biophysics” in “The History of Physics in Cuba”, edited by A. Baracca, J. Renn, H. Wendt , Springer editorial; 2014, p. 337-334. ISBN-10: 9401780404 ISBN-13: 978-9401780407
11. Cabal Mirabal, C., Fernández García, A., Lores Guevara, M. et al. “Kinetics of Complex Biomedical Problems by Magnetic Resonance. Cuban Experiences”. Appl Magn Reson (2018) pp.1/10 https://doi.org/10.1007/s00723-018-0985-2 2

Curie Spin relaxation contribution during the aggregation process of HbS Hemoglobin

C. Cabal[1,2], M. Lores, V. I. Chizhik[3], S. Rodanov[3], J. C. García-Naranjo[1]*

[1]Centro de Biofísica Médica, Cuba
[2]Physics Faculty Havana University, Cuba
[3]San Petersburg State University, Russia
[*]Corresponding author
E-mail: carlos.cabal@quimica.unlp.edu.ar

The Curie-Spin (CS) relaxation mechanism has been well described theoretically [1, 2]. but only a few experimental evidences have been presented [3]. Previous works [4-7] showed a significant increase in the rotational correlation time of the water bound to the hemoglobin S during the aggregation process under sickle cell disease. In this case, the influence of "Curie-Spin" relaxation mechanism to proton relaxation may be expected Based on the reported correlation times [4-7], the contribution of the CS relaxation mechanism to proton relaxation times (T1 and T2) has been estimated in comparison with the contribution of the dipole–dipole relaxation mechanism at the extreme stages of the aggregation process of the hemoglobin S.

The CS contribution to the total spin-spin relaxation rate R2 is about 25% and 50% at the magnetic field of 1.5 T (60 MHz for 1H resonance) during the induction and ending stages of the aggregation process, respectively. At a lower magnetic field, this mechanism gives an insignificant contribution. The CS contribution to the spin–lattice relaxation rate R1 is negligible in the range of magnetic fields investigated.

Therefore, the T1/T2 ratio may change not only because of the R1 dispersion but also due to the CS contribution. The dependence of the T1/T2 ratio on the magnetic field magnitude during the aggregation processes will be discussed in an upcoming work for what higher field experiments on the NMR-relaxation in the presence of the HbS agglutination process need to be done. Definitely, at B0 > 1.5 T, the CS contribution to the spin-spin relaxation will increase even before the ending stage and its contribution might appear to the spin–lattice relaxation. In other words: if T1/T2 ≈ 1, it means that the aggregation process in the blood sample has not started or is reversible, and if this ratio increases, then based on the dipole-dipole model it was previously assumed that the aggregation becomes significant (τR increases).

It is shown here that for studies in high magnetic fields, it is first necessary to evaluate the contribution of CS relaxation, otherwise, the conclusions may be erroneous. Since the CS and dipole-dipole relaxation have different dependences on the magnetic field and molecular mobility, it is advisable to raise the question of choosing the optimal magnetic field for the relaxation method of the sickle cell disease diagnostics. In high field magnetic resonance imaging experiments (modern trend), the contribution of the CS mechanism may also be expected. Thus, to obtain higher contrast in the molecular magnetic resonance imaging (mMRI) high-molecular structures conjugated with certain paramagnetic ions (for example, Pr+3, Sm3+, Fe2+, Fe3+) having short electron relaxation times are used. The mMRI experiments are done in very high field machines and in these cases, the CS contribution should also be considerable.

Acknowledgements

The reported study was funded by RFBR and CITMA according to the research project no 18-53-34003

References

1. M. Gueron, J. Magn. Resonan, 58 (1975)
2. Vega A., Fiat D, Molec. Phys., 347 (1976)

3. P. Caravan, M.T. Greenfield and J.W.M. Bulte, Mag. Reson. Med., 917 (2001)
4. A. Fernández, C. Cabal, J. Losada, E. Alvarez, J. Otero, Hemoglobin, 181 (2005)
5. M.A. Lores-Guevara, C. A. Cabal, Appl. Magn. Reson., 79 (2005)
6. M. Lores, C. Cabal, O.R Nascimento, A.M Gennaro, Appl. Magn. Reson., 121 (2006)
7. M Lores, C. Cabal, R.N. Muller, S. Lauren, Y. Mengana, J. Garcia, *Proceedings of the International Youth School Conference Spinus 2019* (Saint Petersburg, 2019), p.98.
8. Cabal, C., Lores, M., Chizhik, V.I. et al. Assessment of Contribution of Curie-Spin Mechanism in Proton Relaxation During Aggregation Process of Hemoglobin S. Appl Magn Reson (2020). https://doi.org/10.1007/s00723-020-01241-x

Using electronic criterion towards to the halogen bond for prediction ^{31}P NMR chemical shift of phosphine oxides as probe acceptors

Edem R. Chakalov, Alexei S. Ostras, Daniil M. Ivanov, Peter M. Tolstoy

Institute of Chemistry, Saint Petersburg State University, Saint Petersburg, Russia
E-mail: st086266@student.spbu.ru

Introduction

Halogen bond (XB) is actively studied because it is one of the most abundant non-covalent interactions in nature, which is present in solids, in liquids and solutions and in a gas phase; moreover, it has been demonstrated that it plays a notable role in catalytic processes, crystal engineering, in design of drugs and functional materials with numerous applicable properties.

Electronic features of XB

XBs are formed by electron donors (molecules, ions or individual atoms, e.g. Hal, O, S, Se, N) and halogen-containing (primarily Cl, Br, I) molecules and ions. Generally electronegative covalently bound halogens are able to act as electron acceptors due to the anisotropic distribution of electron density (ED) around them. There are two distinct regions: (a) the region of increased ED (nucleophilic site), located perpendicular to the covalent bond and corresponding to negative values of electrostatic potential (ESP) and (b) the region of decreased ED (electrophilic site, positive ESP) located along the covalent bond, the so-called σ-hole, which acts as the electron acceptor in XB (Figure 1).

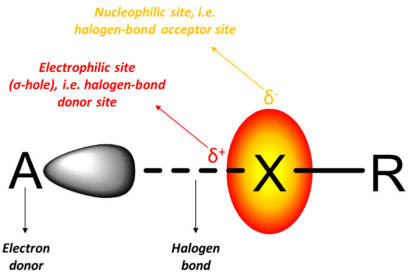

Figure 1. Schematic representation of a halogen bond

In Bader's Quantum Theory of Atoms in Molecules (QTAIM) the presence of XB could be detected as a bond path: the path which follows the ridge of maximum ED between the halogen and electron-donating atom. Along the bond path both the ED and the ESP go through minima. The ED minimum is located closer to the halogen atom, while ESP minimum is located closer to the electron donor [1,2]. The distance between the minima seems to be sensitive to the electronic structure of interacting moieties.

^{31}P NMR chemical shifts and electronic structure of XBs

It stands to reason, that if the electron is donated by the oxygen atom of a P=O group, the XB formation and the corresponding ED redistribution should cause the change of the ^{31}P NMR chemical shift. The question arises, does this shift correlate with the XB strength and/or the distance between ED and ESP minima?

In order to answer this question, we have considered by quantum-chemical calculations 128 complexes formed by trimethylphosphine oxide, $Me_3P{=}O$, with various halogen donors

(Gaussian 16 software, DFT functional M06-2X with basis set def2-TZVPPD, see several examples in Figure 2) [3]. For each complex we have calculated the interaction energy, ΔE, the distance between ED and ESP minima, Δr, and the change of the isotropic ^{31}P NMR chemical shift upon complexation, $\Delta\delta$P.

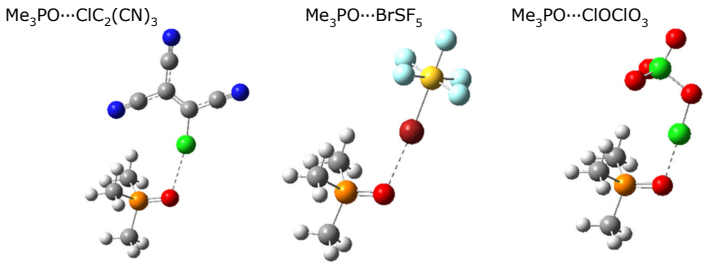

Figure 2. Example of the complexes studied in this work

As an example, in Figure 3 we show the resulting dependence of $\Delta\delta$P on Δr for $Me_3P{=}O$ complexes with bromine-containing halogen donors. We have found that in this and in other cases the phosphorus chemical shift could be used as a spectroscopic descriptor of the electronic structure of XB.

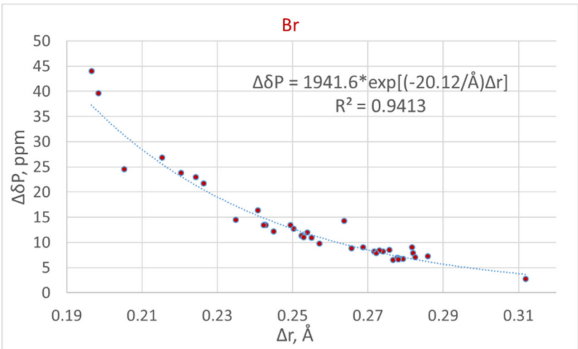

Figure 3. $\Delta\delta P(\Delta r)$ dependence for $Me_3P{=}O\cdots Br$-R halogen-bonded complexes

References

1. E. Bartashevich, S. Mukhitdinova, I. Yushina, V. Tsirelson. – *Acta Cryst.*, B**75**, 117-126 (2019);
2. E. Bartashevich, Y. Matveychuk, V. Tsirelson. – *Molecules*, **24(6)**, 1083-1094 (2019);
3. A. S. Ostras', D. M. Ivanov, A. S. Novikov, P. M. Tolstoy. – *Molecules*, **25(6)**, 1406-1422 (2020);

Development and investigation of pervaporation green high-performance hydroxyethyl cellulose/sodium alginate membranes for dehydration

Mariia E. Dmitrenko, Andrey A. Zolotarev, Vladislav P. Liamin, Anna I. Kuzminova, Anastasia V. Penkova

St. Petersburg State University, 7/9 Universitetskaya nab., St. Petersburg 199034, Russia
E-mail: m.dmitrienko@spbu.ru

Introduction

Membrane processes play an important role and are widely used in various industries for the saving of environment. Pervaporation is one of the most important membrane methods for the separation of liquid mixtures. It is actively applied for the separation of mixtures with low molecular weight components and, especially, for their dehydration. Currently, due to the increased control of the impact of production on the environment, it is important to develop highly efficient pervaporation membranes based on biopolymers with tailored properties.

Results

To develop of novel green high-performance blend membranes for enchanced pervaporation dehydration, biopolymers sodium alginate (SA) and hydroxyethyl cellulose (HEC) were chosen as a membrane material. Several approaches were used for the preparation of membranes with improved properties: (1) the selection of the optimal biopolymer ratio in the matrix, (2) bulk modification by the introduction of fullerenol in blend matrix, (3) the selection of the optimal cross-linking agent, and (4) surface modification by layer-by-layer technique for the deposition of polyelectrolytes. Structure of the developed membranes were investigated by spectroscopic (FTIR and NMR) and microscopic (SEM and AFM) methods. The physicochemical properties were studied by TGA, contact angle and swelling degree measurements. Transport properties of developed HEC/SA membranes were tested in pervaporation dehydration of isopropanol in a wide concentration range. It was demonstrated that the combination of several strategies (bulk and surface modifications) resulted to changes in membrane structure causing improved performance of the membrane.

Acknowledgements

This work was supported by Russian Science Foundation [project No 20-79-10064]. The experimental work of this study was facilitated by the equipment from the Resource Centre of Geomodel, Chemical Analysis and Materials Research Centre, Centre for X-ray Diffraction Methods, Magnetic Resonance Research Centre, Centre for Innovative Technologies of Composite Nanomaterials, Nanophotonics Centre, Cryogenic department, Thermogravimetric and Calorimetric Research Centre and the Interdisciplinary Resource Centre for Nanotechnology at the St. Petersburg State University.

Computer simulation of atactic polymers

Elisaveta V. Fedotova, Andrei V. Komolkin, Sergey G. Polushin

Saint Petersburg State University, 7/9 Universitetskaya nab., St. Petersburg, Russia 199034
E-mail: lizokaf@mail.ru

Introduction

In liquids, structural transitions of the form isotropic phase–isotropic phase are found under changing external conditions, similar to phase transitions of the first kind in solids. In polymers, strong changes in the short-range order and structure of substances in an isotropic melt were observed by the double-refraction method.

Methods and results

In this paper, a computer simulation of the atactic polymer polystyrene-25 with a chain length of 25 monomer units was performed. Each molecule was randomly generated from a sequence of right and left isomers of the monomer unit. The model system consisted of 142 molecules (3550 monomer units in total).

The aim of the simulation was to find out the possibility of ordering benzene rings in the oligomer composition in the isotropic phase. Computer simulation was carried out in the AKMD program [1]. A full-atom model of an atactic polymer was constructed using OPLS-AA potentials [2]. The simulation was performed in an NpT ensemble with periodic boundary conditions. The cubic model cell size was 86.06±0.02 Å at normal pressure and temperature of 20 °C.

The analysis of the relative position of the benzene rings showed that, in contrast to the system of ethylbenzene molecules, the centers of the benzene rings in the polymer are located closer to each other. This indicates the existence of a parallel orientation of the benzene rings, as opposed to the preferably T-shaped orientation of the benzene molecules in the melt and in the crystal.

Thus, the calculated data on the ordering of the benzene rings of polystyrene-25 obtained in this work allow us to better understand the molecular mechanisms that manifest themselves in the temperature dependence of the Kerr equilibrium constant of an isotropic polystyrene melt.

As a result of the calculations, the distributions of the centers of mass of the molecules of ethylbenzene, polystyrene-5 and polystyrene-25 were obtained as a function of the cylindrical distribution around the central molecule.

It turned out that with an increase in the number of monomers in the polymer chain, the orientation order of the benzene rings increases sharply. When comparing the distributions in Figure 1, it turned out that the system consisting of polystyrene-5 molecules, in contrast to the system of ethylbenzene molecules, has new regions of a high density of distribution. They appear close to axis of the ring and to its plane (distance wrom plane of the ring is 3.5-4.1 Å). The system of polystyrene-25 molecules differs from the system of polystyrene-5 molecules by higher density of distribution in these regions. These areas correspond to planar configuration of benzene rings, so in the longer chain the orientational order benzene rings increases.

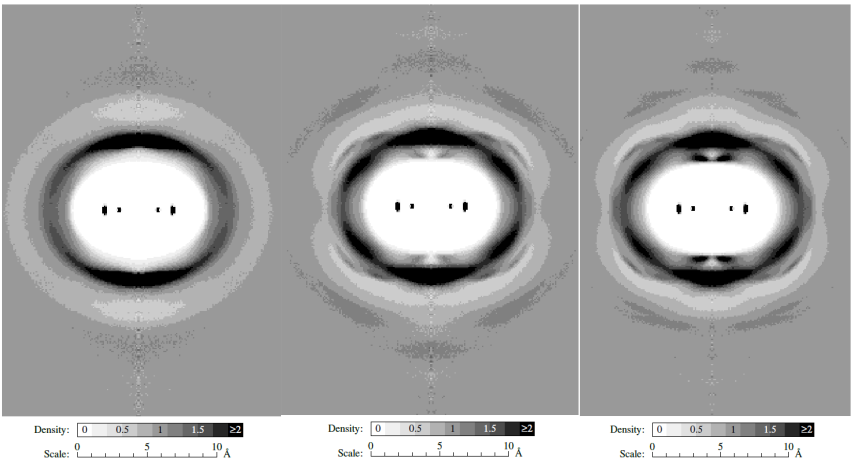

Figure 1. Functions of the cylindrical distribution of the centers of mass of benzene rings in styrene, polystyrene-5, and polystyrene-25 molecules. The axis of the cylindrical coordinate system is directed upwards and coincides with the axis of symmetry C6 of the benzene ring. The center of the distribution shows the position of the carbon and hydrogen atoms of the central molecule. The probability density scale and the image scale are shown below. The gray color of the scale corresponds to the average density of the benzene molecules, the white color shows the excluded volume of the molecule

References

1. A. V. Komolkin, A. Laaksonen, A. Maliniak. Molecular dynamics simulation of a nematic liquid crystal // J. Chem. Phys. (1994), Vol. 101, No. 5, P.p. 4103-4116. DOI: 10.1063/1.467460
2. W. L. Jorgensen, D. L. Severance. Aromatic-aromatic interactions: free energy profiles for the benzene dimer in water, chloroform, and liquid benzene // J. Am. Chem. Soc. (1990), Vol. 112, No. 12, P.p. 4768-4774. DOI: 10.1021/ja00168a022

2D NMR diffusion-relaxation (DT_2) studies of water in hydrophobic carbon nanotubes

L. Gkoura[1], M. Karagianni[1], M. Fardis[1], J. Hassan[2] and G. Papavassiliou[1]

[1]Institute of Nanoscience and Nanotechnology, NCSR Demokritos, 15310 Aghia Paraskevi, Attiki, Greece
[2]Department of Physics, Khalifa University of Science and Technology, 127788, Abu Dhabi, UAE
E-mail: l.gkoura@inn.demokritos.gr

Introduction

In this work, we investigate, through experimental two-dimensional Nuclear Magnetic Resonance (NMR) diffusion–relaxation (D-T_{2eff}) spectroscopy combined with Molecular Dynamics (MD) simulations, water behavior under extreme nanoscale confinement. To analyze different diffusive mechanisms, we examined the size dependence of water dynamics inside Carbon Nanotubes (CNTs) of different diameters (1.1 nm to 6.0 nm) and temperature range $265 \leq T \leq 305$ K.

Behavior of Water inside CNTs

Carbon nanotubes are able to encapsulate many kinds of materials within their quasi-one-dimensional cavities. Many theoretical studies have shown that materials confined within such small cavities, exhibit novel features which do not appear in the bulk material. In this study we examined water adsorbed inside CNTs in spite of the hydrophobic nature of their wall.

Most of the theoretical studies have shown that water inside hydrophobic nano-channels diffuses faster than bulk water and this enhancement depends on the size of the hydrophobic nanochannels.

Herein, we provide experimental evidence of this dependence by the use of two-dimensional nuclear magnetic resonance diffusion–relaxation (D–T_{2eff}) spectroscopy in the stray field of a superconducting magnet, combined with molecular dynamics simulations. We were able to analyze the size dependence of water dynamics inside Carbon Nanotubes (CNTs) of different diameters (1:1–6:0 nm), in the temperature range of 265–305 K.

The nanotube water is shown to resolve in two or more tubular components acquiring different self-diffusion coefficients strongly depending on the CNT diameter. Notably, a favorable CNT diameter range (3.0–4.5 nm) is observed, in which water molecule dynamics at the center of the CNTs exhibits anomalously enhanced water diffusion, non-Arrhenius temperature dependence, and extraordinary fragility. Such result is of significant importance in the efforts to understand the behavior of water inside hydrophobic nanochannels.

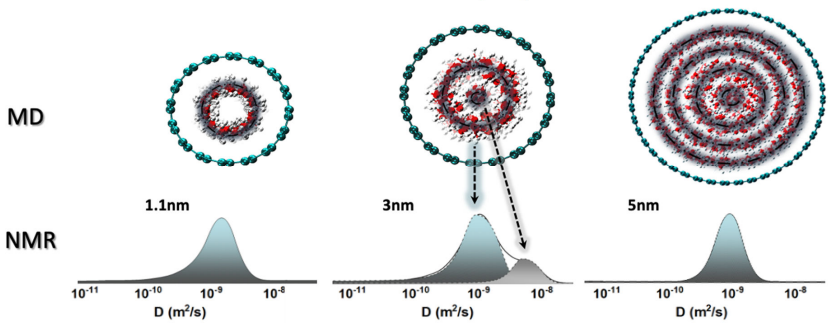

Figure 1. Water diffusion inside CNTs with different sizes (1.1nm, 3nm, 5nm) analyzed by Molecular Dynamic Simulations (MD) and Nuclear Magnetic Resonance techniques (NMR)

Acknowledgements

L. Gkoura, M. Karagianni and M. Fardis acknowledge support of this work by the project "Study of the Peculiar Water Flow in Hydrophobic Carbon Nanotubes using 2D-NMR Spectroscopy" (No. MIS 5047810), co-financed by Greece and the European Union (European Social Fund- ESF) through the Operational Programme Human Resources Development, Education and Lifelong Learning 2014-2020.

References

1. Gkoura, L., G. Diamantopoulos, M. Fardis, D. Homouz, S. Alhassan, M. Beazi-Katsioti, M. Karagianni, A. Anastasiou, G. Romanos, J. Hassan, and G. Papavassiliou. The Peculiar Size and Temperature Dependence of Water Diffusion in Carbon Nanotubes Studied with 2D NMR Diffusion–Relaxation D–T_{2eff} Spectroscopy. *Biomicrofluidics* 14, no. 3 (2020): 034114. https://dx.doi.org/10.1063/5.0005398.
2. Hassan, J., G. Diamantopoulos, L. Gkoura, M. Karagianni, S. Alhassan, S. V. Kumar, M. S. Katsiotis, T. Karagiannis, M. Fardis, N. Panopoulos, H. J. Kim, M. Beazi-Katsioti, and G. Papavassiliou. Ultrafast Stratified Diffusion of Water inside Carbon Nanotubes; Direct Experimental Evidence with 2D D–T_2 NMR Spectroscopy. *The Journal of Physical Chemistry C* 122, no. 19 (2018): 10600-06. https://dx.doi.org/10.1021/acs.jpcc.8b01377.

Supramolecular interaction between macrocyclic Gd (III) complexes and polyaromatic systems as innovative way to enhance relaxivity

Enza Di Gregorio, Silvio Aime, Eliana Gianolio, Giuseppe Ferrauto

Molecular Biotechnology Center, Dept of molecular biotechnologies and health sciences, University of Torino (IT)
E-mail: giuseppe.ferrauto@unito.it

Introduction

MRI is the election imaging technique for the diagnosis and monitoring of numerous diseases. About 40–45% of MRI scans (*ca*. 38 million *per* year) are performed with the use of Gadolinium based contrast agents (GBCAs).

The recent findings related to NSF and Gd-retention strongly required caution in the use of GBCAs [1]. Chemistry becomes central in looking for i) more stable and ii) more efficient GBCAs (*i.e*. enhanced relaxivity). Different routes to enhance relaxivity were exploited as i) the *set-up* of non-covalent binding interactions with macromolecules present in solution (*e.g.* albumin), ii) the increase of the number of coordinated or second sphere water molecules, iii) the increasing of prototropic exchange rates [2, 3].

Herein, we describe the increase of relaxivity attainable through reversible binding interactions between the hydrophobic region of macrocyclic GBCAs and SO^{3-}/OH containing pyrene derivatives (Fig. 1a).

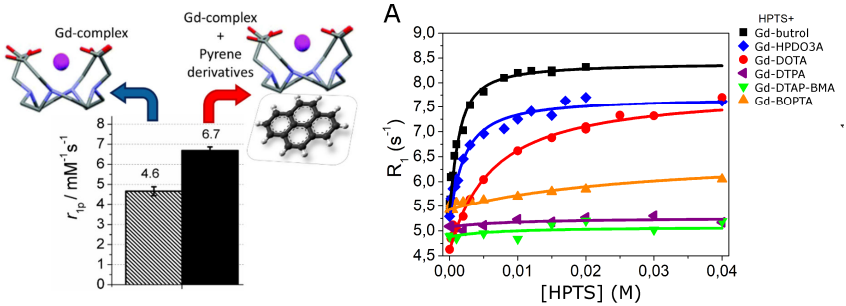

a *b*

Figure 1. a) Enhancement of relaxivity upon supramolecular interaction with pyrene derivatives. b) R_1 of GBCAs (1mM) in the presence of HPTS at variable concentration (0-40 mM)

Methods

Macrocyclic (ProHance, Gadovist, Dotarem) and linear (Magnevist, Omniscan, MultiHance) GBCAs were tested. The increase of relaxivity upon the addition of SO^{3-}/OH containing pyrene derivatives was assessed by ^{1}H-relaxometry and ^{1}H- / ^{17}O-NMR. The binding parameters K_a (*association constant*) and R_b (*relaxivity of the adduct*) between GBCAs and the pyrene derivatives were calculated by using the PRE technique (0.5 T). ^{1}H NMRD profiles were measured *w* or *w/o* of pyrene derivatives at variable B_0 (0.00024 to 1.5 T).

Insights into the formation of the adduct were obtained by high resolution ^{1}H-NMR of YbHPDO3A complex w or w/o of pyrene derivatives (14 T).

Finally, the in vivo proof of concept of the enhancement of contrast was obtained by MRI of tumor-bearing mice pre and post injection of GBCA (7 T) upon injection of Gd-HPDO3A (0.15 mmol/Kg) or Gd-HPDO3A/HPTS adduct (0.15 and 0.45 mmol/Kg).

Results and discussion

A high binding affinity of macrocyclic GBCAs toward pyrene derivatives was observed. The supramolecular adducts display a significant increase of relaxivity. No enhancement was observed for linear GBCAs (Fig. 1b). This is due to the increase of the molecular reorientation time (τ_R) and second sphere water molecules (for the presence of SO^{3-} and OH).

NMR spectra of the Yb-HPDO3A/ pyrene mixture support the formation of the supramolecular adduct. When HPTS/Gd-HPDO3A ratio is 3:1 (m/m), > 90% of Gd-HPDO3A is in the associated adduct and there is a 40% relaxation enhancement in respect to the value observed for Gd-HPDO3A alone (i.e. 6.5 $mM^{-1}s^{-1}$ vs. 9.2 $mM^{-1}s^{-1}$ in serum).

In T_{1w}-MRI of tumor-bearing mice there is the increase of signal enhancement from 53% (upon i.v. of only Gd-HPDO3A) to 125% (upon i.v. of Gd-HPDO3A/HPTS adduct) (Fig. 2).

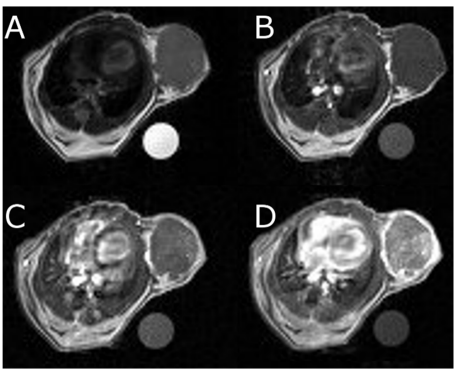

Figure 2. Representative in vivo axial MR images of tumor region in Balb/c mouse bearing subcutaneous TS/A tumor. (A) T_{2w} MR image, (B) uncontrasted (pre) T_{1w} MR image without Gd(III)-CA, (C) T_{1w} MR image after 2 min from injection of Gd-HPDO3A (0.15 mmol/kg), (D) T_{1w} MR image after 2 min from the injection of Gd-HPDO3A (0.15 mmol/kg) and HPTS (0.45 mmol/Kg)

By concluding, the reported results show a novel tool to enhance the relaxivity of GBCAs through the formation of supramolecular adducts at clinical doses.

Acknowledgements

This work received funding from Regione Piemonte (P.O.R. FESR 2014/2020 Bando IR2 – Industrializzazione dei risultati della ricerca – project "Gadoplus"). Funding was also received from the University of Torino (ex 60%, G. F.). Bracco Imaging S.p.A. is gratefully acknowledged for providing Gadoteridol.

References

1. Aime S, *et al.* Magn Reson Imaging. 2009, 30, 1259;
2. Caravan P. *et al.* Chem. Soc. Rev. 2006, 35, 512;
3. Caravan P. *et al.* Acc. Chem. Res. 2009, 42, 851.

The simple method of estimation of a retarder influence on the cement hardening process

Junko Ikeda[1,2], Kazuhisa Hayakawa[3], Innokenty Nikolaev[4,5], Leonid Grunin[4,5]

[1]Mageleka Japan Co., Ltd., 573-66, Nedo, Abiko-shi, Chiba, 270-1168, Japan
[2]Graduate School of Science and Technology, Niigata University, Niigata, Japan
[3]Hayakawa Lab. Saitama, Japan
[4]Resonance Systems GmbH. Seestrasse 28, D-73230, Kirchheim u. Teck, Germany
[5]Volga State University of Technology, Lenin sq. 3, Yoshkar-Ola, Russia
E-mail: j.ikeda@mageleka-japan.com
https://www.mageleka-japan.com

Introduction

It is known that cement mixes with water and is condensed by hydration process. Hydration is accompanied with heat generation during coagulation process, so the calorimetric method of measuring of the setting time is also well known. Calorimetric method is very sensitive but a special equipment is required. The nuclear magnetic relaxation times are very easily measured by TD-NMR and also describes physicochemical processes in the sample. In this article the simple method of measuring of the condensation degree of cement by TD-NMR is described.

Method and Results

Spin-lattice relaxation time (T_1) of the dispersion of water (50 wt %) and Hydoxypropylmethylcellulose (Metolose 90SH-15000 / Shin-Etsu Chemical Co., Ltd.) added to the cement as hardening delay adjusting agent was measured by saturation-recovery pulse sequence. The measurements were carried on at 60 °C. In addition, as the initial viscosity greatly depends on the presence or absence of Metolose the viscosity was measured. A rheometer (ONRH / OhnaTech. Inc) was used to measure the viscosity. Fig. 1 shows the relationship between viscosity and shear rate. The relationship between the relaxation time T_1 and the elapsed time is shown in Fig. 2.

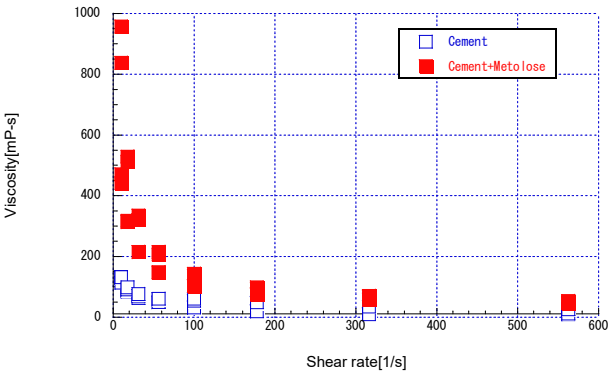

Figure 1. Initial viscosity and shear rate of cement relationship

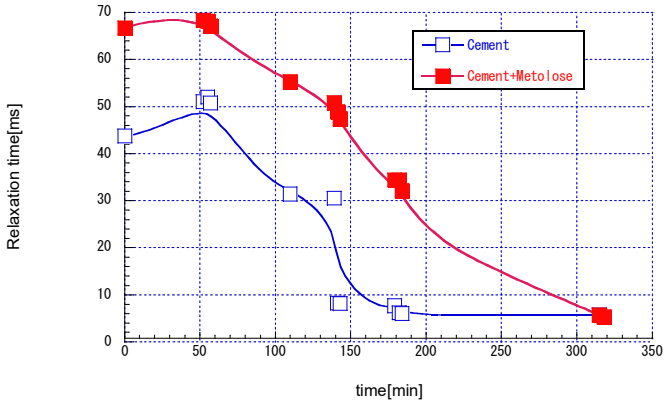

Figure 2. Relaxation time and elapsed time relationship

The T_1 of water at 60 °C is approximately 7200 ms. The relaxation time of the dispersions of cement and cement and Metolose added to water is 70 ms or less which is considerably shorter than T_1 of water. This suggests that water is constrained on the cement surface. From the relationship between the shear rate and the viscosity it can be seen that the initial viscosity in the low shear region of the dispersion containing Metolose approximately by 10 times higher than initial viscosity of the dispersion containing only cement and water. However, the initial relaxation time was shorter in the case of the dispersion containing only cement and water. For example, when a substance like gel containing no particles is measured, the stronger gel strength provides shorter relaxation time. It occurs because relaxation time has a great relationship with molecular motion. It should be noted than T_1 and T_2 behave differently with respect to molecular motion but in the region of the sample when these times are measured the relaxation time can be shortened when the molecular motion intensity decreases. However, the relaxation time was shorter for the low-viscosity cement and water-only dispersion without Metolose. It is considered that the cement restrains a lot of water and the relaxation time is short. On the other hand, it is considered that Metolose added to the dispersion is adsorbed on the surface of the cement particles and water is not easily restrained. After that the relaxation time of both dispersions became shorter over the time. It is considered that the molecular mobility of water became smaller due to the condensation of cement. When the relaxation time was 10 ms or less, the hardness was such that it could be judged that curing had started. It can be said that the hardening of cement and water mixture started in 160 minutes and in 280 minutes for the dispersion with added Metolose. This simple experiment was able to predict the cement hardening delay caused by Metolose and the hardening delay time at 60 °C.

References

1. Catherine L. Cooper, Terence Cosgrove, Jeroen S. van Duijneveldt, Martin Murray Stuart W. Prescott, *The use of solvent relaxation NMR to study colloidal suspensions,* Soft Matter, 9, 7211–7228 (2013)
2. David Fairhurst, Terence Cosgrove, Stuart W. Prescott, *Relaxation NMR as a tool to study the dispersion and formulation behavior of nanostructured carbon materials,* Magnetic Resonance in Chemistry, 54, 521-526(2016)
3. K.Hayakawa, *Relationship between adsorption behavior of methic cellulose on the cement surface and retardatin of setting time, Polymer Prepreprints*, Japan, 38(11), 3Q-07, 3705-3707(1989)

TD-NMR in study of fat melting

Maria Ivanova, Leonid Grunin

Volga State University of Technology, Lenin sq. 3, Yoshkar-Ola, Russian Federation
E-mail: manyunya1107@gmail.com, mobilenmr@hotmail.com

The need to study changes in behavior of fats during crystallization and melting is due to fat is the important component of most foods and affects their organoleptic properties. Based on results of such studies, solutions can be proposed for improving food storage technologies. The aim of this research work is to study the change in behavior of fats during melting under isothermal conditions based on NMR-relaxation data. To determine the ^{1}H NMR-relaxation parameters, Inversion-Recovery (IR) and Carr-Purcell-Meiboom-Gill (CPMG) experiments [1] were chosen.

Spin-lattice relaxation time (T_1) measurements

Butter and olive oils were used as objects of research. We kept test tubes with oils at -10 °C for 4, 8, 10 and 12 hours. Immediately after holding in the freezer, these test tubes were placed in the magnetic system of NMR analyzer 'Spin Track' [2], the temperature of which was maintained at 30 °C by the thermostat. The number of measurements when performing the single run was 100. Simultaneously with the registration of curves of longitudinal magnetization recovery the sample temperature was measured by the infrared thermometer.

Spin-spin relaxation time (T_2) measurements

Sample preparation and experimental algorithm were identical to those presented above. Samples were kept at -10 °C for 4, 8, 12 and 48 hours. We measured spin-spin relaxation times using the CPMG experiment.

Fitting of the data from IR and CPMG experiments by two independent components shows that pre-frozen oil samples contained two fractions. Separation of observed components that change with time according to their own functions indicates that the slow exchange of magnetizations took place between these fractions. Based on the significant difference in relaxation times of components, we assume that one of them was crystallized solid fraction of oil, and the other one was more mobile.

In our opinion, during melting solid fraction of sample interacting with more mobile one partially passes into molten state thus forming liquid phase with latter. This conclusion is confirmed by dependences of amplitudes A_1 and A_2 on time in experiments to study the nature of change in values of T_1 and T_2. In addition, the increase in spin-spin relaxation time of solid component T_{21} with time and sample temperature indicates the increase in mobility of molecules and the sequential partial transition to molten state. The change in value of T_{22} with time and sample temperature has the more complex character. However, we also observe the interaction between two fractions, and, ultimately, their transition to equilibrium molten state.

Based on the data of change in relative solid fraction with time, it is possible to analyze the behavior of fats during melting without resorting to registration of Free Induction Decay. This approach reveals the distribution of crystallized and molten phases of fats and can form the basis for new reliable method of analysis.

References

1. Ray Freeman. Magnetic resonance in chemistry and medicine. Oxford University Press, 2003.
2. http://www.nmr-design.com.

Sensitivity of ^{77}Se chemical shift to the selenium atom surroundings in water media

Valerii V. Karpov, Peter M. Tolstoy, Elena Yu. Tupikina

Institute of Chemistry, Saint Petersburg State University, Saint Petersburg, Russia
E-mail: valerkarp@mail.ru

Introduction

Two proteinogenic amino acids, cysteine and selenocysteine, differ from each other only by replacement of a chalcogen atom. Despite the similarity in chemical formulae, these two amino acids possess different biochemical properties what lead to various functions in organisms of human and mammals. Thus, selenocysteine was found to be a part of very important proteins that protect our bodies from oxidative damage — antioxidant enzymes (such as glutathione peroxidase family proteins GPx1-4 and GPx6 [1]). In such enzymes a selenocysteine residue is usually located in an active center of an enzyme. Also, there are some examples of selenium-containing molecules [2, 3] that possess the similar redox activity but do not resemble a selenocysteine molecule or its residue. One of the selenium-containing potential drug, Ebselen, is being under controlled clinical trial [4, 5].

Probably, a highly polarizable electronic shell of a selenium atom is a touchstone of how enzymes akin to glutathione peroxidase and selenium-containing drugs work. That is why we aimed to investigate the factors that influence on features of outer electronic shell of a selenium atom.

A novel descriptor

One of potential descriptors of Se outer electronic shell can be its chemical shift. It can be available both from quantum chemical calculations and from experiment. And indeed, nucleus of selenium-77 has a spin one half, gyromagnetic ratio of ^{77}Se is 5.115×10^7 rad·s^{-1}·T^{-1}, and its natural abundance is quite high (7.63%).

Enzyme of GPx family metabolize hydrogen peroxide and lipid peroxides. Their structures are well-defined but the mechanistic details of how they work is still not clear. Moreover, there is no understanding of all possible reaction intermediates and hights of thermodynamic barriers. In view of this, theoretical investigation can be fruitful estimating the possibility of some transition states and intermediates formation in real systems.

One of the most probable mechanism includes deprotonation of a selenolate group (R-SeH) and further nucleophilic attack of a peroxide molecule. After this reaction, the peroxide molecule is reduced and a selenium undergoes to an oxidized state (R-SeOH). Then it reacts with glutathione forming a molecule with sulfur-selenium bond (R-SeSG). Following attack of another glutathione molecule leads to a regeneration of an active cite (R-SeH) and formation of glutathione disulfide – oxidized form of glutathione. According to our calculations, an experimental supervision on these processes can be performed using NMR spectroscopy, because ^{77}Se chemical shift is expected to provide information about Se oxidation state of a selenium-containing fragment and thus about possible intermediates (Figure 1). It is important to note, that possible intermediates depend on reaction conditions, chemical structure of model system used and electron structure of its substituents when investigating these catalytic reactions experimentally [6].

Here we demonstrate the possibility of application of ^{77}Se chemical shift as a powerful tool revealing the oxidative state of a selenium atom. Due to the fact that simulation of a whole protein would have been extremely computationally costly, we use model selenium-containing systems that simulate surroundings of a selenium atom that are observed in nature and isolated selenium atom that liken potential drugs and deprotonated selenocysteine residue. Adequacy of this approach can be driven by a central role of a selenium atom in redox processes studied.

Thus, in real systems the size of substituent *R* (Figure 1) is tremendous and in our calculations *R* is taken to be $HOOCCH(NH_2)CH_2$ in case of analysis of oxidized and reduced states.

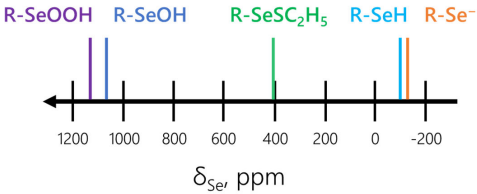

Figure 1. Calculated (MP2/aug-cc-pVDZ) ^{77}Se chemical shift of selenium-containing group within GPx1 catalytic cycle. R = $HOOCCH(NH_2)CH_2$ (in this work)

Taking into account that all mentioned catalytic processes occur in body fluids, it would have been incorrect to perform calculations in vacuum. For this very reason we performed calculation both using the CPCM polarizable conductor calculation model and adding solvent (water) molecules to the first coordination sphere of selenium (Figure 2). The former is time efficient but every so often underestimates the impact of the solvation environment, on the contrary, the latter is quite computationally expensive but is capable to provide reliable thermodynamic barriers data. In our work we have compared calculated NMR data obtained from these two methods with experimental values. It is also important to note that quantum simulations of different model systems can be controversial in terms of intermediates and transition states, that is why it is a vital task to give consideration to the solvent media correctly when describing relational systems.

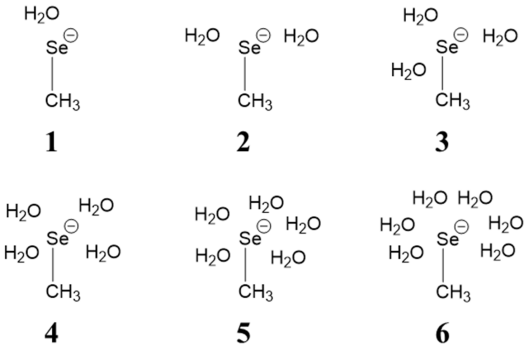

Figure 2. Model systems investigated in our work

Computational details

The calculations were performed using Gaussian16 software package.

Selenocysteine and its derivatives model systems were used in analysis of dependence chemical shift – oxidation state. Geometry optimization and vibrational frequencies calculation were performed on CCSD/aug-cc-pVDZ level of theory. ^{77}Se chemical shielding constants were calculated on MP2/aug-cc-pVDZ using equilibrium geometries obtained by the coupled cluster method.

In the study of hydration $SeCH_3(-)\cdot nH_2O$ (n = 1, 2, 3, 4, 5 and 6) model systems were used. Geometry optimization, vibrational frequencies calculation and chemical shielding calculation were performed on MP2/aug-cc-pVDZ level of theory.

Chemical shifts of selenium atoms were calculated as $\delta = \sigma_{ref} - \sigma$, where σ_{ref} is a shielding constant of dimethyl selenide (2034.37 ppm).

Acknowledgements

This work was financially supported by the RSF grant 20-73-00099. The calculations were performed in the Computer Center of Saint-Petersburg University Research Park (www.cc.spbu.ru).

References

1. R. Brigelius-Flohé, M. Maiorino. – *Biochim. Biophys. Acta.*, **1830**, 3289–3303 (2013);
2. I. Domracheva, A. Gulbe, E. Paegle, P. Arsenyan. – *Chem. Heterocycl. Compd.*, **52**, 551–554 (2016);
3. A. Müller, E. Cadenas, P. Graf, H. Sies. – *Biochem. Pharmacol.*, **33**, 3235–3239 (1984);
4. J. Kil, E. Lobarinas, C. Spankovich, S. K. Griffiths, P. J. Antonelli, E. D.Lynch, C. G. Le Prell. – *Lancet*, **390**, 969-979 (2017);
5. A. L. Sharpley, C. Williams, A. A. Holder, B. R Godlewska, N. Singh, M. Shanyinde, O. MacDonald, P. J. Cowen. – *Psychopharmacology (Berl.)*, **237**, 3773-3782 (2020);
6. D. Bhowmick, S. Srivastava, P. D'Silva, G. Mugesh. – *Angew. Chem. Int. Ed.,* **54**, 8449-8453 (2015).

Two-frequency flat gradiometer for searching explosives hidden under clothing – modeling and experiment

Rustem R. Khusnutdinov[1], G. V. Mozzhukhin[2], A. Konov[1], B. Z. Rameev[2], Yavuz Ozturk[2]

[1]Institute of Electric Power Engineering and Electronics, Kazan State Power Engineering University, Kazan, Russia
[2]Gebze Institute of Technology, Gebze, Turkey
E-mail: khrr@yandex.ru

Introduction

The methods of remote nuclear quadrupole resonance (NQR) detection of explosives and narcotics have been a subject of research for many years (see in [1-3]). Through the development of advanced electronic components, procedures, analysis and signal processing, noise reduction systems, designs spectrometers and sensors become possible to significantly increase the sensitivity of the method. In particular, expanded class of compounds which has been possible to detect. Suitable method for authentication of drugs.

Method two- and three-frequency excitation is used to increase the sensitivity in the detection of the weak NQR signals. In [4-7] is designed dual-frequency theory proposed dual-frequency excitation and multiple-pulse sequence. In [68-10] proposed composite pulses, allowing the signal to move on nonirradiated NQR transition. This technique reduces the "dead time" caused by an overload circuit excitation pulse.

In practice, not always possible to place the object of study (the human body, luggage, mines) inside the sensor NQR spectrometer. In such cases, are flat or surface sensors. Typically circuit inductor is a special form . Of a sufficient number should highlight reel type gradiometer. In [10-12] calculated and shown as the design gradiometer with two related paths created RF field opposite direction allows you to subtract from the final signal noises. Later [13] developed a coil-type gradiometer survey offered a variety of design circuits.

This paper shows the possibility of combining the two-frequency technique and flat type gradiometer coils.

Calculation and simulation

In compliance with the theory for the application of the two-frequency NQR want to use two mutually orthogonal coils. It to be analyzed in the irradiated region where the two RF fields are perpendicular, each of which corresponds to its NQR frequency transition. The accuracy with which the generated orthogonal to the most important single-crystal samples, in which the direction of the axes gap strictly correspond to the crystal axes. In practical terms, we have to deal with powders, in which the nucleus with randomly oriented. This allows you to enter orthogonal deviation of 5-10%. Another challenge is that for any surface coil is important to get the greatest possible distance from the surface of the coil, allowing to fix NQR signals.

To search the area of fields' orthogonality we simulated spatial distribution of the RF magnetic field. We modeled some of the most common types of surface coils:

– a circle round; two circular coils; spiral; two spirals.

In our simulation we calculated constant magnetic field from the coils of different shape. It is possible to substitute RF magnetic field from the alternating current to the constant magnetic field from the direct current because our main interest is the area of the magnetic field orthogonality. Furthermore it is possible, because the length of the electromagnetic wave (tens of meters) is greater than the characteristic size of the conductor. For modeling of the magnetic field from the conductor of arbitrary shape *we* used Biot-Savart-Laplace law in differential form:

$$d\vec{\mathbf{B}}\left(\vec{\mathbf{r}}_0\right)=\frac{\mu_0}{4\pi}\cdot\frac{I\cdot\left[d\vec{\mathbf{r}}\times\left(\vec{\mathbf{r}}_0-\vec{\mathbf{r}}\right)\right]}{\left|\left(\vec{\mathbf{r}}_0-\vec{\mathbf{r}}\right)\right|^3} \tag{1}$$

where $\vec{\mathbf{r}}_0$ is the radius-vector of the point where the magnetic field is calculated, $\vec{\mathbf{r}}$ – the radius vector of the current conductor element, $d\vec{\mathbf{r}}$ – vector of the current's element; the direction of this vector coincide with current direction; the length of the vector equal to the conductor's element length.

The resulting data were normalized to the length of the conductor. The number of elements in the division conductor N = 60,000.

Calculations were performed using a program written in C++ IDE MVS 2005.

The amplitudes and vectors of magnetic field in the case of one field are shown in Fig. 1.

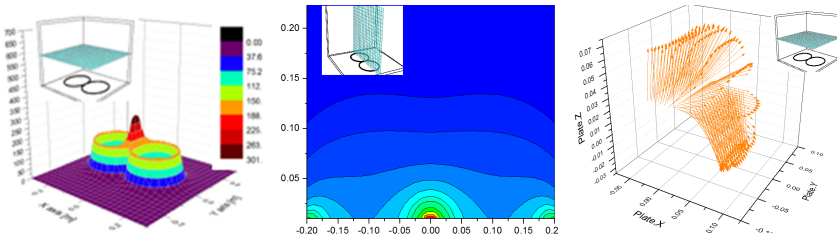

a) *b)* *c)*

Figure 1. Simulation of amplitude and direction of magnetic field for different configuration of coils: a) magnetic field amplitude from the two-loop coil – perpendicular to the plane of this coil; b) the same on parallel plane; c) vector of magnetic field

The simulation for the two intersecting fields was performed for the same types of coils. The area of magnetic field orthogonality was calculated using scalar product of the vectors as follows:

$$\cos\left(\angle\left(\vec{\mathbf{B}}_1\vec{\mathbf{B}}_2\right)\right)=\frac{\vec{\mathbf{B}}_1\cdot\vec{\mathbf{B}}_2}{\left(\left|\vec{\mathbf{B}}_1\right|\cdot\left|\vec{\mathbf{B}}_2\right|\right)}=\frac{B_{1x}\cdot B_{2x}+B_{1y}\cdot B_{2y}+B_{1z}\cdot B_{2z}}{\left(\left|\vec{\mathbf{B}}_1\right|\cdot\left|\vec{\mathbf{B}}_2\right|\right)} \tag{2}$$

where $\vec{\mathbf{B}}_1\cdot\vec{\mathbf{B}}_2$ – is a scalar product of magnetic field vectors, $\left|\vec{\mathbf{B}}_1\right|$, $\left|\vec{\mathbf{B}}_2\right|$ – vectors' lengths.

The cosine of the angle between the two vectors is calculated for each point in space, in which magnetic fields of the coils was previously calculated. During calculations $\Delta\varphi$ = 5° or 10° angle deviation was allowed:

$$\cos\left(\frac{\pi}{2}+\Delta\varphi\right)\le\cos\left(\angle\left(\vec{\mathbf{B}}_1\vec{\mathbf{B}}_2\right)\right)\le\cos\left(\frac{\pi}{2}-\Delta\varphi\right) \tag{3}$$

where $\Delta\varphi$ is the allowable deviation of the angle between the vectors, which was taken as 5° and 10°.

This deviation is allowed, since the powders in contrast to the random orientation of the crystals present in the nuclei of the sample space. The corresponding vector fields are shown in Figure 2.

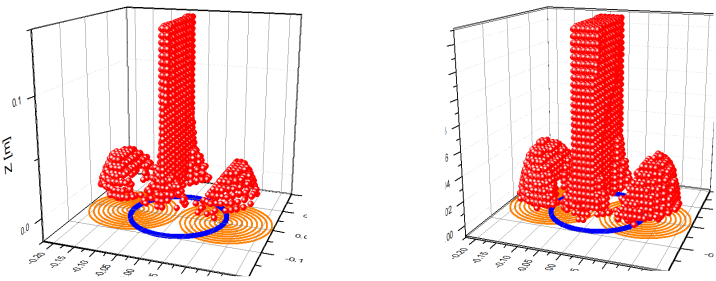

a) *b)*

Figure 2. Space distribution of the points for which the angle between magnetic fields from two coils are orthogonal. The deviation from 90 degrees + / – 5 and + / –10 are shown in a) and b), respectively

Experimental

Measurements were performed on a spectrometer Apollo Tecmag. NQR experiments were carried out on *Apollo Tecmag* NQR/NMR console (0.1−100 MHz) with two-channel transmitter and one-channel receiver modules. The sample of RDX explosive was in the form of about 120 g of a plastic mixture placed inside a tube. The resonance frequencies set contains the following parameters: $\nu_+ = 5047$ kHz (transition between states $0 \rightarrow +1$), $\nu_- = 3359$ kHz (transition between states $0 \rightarrow -1$) and $\nu_0 = 1688$ kHz (transition between states $-1 \rightarrow +1$). Apply a simple two-frequency NQR method. Impulse frequency thumbed ν_0, then applied spin-locking pulse series at the frequency of ν_- [7].

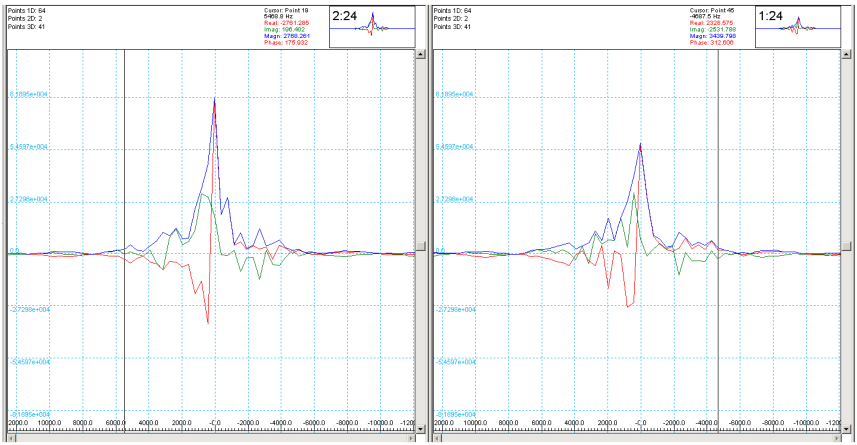

Figure 6. the results of the application the two frequency NQR sensor for human body detection: a) two frequency signal; b) one frequency signal. The distance between surface coil and sample is near 5 cm

References

1. Explosives Detection using Magnetic and Nuclear Resonance Techniques. Series: NATO Science for Peace and Security Series. Subseries: NATO Science for Peace and Security Series B: Physics and Biophysics. Fraissard, Jacques; Lapina, Olga (Eds.) Springer, 2009, 295 p., ISBN: 978-90-481-3060-3.
2. Magnetic Resonance Detection of Explosives and Illicit Materials. Series: NATO Science for Peace and Security Series B: Physics and Biophysics, Apih, T.; Rameev, B.; Mozzhukhin, G.; Barras, J. (Eds.)Springer 2014, X, 168 p. 84 illus., 50 illus. in color
3. G.V. Mozzhukhin, B.Z.Rameev, Nuclear Quadrupole Resonance, In Book: Subsurface sensing (Eds. A.S. Turk, A.K. Hocaoglu, A.A. Vertiy), Wiley-Interscience, ISBN: 978-0-470-13388-0, Hardcover, 920 pages, September 2011, (429-450).
4. Two-frequency saturation in pulsed NQR of14N //V. S. Grechishkin,G. V. Mozzhukhin, N. Ya. Sinyavskii, E. V. Yurepina //Russian Physics Journal 07/1988; 31(8):647-649.
5. Theory of two-frequency excitation in 14 N NQR //D. Ya. Osokin, R. R. Khusnutdinov // Applied Magnetic Resonance 01/2003; 24(2):145-156.
6. Two-frequency multiple-pulse sequences in nitrogen-14 NQR //D. Ya. Osokin,R. R. Khusnutdinov,V. A. Shagalov //Applied Magnetic Resonance 05/2004; 25(3):513-521.
7. The two-frequency nuclear quadrupole resonance for explosives detection.// G. V. Mozjoukhine // Applied Magnetic Resonance. 05/2012; 18(4):527-535.
8. Two-frequency composite pulses in NQR //D. Ya. Osokin, R. R. Khusnutdinov //Applied Magnetic Resonance 01/2006; 30(1):7-11
9. Three-Frequency Composite Multipulse Nuclear Quadrupole Resonance Technique for Explosive Detection // G. V. Mozzhukhin, B. Z. Rameev, R. R. Khusnutdinov, N. Doğan, B. Aktas// Applied Magnetic Resonance 08/2013; 43(4).
10. The Application of the Two Frequency Composite Pulses for NQR Detection of Nitrogen-Based Compounds//G. V. Mozzhukhin, B. Z. Rameev, N. Doğan, B. Aktaş //Journal of Superconductivity and Novel Magnetism 04/2012; 24(1):653-658.
11. A Two-Spiral Flat Coil for Detecting 14 N NQR Signals//G. V. Mozzhukhin,A. V. Efremov,A. V. Bodnya,V. V. Fedotov// Russian Physics Journal 01/2005; 48(9):978-983.
12. Noise-Immune Coil for Unshielded Magnetic Resonance Measurements //Journal of Magnetic Resonance, Volume 131, Issue 1, March 1998, Pages 154-158//B.H. Suits, A.N. Garroway, J.B. Miller
13. Optimizing surface coils and the self-shielded gradiometer //B. H. Suits, A. N. Garroway
14. Simulation of nuclear quadrupole resonance for sensor probe optimization //Junichiro Shinohara, Hideo Sato-Akaba, Hideo Itozaki

Modeling the system of the melt of carbosilane dendrimers

Naira R. Khusnutdinova, Denis A. Markelov

St. Petersburg University, 7-9 Universitetskaya Emb., St Petersburg 199034, Russia
E-mail: nai.khus@yandex.ru

Introduction

Dendrimers are synthetic polymers, macromolecules in which the three-dimensional structure is formed by the regular branching from a single focal point. Branching is usually organized by three structural building blocks: the core block; repeating blocks and the functional groups. The study of structural properties of dendrimers is very important for understanding their physical behavior and interactions with the environment and with other compounds. These studies are also important in the design of structures and in the discovery of new applications. One important application, where translational mobility data can be utilized, is nanoparticle synthesis [1] and drug delivery.

In this work we study the melt of poly(butyl)carbosilane (PBC) dendrimers of different generations (G = 2, 3, and 4) at 600 K by molecular dynamics (MD) simulations.

Computer modeling details and results

A detailed description of the atomic model for dendrimers, the modeling method, including procedures for preparing and balancing the system, are given in [2]. The main details of modeling: two cubic cells for modeling were considered, containing 27 and 125 dendrimer macromolecules. Periodic boundary conditions and the force field Gromos53a6 were used in the Gromacs-4.5.5.2 package [3]. Depending on the number of dendrimer generations the equilibration of the systems was from 100 ns to 400 ns. The MD simulations were continued for 200-2000 ns to collect data to calculate system performance.

To establish the fact of reaching the diffusion mode, the following criterion was used: the slope of the time dependences of mean-square displacement, MSD(t), in a double logarithmic scale should be close to 1.

It was found that before the diffusion regime, a subdiffusion regime is observed, in which the slope of the curve is less than 1 and varies for different generations. This mode is determined by correlations between the autocorrelation function of dendrimer velocities (VACF, C (t)). The slope of the VACF velocity - β should be correlated with the slope of the subdiffusion by the expression Slope (MSD) + |Slope (VACF)| = 2. Our simulation results are close to the expected value of β. Thus, we can conclude that in PBC dendrimer melts a wide region of the subdiffusion regime is observed. It is important to note that this subdiffusion regime was absent in the same dendrimers in a solution [4].

Acknowledgements

Helpful discussions with Dr. Maxim Dolgushev are gratefully acknowledged. MD simulations were carried out in the computing resource center of St. Petersburg State University. This work is supported by Russian Science Foundation (grant № 19-13-00087).

References

1. Yamamoto K. et al. New Horizon of Nanoparticle and Cluster Catalysis with Dendrimers // Chem. Rev. American Chemical Society, 2020. Vol. 120, № 2. P. 1397–1437.
2. Shishkin A.N.; Markelov D.A.; Matveev V.V. Molecular Dynamics Simulation of Poly(butyl)carbosilane Dendrimer Melts at 600 K // Russ. Chem. Bull, 2016. P. 67–74.
3. Abraham M.J. et al. Gromacs: High performance molecular simulations through multi-level parallelism from laptops to supercomputers // SoftwareX. 2015.

4. Khusnutdinova, N. R.; Markelov D.A. Modeling the system of the carbosilane dendrimer of various generations. Magnetic Resonance and Its Applications. Spinus-2020, 2020. P. 93–95

Operando 3D MRI visualization of complex heterogeneous catalytic system using parahydrogen

Elizaveta S. Kononenko, Alexandra Svyatova[1,2], Kirill V. Kovtunov[1,2], Alexey Fedorov[3] and Igor V. Koptyug[2]

[1]Novosibirsk State University
[2]International Tomography Center (ITC SB RAS), Novosibirsk
[3]Department of Mechanical and Process Engineering, ETH Zürich, Switzerland
E-mail: elizaveta.kononenko@tomo.nsc.ru

Introduction

Nuclear magnetic resonance (NMR) and magnetic resonance imaging (MRI) are widely used to provide information about catalytic reactions. Operando imaging of selective heterogeneous hydrogenation of alkynes and dienes has an industrial importance. However, MRI has several limitations, especially during the studies of gas phase, where the spin density of the reactants and products is much lower comparing with the spin density in the liquid phase. In addition, inhomogeneities of the magnetic field caused by the catalytic reactor, rapid diffusion of gases, and short relaxation times of their nuclear spins further complicate the study. Hyperpolarization methods, for example, parahydrogen-induced polarization (PHIP) can help to overcome the limitations associated with low spin density and make possible MRI visualization of hydrogenation processes in the gas phase. The use of model glass tube catalytic reactors with a thin layer of catalyst deposited on them significantly reduces the inhomogeneities of the magnetic field, and the suitable choice of the pulse sequence allows one to get over the limitations associated with diffusion and short relaxation times.

Spatially resolved NMR spectroscopy of heterogeneous gas phase hydrogenation with parahydrogen

In the previous study [1], it was shown that model glass tube catalytic reactor minimizes magnetic field inhomogeneities. Therefore, in this work, 16 glass tube reactors containing Pd, Pt, Rh or Ir nanoparticles dispersed on a thin layer of TiO_2, CeO_2, SiO_2 or Al_2O_3 were used in the hydrogenation of 1,3-butadiene using parahydrogen [2].

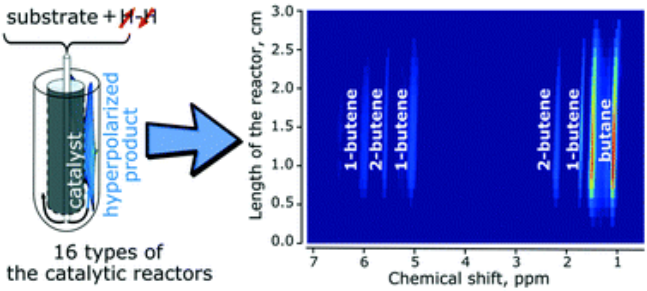

Figure 1. Experimental scheme of spatially resolved NMR visualization of 1,3-butadiene hydrogenation reaction over Ir/SiO_2 catalyst with parahydrogen (from [2])

Gas phase ^{1}H NMR spectra allowed insights into the reaction mechanism of the 1,3-butadiene hydrogenation reaction on those catalysts to be obtained. It was shown that the catalysts containing Ir and Rh nanoparticles demonstrate the highest polarization level in the products, while the catalysts with Pd nanoparticles are the most selective ones towards butene. Spatially resolved ^{1}H NMR spectroscopy with Ir/SiO_2 and Rh/CeO_2 catalysts gave further

mechanistic insight into the reaction by mapping the reagent and product distribution along the length of the reactors. It was shown that in the experiments with Ir/SiO_2 catalyst, the reaction products were distributed along the whole reactor indicating high reaction rates (Fig. 1). The resulted product distribution allowed to suggest that butane is the secondary reaction product. In addition, it was shown that during hydrogenation over the Rh/CeO_2 catalyst butane is formed faster from 1-butene than from 2-butene.

3D MRI of heterogeneous gas phase hydrogenation with parahydrogen

To optimize the operation of a heterogeneous reactor, an important task is to visualize the distribution of reagents and products separately from each other inside an operating reactor. Therefore, this part of the study demonstrates the possibility of selective MRI in the complex catalytic system containing 3 different catalyst coatings (Pd/SiO_2, Rh/SiO_2, Pt/SiO_2) distributed along the axis of a glass tube. Selective MR imaging was done using true-FISP pulse sequence in a pseudo-3D mode. Eight 2D slices with 3 mm thickness were detected one after another, then they were converted into a 3D model using MATLAB (Fig. 2), the resulted spatial resolution was 0.625×0.625×3 mm3/pixel. For each reactant and product, ^1H MRI was done with parahydrogen (pH_2) and normal hydrogen (nH_2) to analyze areas of preferred formation of hyperpolarized products. It was shown that 1-butene is predominantly formed near the reactor surface with Rh nanoparticles. The formation of the hyperpolarized 2-butene was preferentially observed in regions where Rh and Pd were located. As for the hyperpolarized butane, it was preferentially formed on the Pd/SiO_2 catalyst and to a lesser extent on the Pt/SiO_2 catalyst. These results demonstrate the possibility to use MRI as a highly sensitive operando method for detailed studies of the catalytic processes in heterogeneous systems.

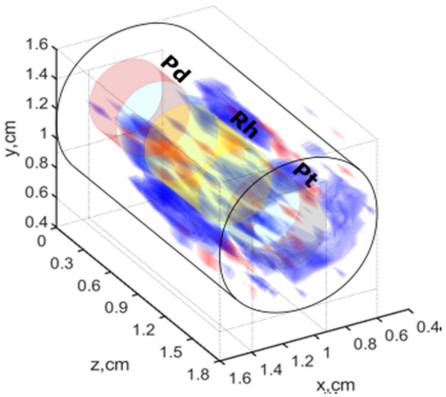

Figure 2. Selective ^1H MRI of hyperpolarized gas without contribution of thermally polarized gas. The selective imaging was done using CH_2 group of 1-butene obtained during heterogeneous hydrogenation of 1,3-butadiene with pH_2 or nH_2. The reaction conditions are: 1,3-butadiene : pH_2 (or nH_2) ratio = 1 : 2, 1.9 mL s^{-1} flow rate, 70 °C. Three areas with the catalysts Pd/SiO_2, Rh/SiO_2, Pt/SiO_2 are labelled. The blue volume around the reactor indicates the formation regions; the red color indicates the consumption regions of 1-butene

Currently, a comparison of experimental data and simulations for the TrueFISP pulse sequence is being carried out for the case of equilibrium and hyperpolarized NMR signals. TrueFISP sequence is shown to be more efficient compared with the FLASH sequence. This analysis will expand the scope of PHIP for MRI.

Acknowledgements

This work was supported by the Russian Science Foundation (grant # 19-13-00047).

References

1. K.V. Kovtunov et al. – ChemCatChem, 11, 969-973 (2018).
2. A. Svyatova et al. – Catal. Sci. Technol, 10, 99–104 (2020).

The ^{1}H NMR and MD study of the interaction of the antiviral agent glycyrrhizin with lipid membranes: an effect on lipid mobility and membrane fusion

Polina A. Kononova[1,2], Ekaterina A. Shelepova[1], Olga Yu. Selyutina[1,3], Nikolay E. Polyakov[1,3]

[1]Voevodsky Institute of Chemical Kinetics and Combustion, Novosibirsk, Russia
[2]Novosibirsk State University, Novosibirsk, Russia
[3]Institute of solid state chemistry and mechanochemistry, Novosibirsk, Russia
E-mail: kononova_polina@bk.ru

Introduction

Glycyrrhizin (glycyrrhizic acid, GA, Fig. 1) is a triterpene glycoside (saponin), the main active component of the licorice root, which is widely used in Chinese medicine. Due to its amphiphilicity, glycyrrhizin is capable of forming micelles and inclusion complexes with drugs in aqueous and aqueous-alcoholic solutions. Many studies show that GA has a wide spectrum of biological activity (antiviral, anti-inflammatory, antioxidant, etc) [1-4]. Glycyrrhizin can inhibit the replication of various viruses, including SARS-coronovirus. In addition, a number of studies have recently appeared indicating the promising use of GA for the therapy of SARS-CoV-2 [5, 6]. Different studies indicates that the mechanism of GA action is connected with the interaction with cell or virus membrane. Therefore, the purpose of this work is to investigate the interaction of glycyrrhizin with cell membranes.

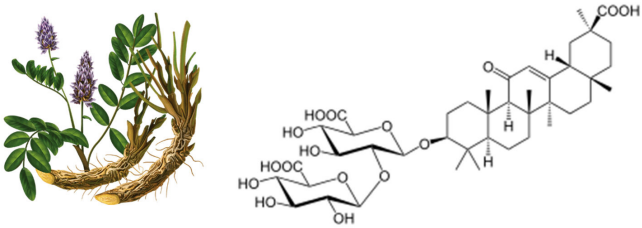

Figure 1. Licorice root glycoside – glycyrrhizic acid

Methods

As a model membrane, liposomes of DOPC, DPPC and POPC were chosen. The NMR spectroscopy allows an observation of the various functional groups of the phospholipid. The addition of paramagnetic ions (shift-reagents) separates the signal from the inner and outer layers of the lipid bilayer. GA influence on the mobility of lipid molecules was studied by NMR-relaxation technique. The spin-spin (T_2) and spin-lattice (T_1) relaxation times are very sensitive to the mobility of the observed groups of protons, so, using NMR technique one can make an assumption about glycyrrhizin localization in the membrane. The T_1 relaxation parameter is sensitive to high frequency lipid motions such as trans-gauche methylene isomerization, whereas the T_2 time is sensitive to low frequency lipid motions (lateral diffusion) [7, 8]. Also, the effect on molecular mobility was characterized by the determination of the change of the phase transition temperature. To confirm assumptions about glycyrrhizin localization in the membrane, molecular dynamics simulation was also carried out.

Results

A strong dependence of lipid mobility on glycyrrhizin concentration was detected. The decrease of the spin-lattice relaxation times with increasing glycyrrhizin concentration for all types of liposomes was observed. It could mean that glycyrrhizin incorporates into lipid

bilayer, affecting the mobility of the lipids. This hypothesis was also confirmed by the results of molecular dynamics simulation, which demonstrated that GA could incorporate into membrane and to form the stable self-associates inside the membrane.

Molecular dynamics simulations show that the formation of GA self-associates in lipid bilayer depends on bilayer composition. NMR experiments show that the effect of GA on the spin-spin relaxation times is observed only for DPPC liposomes and for mixture of DPPC and DOPC. There is no effect of GA for less ordered lipid DOPC (Figure 2). It could mean that glycyrrhizin tends to form associates in more ordered membranes.

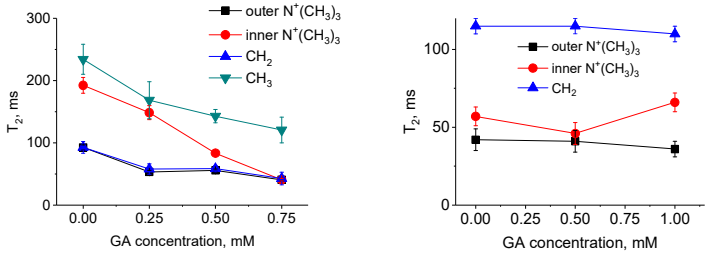

Figure 2. The dependence of spin-spin relaxation time on GA concentration a) in DPPC-DOPC mixture, b) in DOPC

It is known that the process of self-association of glycyrrhizin depends on the acidity of the medium [9]. Therefore, we studied the effect of pH on glycyrrhizin behavior in membrane. The ^{1}H NMR spectra of phospholipid POPC with glycyrrhizin shows a drop in intensity and an increase in signal width, when pH gradually increases. This may indicate membrane fusion and consequent broadening and disappearing of the signal from large liposomes. The spin-spin relaxation time decreases with increasing pH for DOPC with glycyrrhizin. We suggest, that glycyrrhizin in the deprotonated form (in the neutral and alkaline media) accumulates on the membrane surface; in the protonated form GA is located inside the lipid bilayer. These results are also confirmed by molecular dynamics simulation.

The study of the phase transition temperature was performed with DPPC liposomes and DPPC-DOPC liposomes. Glycyrrhizin increases the collectivity of the phase transition (smaller phase transition width) and increases its temperature (Fig. 3).

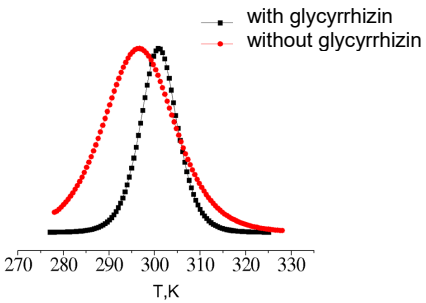

Figure 3. Phase transition in the lipid membrane. Change in the temperature and the collectivity of the transition in the presence of 0.75 mM of glycyrrhizin

Discussion and Conclusions

It was found that glycyrrhizin has an effect on lipid mobility. A decrease in lipid molecular mobility was observed with an increase in glycyrrhizin concentration. We assume that this is due to penetration of glycyrrhizin molecules into bilayer and formation of glycyrrhizin associates in ordered bilayers. In the deprotonated form, the glycyrrhizin only sticks to the surface of the lipid membrane. Lipids are greatly involved in the processes of the fusion of the viral particle with the host cell, and glycyrrhizin, affecting the lipid mobility, could influence this process. Obtained results are important for understanding the mechanisms of glycyrrhizin biological activity, in particular, in aspects of GA use as antiviral agent affecting virus-cell membrane fusion.

Acknowledgements

The study was financially supported by the Council for grants of the President of the Russian Federation (grant № MK-1580.2021.1.3).

References

1. Fiore C, Eisenhut M, Krausse R, Ragazzi E, Pellati D, Armanini D, Bielenberg J., Antiviral effects of Glycyrrhiza species, Phytother Res. 2008; 22(2):141-8;
2. Lee Jia Ming and Adeline Chia Yoke Yin, Sun ZG, Zhao TT, Lu N, Yang YA, Zhu HL, Research Progress of Glycyrrhizic Acid on Antiviral Activity, Mini Rev Med Chem. 2019;19(10):826-832;
3. Pompei R, Pani A, Flore O, Marcialis MA, Loddo B, Antiviral activity of glycyrrhizic acid, Experientia. 1980, 36(3):304
4. Selyutina O.Yu., Polyakov N.E. Glycyrrhizic acid as a multifunctional drug carrier – From physicochemical properties to biomedical applications: A modern insight on the ancient drug // International Journal of Pharmaceutics. 2019. V. 559. C. 271–279.
5. Julian Chrzanowski Alicja Chrzanowska Wojciech Graboń, Glycyrrhizin: An old weapon against a novel coronavirus, Phytotherapy Research, 2020 https://doi.org/10.1002/ptr.6852
6. Christian Bailly. Gérard Vergoten, Glycyrrhizin: An alternative drug for the treatment of COVID-19 infection and the associated respiratory syndrome? Pharmacology & Therapeutics Volume 214, 2020, 107618, https://doi.org/10.1016/j.pharmthera.2020.107618
7. J. Gabrielska, M. Gagoś, J. Gubernator, W.I. Gruszecki, Binding of antibiotic amphotericin B to lipid membranes: a 1H NMR study, FEBS Lett. 580 (2006) 2677–2685, https://doi.org/10.1016/j.febslet.2006.04.021.
8. J.F. Ellena, L.S. Lepore, D.S. Cafiso, Estimating lipid lateral diffusion in phospholipid vesicles from carbon-13 spin-spin relaxation, J. Phys. Chem. 97 (1993) 2952–2957, https://doi.org/10.1021/j100114a021.
9. Petrova, S., Schlotgauer, A., Kruppa, A., et al. Self–Association of Glycyrrhizic Acid. NMR Study // Zeitschrift für Physikalische Chemie. 2016. V. 231. C. 839–855.

Ferromagnetic resonance of magnetic multilayered structures

Oksana Koplak[1,2], Roman Morgunov[1,2]

[1]Institute of Problems of Chemical Physics, 142432 Chernogolovka, Russia
[2]I.M. Sechenov First Moscow State Medical University, Ministry of Health of Russia, 119991 Moscow, Russia
E-mail: o.koplak@gmail.com
https://sci-lab.ru/

Introduction

Engineering of magnetic multilayered structures such as logic spin valves based on giant magnetoresistance (GMR) conquers successfully a niche in the industry of magnetic memory elements, reading and recording devices, etc. [1, 2]. Series of the previous works devoted to the ferromagnetic resonance (FMR) analysis of GMR platforms (as well as CoFeB thin films) provided major contribution to understanding of spin dynamics in multilayered devices with perpendicular anisotropy [3, 4]. However exchange and magnetostatic interaction between ferromagnetic layers, contribution of nonresonant absorption dependent on magnetoresistance, spin polarization pumping by microwave power, space redistribution of spin-polarized charge carriers and many other processes contributes to FMR effects of the spin valves [5]. The aim of our work is analysys of ferromagnetic resonance in a multilayered structures MgO/CoFeB/Ta/CoFeB/MgO manifesting perpendicular magnetic anisotropy (PMA).

Anisotropic FMR spectra and asymmetry of the FMR line

The multilayer structures of MgO/CoFeB (0.9 nm)/MgO/Ta (sample I) and MgO/CoFeB (0.9 nm)/Ta(0.8 nm)/CoFeB (0.74 nm)/MgO/Ta (sample II) were grown on substrates of undoped GaAs (001) by the magnetron sputtering method. Anisotropic FMR spectra for monolayer and bilayer recorded at room temperature for different angles θ between the magnetization vector and the normal to the sample plane are shown in Fig. 1 a-c. The magnetic anisotropy constants was found from standard approximations of the resonance field dependence on polar angle. The differences between the anisotropy constants have been detected in a single-layer film of MgO/CoFeB/MgO/Ta and the spin valve MgO/CoFeB/Ta/CoFeB/MgO/Ta. These differences are explained by dipole magnetic interaction between ferromagnetic layers.

The FMR spectrum at θ = 60° was integrated and adsorption power field dependence P(H) was chosen for analysis of the lineshape (Fig. 1d). In Fig. 1d one can see approximations by common functions (two Lorenz (1) or Gauss lines (2), Landau-Lifshitz- Hilbert (3), Bloch-Bloembergen (J)). However, asymmetrical long wings of the P(H) dependence do not satisfy to standard FMR functions. Effect of ferromagnetic layers interaction or special conditions of electrical conductivity in spin valve should be considered to explain FMR line shape. The linewidth was determined by the sum of three components: the broadening of ΔHG due to the finite time damping of spin precession (defined by Hilbert parameter G), the broadening of ΔH_{2mag} due to the two-magnon scattering, and inhomogeneous broadening of ΔH_{inh}. The damping factor of spin precession 0.034 exceeds the 0.004–0.027 range convenient for applications CoFeB in spintronics. The main part of the linewidth corresponds to inhomogeneous widening. The FMR line shape can be explained by contribution of standard FMR Lorenz line and nonresonant contribution to microwave cavity Q-factor provided by inverse spin Hall effect (ISHE) due to change of the sample conductivity.

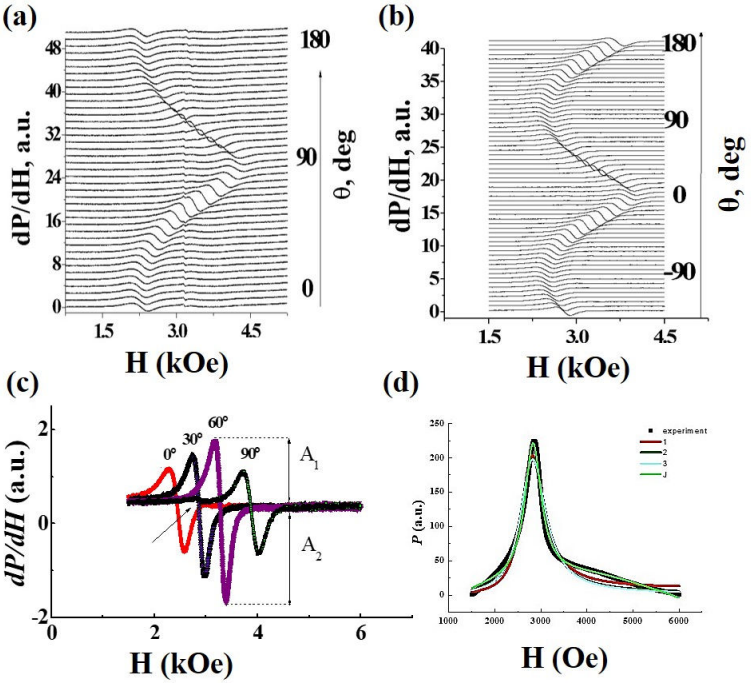

Figure 1. Series of FMR spectra for monolayer sample I (a) and bilayer sample II (b) in θ = 0-180° orientations of the magnetic field H relative of the normal to the plane of the sample. Anisotropic FMR spectra for bilayer sample recorded at 296 K for few different angles θ between the magnetization vector and the normal to the sample plane (c). The values of the angle θ are labeled in the figure. The A_1 and A_2 are amplitudes of the left and right parts of the derivation of the FMR signal. (d) FMR absorption spectra for monolayer sample I recorded in θ= 60° orientation. Solid white line is approximation described in text

Acknowledgements

This work is supported by the funding from the Ministry of Science and Higher Education of the Russian Federation (Grant No. 13.1902.21.0006).

References

1. S. Ikeda, et al. A perpendicular-anisotropy CoFeB–MgO magnetic tunnel junction, Nat. Mater. 9 (2010) 721–724.
2. X. Wang, Metallic Spintronic Devices, CRC Press, FL, USA, 2014
3. C. Li, et al. Tunable zero-field ferromagnetic resonance frequency from S to X band in oblique deposited CoFeB thin films, Sci Rep 5 (2015) 17023.
4. R. Morgunov, et al. Remote microwave monitoring of magnetization switching in CoFeB/Ta/CoFeB spin logic device, Appl. Phys. Lett. 110 (2017) 212403.
5. R. Morgunov, et al. Ferromagnetic resonance of CoFeB/Ta/CoFeB spin valves versus CoFeB film

2D NMR structure determination of 3,4-dihydro-1,2,4-triazine intermediate in novel Rh(II)-catalyzed transannulation reaction

A. Koronatov, M. Novikov

Institute of Chemistry, Saint Petersburg State University, 198504, Universitetskii prospect 26, Petergof, Saint Petersburg, Russia
E-mail: koronatov@bk.ru

Introduction

1,2,3-Triazoles are attractive compounds for various applications in different fields of chemistry. Transannulation reactions of their derivatives are usually catalyzed by transition metal complexes or light irradiation. The reactions proceed via the formation of metallocarbenes, which, when reacting with alkynes, nitriles, imines, and other unsaturated compounds, afford a wide variety of heterocyclic skeletons. Unfortunately, range of such triazoles, which could undergo aforementioned transformation, was limited to 1-sulfonyl-1,2,3-triazoles, 1-perfluoroalkyl-1,2,3-triazoles, and [1,2,3]triazolo[1,5-*a*]pyridines until recently.

However, in 2020 our research group discovered the first example of transannulation reaction with inactivated 1-alkyl-4-aryl-1,2,3-triazoles **1** with diazoesters **2** under rhodium(II) catalysis [1]. In fact, this approach gave the opportunity to synthesize variously substituted 3-alkoxy-4-pyrrolin-2-ones **3** (their structures were determined by NMR and X-ray studies). The investigation of reaction mechanism showed that it proceeded through unstable 3,4-dihydro-1,2,4-triazine **4**, which could be detected and isolated if the reaction was carefully monitored. Structure of the compound **4** in one case was proved by HRMS and NMR (^{1}H, ^{13}C and 2D NMR). On the contrary, when the aryl substituent at C4 position of triazole ring was replaced with alkyl we did not observe the transannulation product **3**, so it was proposed that stable triazole ylide **5** was formed.

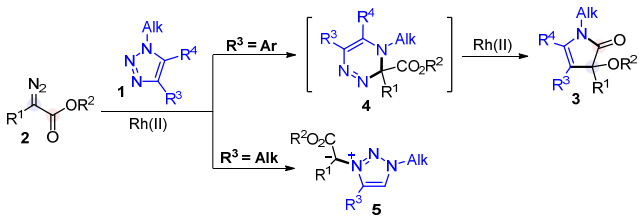

Experimental section

As was mentioned before, one of the intermediate, in particular compound **4a**, could be successfully isolated and it was shown by HRMS–ESI experiments, that it has formula $C_{14}H_{14}F_3N_3O_2$. Thus, four possible structures (**A**–**D**, figure 1) can be proposed considering the reaction mechanism.

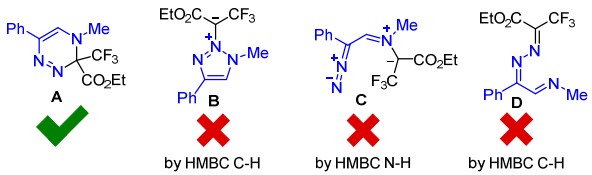

*Figure 1. Suggested structures for compound **4a***

Unfortunately, basic NMR techniques (^{1}H and ^{13}C NMR) did not reveal any additional information regarding the structure of **4a**. Therefore, 2D NMR of this compound was studied (figure 2). Obtained data was sufficient enough and we concluded that only one possible structural formula fitted all the criteria – 3,4-dihydro-1,2,4-triazine. To the best of our knowledge, it was the first example of this heterocyclic scaffold bearing such functionalization. Probably, it was the reason of its instability and, consequently, the reason why this unusual transannulation reaction proceeded.

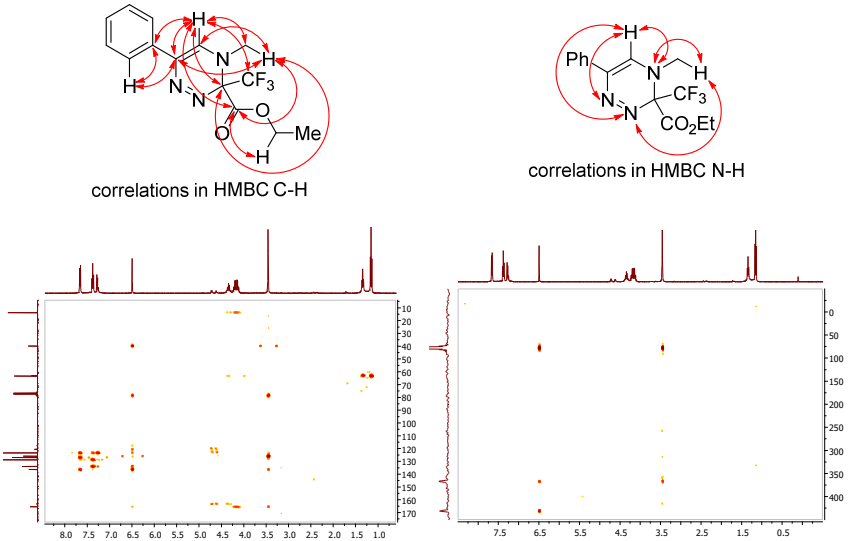

*Figure 2. Correlations in HMBC C-H and HMBC N-H spectra of **4a***

In the same manner, it was impossible to verify the structures of triazolium ylides **5** by X-ray crystallography. Consequently, we proved its structural formula by analysis of ^{1}H, ^{13}C, 2D NMR spectra and HRMS.

Acknowledgements

We gratefully acknowledge the financial support of the Russian Science Foundation (20-13-00044). This research used resources of the Magnetic Resonance Research Centre, Chemical Analysis and Materials Research Centre, Centre for X-ray Diffraction Studies, Computing Centre, and Chemistry Educational Centre of the Research Park of St. Petersburg State University.

References

1. Alexander N. Koronatov, Nikolai V. Rostovskii, Alexander F. Khlebnikov, Mikhail S. Novikov *Organic Letters* **2020**, 22, 20, 7958–7963.

The ^{1}H NMR study of lipid peroxidation processes involving chelate complexes of thiosemicarbazone Dp44mT

Vladimir E. Koshman[1,2], Olga Yu. Selyutina[1], Nikolay E. Polyakov[1]

[1]Voevodsky Institute of Chemical Kinetics and Combustion, Novosibirsk, Russia
[2]Novosibirsk State University, Novosibirsk, Russia
E-mail: kosmanvova2010@mail.ru

Introduction

Oxidative stress plays an important role in the functioning of living systems, and an important aspect of this problem is the oxidation of lipids formed the basis of the cell membrane. It is known that lipid oxidation leads to a change in the packing and ordering of the lipid bilayer [1, 2]. The study of the process of lipid peroxidation makes practical sense, since controlled oxidative stress can potentially be used in anticancer therapy. Our task was to investigate the effect of thiosemicarbazone Dp44mT (2-(Di-2-pyridinylmethylene)-N,N-dimethyl-hydrazinecarbothioamide, Fig. 1) on the process of lipid peroxidation in model systems involving iron and copper ions. Thiosemicarbazones (TSC) are of great interest to scientists from various fields of science, due to the wide range of their chemical and biological activity. Their anticancer activity has always been associated with the ability to inhibit ribonucleotide reductase. However, recent studies indicate a major role of oxidative stress in the antitumor activity of TSC [3].

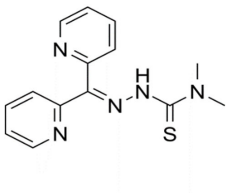

Figure 1. Structural formula of thiosemicarbazone Dp44mT

Methods

The interaction of Dp44mT-metal complexes with the lipid bilayer and their role in the reaction of lipid peroxidation was studied on model systems by ^{1}H NMR and optical spectroscopy. Linoleic acid (LA) micelles and DHPC/DLPC (dihexanoylphosphatidylcholine/dilauroylphosphatidylcholine) bicelles were choosen as model systems. The initiation rate of lipid peroxidation was studied using the decay of intensity of the signal of the bis-allylic proton. Reaction products were dried and dissolved in $CDCl_3$.

Results and Discussion

^{1}H NMR spectra of initial linoleic acid sample and the products of reaction with H_2O_2 and $FeSO_4$ are given at the Figure 2. It should be noticed that during the reaction, sediment was observed in the solution. To study the nature of this sediment, samples were centrifuged, water was removed and the sediment was dissolved in $CDCl_3$. It is noticeable that the line width of the reaction products is significantly higher than the line width of initial LA. It could mean the presence of some oligomers with the high molecular mass. So, the main oxidation products of the reaction in micelles are the polymerization products.

Kinetics of DLPC oxidation in bicelles in the reaction with H_2O_2 for samples with Dp44mT in the absence and in the presence of ascorbic acid were studied. It was found that in

the absence of ascorbic acid, Dp44mT almost completely inhibits the reaction. At the same time, in the presence of ascorbic acid, Dp44mT complexes become redox active. The changes in redox activity of chelate complexes in the presence of ascorbic acid could be caused by the formation of mixed complexes of ascorbic acid, chelator and metal ion. To test the hypothesis of formation of such mixed complexes with ascorbic acid, optical absorption experiments were done.

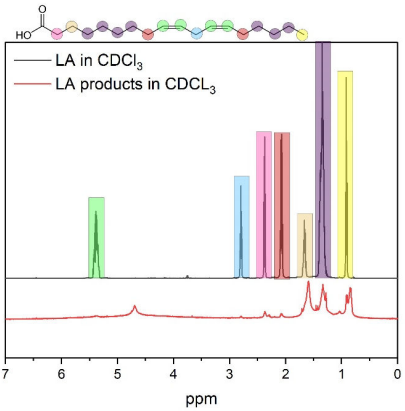

Figure 2. ^{1}H NMR spectra of LA and reaction products in $CDCl_3$ in the absence of chelators

Optical absorption spectra were recorded for the mixture of 0.05 mM of $FeSO_4$, 0.1mM of Dp44mT and ascorbic acid with the concentration in the range of 0-0.8 mM in PBS. pH remained the same and equal to 7.5 for all samples. As could be seen from Fig. 3 an additional peak at 620 nm arise with the increase of ascorbic acid concentration. Ascorbic acid has a single absorption peak at 250 nm, and Fe(III)-Dp44mT complex also do not have an absorption peak in the range of 500-700 nm. It means the formation of the mixed complexes Fe-Dp44mT-ascorbic acid.

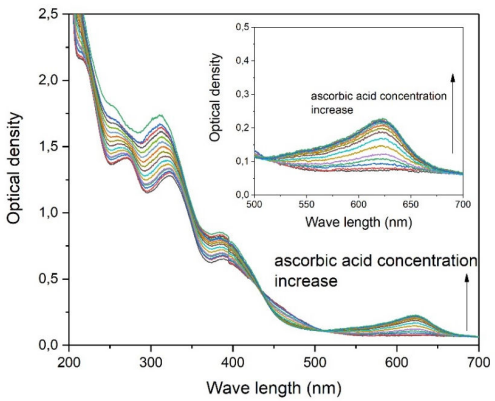

Figure 3. Optical absorption spectra of the samples containing 0.05 mM of $FeSO_4$, 0.1 mM of Dp44mT and ascorbic acid with the concentration in the range of 0-0.8 mM

Conclusions

The effect of thiosemicarbazone Dp44mT on the lipid peroxidation reaction was investigated by ^{1}H NMR spectroscopy. It was found that Dp44mT almost completely inhibits the peroxidation reaction. However, after the addition of ascorbic acid Fe-Dp44mT complexes became redox-active. This may be due to the formation of mixed complexes of ascorbic acid, chelator, and metal ions.

Dp44mT interaction with the bilayer occurs via binding of the sulfur atom with phospholipid. Fe-Dp44mT complex formation could block the interaction of the Dp44mT with bilayer, so Dp44mT remains able to form mixed complexes with ascorbic acid.

Acknowledgements

The study was financially supported by the RFBR (grant №20-33-70019).

References

1. P. Jurkiewicz, A. Olżyńska, L. Cwiklik, E. Conte, P. Jungwirth, F.M. Megli, M. Hof, Biophysics of lipid bilayers containing oxidatively modified phospholipids: insights from fluorescence and EPR experiments and from MD simulations, Biochim. Biophys. Acta. 1818 (2012) 2388–2402.
2. J. Wong-ekkabut, Z. Xu, W. Triampo, I.-M. Tang, D.P. Tieleman, L. Monticelli, Effect of Lipid Peroxidation on the Properties of Lipid Bilayers: A Molecular Dynamics Study, Biophys. J. 93 (2007) 4225–4236.
3. D.R. Richardson, D.S. Kalinowski, V. Richardson, P.C. Sharpe, D.B. Lovejoy, M. Islam, P.V. Bernhardt, 2-Acetylpyridine Thiosemicarbazones are Potent Iron Chelators and Antiproliferative Agents: Redox Activity, Iron Complexation and Characterization of their Antitumor Activity, J. Med. Chem. 52 (2009) 1459–1470.

Structure and mobility of elastomers studied by the signals of primary and stimulated echoes

Tatiana P. Kulagina[1], Grigorii E. Karnaukh[1], Irina Yu. Golubeva[1,2]

[1]Institute of Problems of Chemical Physics RAS, Semenov prospec 1t, Chernogolovka, Moscow region, 142432, Russia
[2]Moscow State University, Moscow
E-mail: tan@icp.ac.ru

Introduction

A general approach to deriving formulas for calculating the signals of primary and stimulated spin echoes was developed and applied to obtaining data on random processes in linear and cross-linked polymers with different topological structures [1].

The method of NMR relaxation allows define topological structure and molecular mobility in elastomers (EL) [2, 3]. Self-diffusion in polymers is responsible for specific features of many physicochemical processes, including the establishment of a thermodynamically equilibrium structure. To determine the self-diffusion coefficient (D) the pulsed (or constant) field gradient NMR stimulated echo method is often used.

In this work the theory of primary and stimulated echoes in EL containing three spin groups is suggested.

General theoretical approach to calculating spin echo signals

On the base of general approach to deriving formulas for calculating the of spin echoes decay signal in view of the additivity of the displacements $r(t_i, t_j)$ over the time interval $[t_i, t_j]$, for each realization of the random process, the following equality holds: For the correlation of the displacements the next expression is valid:

$$\langle r(t_1,t_2)r(t_3,t_4)\rangle = \frac{1}{2}\left(\langle r^2(t_1,t_4)\rangle + \langle r^2(t_2,t_3)\rangle - \langle r^2(t_1,t_3)\rangle - \langle r^2(t_2,t_4)\rangle\right) \quad (1)$$

For steady-state process we obtain:

$$\langle r^2(t_1,t_2)\rangle = \langle r^2(0,t_2-t_1)\rangle = \langle r^2(t_2-t_1)\rangle \quad (2)$$

Using formula (3), (4), we obtained expressions for the mean squares of displacements for echoes 1 (primary echo), 4, and 5, the following expression was derived:

$$\left\langle \left(r(0,\tau) - r(\tau,2\tau)\right)^2 \right\rangle = 4\langle r^2(\tau)\rangle - \langle r^2(2\tau)\rangle \quad (3)$$

where τ is a time between pulses.

Analogously, with the use of condition (5), the following equations for echo 2 (stimulated echo) and echo 3 were obtained:

$$\left\langle \left(r(0,\tau_1) - r(\tau_1+\tau_2, 2\tau_1+\tau_2)\right)^2 \right\rangle = 2\langle r^2(\tau_1)\rangle + 2\langle r^2(\tau_1+\tau_2)\rangle - \langle r^2(2\tau_1+\tau_2)\rangle - \langle r^2(\tau_2)\rangle \quad (4)$$

$$\left\langle \left(r(0,\tau_1) - r(\tau_1,\tau_1+\tau_2) + r(\tau_1+\tau_2, 2\tau_2)\right)^2 \right\rangle =$$
$$= 2\langle r^2(\tau_1)\rangle + 4\langle r^2(\tau_2)\rangle + \langle r^2(2\tau_2)\rangle + 2\langle r^2(\tau_2-\tau_1)\rangle - 2\langle r^2(\tau_1+\tau_2)\rangle - 2\langle r^2(2\tau_2-\tau_1)\rangle \quad (5)$$

Equations (3) – (5) are valid for any random stationary processes.

Primary and stimulated echo signals

In the method of stimulated echo NMR without gradient of an external magnetic field in a result of the impact on a spin system of three pulse sequence RF pulses there are five spin echo signals are observed (echo 1-5) at time points: $2\tau_1$, $\tau_2 + 2\tau_1$, $2\tau_2$, $2\tau_2 + \tau_1$, $2\tau_2 + 2\tau_1$, where

τ_1 – the time interval between the first and second pulses, $\tau 2$ – the time interval between the second and third pulses.

According to the theory of a spin echo [1], the amplitude of the *i*-th echo signal A_{id} is connected with mean squares of random change of phase (phase shift) due to the changes in the local magnetic field at the spin of the nuclei by ratio:

$$A_{id} = \exp\left[-\frac{1}{2}\left\langle \delta^2 \varphi_i \right\rangle\right] \tag{6}$$

To determine a relationship with the mean squares of the shifting nuclei are obtained formulas, which are valid for any random processes [1]. Formulas (3) – (6) were applied for getting attenuation formulas of the spin echoes.

Primary echo signal was expressed as [3]

$$A_r(t,\tau) = \frac{G^2(t)G^2(\tau)}{G(t+\tau)} \tag{7}$$

Expression of primary echo after the second pulse in EL with group of three-spin is the next:

$$A(t) = A_3(t)A_r(t) \tag{8}$$

where $A_3(t)$ is the spin echo of three spin group with arbitrary constant DDI [2].

In view of (1) the stimulated echo signal was obtained, which was observed at the time point $\tau_2 + 2\tau_1$:

$$A_2(\tau_1,\tau_2) = \exp\left[-\frac{1}{2}\left(2\left\langle \delta^2\varphi(\tau_1)\right\rangle - \left\langle \delta^2\varphi(\tau_2+2\tau_1)\right\rangle + 2\left\langle \delta^2\varphi(\tau_2+\tau_1)\right\rangle - \left\langle \delta^2\varphi(\tau_2)\right\rangle\right)\right] \tag{9}$$

Whence, in respect that, formulas (6), (8) we obtain the functional relations between the stimulated echo signals and the FID:

$$A_2(\tau_1,\tau_2) = \frac{G^2(\tau_1)G^2(\tau_2+\tau_1)}{G(\tau_2+2\tau_1)G(\tau_2)} \tag{10}$$

Topological Structure and Anomal Diffusion in Elastic Polymers

In the present work, we suggested a common theoretical approach to calculation of the diffusion attenuation signals of all spin echoes and the mean squared displacement as function of time $<S^2(t_d)>$, where t_d is the time delay between pulses of magnetic field gradient [1]. It was shown that dependence of $<S^2(t_d)>$ on t_d for polymer networks is non linear.

Calculations of self-diffusion coefficient (D) were performed with $t_d = 80$ and $t_d = 400$ where the plot of $<S^2(t_d)>$ versus t_d is conditionally linear and the condition $\frac{t}{N_0} \gg 1$ is met. It was shown that molecular-weight distribution (MWD) has no effect on D at $t_d = 400$ since the chain length distribution is not manifested in the correlation function. However, at shorter t_d times, different MWDs can be observed (Fig. 1).

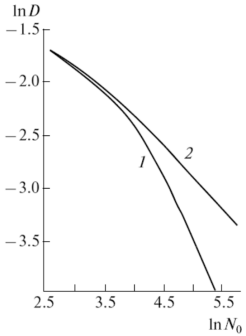

Figure 1. Log–log dependence of self-diffusion coefficient on the mean chain length N_0 at t_d = 80 for the (1) Gaussian and (2) exponential chain length distribution function

A theory of the line shape and spin echoes in elastic polymers with three-spin groups is proposed. Computer simulation of the signals showed the influence of $G_3(t)$ on FID and primary echo signals. That allows getting more information about the structure and mobility of polymer chains.

Acknowledgements

Work is performed on the theme of the state task № AAAA-A19-119071190017-7.

References

1. T. P. Kulagina, G. E. Karnaukh, A. N. Kuzina, L. P. Smirnov. *Russian Journal of Phys. Chem. B.* **7,** 170-176 (2013).
2. T. P. Kulagina, G. E. Karnaukh, I. Yu. Golubeva. *J. Applied Magnetic Resonance* **55**, 155-163 (2020).
3. I. Yu. Golubeva, G. E Karnaukh, T. P. Kulagina. *Proceedings 17-th International School-Conference Spinus-2020* ,182-184 (2020),.

Protein intermolecular interactions according to the translational diffusion by PFG NMR and DLS

Aleksandra Kusova, Aleksandr Sitnitsky, Yuriy Zuev

Kazan Institute of Biochemistry and Biophysics, Russian Academy of Sciences, Lobachevsky Str., 2/31 Kazan, Russian Federation.
E-mail: alexakusova@mail.ru

Introduction

Determination of protein-protein interactions in water environment at low and high protein concentrations is important for understanding of biological processes in vitro and in cellular environment, as well as for development and optimization of biotechnological processes [1, 2]. The role of weak intermolecular interactions is risen sharply in concentrated protein solutions where they affect viscosity, phase separation, solubility, and aggregation, altering protein functioning and causing the problems in creating protein products.

One of the longstanding approaches to estimate intermolecular interactions in different systems was the analysis of translational diffusion of molecules and particles in viscous liquid medium. The concentration dependence of the Fg diffusive mobility was obtained using the Dynamic Light Scattering (DLS) and Pulsed Field Gradient Nuclear Magnetic Resonance (PFG NMR) techniques. It should be noted, that the applied experimental approaches observe different diffusion effects denoted by the self-diffusion coefficient D_s (PFG NMR) and collective diffusion coefficient D_c (DLS). The difference in the D_s and D_c concentration dependences reflects different molecular effects, observed and averaged over the observation time in these two experimental approaches [3, 4]. Concentration dependences of for rod-shaped fibrinogen (Fg) and spherical chymotrypsin (ChTr) diffusivity are analyzed within the combination of friction formalism of nonequilibrium thermodynamics and the DLVO theory with porous particle model to obtain information about protein interaction.

Experimental

The lyophilized bovine Fg with molecular weight of 340 kDa (Calbiochem, USA) was studied in phosphate buffer (25 mM, pH = 7.4) at T = 30°C. The stock solution was purified from low molecular weight impurities using the Zeba Micro Spin Desalting Columns (40 kDa). Lyophilized ChTr with molecular weight of 24.8 kDa from bovine pancreas, type II, (SIGMA-ALDRICH, USA) was studied in water solutions at T = 30 °C, pH = 3 (adjusted by microliter amounts of HCl). The ^{1}H NMR diffusion experiments were performed on the Bruker AVANCE III NMR spectrometer, operating at ^{1}H 600.13 MHz and equipped with the standard z-gradient inverse triple resonance high resolution probe (TXI, 5 mm) with a maximum field gradient of 55 G cm^{-1}. Translational diffusivity was also analyzed by means of the DLS technique using Photocor Complex (Photocor), equipped with a He–Ne laser (λ = 632.8 nm). Protein solutions were filtered before the measurements through the 0.2 μm polytetrafluoroethylene (PTFE) membrane directly into the cuvette with protein concentration controlled after filtration.

Results and discussion

The concentration dependence of the Fg and ChTr self-diffusion coefficient, obtained with the PFG NMR technique, is presented in Figure 1. The initial near-horizontal regions of the curves characterize the dilute solutions with the protein self-diffusion coefficients equal to $4.05 \cdot 10^{-11}$ m^2/s and $1.05 \cdot 10^{-10}$ m^2/s for Fg and ChTr, respectively. Protein concentration of the onset of deviations from the initial near-horizontal region for the Fg self-diffusion coefficient is much smaller than for ChTr, being the evidence that Fg proceeds from the dilute (low-interaction) conditions to the interactive ones at significantly lower protein concentration.

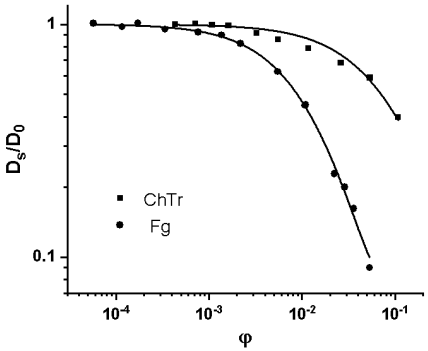

Figure 1. The generalized concentration dependences of self-diffusion coefficient $D_s(\varphi)$ for Fg (circles) and ChTr (squares) depicted by the Vink algorithm (lines). φ is the protein volume fraction

The Fg and ChTr diffusive mobility was analyzed using the DLS technique. Data is presented in Figure 2. The extremes on the concentration dependences of collective diffusion coefficient indicate the nature of the prevailing intermolecular interaction in protein solution.

To analyze the protein intermolecular interactions from the experimental data $D_c(\varphi)$ we used the phenomenological approach based on the frictional formalism of non-equilibrium thermodynamics, Vink approach [5]. The fitting of experimental results (Fig. 1 and Fig. 2) shows that the Vink algorithm depicts well the obtained data on collective diffusion for Fg and ChTr in a wide concentration range.

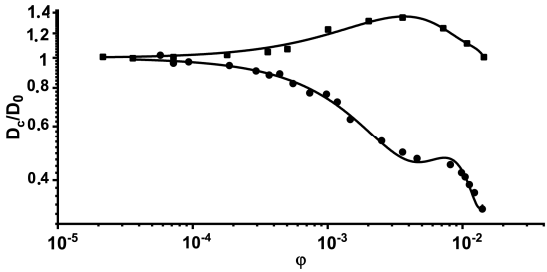

Figure 2. The generalized concentration dependences of collective diffusion coefficient $D_c(\varphi)$ for Fg (circles) and ChTr (squares) depicted by the Vink algorithm (lines). φ is the protein volume fraction

From the approximation of experimental data we obtained the set of virial coefficients for Fg and ChTr. In dilute solutions the total interaction potential is determined by the pairwise interactions characterized by second virial coefficient. We used the potential of mean force and the "porous" colloid particle model in combination with the DLVO theory to characterize second virial coefficient values for spheroidal ChTr and for the rod-shaped Fg [6, 7].

On the basis of performed calculations we estimated the different contributions to the overall intermolecular interaction in the studied protein systems. Figure 3 depicts the comparative contributions from electrostatic and van der Waals interaction to the total interaction potential of two protein molecules for the cases of Fg and ChTr. According to obtained results the electrostatic interactions are the dominant ones in the case of ChTr while the most pronounced effect for Fg molecules is proceeded from the van der Waals forces.

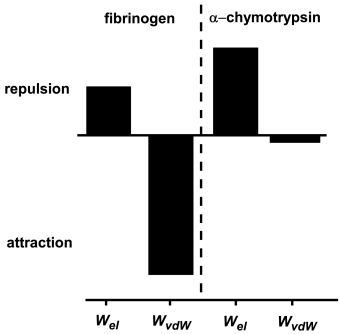

Figure 6. Schematic representation of contributions of electrostatic and van der Waals intermolecular interactions for ChTr, and Fg. The maximum deposit is taken as 100% for every protein

Conclusions

In this work we made the complementary use and subsequent theoretical analysis of the self- (PFG NMR) and the collective (DLS) diffusion to extend proposed early approach to evaluate protein-protein interactions of strongly rod-shaped fibrinogen (Fg) in comparison with the spheroidal one ChTr. The contributions of the main types of protein-protein interactions were estimated. The most pronounced deposit for Fg molecules is determined by the van der Waals attraction while for ChTr (which agree with our previous data with another model of electrostatic potential used here for comparison) the electrostatic repulsion gives the main contribution in protein-protein interactions.

Acknowledgements

This work was partly supported by the government assignment for Federal Research Center Kazan Scientific Center of Russian Academy of Sciences and the Russian Foundation for Basic Research [Grant N 20-04-00157].

References

1. D.H. Williams, E. Stephens, D.P. O'Brien, M. Zhou, Understanding noncovalent interactions: ligand binding energy and catalytic efficiency from ligand-induced reductions in motion within receptors and enzymes, Angew. Chem. 43 (2004) 6596–6616.
2. W. Wang, Protein aggregation and its inhibition in biopharmaceutics, Int. J. Pharm. 289 (2005) 1–30.
3. C. Le Bon, T. Nicolai, M.E. Kuil, J.G. Hollander, Self-diffusion and cooperative diffusion of globular proteins in solution, J. Phys. Chem. 103 (1999) 10294–10299.
4. A.M. Kusova, A.E. Sitnitsky, D.A. Faizullin, Yu.F. Zuev, Protein translational diffusion and intermolecular interactions of globular and intrinsically unstructured proteins. J. Phys. Chem. A 123 (2019) 10190–10196.
5. H. Vink, Mutual diffusion and self-diffusion in the frictional formalism of non-equilibrium thermodynamics, J. Chem. Soc. Faraday Trans. 1 81 (1985) 1725–730.
6. Ohshima, H. *Biophysical Chemistry of Biointerfaces*; John Wiley and Sons, Hoboken; New Jersey; 2010.
7. Coen, J.; Blanch, H. W.; Prausnitz, J. M. Salting Out of Aqueous Proteins: Phase Equilibria and Intermolecular Potentials. AIChE Journal 1995, 41, 996–1004.

Spin kinetics of gaseous ^{3}He in oriented aerogels

V. Kuzmin[1], K. Safiullin[1], A. Stanislavovas[1], M. Tagirov[1,2]

[1]Kazan Federal University, 420008, Kremlevskaya 18, Kazan, Russian Federation
[2]Institute of Applied Research, Tatarstan Academy of Sciences, Kazan, 420111, Russian Federation

Introduction

Aerogels with open-pore space have a various fields application [1] as thermal insulation, microelectronics and Cherenkov Counters. Confinement in chaotic and oriented aerogels have significant effects not only on ^{4}He superfluidity [1-4] but also on properties of ^{3}He NMR in superfluid phases and normal state at low and very low temperatures [5-8]. Therefore, the characterization of their porous structure and magnetic properties is of increasing interest.

Experimental

In the present study the ^{3}He gas self-diffusion and spin-lattice relaxation studies in ordered Al_2O_3 aerogels of different density (82, 125, 180, 597 and 920 mg/cm^3) were performed. The high density samples (597 and 920 mg/cm^3) were fabricated from low density samples (82 and 125 mg/cm^3) by soaking in the Milli-Q water for 20 minutes and drying at the room temperature for 48 hours [9].

The relaxation study was carried out using pulsed NMR methods in the temperature range of T = 1.5 - 4.2 K at frequency of about f_0 = 16 MHz (H_0 = 490 mT). The diffusion study was carried out at the same conditions with additionally applied constant external magnetic field gradient of G = 2.2 mT/cm.

Results

The excluding of the “fast-exchange” [10] process between ^{3}He adsorbed layer and gas phase and corresponding surface relaxation influence on ^{3}He gas relaxation by ^{4}He pre-plating leads to the increase of T_1 by order of magnitude. Nonetheless, the observed T_1 lies in the range 1 - 10 s in gas in the aerogels which is much less than in bulk ^{3}He gas [11]. Therefore, in this case the ^{3}He gas relaxation should be governed by other rather weak remained relaxation mechanisms. The mechanism a of dipole-dipole relaxation of ^{3}He gas in restricted geometry considered in [12] is omitted as being negligible for large pores and open pore geometry in aerogels. We suppose that the longitudinal relaxation of ^{3}He in gas is governed by a motion in macroscopic inhomogeneous magnetic field produced by aerogels magnetism. We discuss a realisation of possible motion regimes [13] in aerogels and possible sources of inhomogeneity: the paramagnetic centers in the aerogel, the diamagnetic susceptibility of the fibers and a possible existence of “dirty” aerogel fibers surrounded by “clean” fibers. In the latter case the nuclear magnetic relaxation should be governed by the time needed for atoms to diffuse to magnetically “dirty” fibers.

The apparent diffusion of ^{3}He atoms in the aerogels is slower than expected for free gas which also indicates on the “fast-exchange” process [10] that influences gas diffusion. The ^{4}He pre-plating allows to avoid the ^{3}He adsorption and to directly assess diffusion in gas phase in aerogels. It was found that the diffusion of ^{3}He atoms in gas is also slower than is expected for ideal gas at low pressure range. The simplest Knudsen model which takes place at low pressures cannot describe the ^{3}He slow gas diffusion at low temperatures. Problems with an application of Knudsen diffusion model are described by Bhatia and Nicholson [14]. Authors show that Knudsen model overpredicts the value of the diffusivity, because it neglects distant van der Waals interactions between the walls and the diffusing atoms in gas.

More details will be presented in oral report.

Acknowledgements

This work was financially supported by the Russian Science Foundation (grant RSF 20-42-09023).

References

1. Yu. K. Akimov, Instrum. Exp. Tech., 46, 287 (2003).
2. Gibbs M et. al., Physica B, 462, 213 (1995).
3. Sokol P et. al., Nature, 379, 616 (1996).
4. Sokol P et. al. Physica B, 241, 929 (1997).
5. Dmitriev V V et. al. Phys. Rev. Lett., 115, 165304 (2015).
6. Candela D and Kalechofsky N, J. Low Temp. Phys., 113, 351 (1998).
7. Dmitriev V V et.al., JETP Lett. 101, 808 (2015).
8. Zhelev N et. al., Nat. Commun., 7, 12975 (2016).
9. V. V. Volkov et. al., Instrum. Exp. Tech., 60, 737 (2017).
10. Collin E et. al., Phys. Rev. B: Condens. Matter Mater. Phys., 80, 094422 (2009).
11. Chapman R and Richards M G, Phys. Rev. Lett., 33, 18 (1974).
12. J.-P. Korb, Shu Xu, and J. Jonas, J. Chem. Phys., 98, 2411 (1993).
13. Pignol G. et al.: Phys. Rev. A, 92, 053407 (2015).
14. Bhatia S.K. and Nicholson D., Chem. Eng. Sci. 66, 284 (2011).

The correlation of structure with transport properties of novel pervaporation sodium alginate membranes modified by Zr-MOFs

Anna I. Kuzminova, Anastasia V. Penkova

St. Petersburg State University, St. Petersburg, 199034 Russia
E-mail: ai.kuzminova@mail.ru

Introduction

Pervaporation is the one of the most popular processes for the separation of low molecular weight components, which allows the separation of mixtures of isomers, azeotropic mixtures and thermally unstable mixtures, the separation of which is difficult by traditional methods. Currently, the improvement of the transport properties of polymer pervaporation membranes occurs due to the creation of mixed matrix membranes (MMMs), by modifying the polymer matrix with an inorganic and/or organic filler. The introduction of an inorganic and/or organic filler into the polymer matrix of the membrane makes it possible to obtain tailoring properties.

In the present work the novel green membranes based on biopolymer sodium alginate (SA) were prepared by introducing the three metal-organic frameworks (Zr-MOFs): UiO-66, UiO-66(NH_2)-EDTA and UiO-66(NH_2)-AcOH into the SA matrix. The improvement of the transport properties of the membranes based on SA modified by Zr-MOFs was expected due to the porous structure, hydrophilic/hydrophobic properties, excellent chemical and thermal stability of the Zr-MOFs. The most important investigation of Zr-MOFs inclusion in SA matrix is analysis of membranes by spectroscopic methods. Among these methods, nuclear magnetic resonance (NMR) is the best tool for the investigation of polymer nanocomposite materials. NMR allowed to study the interaction between Zr-MOFs and polymer SA matrix and to confirm the complex structure of MMMs in the present work. The additional characterizations of the polymer samples were studied by Fourier-transform infrared spectroscopy, scanning electron microscopy, atomic force microscopy, thermogravimetric analysis, and swelling experiments. Transport properties of the developed membranes were investigated by pervaporation during separation of water-isopropanol mixtures at 22 °C.

Acknowledgements

The reported study was funded by RFBR, project number 19-38-90008. The experimental work of this study was facilitated by the equipment from the Resource Centre of Geomodel, Chemical Analysis and Materials Research Centre, Centre for X-ray Diffraction Methods, Magnetic Resonance Research Centre, Centre for Innovative Technologies of Composite Nanomaterials, Nanophotonics Centre, Cryogenic department, Thermogravimetric and Calorimetric Research Centre and the Interdisciplinary Resource Centre for Nanotechnology at the St. Petersburg State University.

Mn-based silica nanoparticles as potential MRI probes

Daniela Lalli[1], Fabio Carniato[1], Giuseppe Ferrauto[2], Enzo Terreno[2], Mauro Botta[1]

[1]Department of Sciences and Technological Innovation, University of Eastern Piedmont "Amedeo Avogadro", Viale Teresa Michel 11, 15121-Alessandria, Italy
[2]Molecular Imaging Center, Department of Molecular Biotechnology and Health Sciences, University of Torino- Via Nizza 52, 10126 Torino, Italy
E-mail: daniela.lalli@uniupo.it

Over the last decade, a wide range of nanoparticle-based paramagnetic contrast agents (CA) have been developed as potential high efficiency probes for magnetic resonance imaging (MRI). Such nanoprobes have the advantage of accumulating large payload of paramagnetic metal-chelates into biocompatible nanosized systems, thus allowing for dose reduction, minimization of the metal release, and increase of the image contrast.

A detailed physico-chemical characterization of the silica nanoparticles before and after the surface modification was carried out to assess the structural and surface properties of the hybrid material.

^{1}H-NMR relaxometric investigations of the aqueous suspensions of these hybrid materials decorated on the surface with a Mn(II)-CDTA derivative, as a function of applied magnetic field strength and temperature, provide insights into the dynamic properties of functionalized silica nanoparticles. In particular, at clinical field strengths (42 MHz), a 117 % enhancement of longitudinal relaxivity (r_{1p}) of the materials was observed, compared to the free Mn(II)complex (r_{1p} from 5.2 to 11.3 mM^{-1} s^{-1}, at 298 K) due to the reduction of the rotational tumbling motions of the Mn(II)complex conjugated to the nanospheres.

Finally, the Mn(II)complex anchored onto the silica nanospheres show good colloidal and chemical stability in aqueous solution and in biologic matrices (Seronorm solution), which opens the way for molecular imaging in vivo applications.

Investigation of novel pervaporation membranes based on sodium alginate – fullerene derivative composites

Vladislav P. Liamin, Mariia E. Dmitrenko, Sergey S. Ermakov, Anastasia V. Penkova

St. Petersburg State University, 7/9 Universitetskaya nab., St. Petersburg 199034, Russia
E-mail: lyamin.vlad.322@gmail.com

Introduction

Membrane separation methods are the most promising field of sustainable processes due to their beneficial characteristics, namely, waste-free, environmentally friendly, low-energy and compact equipment. Pervaporation is a membrane process actively and effectively used for the separation of close-boiling and thermally unstable substances, azeotropic and isomer mixtures, in particular, for dehydration. The rapid development of this method requires the research of new high-effective green membranes. One of the most perspective ways to improve characteristics of polymer membranes is the introduction of carbon nanoparticles into a well-known polymer matrix. In this work, biopolymer sodium alginate (SA) was used as a membrane material, while water-soluble fullerene derivatives (fullerenol and arginine-derivative fullerene) were used as modifiers for the development of novel green high-effective membranes for pervaporation dehydration.

Membrane investigation

The optimal conditions for preparation and cross-linking of SA membranes were developed. The structural characteristics of developed composites and membranes based on them were studied by spectroscopic (NMR and FTIR) and microscopic (SEM and AFM) analysis methods. The physicochemical properties were evaluated by the thermogravimetric analysis, sorption experiments and contact angle of water measurements. Transport characteristics of SA and SA-fullerene derivative membranes were tested in pervaporation dehydration of isopropyl alcohol in a wide concentration range (12-90 wt.% water).

Results

It was demonstrated that the introduction of fullerene derivatives in SA matrix led to the significant changes in the surface and inner structure of membranes (confirmed by analysis methods, in particular by NMR spectroscopy) resulting to the improved transport properties of modified SA membranes.

Acknowledgements

This work was supported by Russian Science Founda-tion [project No 19-73-00105]. The experimental work was facilitated by equipment from the Resource Centers for Nanotechnology, Magnetic Resonance, Thermogravimetric and Calorimetric Research Centre, Chemical Analysis and Materials Research Centre, Cryogenic Department and Centre "Nanofabrication of Photoactive Materials (Nanophotonics)" at the St. Petersburg State University.

Correlation times and water fractions distribution in HbA and HbS intracellular solutions

Manuel Arsenio Lores Guevara[1], Carlos Alberto Cabal Mirabal[1,2], Robert N. Muller[3], Sophie Laurent[3], Fabian Tamayo Delgado[1], Juan Carlos García Naranjo[1]

[1]Centro de Biofísica Médica. Universidad de Oriente. Patricio Lumumba S/N. CP: 90500. Santiago de Cuba, Cuba.
[2]Facultad de Física, Universidad de la Habana, Cuba.
[3]Laboratoire de RMN et d'Imagerie Moléculaire. Service de Chimie Générale, Organique et Biomédicale. Faculté de Médecine et de Pharmacie. Université de Mons. Belgique.
E-mail: manuellores2@gmail.com
http://www.uo.edu.cu

Introduction

The correlation times and water fractions were evaluated in intracellular samples of hemoglobin A (HbA) and hemoglobin S (HbS) at 310 K. The HbA and HbS samples were obtained from whole blood of voluntary donors and patients respectively, and processed by classical methods (centrifugation, decanting and freezing). The correlation times and water fraction values were calculated starting from the NMRD profiles (20 KHz – 20 MHz) using a Fast Field Cycling NMR Relaxometer (Stelar FFC 2000 Spinmaster) and Minispec relaxometers (Mq20, Mq60).

Results

A three sites exchange model was successfully used to fit the NMRD profiles considering a Dipole-Dipole interaction between the intramolecular water protons with a mono exponential autocorrelation function.

$$\frac{1}{T_1} = 2c\left[P_b\left(\frac{\tau_{cb}}{1+(\omega\tau_{cb})^2} + \frac{4\tau_{cb}}{1+4(\omega\tau_{cb})^2}\right) + P_h\left(\frac{\tau_{ch}}{1+(\omega\tau_{ch})^2} + \frac{4\tau_{ch}}{1+4(\omega\tau_{ch})^2}\right)\right] + \frac{1}{T_{1f}}$$

Distributions of correlation times ($10^{-7}$to $10^{-11}s$) and water fractions (P_b=4.04 $*$ 10^{-4}, P_h = 3.99 $*$ 10^{-3} and $P_f \approx 1$) were obtained after describe the experimental profile, using the three sites exchange model, with similar quality that commonly used empirical approximation (Cole-Cole expression).

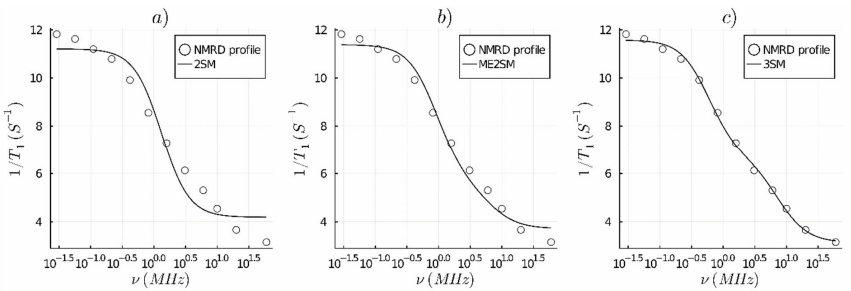

Figure 1. Typical NMRD profiles of HbA and HbS intracellular solutions obtained at 310 K. The experimental result has been fitted to: a) a two sites exchange model with two correlation times, b) a two sites exchange model with four correlation times and c) a three sites exchange model with three correlation times

Acknowledgements

This work was supported by the FNRS (Fonds National de la Recherché Scientifique) from Belgium, and the researchers of the NMR laboratory of the University of MONS. The authors also want to thanks to the ULB Brussels University Hospital for its support.

Ionic liquid crystals studied by solid-state NMR spectroscopy

Debashis Majhi[1,2], Jing Dai[1], Boris B. Kharkov[3], Andrei V. Komolkin[4], Sergey V. Dvinskikh[1,3]

[1]Department of Chemistry, KTH Royal Institute of Technology, Stockholm, 10044, Sweden,
[2]School of Chemistry, Tel Aviv University, Ramat Aviv, 6997801 Tel Aviv, Israel.
[3]Laboratory of Bio-NMR, St. Petersburg State University, St. Petersburg, 199034, Russia
[4]Physics Faculty, St. Petersburg State University, St. Petersburg, 199034, Russia
E-mail sergeid@kth.se

Ionic liquid crystals (ILCs) belong to a special class of ionic liquids with mesogenic functionalities which show thermotropic liquid crystal behaviour. The molecular design of ILCs is commonly based on cations and anions of conventional ionic liquids by addition of one or more long alkyl chains. The ionic character and rod-shaped structure of cations favour the formation of layered phases (Fig. 1). There are several types such as ammonium, imidazolium, pyridinium based ILCs reported, among these monocationic imidazolium-based salts are the most studied ones. Recently, dicationic ionic liquid crystals have also been presented.

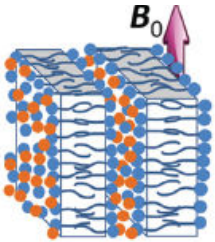

Figure 1. Illustration of ionic smectic A layers aligned in the magnetic field B_0

We report investigation of the molecular and local bond orientational ordering in a series of ILCs with imidazolium-based mono- and di-cations and number of anions varying in structure, ionic radius, negative charge localization, and hydrogen bonding properties. Molecular and local bond order parameters are estimated via measurement of dipolar spin couplings. A large anisotropy of diamagnetic susceptibility of mesogenic functional groups in ILCs induces macroscopic molecular alignment in the presence of a strong magnetic field of an NMR spectrometer. In this case, NMR spectra are obtained with high resolution and site-specific anisotropic spin couplings are straightforwardly accessed. We quantify the orientational order of C-H bonds of a long-chain imidazolium-based cation in an ionic smectic phase. Molecular order parameter S is estimated. The results revealed the trends in the orientational order in ionic liquid crystals and contributed to a better understanding of interparticle interactions driving smectic assembly in ionic mesogens [1-7].

References

1. J. Dai, B. B. Kharkov, S. V. Dvinskikh, Crystals, 2019, 9, 18.
2. J. Dai, D. Majhi, B. B. Kharkov, S. V. Dvinskikh, Crystals, 2019, 9, 495.
3. D. Majhi, J. Dai, A. V. Komolkin, S. V. Dvinskikh. *PCCP*, 2020, 20, 13408
4. D. Majhi, A. V. Komolkin, S. V. Dvinskikh. *Int. J. Mol. Sci.*, 2020, 21, 5024
5. S. V. Dvinskikh. *Liq. Cryst.* 2020, 47, 1975-1985
6. D. Majhi, S. V. Dvinskikh. *Sci. Rep.,* 2021. https://doi.org/10.1038/s41598-021-85021-y
7. M. Cifelli, V. Domenici, V. I. Chizhik, S. V. Dvinskikh, Appl. Magn. Reson. 2018, 4, 553.

The ^{1}H NMR and CIDNP study of the interaction of nonsteroidal anti-inflammatory drug ketoprofen with L- and D-tryptophan

A. V. Mastova, O. Yu. Selyutina, N. E. Polyakov

Institute of chemical kinetics and combustion SB RAS
E-mail: mastova-anna99@yandex.ru

Introduction

Ketoprofen (KP) is nonsteroidal anti-inflammatory drug (NSAID) with analgesic and antipyretic effects. It reversibly inhibits cyclooxygenase-1 and -2 (COX-1 and COX-2) enzymes, which regulates production of pro-inflammatory prostaglandin precursors. Although the anti-inflammatory role of two KP enantiomers is not fully characterized, it is known that R-KP is a weak cyclooxygenase inhibitor [1], being 100 to 1000 times less potent than the S-enantiomer in vitro. In the present study, we attempt to study the role of chirality in the mechanism of interaction of ketoprofen with enzymes.

Experimental part and results

As a model of the interaction of KP with the active sites of cellular receptors and enzymes [2], the photoinduced interaction of KP with the stereoisomers of the amino acid tryptophan (Trp) was studied in this work (Fig.1). Of particular interest is the study of the stereoselectivity of these processes in model lipid membranes (bicelles). Bicelles consist of two types of lipids - DMPC and DHPC in a ratio of 1:2 (Fig. 2)

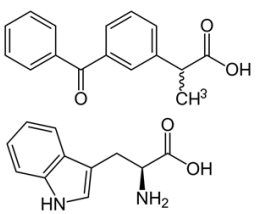

Figure 1. Structures of ketoprofen and tryptophan

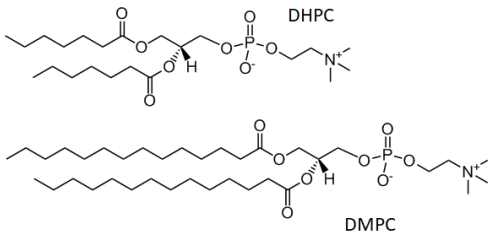

Figure 2. Structures of DHPC and DMPC

^{1}H NMR and chemically induced dynamic nuclear polarization (CIDNP) methods revealed differences in the interaction of KP with Trp isomers in the buffer solution and within the membrane system (Fig. 3). The ROESY method revealed the interaction between the protons of KP and L- and D-Trp in the bicelles, which indicates the formation of associates of ketoprofen with tryptophan in the lipid bilayer (Fig. 4). Also, it revealed an interaction between Trp and lipid protons, and KP and lipid protons, which indicates the incorporation of Trp and KP molecules into the bicelles.

Observation of CIDNP effects in photoreaction of KP with L- and D-Trp in bicelles is the strong evidence of the radical mechanism of this reaction. In addition, there is the difference in the degree of decomposition of lipids: in the deoxygenated system with L-tryptophan, the integral intensity of the peak corresponding to the CH_2 groups of lipids decreased by 28%, but in the system with D-tryptophan by 15%. The dependence of the CIDNP effects on the presence of oxygen in the system was also investigated. It was found that the saturation of the sample with oxygen leads to an increase in the CIDNP intensity and to the acceleration of lipid oxidation (Fig. 5).

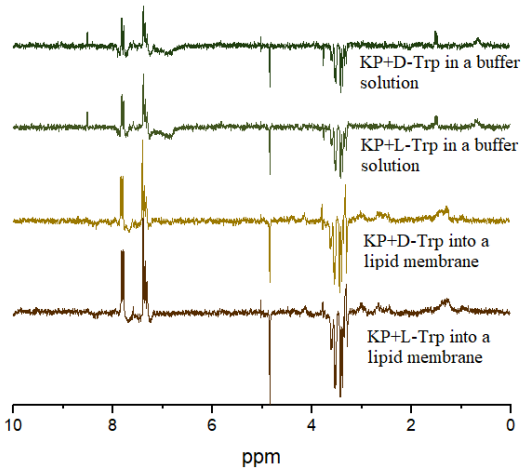

Figure 3. CIDNP spectra of different solutions

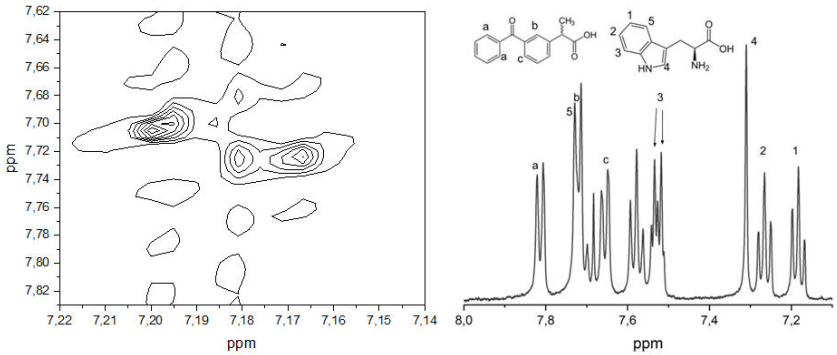

Figure 4. ROESY spectrum of KP+D-Trp+bicelles solution (left), NMR spectrum of KP+Trp solution (right)

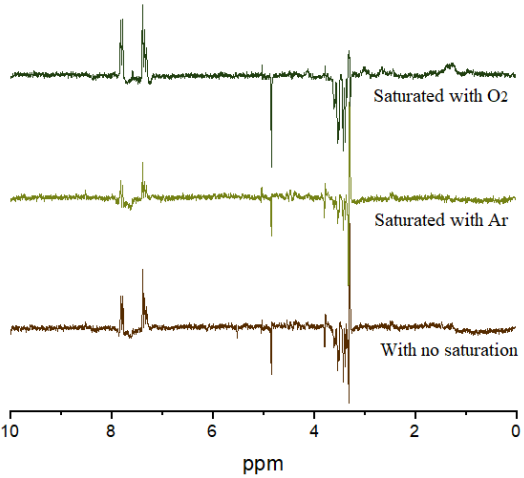

Figure 5. CIDNP (308 nm) spectra of KP (2 mM)+D-Trp (4 mM)+bicelles (12 mM) solution with different degree of oxygen saturation.

Conclusions

The obtained data let us suggest that:

- The photochemical reaction of tryptophan and KP follows a radical mechanism
- Tryptophan and KP interacts differently in homo- and heterogeneous solutions
- S-ketoprofen interacts stereoselectively with tryptophan isomers in a heterogeneous solution
- The presence of oxygen in the system increases the polarization of tryptophan and accelerates the decomposition of lipids.
- The photoinduced formation of the ketyl radical of KP leads to the oxidation of membrane lipids and may be the cause of phototoxicity of KP.

Further study of this system may lead to a better understanding of the mechanism of interaction of the enzyme with the nonsteroidal anti-inflammatory drug ketoprofen, as well as to more effective and safe use of the drug.

References

1. G. Marconi, e.a., Stereoselective interaction of ketoprofen enantiomers with β-cyclodextrin: ground state binding and photochemistry. Photochem. Photobiol. Sci., 2011, 10.
2. A. Ageeva, e.a., Stereoselectivity of Electron and Energy Transfer in the Quenching of (S/R)-Ketoprofen-(S)-Tryptophan Dyad Excited State. International Journal of Molecular Sciences. 2020, 21, 5370; doi:10.3390/ijms21155370.

Study of doped chalcopyrite $Cu_{1-x}Pd_xFeS_2$ compounds by $^{63,65}Cu$ NMR and EPR methods

Vadim L. Matukhin[1], Andrey N. Gavrilenko[1], Iliya G. Sevastianov[1], Sergei B. Orlinskii[2], Ecaterina V. Schmidt[1], Stanislav O. Garkavyi[1], Jiri Navratil[3], Pavel Novak[3]

[1]Kazan State Power Engineering University, Krasnoselskaya, 51, Kazan 420066, Russian Federation
[2]Kazan Federal University, Kremlyovskaya, 18, Kazan 420008, Russian Federation
[3]Institute of Physics of the Czech Academy of Sciences Cukrovarnicka 10/112, 16200, Praha 6, Czech Republic
E-mail: ang_2000@mail.ru

Introduction

Highly efficient thermoelectric materials have been attracting much attention because of their potential applications, especially for energy harvesting by waste heat. Recently, it has been proposed to use magnetic semiconductors as effective thermoelectrics [1]. One characteristic feature of magnetic semiconductors is the strong coupling between carriers and the spins of magnetic ions. This strong interactions may to a large effective mass of carriers, which can enhance the Seebeck coefficient with good carrier conduction. One of the representatives of this class of compounds is the well-known semiconductor mineral chalcopyrite $CuFeS_2$.

Recent first-principle studies suggested a possible enhancement of thermoelectric properties of this compound, especially by a dilute doping [2, 3]. Therefore, a detailed understanding is necessary for the achievement of highly efficient thermoelectric compounds.

In this work, we present a study of a series of $Cu_{1-X}Pd_XFeS_2$ (x = 0-0.02) compounds by $^{63,65}Cu$ NMR in local field and EPR methods. Previously, the thermoelectric and transport properties of hot-pressed $Cu_{1-X}Pd_XFeS_2$ (x=0-0.1) sample pellets were studied in [4].

Experiment

Polycrystalline samples with the nominal composition of $Cu_{1-X}Pd_XFeS_2$ (x=0, 0.01, 0.02) were synthesized from a mixture of pure elements obtained from Sigma-Aldrich, including Cu (4 N shots), Pd (4 N powder), Fe (4 N granular) and S (5 powder). The synthesis of the samples is described in Ref. [4].

The spectral parameters of $^{63.65}Cu$ NMR in a local field in $CuFeS_2$ were measured on a Tecmag Redstone multi-pulse NQR/NMR spectrometer. Measurement of the NMR line shape was performed using quadrature detection by recording spin echo signals with step-by-step passage of the frequency range and signal accumulation.

The EPR spectra of 3 samples $Cu_{1-X}Pd_XFeS_2$ (x = 0, 0.01, 0.02) were studied on a Bruker stationary X-ray spectrometer ESP-300 in the temperature range 15-300 K. The masses of the samples were approximately the same.

Results and discussion

A detailed study of the shape of the resonance lines revealed their asymmetric nature with a more gentle decay in the high-frequency region.

The experimental Cu NMR spectrum of the compounds at 77 K can be considered as a superposition of two Cu NMR spectra: the first spectrum consisting of low-frequency resonance lines assigned to the main phase and the second spectrum consisting of high-frequency lines due to resonance centers located in defective areas of crystalline structure.

A broadening of the resonance lines may be the result of an increase in the number of defects in the crystal lattice of the compound, leading to a larger spread of EFG on the resonant copper nuclei. The formation of such defects (Fe_{Cu}^{2+} antisite (AS) defects as proposed in [4]) is caused by the formation of the PdS phase in the chalcopyrite matrix, with increasing nominal

content of Pd. The frequency shift of the resonance lines can be explained by the Ruderman-Kittel-Kasuya-Yosida (RKKY) interaction [5]. This is supported by the increased conductivity observed for $Cu_{0.98}Pd_{0.02}FeS_2$ sample [4].

The EPR spectra of all samples have their own characteristics.

A significant shift of the center of the line to the right and its narrowing in the $CuFeS_2$ sample (0% Pd) occur in the temperature range 100 – 130 K.

At the low temperature T = 15 K, unlike the previous sample without Pd, a part of the wide ferromagnetic signal is practically absent in the sample with a Pd content of 1%; however, a presumably paramagnetic signal with the g factor g = 2.08 and a width of the order of 1 kG is observed (Fig. 1), which gradually weakens and narrows with increasing temperature. In the sample with 2% Pd, the signal near g = 2.00 has a lower intensity (Fig. 1). It repeats the behavior of the signal in the sample with 1% Pd when heated.

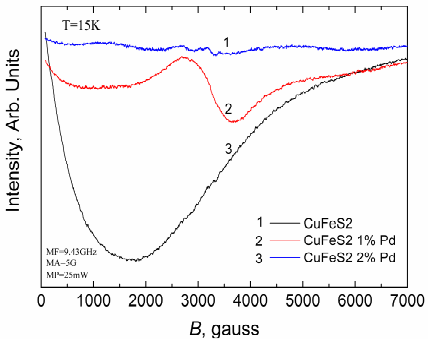

Figure 1. Measured EPR spectra at the temperature 15 K of $CuFeS_2$ (1), $Cu_{0.99}Pd_{0.01}FeS_2$ (2) and *$Cu_{0.98}Pd_{0.02}FeS_2$ (3) samples*

At 150 K and higher, the nature of the temperature dependence is the same for all samples. The shape of the lines of all samples is the same in this temperature range too, although there is a difference in intensities. The EPR spectra of the samples at 300 K are shown in Fig. 2.

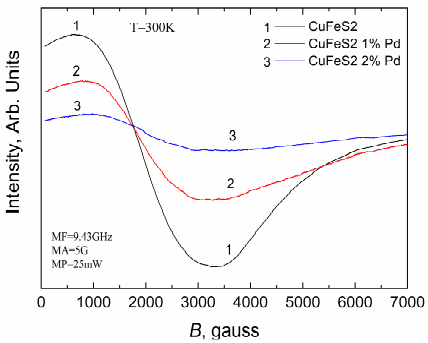

Figure 2. Measured EPR spectra at the temperature 300 K of $CuFeS_2$ (1), $Cu_{0.99}Pd_{0.01}FeS_2$ (2) and *$Cu_{0.98}Pd_{0.02}FeS_2$ (3) samples*

Conclusions

The broadening of the NMR resonance lines may be the result of an increase in the number of defects in the crystal lattice of the compound, leading to a larger spread of EFG on the resonant copper nuclei. Such defects can be Fe_{Cu}^{2+} antisite (AS) defects. The formation of such defects is caused by the formation of the PdS phase in the chalcopyrite matrix, with increasing nominal content of Pd. Thus, it was shown that the Cu NMR method in a local field can be used to assess the defectiveness of polycrystals of $Cu_{1-X}Pd_XFeS_2$ (x=0-0.02) compounds.

A rapid change in the shape of the EPR spectrum was found in the temperature range 100 K – 130 K in the $CuFeS_2$ sample, which presumably corresponds to a possible structural phase transition.

In the EPR spectra of a $CuFeS_2$: Pd 1% sample at a temperature of T = 15 K a presumably paramagnetic signal with the g-factor of g = 2.08 and the width of the order of 1 kG is observed, which may be associated with the appearance of antisite defects.

Acknowledgements

We are grateful for the financial support from the Czech Science Foundation, Project No18-12761S.

References

1. N. Tsujii. – *J. Electron. Mater.,* **42**, 1974 (2013).
2. H. Takaki, K. Kobayashi, M. Shimono, N. Kobayashi, K. Hirose, N. Tsujii, and T. Mori. – *Mater. Today Phys*., **3**, 85 (2017).
3. H. Takaki, K. Kobayashi, M. Shimono, N. Kobayashi, K. Hirose, N. Tsujii, and T. Mori. – *Appl. Phys. Lett*., **110**, 072107 (2017).
4. J. Navratil, J. Kasparova, T. Plechacek, L. Benes, Z. Olmrova-Zmrhalova, V. Kucek, and C. Drasar. – *J. Electron. Mater*., **48,** (2019).
5. T. Koyama, M. Matsumoto, S. Wada, Y. Muro and M. Ishikawa. – *J. Phys. Soc. Jap.,* **70**, 3667 (2001).

Quadrupole coupling constants in compounds with aminogroups in liquids

G. V. Mozzhukhin[1], G. S. Kupriyanova[2], S. Mamadazizov[2,4], M. Vafandar[1], B. Z. Rameev[1,3]

[1]Gebze Technical University, 41400 Gebze/Kocaeli, Turkey.
[2]Baltic Federal University by Immanuel Kant, 236041 Kaliningrad, Russian Federation
[3]E. Zavoisky Kazan Physical-Technical Institute, 420029 Kazan, Russian Federation
[4]School of Arts and Sciences, University of Central Asia, 736000, Khorog, Tajikistan
E-mail: mgeorge@yandex.ru; http://www.gtu.edu.tr

Introduction

There are several direct methods for the measurements of nuclear quadrupole interaction constants (NQC), such as methods based on nuclear quadrupole spectroscopy (NQS) for solid samples and molecular beam methods for gaseous samples [1].

Nuclear Magnetic Resonance (NMR) of ^{14}N allows detecting NQC from linewidths [2]. In the case of ^{14}N NMR in liquids, the linewidth and relaxation parameters are mainly determined by quadrupole interactions. In the case of isotropic stochastic rotational motions in liquids, the correlation function is determined by one exponential dependence with a characteristic correlation time τ_c [3]. In this situation we applied the following famous approximations [4]: i) narrowing limit $(\omega_0\tau_c)^2 << 1$ is valid; ii) substances have isotropic molecular reorientation. In this approximation, the transverse and longitudinal relaxation times are equal, and the following expression for the quadrupole contribution to relaxation can be used.

$$\left(\frac{1}{T_1}\right)_Q = \left(\frac{1}{T_2}\right)_Q = \frac{3}{8}\left(1+\frac{\eta^2}{3}\right)\left(\frac{e^2Qq_{zz}}{\hbar}\right)^2\tau_c \qquad (1)$$

where $(T_1)_Q$ and $(T_2)_Q$ are longitudinal and transverse relaxation times correspondently, η is asymmetry parameter, $e^2q_{zz}Q/\hbar$ is a nuclear quadrupole coupling constant Qc. We have neglected η in equation (1) because the maximum error introduced by omitting asymmetry parameter η in calculating τ_c is about <10% [5].

If the characteristic correlation time τ_c can be calculated or extracted from another experiments, NQC might be obtained from the relaxation parameters. In this work, the relaxation measurements of ^{14}N NMR for several liquids containing nitrogen compounds were performed. The correlation times of rotational motion τ_c were calculated by using of the theoretical models, and the NQC of some molecules with NH_2 and NO_2 groups were evaluated. The results were evaluated by application of quantum mechanical calculations of NQC.

Experimental

Our experimental device was assembled with use a home-made permanent magnet system with a magnetic field of 0.575 T, home-made NMR probe with a resonance frequency of about 1.770 MHz, Kea2 NMR console.

We studied some molecules with NH_2 and NO_2 groups in liquids. An aqueous solution of glycine NH_2-CH_2-COOH (is about 15% concentration in water solution), of urea $CO(NH_2)_2$(is about 30%) and (~40%) of sodium nitrite ($NaNO_2$) obtained from powder (Merck KGaA, powder percentage 99%) were examined.

We used the Carr-Purcell-Meiboom-Gill (CPMG) sequence for T_2 measurements and inversion-recovery [1] for T_1 measurements. The measurements were carried out at room temperature and on a sample with a volume of 1 mL.

Theoretical models

In NMR spectroscopy, the Stokes – Einstein-Debye (SED) model is the most widely used. In the SED model, a molecule is considered as a sphere experiencing resistance in a viscous medium, the rotational correlation time τ_c depends on the macroscopic parameters of viscosity σ and temperature T [4-6]:

$$\tau_C = \frac{4\pi a^3}{3kT}\sigma = \frac{V_{mol}}{kT}\sigma\,, \tag{2}$$

where V_{mol} is the molecular volume determined by the Stokes radius, k is the Boltzmann constant. The authors in ref. [5, 9] note that relations τ_c / τq (for quadrupole relaxation) are in range from 5.5 to 20 for different liquids. This indicates that the friction limitation should be lower than the Stokes coefficient. In order to improve this model, Gierer and Wirtz (GW) [9] proposed the idea of the microviscosity coefficient as a dimensionless coefficient depending on the ratio of the radii of the solution a and the solvent a_s. The rotational correlation time in GW model is

$$\tau_{GW} = f\,\frac{V_{sphere}}{kT}\sigma, \tag{3}$$

$$\text{where } f = [\ 6\ (\ as / a\ ) + (as / a\ )^{-1}\ ]^{-3}. \tag{4}$$

The value of the microviscosity coefficient for a pure liquid is f = 0.16 [6, 10]. While the GW model uses a spherical representation of molecules, the models proposed by Hu-Zwanzig (HZ) and Youngren-Acrivos (YA) are based on spheroidal and ellipsoidal representations, respectively [6]. The rotational correlation time in YA model is

$$\tau_{YA} = \beta i\,\frac{V_{ellipsoid}}{6kT}\sigma, \tag{4}$$

βi are parameters that were calculated and given in [4, 7]. Model YA gives acceptable results for most small or rigid molecules [4]. All near-spherical molecules such are treated by the GW model.

The Lamb model is used to calculate the volume of planar molecules in the approximation of hexagonal close packed solid sphere [5, 9, 11, 12] and with using the concept of Van der Waals [9, 10]. The structural data for calculating the required parameters in (1) - (4) were taken from [13-16].

DFT calculations were performed using the GAUSSIAN09 package [13] with the basis set b3pw91/6-311++g. It was shown in [12] that calculated NQC are close to experimental, when the local environment of the atom was correctly reproduced. Thus, the cluster are created by the way in which one of molecules are surrounded by all neighbors (see fig. 1). We used the structural data for urea and glycine from ref. [15] and [16].

Results and discussion

Our measurements show that relaxation parameters T_1 and T_2 in NMR of ^{14}N nuclei in liquids are approximately equal. Thus, we presented in Table 1 only data for T_1. Experimental values of T_1 have allowed us to extract τ_c directly by means of Eq. (1) in the case of known NQC [15].

It can be seen that the calculated values for the correlation times of urea, glycine, and previously studied aminomethane, $NaNO_2$, CH_3NH_2 [13] are in satisfactory agreement with experiment and literature data, which allows us the model to be used to estimate the quadrupole interaction constants.

Table 1. ^{14}N NMR relaxation parameters of tested liquids and NQR constants

Material	T_1, ms	$e^2q_{zz}Q/\hbar$, MHz (*)exp	$e^2q_{zz}Q/\hbar$, MHz (ref)	$e^2q_{zz}Q/\hbar$, MHz (cal)	Viscosity [24], mPa·s [18]
Glycine NH_2-CH_2-COOH	4.3±0.4	1.7	1.257 (T=77K) (η=0.5) [17]	1.544 (η=0.285)	0.880
Urea $CO(NH_2)_2$	0.95±0.1 1.34 [22]	3.7	3.51 (η=0.342) [22] 3.99±0.4 [6]	3.751 (η=0.54)	1.627 [20]
Acetamide CH_3CONH_2	-	-	2.469 (η=0.412)[22]	3.102 (η=0.47)	2.05
Formamide $HCONH_2$ [21]	2.06 [21] 1.27 [22]	2.57	2.56	-	3.75

Acknowledgements

The work was supported by TUBITAK grant under the Programme 2221 for Visiting Scientist (G. S. Kupriyanova). Authors also acknowledge a partial support by East Marmara Development Agency (MARKA, project No. TR42/16/ÜRETİM/0013) and by Research Fund of Gebze Technical University (grants Nos. BAP 2015-A-19 and BAP 2017-A-105-44).

References

1. E. A.K Luken, Nuclear Quadrupole Coupling Constants, Academic Press, New York, 1969
2. W.B. Moniz and H.S. Gutowsky, Nuclear Relaxation of N-14 by Quadrupole Interactions in Molecular Liquids, J. Chem. Phys. 38 (1963) 1155-1162.
3. A. Abragam, The Principles of Nuclear Magnetism, The Clarendon Press, Oxford, (1961) 314 p.
4. M. Witanovski, Nitrogen NMR. Spectroscopy, Pure and Applied Chemistry 37 (1974) 225-233.
5. R.T. Boere, R.G. Kidd, in: G.A. Webb (Ed.), Annual Reports on NMR Spectroscopy, vol. 13, Academic Press, New York (1982) 319 p.
6. J.T. Edward, Molecular volumes and the Stokes–Einstein equation, J. Chem. Educ. 47 (1970) 261-270.
7. G.J. Jenks, NMR Investigation of the Nitrogen Quadrupole Coupling Constant in Liquid Samples, J. Chem. Phys. 54(2) (1971) 658-663.
8. A. Gierer and K. Wirtz, Zeit. Naturforsch., 1953, AS, 532
9. G. K. Youngren and A. Acrivos, J. Chem. Phys., 1975.63, 3846
10. H. Lamb, Hydrodynamics, Dover, New York (1932) 605 p.
11. J.T. Edward, Molecular volumes and the Stokes–Einstein equation, J. Chem. Educ. 47 (1970) 261-270.
12. D.J.F.M.J. Frisch, G.W. Trucks, H.B. Schlegel, G.E. Scuseria, M.A. Robb, J.R. Cheeseman, G. Scalmani, V. Barone, G.A. Petersson, H. Nakatsuji, X. Li, M. Caricato, A. Marenich, J. Bloino, B.G. Janesko, R. Gomperts, B. Mennucci, H.P. Hratchian, J.V. Ort, Gaussian, Revision D.01, Gaussian Inc, Wallingford CT, 2016.
13. G.V. Mozzhukhin, G.V. Kupriyanova, S.Sh. Mamadazizov, A. Maraşlı, B.Z. Rameev, Low-field 14N nuclear magnetic resonance for detection of dangerous liquids, Chemical Physics, Volume 513, Pages 129-134, September 2018.
14. V.Nikolic, M.Stankovic, L.Nikolic, D.Cvetkovic, A.Kapor, M.Cakic, Chemical Industry and Chemical Engineering Quarterly, 2005, 1, 69
15. T.N.Drebushchak, E.V.Boldyreva, E.S.Shutova, Acta Crystallographica Section E: Structure Reports Online, 2002, 58, o634
16. J.M.Lehn, J.P.Kintzinger. Nitrogen NMR, 1973, p.86.

17. G.V. Mozzhukhin, G.V. Kupriyanova, S.Sh. Mamadazizov, A. Maraşlı, B.Z. Rameev, Low-field ^{14}N nuclear magnetic resonance for detection of dangerous liquids, Chemical Physics, Volume 513, Pages 129-134, September 2018.
18. D. T. EDMONDS AND P. A. SPEIGHT, Phys. Lett. A 35, 325 (1971).
19. D.S. Viswanath, T.K.Ghost, D.H.L.Prasad, N.V.K.Dutt and K.Y.Rani, Viscosity of liquids:Theory, Estimation, Experiments and Data, Springer, The Netherlands, ISBN-10 1-4020-5482-3, 2007. and technical datasheets from http://www.viscopedia.com/viscosity-tables ; http://angus.com; http://www.chemtradelogistics.com
20. Halonen, S., Kangas, T., Haataja, M. *et al.* Urea-Water-Solution Properties: Density, Viscosity, and Surface Tension in an Under-Saturated Solution. *Emiss. Control Sci. Technol.* **3,** 161–170 (2017).
21. H. Weingartner, M. Holz, and H. G. Hertz. Journal of Solution Chemistry, Vol. 7, No. 9, 1978
22. M.I. Burgar, Thomas E. St. Amour, and Daniel Flat. $^{17}0$ and ^{14}N NMR Studies of Amide Systems. *J. Phys. Chem.* 1981, 85, 502-510
23. S. Kojima, M. Minematsu, and M. Tanaka, *J. Chem. Phys.,* 31, 271 (1959)

Time domain NMR Pake-Doublet analysis of sorption cycles experiments of cement materials

Anastasiia Nagmutdinova[1], Leonardo Brizi[2], Paola Fantazzini[2], Villiam Bortolotti[1]

[1]Department of Civil, Chemical, Environmental and Materials Engineering, University of Bologna, Italy
[2]Department of Physics and Astronomy, University of Bologna, Italy
E-mail: anastas.nagmutdinov2@unibo.it
https://www.unibo.it/sitoweb/anastas.nagmutdinov2

Introduction

NMR (Nuclear magnetic resonance) relaxation techniques of ^{1}H nuclei have contributed in recent years to improve the knowledge of the nanoscale structure and water location during cement hydration. The dependence of longitudinal (T_1) and transverse relaxation (T_2) times on correlation times for molecular motion, allows the separation of lower mobility from higher-mobility ^{1}H nuclei on the basis of their free induction decay (FID) signals.

In many solids the main contribution to the local field experienced by a spin is due to one nearest-neighbour spin. Therefore, the absorption line can be supposed to come from a Gaussian- broadened two-spin interaction, where the broadening is due to the other neighbours. Pake [1] has showed an analytical expression for such an absorption line assuming spin ½ and Look *et al.* [2] succeeded in computing the Fourier transform of the Pake expression to determine the correspondence function in time. We used this function in the fitting procedure with experimental data to obtain information on the cement structures.

Origin of Pake-Doublet pattern

The dipolar coupling in a sample influences the shape of the NMR signal in time and frequency domain. Neighbouring nuclei in addition to external applied magnetic field B_0 influence the magnetic environment of the absorbing nuclei. In gases, liquids and some solids this influence is quite insignificant compared to the inhomogeneities of the external field. But for the crystalline solids, atomic nuclei usually are in certain lattice positions. In this case, the interaction of static magnetic dipoles is expected to determine line widths and shape for the nuclei with spin 1/2. Interacting nuclei produce a field, which component along B_0 will alter effective field. Different resonance frequencies are produced as this local component varies as $3\cos^2\theta - 1$, where θ − angle of inter-nuclear vector and B_0. The two lines splitting decrease with the cube of the inter-nuclear distance (Eq. 2) [3].

Solid phases in cement

In this study we will be focusing on the exploration of solid phases in cement materials during sorption cycles.

Hydrated cement past is a complex material with complex porosity and several solid phases. Portlandite (calcium hydroxide, $Ca(OH)_2$) and Ettringite ($3CaO.Al_2O_3.3CaSO_4.32\ H_2O$) could be named as mane solid phases. Through previous years there are many studies done on the solid phases in cement materials [4].

Methods and materials

All experiments were performed using White Portland Cement (Aalborg Cement). Fresh pastes were mixed at different water-to-cement ratios by mass, casted into glass tubes and left for 28 days underwater. Samples were dried in a home-made RH chamber. Samples were examined gravimetrically, till equilibrium was reached.

A relaxometer composed by a permanent magnet (ARTOSCAN, ESAOTE, Genova) with a magnetic field B0 ≈ 0.2 T, a 10 mm solenoid coil and a console (Stelar, Mede) were used at 25 °C to perform NMR experiments.

Relaxation time data of the solid components was acquired using Logarithmically distributed Aperiodic-Pulse-Sequence Saturation Recovery (LAPSR) pulse sequence $((\pi_x)_{10} - ((\pi/2)_x - t_l - (\pi/2)_x - \text{FID acquisition})_n)$. Data analyse is discussed further.

Pake function in time domain and fitting

For the dipolar coupled spin 1/2, a physically founded model is obtained by considering that the FID signal can be fitted with $G(t)$, the inverse Fourier transform of the Pake doublet. $G(t)$ is the sum of a Gaussian modulated by an oscillating term, plus an exponential for the "liquid component" (free water).

$$G(t) = \alpha A\sqrt{8\pi}\, e^{-\frac{1}{2}\beta^2 t^2}\left[\frac{\cos(\alpha t)}{\sqrt{\alpha t}} C\left(\sqrt{\frac{6}{\pi}\alpha t}\right) + \frac{\sin(\alpha t)}{\sqrt{\alpha t}} S\left(\sqrt{\frac{6}{\pi}\alpha t}\right)\right] \quad (1)$$

Where C(x) and S(x) are the Fresnel integrals, β is a parameter that accounts for dipolar interactions between non-nearest neighbour ^{1}H nuclei, and α is related to the proton-proton distance as:

$$\alpha = \frac{3}{4}\frac{\mu_0}{4\pi}\frac{\gamma^2 \hbar}{r^3} \quad (2)$$

where r is the distance between the two interacting nuclei, γ is the gyromagnetic ratio, μ_0 is the magnetic permeability of free space, and $\hbar$ the reduced Planck constant.

With the use of Pake-Doublet function in the time domain, as computed by Look *et al.*, (Eq. 1), it is possible to distinguish different populations of less-mobile ^{1}H, monitor their evolution and have information on proton-proton distance of these components (Eq. 2).

With the use of homemade scripts and Psi-Plot software [5] fittings were performed for the cement samples at different RH levels. It was found, that the best fit is obtained by using two solid-like components and one liquid-like component.

An example of the fitting for the cement sample, dried to 50 % RH is shown in the Fig. 1a. With the use of this fitting procedure changes to the solid component through drying are shown in the Fig. 1b and corresponding T_g relaxation time and proton-proton distances are shown in Table 1.

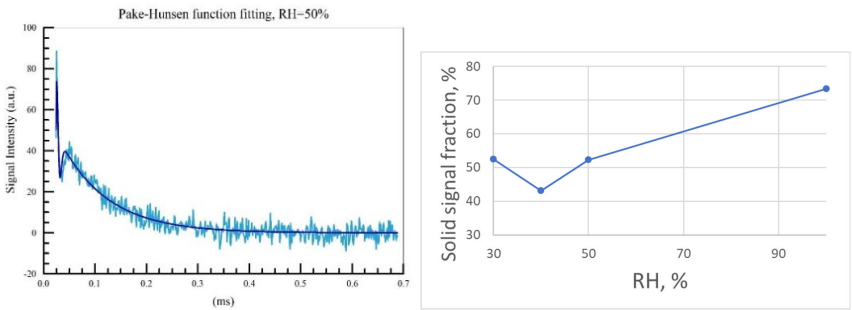

a) *b)*

Figure 1. a) Part of the FID representing the solid long component, where solid line is Eq. 2 fit, b) Fraction of the solid signal through drying process in respect to the total signal (liquid+solid)

Table 1. Relaxation time and proton-proton distance of the two solid components evolution through drying

RH,%	T_{21g} (ms)	Proton-proton distance R_1 (Å)	T_{22g} (ms)	Proton-proton distance R_2 (Å)
100	0.011	1.76		
75	0.011	1.47	0.045	2.00
50	0.015	1.37	0.041	1.89
40	0.013	1.39	0.040	1.91
30	0.014	1.39	0.042	1.92

From these results, and other repetition experiments showing the same behaviour, it seems that solid signal intensity decreased down to 40% RH and increased just after. The trend is similar to what was found by Maruyama et al. But to verify this evolution, more experiments with more sampling points are needed.

From the proton-proton distance R_1, by comparing the value to one obtained by SAX or SANS measurements, this component was associated to ettringite.

Similar trend is observed for oven-dried samples, but with some decrease of proton-proton distance (not showed here). This might suggest the densification of the structure, when particles are brought closer together.

It seems, that changes of the solid components happened, as suggested from T_1 measurements. These experiments suggest that Pake-Doublet analysis could be used for observation of cement solid components during sorption experiments.

As far we know so far, there were not studies done on Pake doublet observation of cement materials during sorption cycles.

Acknowledgements

This work is supported by Horizon 2020 – Marie Skłodowska-Curie – Innovative Training Network (ITN) – 2017 Actions. Grant Agreement no. 764691.

References

1. G. E. Pake. J. Chem. Phys. 1948, 16, 327−336.
2. D. C. Look, I. J. Lowe, J. A. Northby. J. Chem. Phys. 1966, 44, 3441−3452.
3. B. Cowan, Nuclear Magnetic Resonance and Relaxation, Cambridge Un., 2005. P. 434.
4. Y. Aono et al., Nano-structural changes of C-S-H in hardened cement paste during drying at 50□C, Journal of Advanced Concrete Technology, V.5, n.3, pp: 313-323, 2007.
5. PSI-PLOT, Poly Software International, Pearl River, NY, U.S.A.

Broadband high resolution NMR studies of Topological Matter

W. Papawassiliou[1], J. P. Carvalho[1], M. Fardis[2], H. J. Kim[3], G. Papavassiliou[2], A. J. Pell[1]

[1]Department of Materials and Environmental Chemistry, Arrhenius Laboratory, Stockholm University, Svante Arrhenius väg 16 C, SE-106 91 Stockholm, Sweden
[2]Institute of Nanoscience and Nanotechnology, NCSR Demokritos, 15310 Aghia Paraskevi, Attiki, Greece
[3]Electron Microscopy Research Center, Korea Basic Science Institute, 169-148 Gwahak-ro, Yuseong-gu, Daejeon 34133, Republic of Korea
E-mail: wassilios.papawassiliou@mmk.su.se

Topological Materials represent a new quantum state of matter, enclosing a number of striking similarities with states of matter in High Energy Physics, such as Axions (particles that do not obey classical Maxwell electrodynamics and are expected to explain the missing dark matter of the Universe), or Majorana Fermions (particles with a dual particle-antiparticle nature) that have been predicted but never observed. Over the last years studies have been focused in topological insulators, which are non-trivial insulators hosting protected metallic electron states on their surface, as well as Dirac and Weyl semimetals (WSM) with protected electron states in their bulk interior. In all these materials the emerging new Physics is related with the fact that electron energy bands acquire a non-trivial robust topology with bands crossing linearly (E~k) at specific points of the Brillouin zone, the so called Dirac or Weyl nodal points.

Currently, the state-of-the-art method to observe topological electrons is Angle Resolved Photoemission Spectroscopy (ARPES). However, despite the great effectiveness of ARPES, there is a particular shortage in experimental methods, showing at atomic scale resolution how topological electrons spread in real space and interact with non-topological electrons and the crystalline structure; especially their elementary excitations in the vicinity of the nodal points.

In this work by combining advanced broadband high resolution NMR methods with DFT calculations and High Resolution Transmission Electron Microscopy, we succeeded for the first time to detect topological electrons on the surface of ultrafine Bi_2Te_3 nanoplatelets[1]. Herein, we will illustrate how surface electron orbital currents determine the topological properties and will discuss the role of otherwise invisible elementary excitations through spin-lattice (T_1) and spin-spin (T_2) NMR relaxation studies.

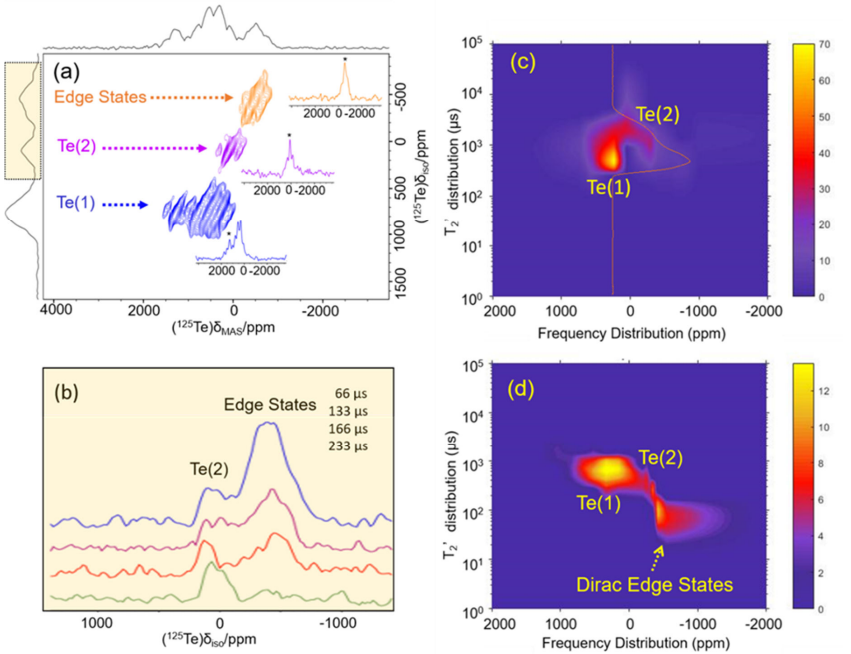

Figure 1. ***a.*** *2D ^{125}Te adiabatic Magic Angle Turning (aMAT) NMR spectrum of Bi_2Te_3 nanoplatelets. Blue and magenta colour contours indicate signals from the bulk interior of the nanoplatelets, while the orange colour contours show signals from the surface Te sites, shielded by the orbital motion of the Dirac electrons.* ***b.*** *The expanded isotropic projections of ^{125}Te MAT NMR spectrum acquired at four different evolution times.* ***c.*** *The ^{125}Te NMR T_2' distribution as a function of the resonance frequency of microcrystalline (bulk) Bi_2Te_3.* ***d.*** *The ^{125}Te NMR T_2' distribution as a function of the resonance frequency of the Bi_2Te_3 nanoplatelets*

References

1. Papawassiliou, W., Jaworski, A., Pell, A. J. et al. Resolving Dirac electrons with broadband high-resolution NMR. *Nature Communication* **11**, 1285 (2020).

The first observation of NMR in ^{169}Tm in magnetically diluted Van Vleck paramagnet $LiTm_{0.02}Y_{0.98}F_4$

A. S. Parfishina[1], A. V. Egorov[2], A. G. Kiiamov[1], S. L. Korableva[1], D. S. Nuzhina[1], A. A. Rodionov[1], I. V. Romanova[1], K. R. Safiullin[1], M. S. Tagirov[1,2]

[1]Kazan Federal University, 420008, Kazan, Russian Federation
[2]Tatarstan Academy of Sciences, Institute of Applied Research, Russia, 420111, Kazan
E-mail: arina.parfishina@gmail.com

Introduction

Van Vleck paramagnets (VVP) are compounds with a singlet or non-magnetic doublet ground state. Single crystals with rare-earth ions which have an even number of electrons on an unfilled 4f-shell (e.g. Ho^{3+}, Pr^{3+}, Eu^{3+}, Tb^{3+}, Tm^{3+}) are widely known examples of VVP [1]. $LiYF_4$ crystals activated by Ho^{3+}, Er^{3+}, Tm^{3+}, Dy^{3+} ions are frequently used in lasers as a converter of the frequencies from radiation to the infrared and visible spectral regions [2].

Van Vleck paramagnets could be researched by NMR method due to gigantic induced magnetic moment at the 4f-shell and, consequently, a huge hyperfine magnetic field at the his own nucleus. Detailed study of the NMR spectra and relaxation characteristics in the concentrated Van Vleck paramagnets were reviewed earlier in work [1]. We report the first NMR study of ^{169}Tm nucleus in a magnetically diluted single crystal VVP $LiTm_{0.02}Y_{0.98}F_4$ and compared our results with $LiTmF_4$.

Sample and experiment

The single crystal $LiTm_{0.02}Y_{0.98}F_4$ has a tetragonal structure of scheelite ($CaWO_4$) with the space group C_{4h}^6 [3]. NMR studying of the VVP single crystal was carried out using pulse home-built spectrometer. The range of magnetic field was 0–0.8 T, working frequencies were 14.15 MHz and 8.43 MHz, temperature region was 2–4.2 K.

Experimental results

We observed a strong anisotropy of the effective gyromagnetic ratio in the single crystal $LiTm_{0.02}Y_{0.98}F_4$. It matches with results for $LiTmF_4$, obtained earlier [1]. An angular dependence of the spin-lattice relaxation rate (T_1^{-1}) were measured and anisotropy close to the direction *[001]* were obtained. An angular dependence of the spin-spin relaxation rate (T_2^{-1}) relatively to a crystallographic axis were measured and calculated. The inhomogeneous linewidth was obtained and compared with the results for the concentrated VVP $LiTmF_4$ [1]. Temperature dependencies of the spin-lattice and spin-spin relaxation rates were measured. The interval between the singlet ground state to the first excited doublet state was determined equals to 25.9±0.2 cm^{-1} in approach of two-phonon Aminov-Orbach relaxation process. The value of splitting between the ground singlet and excited doublet for the concentrated $LiTmF_4$ is 31 cm^{-1} [4]. According to this result, we assumed different roots of correlation time in cases of diluted and concentrated Van Vleck paramagnets $LiTmF_4$.

Acknowledgements

This work was supported by the Russian Foundation for Basic Research, grant no. №18-42-160012 r_a.

References

1. Aminov L.K., Teplov M.A.: Sov. Phys. Usp. **28** 762-783 (1985)
2. Walsh. B.M.:Laser Physics. **19** 855-866 (2009)
3. Garcia E., Ryan R.R.:Acta Cryst.C. **49** 2053-2054 (1993)
4. Romanova, I.V., Tagirov, M.S. Magn. Reson. Solids **21**, 19412 (2019)

The role of radicals in the formation of pathogenic organomineral formations in the body

Alina A. Pichugina, Larisa V. Tsyro

Institute of Natural and Technical Sciences, Surgut State University, Lenina avenue 1, Surgut, Russian Federation
E-mail: alina.com9@mail.ru
http://www.surgu.ru

Introduction

Pathogenic organomineral formations are compounds containing organic and inorganic components. Such pathogenic formations include gallstones, urinary, salivary and dental calculi [1, 2]. The mechanism of formation of such organomineral aggregates is not completely clear and is controversial. As you know, many processes in living organisms are of a radical nature [3]. The accumulation of excess radicals leads to disruption of the body's work and initiates processes leading to the formation of one or another type of disease, including the formation of pathogenic organomineral aggregates [4, 5]. The method that allows direct detection of particles with an unpaired electron is electron paramagnetic resonance [6, 7].

In this work, samples of urinary and gallstones were studied using the method of electron paramagnetic resonance.

Research Methods

The objects of the study were gallstones (cholesterol, pigment and mixed types) and urinary stones (phosphate, oxalate, uranium and cystine types) removed from patients in the Tomsk region.

EPR spectra of the samples were obtained on a JOEL-FA200 spectrometer, under the following shooting conditions: t = 25 °C, microwave frequency ~ 9.4 GHz, modulation frequency 100 kHz, sensitivity $7 \cdot 10^9$ spin / 0.1 mT, maximum magnetic field sweep 500 mT, modulation width 1 mT, field sweep time 4 min. The sample was analyzed in a quartz ampoule 5 mm in diameter.

Results

By the method of electron paramagnetic resonance, it was found that all the studied samples of gallstones and urinary stones contain paramagnetic centers related to various molecules with unpaired electrons.

Figure 1 shows examples of EPR spectra of gallstones and urinary stones. So in the EPR spectra of cholesterol type of gallstones, a narrow line is observed in the region of the g-factor 2.003, which can be attributed to bilirubin radicals and radical ions $CO_2^{\cdot -}$, $CO_2^{\cdot 3-}$, $CO_3^{\cdot -}$, $CO_3^{\cdot 3-}$. In the EPR spectra of pigment and mixed types of gallstones, in addition to the signal related to bilirubin radicals and radical ions, there is a broad line with a g-factor of ~ 4.2, which refers to the paramagnetic centers of high-spin iron (III) with a nuclear spin of 5/2. In addition to these lines in the EPR spectra of pigment and mixed types of gallstones, there is a wide line in the region of the g-factor ~ 2.4–2.05. Interpretation of this line is difficult due to the superposition of signals inherent in the Mn^{2+} centers in the rhodochrosite and Cu^{2+} phase, in the form of two signals $g_{\parallel} = 2.37$ and $g_{\perp} = 2.05$, associated with four nitrogen atoms from the tetrapyrrole rings of bilirubin. Another feature of the pigment type of gallstones is the presence of an additional six lines in each line of the EPR spectrum sextet. Each such sextet is well resolved and is characteristic of the hyperfine splitting of the Mn^{2+} ion with a nuclear spin of 5/2.

In the EPR spectra of urinary stones (Fig. 1), there is a narrow line in the region of the g-factor of ~ 2.003, related to organic radicals such as, $\dot{C}_2O_4^-$, $-CH_2\dot{C}(CH_3)-R$ and $\dot{C}O_2^-$. In addition to the narrow line in the EPR spectra, there is also a wide line in the region of the g-factor ~ 2.4–2.3, the interpretation of which is difficult due to the complex chemical composition of urinary stones. However, it can be assumed that this line is characteristic of the Cu^{2+}, Mg^{2+} and Fe^{2+} centers with a nuclear spin of 3/2, which form various complexes with organic compounds that are part of the urinary stone. Also, in addition to the signals presented above, a weak signal with a g-factor of ~ 4.2 can be observed in the EPR spectra. This signal can be attributed to the Fe^{3+} and Cu^{2+} paramagnetic centers.

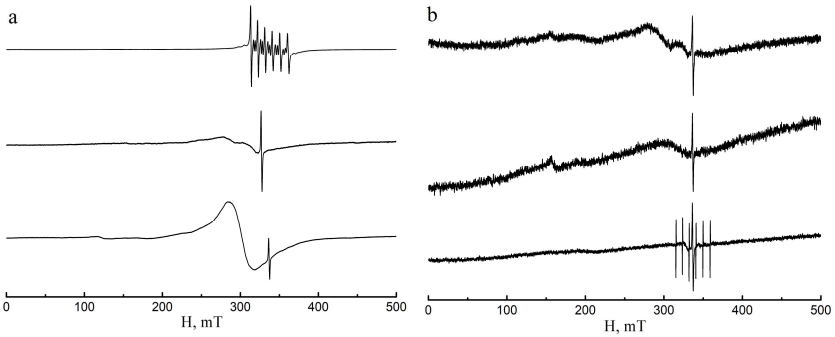

Figure 1. EPR spectra of gallstones (a) and urinary (b) stones

The radical processes taking place in the human body can have both a positive and negative effect on the functioning of the body. If the body does not work properly, negative radical processes begin to occur (the formation of various types of organomineral aggregates occurs, an abscess occurs, various kinds of tumors, etc.), as a result of which there is an excessive accumulation of radicals that the body is trying to remove. According to the study carried out, various kinds of radicals and paramagnetic centers are present in gallstones and urinary stones, and the concentration of such centers reaches about 10^{17}–10^{18} spin/g. Based on this, we can assume the following mechanism for the formation of organomineral aggregates - when an excessive amount of paramagnetic centers accumulate, their direct participation in reactions occurring in the body, including reactions with organic compounds, occurs, i.e. the formation of negative complex compounds, for example, various metal bilirubinates or undesirable uric acid salts, occurs. Further, molecules that do not have paramagnetic centers accumulate around such complexes, as a result of which a so-called associate is formed. Such an associate can be found in the body both in a free form and take a direct part in various radical processes with further enlargement of such an associate to an aggregate, the removal of which from the body is difficult.

Thus, in the work by the method of electronic paramagnetic resonance, it was shown that gallstones and urinary stones contain paramagnetic particles, which are directly involved in the formation of these organomineral aggregates.

References

1. O. A. Golovanova, O. V. Frank-Kamenetskay, Yu. O. Punin. – *Russian Journal of General Chemistry*, **81**, **6**, 1392-1406 (2011).
2. I. A. Abboud. – *Enviton Geochem Health*, **30**, 445-463 (2008).

3. Yu. A. Vladimirov. – *International Soros Science education Program – ISSEP*, **6**, **12**, 13-19 (2000).
4. F. G. Unger, L. V. Tsyro, A. A. Pichugina, D. A. Afanasiev, S. A. Kiselev. – *Herald of the Bauman Moscow State Tech. Univ, Nat. Sci.*, **4**, 107-122 (2016).
5. T. Sanikidze, E. Chikvaidze. – *Radiation Protection Dosimetry*, **172**, **1-3**, 317-324 (2016).
6. G. Elek, A. Rockenbauer. – *Wiener Klinische Wochenschrift*, **60**, 33-35 (1982).
7. R. Koseoglu, E. Koseoglu, F. Koksal, E. Basaran, D. Demirci. – *Radiation Measurements*, **40**, 65-68 (2005).

Electron spin resonance method data for core samples from the Tomsk region deposits

Alina S. Rakhimova, Alina A. Pichugina, Larisa V. Tsyro

Institute of Natural and Technical Sciences, Surgut State University, Lenina avenue 1, Surgut, Russian Federation
E-mail: lina.buyankina@mail.ru
http://www.surgu.ru

Introduction

The data obtained by the electron spin resonance method (ESR) are widely used in geological exploration. For example, in the study [1], for studying rocks (cores) of the Caspian region deposits geological section of exploratory wells by the ESR method was found that in addition to divalent manganese, the intensity of ESR signals of vanadium (IV) and organic free radicals (FR) in rock extracts can be as an indicator of oil content.

The ESR method make it possible to state that the vast majority of rocks have molecules with open orbitals, and the specific quantity of spins per unit volume of the pattern can be compared with the Avogadro number, and sometimes can be higher than it.

In the works of P. N. Nasirov [1, 2], the types of electron paramagnetic resonance spectra of high-spin Mn^{2+} ions recorded in terrigenous core rock obtained from various oil and gas wells from different depths of the Caspian region were studied. It was found that the content of Mn^{2+}, which is located in the cubic symmetry lattices minerals sharply increases in the layers of rocks that are close to the productive horizon. It can be assumed that this phenomenon is associated with the reducing effect of the hydrocarbon medium on the redox equilibrium between different manganese ions [3].

The shape of the ESR spectrum is different for each lithotype of core rock and oils of individual layers [4].

Research Methods

The experiment of cores spin properties study was carried out on an EPA-2M spectrometer with reference ruby rods embedded in the resonator, tested for the intensity of vanadylacetylacetonate [5].

A dry sample, previously grounded into powder, was spilled into the ampoule tested for intensity, which was placed in the ESR spectrometer resonator (microwave field $\lambda = 3.2$ cm). The shooting spectrum conditions: the electromagnet field was changed in the range of 60-520 mT; the time of the magnetic field sweep was 42 s; the amplitude of the RF modulation was 0.25 mT; the sensitivity was selected. The sample resonant absorption of the microwave energy was recorded by an amplitude-digital converter on a computer. The obtained spectra were processed using a program that includes integration and calculation of the area under the integral curve. The area was measured in abstract units, which were then converted to the concentration of spin centers (SC). By the spin center (SC) we mean any particle, such as atomic or molecular system, among the spin orbitals (described by the wave function square), where there is such orbital (or there are such orbitals), which are inhabited by a single electron.

Results

To obtain and study the electron spin resonance spectra, core models that selected from various depths of the Archinskoye, Gerasimovskoye, Kalinovskoye, Moiseyevskoye, Nizhne-Tabaganskoye, Severo-Kalinovskoye, and Solonovskoye deposits of the Tomsk Region are explained.

On Fig. 1 the differential and integral forms of the ESR spectrum of the Archinskoye field (well 45) are presented. Three peaks of ruby standards are recorded on the spectra: 50 mT - R_1; 220 mT - R_2, g = 2.4332; 406.32 mT - R_3, g = 1.3570.

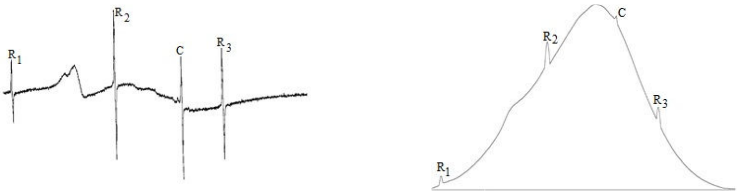

а *б*

Figure 1. ESR-spectrum of the Archinskoye field core (well 45): a-differential form; b-integral form

The analysis of the line shape allows us to draw important conclusions about the electronic complementary abilities. Each substance has its own characteristic spectrum and an g-factor. The cores of the Archinskoye, Gerasimovskoye, Kalinovskoye, Moiseyevskoye, Nizhne-Tabaganskoye, Severo-Kalinovskoye, and Solonovskoye deposits contain organic substance, as well as Fe*; V**; V****; Mn**; Fe*; Fe**.

In Fig. 2 and 3 the dependences of the C_{com} and C_C on the depth of studied deposits core sampling is shown.

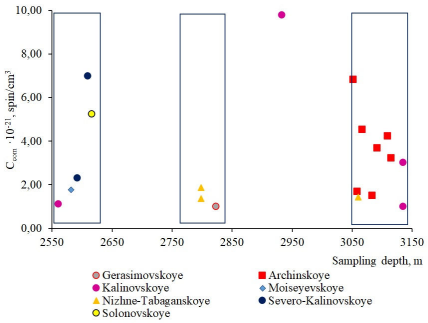

Figure 2. The dependences of the C_{com} on the sampling depth

The obtained dependences for the studied deposits cores demonstrate the following regularities for three depth ranges:

The total number of spin centers in the range of 2550-2650 m varies from 1×10^{21} to 7×10^{21} spin/cm^3, in the range of 2750-2850 m – from 1×10^{21} to 2×10^{21} spin/cm^3, in the range of 3050-3150 m-from 1×10^{21} to 7×10^{21} spin/cm^3; in the depth range from 2850-3050 m, only one core sample was used for the study and it demonstrated the maximum value of the spin centers number – 10^{22} spin/cm^3. Thus, the dynamics of preserving the total spin centers number in the specified depth ranges is observed in these deposits.

The concentration of spin centers for organic matter cores in the range 2550-2650 m varies in the range from 2×10^{18} to 10×10^{18} spin/cm^3, in the range 2750-2850 m – 1×10^{18} to 5×10^{18} spin/cm^3, in the range 3050-3150 m – 0.2×10^{18} to 11×10^{18} spin/cm^3; in the depth range from 2850-3050 m for the study was only one core sample that showed the average of the number of spin centers – 5×10^{18} spin/cm^3. Thus, the dynamics of the conservation of the spin centers number for organic substance in the specified depth ranges is observed in these deposits.

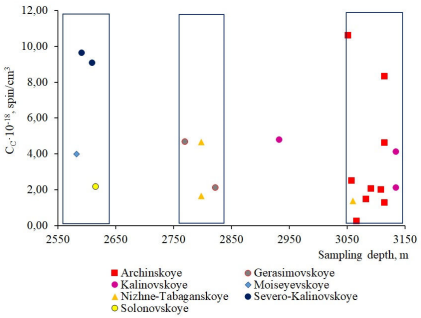

Figure 3. The dependences of the C_c on the sampling depth

The review of a large number of core spectra obtained by the ESR method for studied deposits various rocks allows us to conclude that the nature of the spin centers in the relates. For all the spectra, similar line shapes are observed. They are repeated for cores of different rocks and different deposits. It happens due to the fact that the chemical composition of different rocks differs slightly, core materials differ in the degree of cementation. The intensity of the line depends on the concentration of spin centers; the change in the shape of the line, and the displacement of the peaks depends on the radical structure.

The ESR spectra of all rocks types have a high intensity, a wide line, and a rather complex and unresolved appearance. The spectra analysis indicates the presence of multi – spin atoms with zero nuclear spin in the samples - an unresolved fine interaction (for example, iron group atoms). Elements of a more or less resolved hyperfine structure, which appear in peaks systems of 6 lines, indicate the presence of low-spin atoms in the rock with a nuclear spin of 5/2 (for example, manganese, aluminum, isotopes of magnesium, oxygen). The hyperfine structure of a narrow peak in the g ~ 2 region in such samples cannot be obtained due to the duration of lattice spin–relaxation processes, as evidenced by the low power of this absorption peak microwave saturation. At the same time, short relaxation times are typical for all other signal carriers, the saturation parameters for which are achieved only at a very high microwave power of the klystron. Thus, the spectra show the existence of associative combinations with unpaired electrons, containing multi-spin elements with zero nuclear spin and elements with nuclear spin 5/2, located near one unpaired electron. The intensity of the spectra indicates only a small admixture of breccia of diverse phase composition crystal structures, the spin structure of which is problematic. According to this feature, the studied core powders could be identified with poorly cemented nanomaterials of various compositions.

References

1. P.N. Nasirov, G.O. Sultangaliev. – Bulletin of the Moscow State Regional University. Series: natural sciences, 4, 58-60 (2009).
2. P.N. Nasirov. – Express information. Series Development of oil fields and methods of enhanced oil recovery. – VNIIOENG, 9, 14-17 (1992).
3. P.N. Nasirov, C.P. Solodovnikov. – Oil industry, 11, 31-32 (1992).
4. A.A. Frolov. – Innovative technologies in the oil and gas industry, 166-167 (2015).
5. F.G. Unger, L.N. Andreeva. – Fundamental aspects of oil chemistry. The nature of resins and asphaltenes (in Russian). – Novosibirsk: Nauka, 1995.

Pillar[5]arene complexes with palindromic DNA decamer and plasmid DNA

Polina V. Skvortsova[1], Dmitriy N. Shurpik[2], Natalia E. Gogoleva[1], Sufia A. Ziganshina[3], Ivan I. Stoikov[2], Bulat I. Khairutdinov[1]

[1]Kazan Institute of Biochemistry and Biophysics, FRC Kazan Scientific Center of RAS, 2/31 Lobachevsky Str., Kazan 420111, Russian Federation
[2]Kazan Federal University, Kremlyovskaya Str., Kazan 420008, Russian Federation
[3]Zavoisky Physical-Technical Institute, FRC Kazan Scientific Center of RAS, Sibirsky tract 10/7, Kazan 420029, Russian Federation
E-mail: skvpolina@gmail.com

Introduction

The development of systems for the efficient transfer of genetic material is one of the most promising scientific areas of medical therapy and diagnostics. Such systems can be based on the use of supramolecular platforms. Pillar[5]arenes are a class of new macrocyclic compounds that can potentially act as universal platforms for creating transport systems for the delivery of plasmid DNA into the cell, which can be used for biomedical applications.

DNA-pillar[5]arene complex

Positively charged pillar[5]arene was chosen to interact with negatively charged DNA. Figure 1 shows the structural formula of the investigated pillar[5]arene. We have studied pillar[5]arenes with iodine and chlorine counterions.

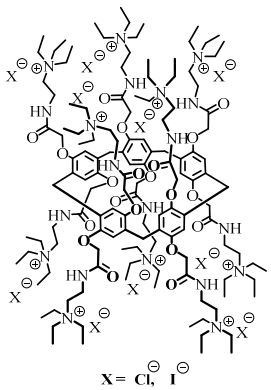

Figure 1. Pillar[5]arene structure

For the transport of genes across the membrane, the plasmid must be compacted. A necessary condition for the compactizaon of a plasmid with pillar[5]arene is their interaction and the possibility of complex formation. High-resolution NMR spectroscopy is a powerful method for detecting intermolecular interactions. However, this method imposes restrictions on the size of the studied molecules. Using NMR, it is impossible to obtain structural information about a complex with a plasmid molecule containing hundreds or thousands of nucleotides. Therefore, the palindromic DNA decamer was used to study the structure of the pillar[5]arene-DNA complex.

The NOESY spectra of the oligonucleotide (ONu) and the mixture of pillar[5]arene with the oligonucleotide were recorded and signal assignment for them were made. The NOESY spectra exhibit cross-peaks between spatially close atoms.

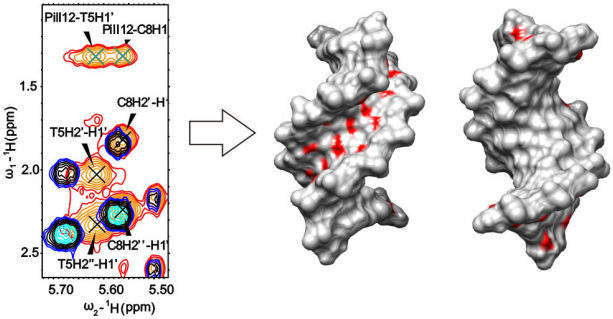

Figure 2. Fragment of superposition of NOESY spectra for ONu (blue-black signals) and ONu-pillar[5]arene-I⁻ mixture (yellow-red signals). Chemical shift changes of ONu signals and new intermolecular cross-peaks (green) appeared after adding pillar[5]arene to ONu mixture indicate complex formation. Visualization of ONu binding sites for pillar[5]arene-I⁻ protons was made based on the data on intermolecular cross-peaks

Figure 2 shows the map of the binding interface of the palindromic oligonucleotide to pillar[5]arene-I⁻, obtained from NOESY spectra. The terminal ethyl groups of pillar[5]arene-I⁻ are spatially close to the atoms of the minor groove of the ONu when interacting. Almost similar cross peaks were observed in the case of pillar[5]arene-Cl⁻ and the interaction also occurs along the minor groove of the ONu.

A model of the resulting complex was constructed using the molecular docking method (in AutoDock4.3 program) based on the experimental data and shown on figure 3.

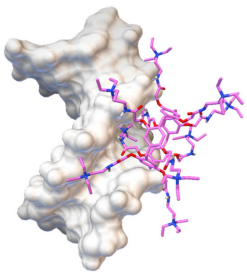

Figure 3. Model of the pillar[5]arene-ONu complex

Plasmid compactization

The ability of pillar[5]arene-I⁻ and pillar[5]arene-Cl⁻ to compact the plasmid was shown using AFM. The plasmid pEGFP-N1 was a circular structure as seen in the figure 4. It can also been see several overlays of the plasmid on itself. The plasmid molecules take the form of dense particles with non-condensed free regions emerging from the center when pillar[5]arene-Cl⁻ is added. With the addition of pillar[5]arene-I⁻ only dense particles are observed, non-condensed areas are not visible. Thus, pillar[5]arene-I⁻ condenses the plasmid more efficiently at the same concentrations than pillar[5]arene-Cl⁻.

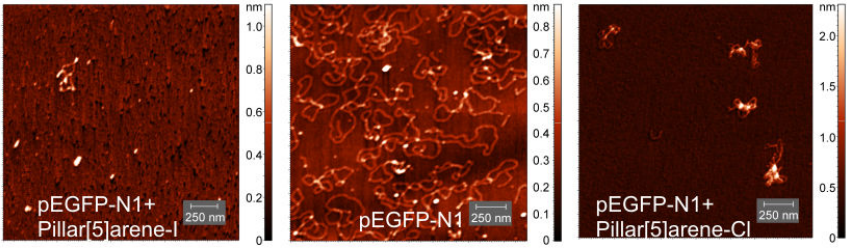

Figure 4. AFM images of pEGFP-N1 plasmid in a free state (center),mixtures plasmid-pillar[5]arene-I^- (z_+/z_- = 1) (left) and plasmid-pillar[5]arene-Cl^- (z_+/z_- = 1) (right). DNA concentration in all cases was 1 nM

Bacterial transformation efficiency

pEGFP-N1 plasmid has a part of the sequence responsible for resistance to canomycin. The E. coli Nova Blue cells were grown in a canomycin rich environment. Only cells that are resistant to this antibiotic survive in this case. To determine the efficiency of transformation in the presence of various concentrations of pillar[5]arenes 1 nM of pEGFP-N1 plasmid DNA was incubated with different concentrations of pillar[5]arenes.

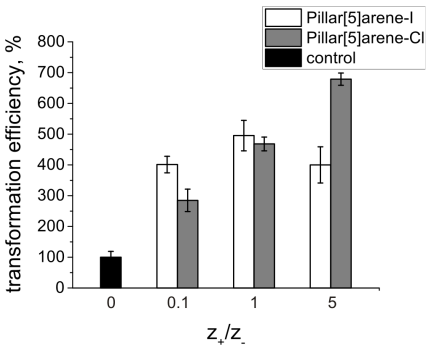

Figure 5. Effect of pillar[5]arenes concentration on the transformation efficiency of pillar[5]arene-I^- (white) and pillar[5]arene-Cl^- (gray).

The transformation efficiency for pillar[5]arene-I^- reached ~ 400-500% when the lowest of the investigated concentrations was added. A further increase in concentration did not lead to an increase in the transformation efficiency. For pillar[5]arene-Cl^-, the transformation efficiency increases with increasing concentration and reaches ~ 700% at the charge ratio z_+/z_- = 5.

Thus, it can be concluded that investigated pillar[5]arene can be used for the transport of genetic material and its properties depend on the counterions type.

Acknowledgements

This work was performed by the financial support from the government assignment for Federal Research Center (FRC) Kazan Scientific Center of Russian Academy of Sciences (RAS)

The authors gratefully acknowledge the Assigned Spectral-Analytical Center of FRC Kazan Scientific Center of RAS for possibility to fulfill the NMR experiments.

Spin properties of the water-Portland cement system

Larisa V. Tsyro, Alina A. Pichugina

Institute of Natural and Technical Sciences, Surgut State University, Lenina avenue 1, Surgut, Russian Federation
E-mail: tsyro@xf.tsu.ru
http://www.surgu.ru

Introduction

Cement is one of the main building materials. Improving cement properties at minimal cost is positioned as one of the most important tasks in cement chemistry. Most of the research aimed at improving the technology of cement production is based on the achievements of modern chemistry and physics: quantum mechanics, thermodynamics of the necessary processes of synergetics and solid state physics, etc. Water plays an important role in the cement hardening process. With a change in the concentration of water in the system, the rate of the elementary stages of the reaction changes, which leads to different strengths of the cement. The solidification process is also influenced by temperature: as it decreases, the structure and dynamics of water changes.

Today, there are many directions in the chemistry of cement, which are designed to improve the properties of the final material, but, unfortunately, scientists do not consider this problem from the standpoint of spin chemistry. The modern interpretation of the processes occurring during the hardening of the cement paste is based solely on charges. This approach is insufficient, because, despite numerous studies in this area, a unified and generally accepted theory of hardening of binding systems has not yet been created, the true nature of the forces leading to the strengthening of the structure and synthesis of the strength of the cement stone has not been revealed.

The discovery in the literature of the presence of a radical mechanism in the process of cement hardening is a clear demonstration of the possibilities of spin chemistry techniques. This formed the basis for using the electron spin resonance (ESR) method in the work. The use of the ESR method for studying cement systems in comparison with other physicochemical methods is quite rare among researchers. This method makes it possible to study the change in the total spin component of cement systems, i.e., the quantitative changes of all particles by open spin orbitals. These particles characterize the system during hardening by analyzing the spectrum in a wide sweep range of the magnetic field using direct radio spectroscopy in order to find new correlations with the properties of the resulting material. Consideration of the tendencies of the processes occurring in the cement system from the standpoint of spin interactions makes it possible to state that the hardening of cement and other similar binders occurs due to the participation of spin centers with the formation of new phase states leading to the formation of a cement stone.

Research Methods

The ESR method was used to analyze the cores. Preliminary preparation consisted of grinding a core sample in ball mills. The powder thus obtained was placed in an ampoule made of quartz glass, the ampoule was placed in the resonator of an ESR spectrometer. A spectrometer of the SE/X brand operating in the X-band was used. The device was tuned (the corresponding microwave modulation was selected), the spectrum was recorded. Conditions of spectrum shooting: a) field width 700 mT; b) sweep time 16 min; c) ν 9 GHz; d) the sensitivity was selected depending on the sample. Microwave modulation was selected in such a way that saturation would not occur for the sample.

Results

The ESR study used Portland cement X. To obtain a solid mass, the cement was mixed with tap water and distilled water in a W/C ratio of 0.1–0.7 at a temperature of 23 °C. The total concentration of spin centers of cement systems is of the order of 10^{-20} spin/g (depending on the water-cement ratio). Figure 1 shows the dependences of the total SC concentrations for samples mixed at 23 °C on the water-cement ratio, constructed from the results of calculations. It is noted that "seasoned" water cement system in a solid state comprises a minimal amount of particles with open spin-orbitals than the original cement. A decrease in the number of spin centers indicates an increase in the so-called cross-links in cement, which in turn contribute to an increase in the strength of the material [1].

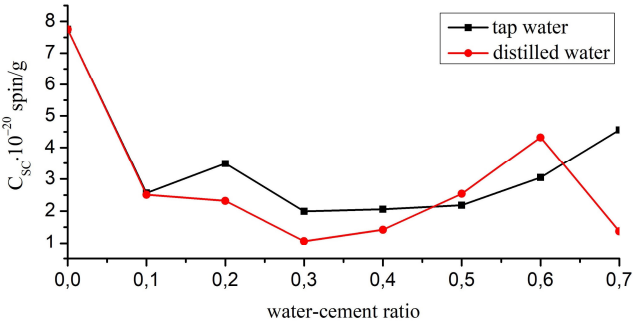

Figure 1. Dependence of the total concentration of SC on the water-cement ratio at 23 °C

It was also revealed that at a temperature of 23 °C (Fig. 1), the concentration of spin centers in the "cement + distilled water" system is lower than in the "cement + tap water" system. Probably, the hardness salts found in tap water can interact with this system (influence it) to one degree or another, introducing new and their own spin centers into it. This can also interfere with the recombination of molecules with open spin-orbitals. As a result, their concentration in cement hardened in tap water can be higher and its strength lower than in cement hardened in distilled water.

The concentration of spin centers in the region of the unresolved line with g ~ 2 was about 10^{-19} spin/g (Fig. 2).

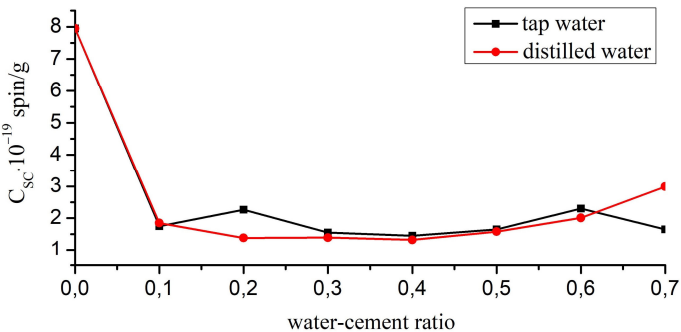

Figure 2. Dependence of the concentration of SC in the range g ~ 2 on the water-cement ratio at 23 °C

The recommended water-cement ratio is 0.4 (standard conditions), at which the resulting cement stone has high strength characteristics. The analysis of the given dependences for objects with both tap water and distilled water showed that the lowest concentration of spin centers is in the range of 0.3-0.5.

The hardening process in distilled water can be complicated by the absence of additional SC, low dissociation of water or low diffusion, due to an increase in the density of the system. It is known that hardness salts are a concentrate of spin centers [2]. Their presence in tap water allows them to participate in recombination in the process of cement hardening, leading to a decrease in SC, which is not observed in distilled water.

The data obtained are consistent with the mathematical model described in [3]. The work shows that the strength of densely laid concrete decreases as the amount of water in the concrete mixture increases. As the water consumption increases (at constant C), the volume of the cement paste increases, and its viscosity decreases. The maximum on the strength curves (W/C = 0.37) corresponds to the optimal water consumption for the given method of compaction, at which the mixture is placed most tightly. Excess water forms many fine capillary pores and cavities in cement stone and concrete. Therefore, the density and strength of concrete decreases [3, 4].

It has been shown by the method of electron spin resonance that during the hardening of cement, the content of spin centers in the samples changes, and different water-cement ratios lead to their different numbers, but the order of magnitude does not change. The range of water-cement ratio of 0.3-0.4, which is recommended by GOST for use from the standpoint of strength characteristics, is consistent with the minimum value of the number of spin centers in this range.

References

1. D.A. Afanaciev, L.V. Tsyro, Yu.S. Sarkisov, F.G. Unger, S.A. Kisilev, A.F. Unger. – *Siberian Journal of Science*, 5, 247-260 (2012).
2. L.V. Tsyro, L.N. Andreeva, S.Ya. Alexandrova, F.G. Unger. – *Journal water: chemistry and ecology*, 4, 66-73 (2011).
3. A.I. Schumkov. – *Concrete Technologies*, 3-4, 40-41 (2011).
4. V.G. Haach, G. Vasconcelos, P.B. Lourenço. – *Construction and Building Materials*, 25, 6, 2980-2987 (2011).

Nanoconfined water in pillared zeolites probed by ^{1}H NMR

A. S. Tyurtyaeva[1], D. Nefedov[1], A. Antonenko[1], R. Yocupicio-Gaxiola[2], M. G. Shelyapina[1], V. Petranovskii[3]

[1]Saint Petersburg State University, 7/9 Universitetskaya nab., Saint Petersburg 199034, Russia
[2]Centro de Nanociencias y Nanotecnología, Universidad Nacional Autónoma de México, Ensenada, B.C., 22860 México
[3]Centro de Investigacíon Científica y de Educacíon Superior de Ensenada, Apdo. 22860, Ensenada, B.C., México
E-mail: st064982student.spbu.ru

Introduction

Pillared zeolites, which represent zeolite layers stacked together and separated by pillars, besides micropores and microchannel typical for 3D zeolites possess macroporosity. The interlayered distance in pillared zeolites is normally about few nanometers, and these macropores may host larger molecules that micropores. This provides great opportunities to creation new composite materials and many practical applications including catalysis, CO_2 capture etc. At normal conditions zeolites are hydrated. Moreover, water is a promoter of many physical and chemical processes that take place in porous materials. From this perspective study of dynamics of such nanoconfined water is of special interest. Water molecules exhibit ability to form an extensive hydrogen-bonding network among themselves, so-called bulk water. In restricted geometries water molecules can also interact with surface. Due to a competition between the surface-water and water–water interactions new structures of water may appear. Both water structure and dynamics can be probed by proton nuclear magnetic resonance (NMR). As soon as ^{1}H chemical shift is sensitive to the structure and binding of individual water molecules, one can use it to study their local environment.

In our previous study we reported on a control of successive structural changes and states of the zeolite framework atoms and organic compounds at all stages of the synthesis of pillared zeolites with mordenite (MOR-P) and ZSM-5 (MFI-P) structures [1]. The formation of layered structures (with layer thickness of about 0.9 nm) separated by pillared of amorphous SiO_2 was confirmed. The interlayer distance was found to be equal to 4.0 and 5.2 nm for MOR-P and MFI-P, respectively. It should be noted that a partial drop out of Al from the zeolite frameworks in pillared zeolites were observed.

In this contribution we report on the results of our ^{1}H NMR study of the dynamics of water molecules confined in interlamellar space of pillared mordenite and ZSM-5 zeolites.

Experimental section

The synthesis procedure can be fined in Ref. [2]. ^{1}H NMR experiments were done applying a Bruker Avance IIITM 400 MHz solid-state NMR spectrometer using a double-resonance 4 mm low temperature magic angle spinning (MAS) probe. The rotation frequency was equal 12 kHz. The temperature was changed within a temperature range from 173 to 293 K and controlled with accuracy 0.5 K.

Results and discussion

There are a large number of different OH-containing species in zeolites, and quite often these signals overlap each other. Depending on the local environment, each proton is characterized by its own chemical shift. For the both MOR-P and MFI-P samples the ^{1}H MAS NMR signal shape near room temperature can be quite well described by two Lorentzian lines.

An example of such a spectrum for MOR-P at 273K is shown in Figure 1. The both lines can be attributed to water protons: the L2 signal at 5.1 ppm corresponds to bulk water, whereas the L1 line at 2.7 ppm is caused by protons of water molecules, which interact with silanol groups on the inner surface.

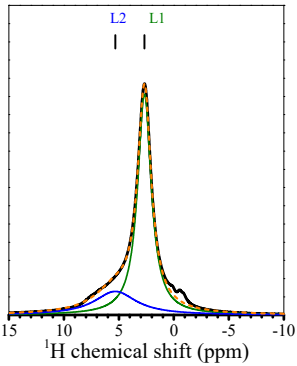

Figure 1. Decomposition of the ^{1}H MAS NMR spectrum for MOR-P at 273 K

The ^{1}H NMR spectra of the studied compounds evolve as temperature increasing. Figure 2 represents temperature changes of spectral parameter of the both lines: chemical shifts, δ, and full width at half maximum (FWHM), $\Delta\nu_{1/2}$. All the dependencies exhibit complex behavior. For MOR-P and MFI-P δ_{L1} decreases slightly in the temperature range from 293K to 217 K slightly decreases and then increases (with a local minimum at 264 K). δ_{L2} for MFI-P sharply increases when temperature is varied from 291 to 264 K, then reaches a plateau. Between 217 and 198 K it sharply decreases for MFI-P and with further cooling does not change.

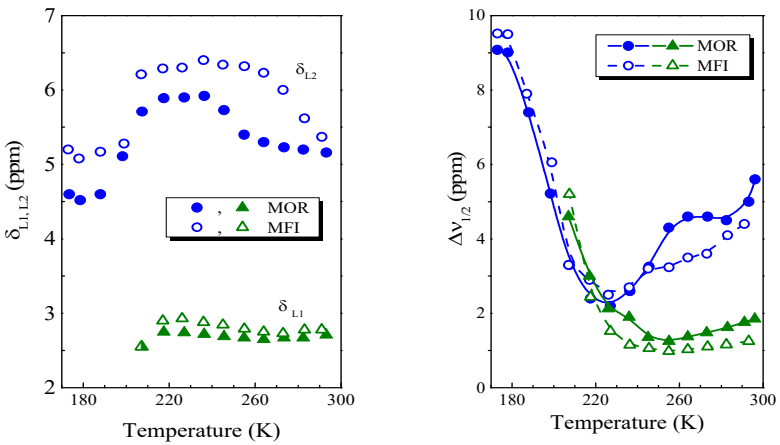

(a) *(b)*

Figure 2. (a) – temperature dependence of the ^{1}H chemical shift of the L1 and L2 lines; (b) – $\Delta\nu_{1/2}$ of the L1 and L2 lines versus temperature in MOR-P and MFI-P. Triangles and circles correspond to L1 and L2, respectively; close symbols – MOR-P, open symbols – MFI-P

For MOR-P, the temperature dependence of δ_{L2} has a less sharp increase and reaches a local maximum at a temperature of 255 K. Between 217 and 188 K chemical shift decreases down to 4.6 ppm for MOR-P and after remains almost constant. It is worth noting that as compared to MOR-P, MFI-P exhibits indicates stronger hydrogen bonding.

As one can see from Figure 2(b), the temperature behavior of the individual linewidths is rather similar for the both sample: $\Delta\nu_{1/2}$ of L1 first decreases slightly, and then increases rapidly at temperatures below 227 K. This temperature dependence of $\Delta\nu_{1/2}$ is typical of the motion of atoms in solids. However, the $\Delta\nu_{1/2}$ of L2 exhibits very complex behavior in the range from 293 to 237 K. In general, this indicates that in the temperature range from 199 to 293 K, there are at least three for MFI-P and four for MOR-P modes of water behavior. For the both samples the water freezing occurs at about 180 K.

Conclusion

To study water mobility in interlayer space of pillared zeolites with mordenite and ZSM-5 structure ^{1}H MAS NMR spectra were recorded. It was found out that water in the interlayer space of zeolites strongly interacts with inner surface formed by both zeolite layers and amorphous SiO_2 pillars. An interplay between water-water and water-surface interactions are strongly affected by temperature. In the studied pillared zeolites the temperature of freezing of nanoconfined water is about 180 K.

Acknowledgements

The work was supported by the Russian Foundation for Basic Research (project No. 18-53-34004). The materials were synthesized by R.I. Yocupicio-Gaxiola. The studies were performed at the Research Park of Saint Petersburg State University (Centre for Diagnostics of Functional Materials for Medicine, Pharmacology and Nanoelectronics).

References

1. M.G. Shelyapina, R.I. Yocupicio-Gaxiola, I.V. Zhelezniak, M.V. Chislov, J. Antunez-Garcia, F.N. Murrieta-Rico, D.H. Galván, V.P. Petranovskii, S. Fuentes-Moyado. Local Structures of Two-Dimensional Zeolites- Mordenite and ZSM-5-Probed by Multinuclear NMR. *Molecules* ***25*** (2020) 4678.
2. R.I. Yocupicio-Gaxiola, V. Petranovskii, J. Antúnez-García, S. Fuentes Moyado, One-pot synthesi of lamellar mordenite and ZSM-5 zeolites and subsequent pillaring by amorphous SiO_2, *Appl. Nanosci*. **9** (2019) 557.

Rotational motion of ions in alkylammonium nitrate ionic liquids by molecular dynamics simulation method

Milosh Ubovich, Andrei V. Egorov, Vladimir I. Chizhik

Faculty of Physics, Saint-Petersburg State University, Russia
E-mail: ubovich.milosh@yandex.ru

Introduction

Alkylammonium nitrate protic ionic liquids (AN PILs) are considered as perspective electrolytes for advanced fuel cells. In the present study a subset of three alkylammonium nitrate PILs: ethyl-, propyl-, and butylammonium nitrates (Fig. 1), was investigated by molecular dynamics simulations.

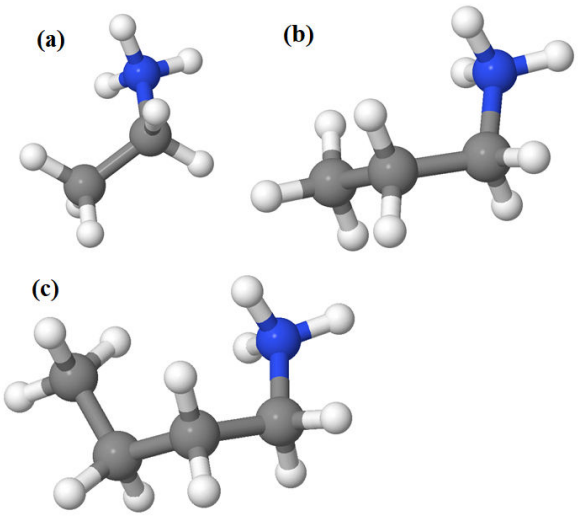

Figure 1. A schematic representation of cations ethyl- (a), propyl- (b), and butylammonium (c) nitrates

Simulation details and results

For each of three AN PILs a model system of 300 nitrate and 300 alkylammonium ions in a cubic periodic cell was simulated in the isothermal–isobaric ensemble at 298 K and 1 atm employing the MDynaMix simulation package [1]. The cations were modeled using the potentials described in Refs. [2-4]. Model nitrate anion (Fig. 2) was treated as a four-site planar structure with a central N atom and three O atoms at a distance of 1.22Å with all O-N-O angles of 120° [5]. Its intermolecular interactions were described as the sum of Coulomb and Lennard-Jones (6-12) potentials. Three different potential parameters sets, taken from Refs. [6-8], were considered.

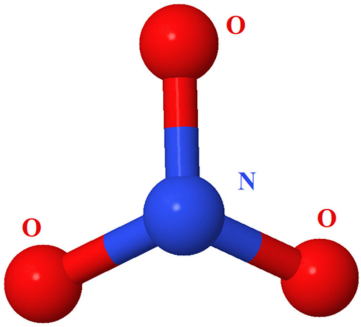

Figure 2. A schematic representation of nitrate anion

To describe the reorientational motion of ions the normalized time autocorrelation functions of various intramolecular vectors were calculated. A special attention was given to the reorientational correlation time of the C-H molecular vectors of the methyl and methylene groups of the cations. The effect of the alkyl chain length on the dynamical properties of alkylammonium nitrate PILs was studied in details.

References

1. A. P. Lyubartsev, A. Laaksonen. − Comp. Phys. Comm., 128, 565-589 (2000).
2. T. Mendez-Morales, J. Carrete, O. Cabeza, et al. – J. Phys. Chem. B, 118, 761-770 (2014).
3. V. Gomez-Gonzalez, B. Docampo-Alvarez, O. Cabeza, et al. – J. Chem. Phys., 143, 124507 (2015).
4. T. Mendez-Morales, J. Carrete, J. R. Rodriguez, et al. − Phys. Chem. Chem. Phys., 17, 5298-5307 (2015).
5. C. Ebner, R. Sansone, S. Hengrasmee, M. Probst. − Int. J. Quant. Chem., 75, 805-814 (1999).
6. T. Megyes, S. Balint. − J. Phys. Chem. B, 113, 4054-4064 (2009).
7. Y. Umebayashi, W.-L. Chung, T. Mitsugi, et al. – J.Comput. Chem. Jpn., 7, 125-134 (2008).
8. A. Laaksonen, H. Kovach. – Can. J. Chem., 72, 2278-2285 (1994).

Use of TD-NMR approaches for characterisation of bovine and porcine gelatin based soft candies

Sirvan Sultan Uguz[1], Leonid Grunin[2,3], Mecit Halil Oztop[1], Deniz Gunalan[1]

[1]Department of Food Engineering, Middle East Technical University, Ankara, Turkey
[2]Resonance Systems GmbH
[3]Department of Physics, Volga State University of Technology, Yoshkar-Ola, Mari El, Russian Federation, Russian Federation

TD-NMR technique mostly involves the use of T_1 (spin-lattice) and T_2 (spin-spin) relaxation times to explain the changes occurring in food systems. However, these relaxation times are affected from many factors and might not always be the best indicators to work with in food related TD-NMR studies. In this study, to our knowledge, the of *non-conventional* TD-NMR approaches of *Solid Echo/Magic Sandwich Echo and Spin Diffusion* in food systems were used for the 1st time. As the system of interest, soft confectionery gels were selected due to the simplicity of their composition and the flexibility of preparing standardized formulations. Soft confectionary gelatin gels were formulated and conventional (T_1, T_2) and non-conventional (SE, MSE and Spin Diffusion) TD-NMR experiments were performed. Gelatin-based candies were prepared with the same formulations by just one syrup type but by using bovine and porcine gelatin as the polymer sources. ºBrix and water activity (a_w) were also measured as the complementary experiments to NMR. T_1 times did not differ ($p > 0.05$) whereas T_2 times were found to be higher for the bovine gels despite their lower water activity. On the other hand, SE/MSE experiments which were performed to calculate the crystallinity of the samples yielded valuable results. Crystallinity values calculated from SE/MSE did not show differences with respect to gelatin source ($p > 0.05$). Spin Diffusion experiments were performed by using *Goldman-Shen* pulse sequence and the interface thickness (*d*) was calculated after a detailed data analysis. Interface thickness values calculated from SD experiments showed that porcine gelatin-based candies were more stable compared to bovine samples ($p < 0.05$).

Results showed that non-conventional NMR approaches had high potential to be utilized in food systems for quality control purposes.

Poster Session

Double step spin transition in binuclear Fe-Fe helicates with incapsulated anion by NMR spectroscopy

D. Yu. Aleshin[1,2], A. A. Pavlov[2], G. Aromi[3], V. V. Novikov[2]

[1]D. Mendeleev University of Chemical Technology of Russia, Moscow, Russian Federation
[2]A. N. Nesmeyanov Institute of Organoelement Compounds of RAS, Moscow, Russian Federation
[3]Departament de Quimica Inorganica i Organica, Universitat de Barcelona, Barcelona, Spain
E-mail: dima.aleshin26@gmail.com

Introduction

Spin crossover iron(II) complexes are perspective materials for data storage on the molecular level [1]. Thermodynamic parameters (e.g. enthalpy, entropy) of transition between low spin and high spin states have crucial importance for understanding spin equilibrium. Wide-used magnetometry and heat capacity methods provide full information about spin state of a molecule in solid state. For solutions, the Evans method is usually used in despite of low measurement accuracy. Paramagnetic NMR spectroscopy seems to be the most promising method to probe spin transition in a solution as long as it allows to overcome disadvantages of the Evans method [2, 3].

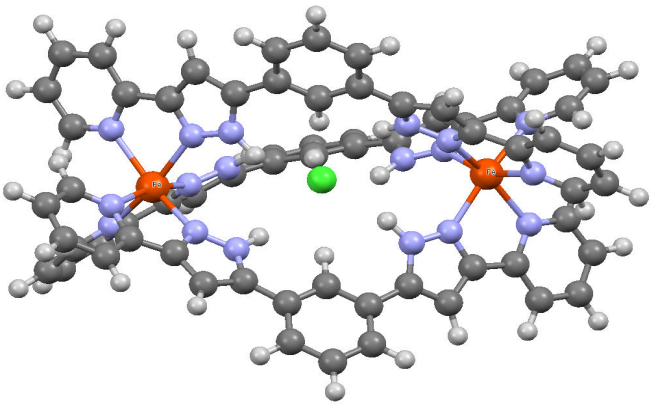

Figure 1. Structure of studied binuclear iron(II) complexes

Results

Here we report about the use of paramagnetic NMR spectroscopy to determinate double step spin transition and his thermodynamic parameters in binuclear Fe-Fe helicates with encapsulated anions (Fig. 1). Correlations between spin equilibrium parameters and encapsulated anion were revealed. The proposed approach is based on analysis of paramagnetic chemical shift temperature dependence. Obtained thermodynamic parameters were compared with solid state measurements [4].

Acknowledgements

This study was financially supported by the Russian Science Foundation (project no. 20-73-00194). Synthesis was performed with the financial support of the Council of the President of the Russian Federation (project no. MK-1301.2021.1.3).

References

1. K. S. Kumar, M. Ruben, Coordination Chemistry Reviews, 2017, 346, 176 – 205.
2. A. A. Pavlov, G. L. Denisov, M. A. Kiskin, V. V. Novikov, Inorg. Chem., 2017, 56, 24, 14759 – 14762.
3. H. Petzold, P. Djomgoue, G. Horner, J. M. Speck, T. Ruffer, D. Schaarschmidt, Dalton Trans., 2016, 45, 13798 – 13809.
4. M. Darawsheh, L. A. Barrios, O. Roubeau, S. J. Teat, G. Aromi, Chem. Eur. J., 2016, 22, 25,8635 – 8645.

Molecular dynamic of bound water in Antarctic lichenized fungus *Umbilicaria antarctica* Frey & I.M. observed by sorption isotherm and ^{1}H-NMR

Aleksandra Andrzejowska[1*], Karol Kubat[1], Angelica Casanova-Katny[2], Kazimierz Strzałka[5,6], Maria Olech[3,4] and Hubert Harańczyk[1]

[1]*M. Smoluchowski Institute of Physics, Jagiellonian University, Cracow, Poland,*
[2]*Faculty of Natural Resources, Catholic University of Temuco, Chile,*
[3]*Institute of Botany, Jagiellonian University, Cracow, Poland,*
[4]*Institute of Biochemistry and Biophysics, Polish Academy of Sciences, Warsaw, Poland,*
[5]*Malopolska Centre of Biotechnology, Jagiellonian University, Cracow, Poland,*
[6]*Faculty of Biochemistry, Biophysics and Biotechnology, Jagiellonian University, Cracow, Poland*
[*]*Corresponding author*
E-mail: aleksandra.pacura@student.uj.edu.pl

Antarctic lichenized fungi may survive extremely low temperatures and high desiccation. This research is focused on molecular mechanisms of these abilities.

The Antarctic lichen *Umbilicaria Antarctica* collected from the sites on rocks of Isla Robert, Southern Shetlands, maritime Antarctics, on July 7th, 2018, at Chilean 54. ECA (54 Expedition Cientifica Antartica). The rate and the sequence of saturation of three bound water fractions was tested.

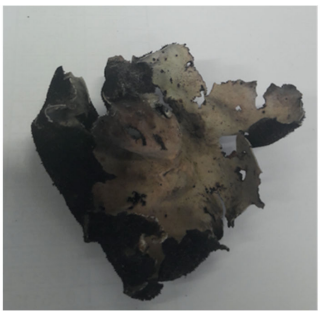

Figure 1. Thallus of Umbilicaria antarctica

Gaseous phase hydration and dehydration courses, sorption isotherm, ^{1}H-NMR spectrometry and relaxometry was used to monitor molecular dynamics of water in *U. antarctica* thalli. The hydration courses revealed bound water fractions: (i) a very tightly bound water A_0^h = 0,01(1) still present after dehydration over the silica gel, (ii) a tightly bound water fraction A_1^h = 0,08(1) with the hydration time t_1^h = 2,4(3) h, and (iii) a loosely bound water fraction with the hydration time t_2^h = 27(3) h. For $p/p_0 \geq$ 88% the total level of bound water significantly increases up to *ca*. 0,6 which may be interpreted as a recovery of life activity in *U. antarctica*. The dehydration kinetics is well described by a single-exponential function with the dehydration time t^d = 10(1) h. The sorption isotherm showed the multilayer sorption fitted well by a sigmoidal function. We fitted two models of the sorption process, namely a classic Brunauer-Emmett-Teller (BET) model, and a newer Dent model (Guggenheim-Anderson-de Boer = GAB). The GAB fits yield the value of primary binding sites contribution equal to $\Delta M/m_0$ = 0,05(1), as expressed in units of dry mass, m_0. The fraction of unoccupied binding

sites at p/p_0 = 100% equals $1/b_1$ = 0,01%, which may suggest elevated hydrophilicity level of the surface of *U. antarctica* thallus.

^{1}H-NMR spectra and relaxation times distinguish two signals of bound water: (i) a tightly bound water, and (ii) a loosely bound water fraction. ^{1}H-NMR spectrum is fitted well by superposition of Gaussian function (from partially immobilized protons of solid matrix) and one (up to $\Delta m/m_0 = 0.42$), or two Lorentzian function. The half-width of the solid Gaussian line component is equal to $\nu_G \approx 45$ kHz and does not change significantly with the increasing hydration level. The half-width of the first Lorentzian, coming from restricted in mobility tightly bound water fraction, decreases with the increased hydration level up until $\Delta m/m_0 = 0.45$ and does not change with higher hydration levels. The half-width of the second Lorentzian, coming from a loosely bound water fraction, also decreases with the increased hydration level across the entire measurement range. For tightly bound and loosely bound water the peak positions of the Lorentzian lines are different, which may be attributed to the difference in chemical shifts.

^{1}H-NMR FID (Free Induction Decay) function is fitted well by a superposition of one Gaussian function (protons of thallus solid matrix) and one (up to $\Delta m/m_0 = 0.30$) or two exponential functions. First exponentially relaxing signal comes mainly from tightly bound water relaxes with $T^*_{2L_1} \approx 100$ μs. Second exponential function is a signal coming from loosely bound water relaxing with $T^*_{2L_2} \approx 1000$ μs. *U. antarctica* thallus contains a water-soluble solid fraction. The saturation concentration of water-soluble solid fraction, $c_s = 0.55(9)$, and the dissolution effect is detected at least up to $\Delta m/m_0 = 0.7$.

Acknowledgements

This research was performed thanks to INACH (Instituto Antártico Chileno, Ministerio de Relaciones Exteriores, Chile): Sistema de Proyectos INACH, RT_27_16.

Computer simulation and NMR study of the temperature dependencies of the structural and dynamic characteristics of Lys2Arg peptide dendrimers

Valeriy V. Bezrodnyi[1,2], Sofia E. Mikhtaniuk[1,2], Oleg V. Shavykin[1,2], Igor M. Neelov[1,2], Nadezhda N. Sheveleva[1], Denis A. Markelov[1]

[1]St. Petersburg State University, 7/9 Universitetskaya nab., 199034 St. Petersburg, Russia
[2]St. Petersburg National Research University of Information Technologies, Mechanics and Optics (ITMO University), Kronverkskiy pr. 49, 197101 St. Petersburg, Russia
E-mail: v.v.bezrodniy@mail.ru, kupala-89@mail.ru

Introduction

New peptide dendrimers based on lysine dendrimer [1-4] but with additional spacers consisting of two aminoacid residues were recently studied experimentally by NMR [5-7] and tested as gene carrier successfully [8-9]. For Lys2Arg dendrimer with double Arg spacers the unusual slowing down of the orientational mobility of 2Arg spacers was revealed in comparison with similar 2Lys spacers in Lys2Lys dendrimer. It has been suggested that this unexpected behavior is caused by the Arg-Arg pairing effect in water, which leads to entanglements between dendrimer branches. We determine the reason for this slowing down using atomistic molecular dynamics simulation [10] of this dendrimer. The details of MD method [10] and structures of united atoms and full atomic models used for linear polymers [10-17], polyelectrolytes [18-25] and branched polymers [26-36] were described by us earlier.

The structural characteristics

Recently, it was shown [8] that a novel peptide dendrimer with Lys-2Arg repeating units developed for gene delivery provide better transport properties for si-RNA molecules than the similar dendrimers with Lys-2Gly and Lys-2Lys repeating units [9]. In this work, we performed MD simulation of the Lys-2Arg dendrimer studied earlier by NMR.

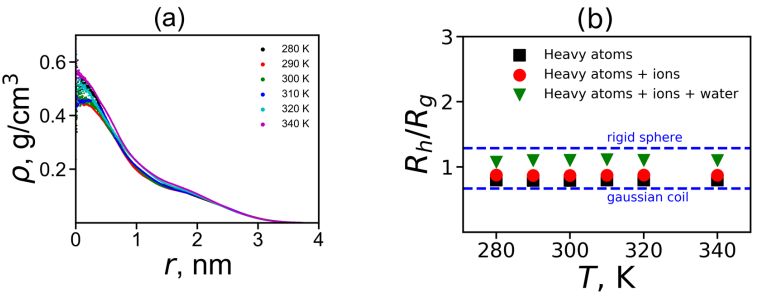

Figure 1. (a) The radial density distribution function of the Lys-2Arg dendrimer atoms at different temperatures. (b) The characteristic ratio R_h (in the Kirkwood approximation) to the radius of gyration R_g for Lys-2Arg for three alternative ways of calculations: taking into account the heavy atoms of this dendrimer only, for heavy atoms in the dendrimer and ions, for all heavy atoms in the system (carbons, nitrogens, and oxygens of the dendrimer; Cl ions; oxygens of water molecules)

Moreover, we compared the structure and the mobility of Lys-2Arg dendrimer [1] with characteristics of the Lys-2Lys dendrimer [2] obtained from the previous NMR experiments and MD simulation. We found that the size and shape of the Lys-2Arg dendrimer are very close to those of Lys-2Lys. The internal structure of both dendrimers is also very similar. The terminal

groups of these dendrimers are evenly distributed over the surface of both dendrimers. Lys-2Arg and Lys-2Lys have similar electrostatic characteristics (charge distribution, zeta potential etc). Most of the structural and electrostatic properties of both dendrimers are also independent of temperature, i.e. these dendrimers form similar stable nanocontainers.

The dynamic characteristics

Local orientational mobility of the inner and terminal lysine groups in each dendrimer is different. This difference in the mobility is approximately the same in both dendrimers and very close to that one obtained from NMR. However, the MD simulation carried out in this paper confirms the significant difference in the mobility of the side CH_2-N groups in the Lys-2Arg dendrimer in comparison with the same CH_2-N groups in the Lys-2Lys dendrimer obtained earlier in NMR experiment [1, 2].

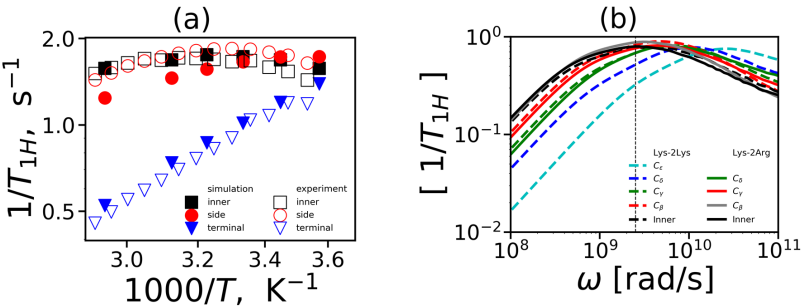

Figure 2. (a) The ^1H NMR spin-lattice relaxation rate $1/T_{1H}$ as a function of inverse temperature 1000/T for the inner, side and terminal CH_2 groups at the fixed frequency $\omega_H/2\pi$=400 MHz from the simulation and experimental data for Lys-2Arg; (b) the frequency dependencies of $[1/T_{1H}]$ in the susceptibility representation for H-H vector in the inner and the different types of CH_2 groups in side segments at T=310 K

We have revealed that this difference is due to the larger distance from the NMR active side CH_2-N group to the end of the side segment in the 2Arg spacer than the distance from a similar group in 2Lys spacer. We obtained also that if we calculate in simulation the mobility of other CH2 groups which have the same distance from the end of side segments then their mobility in Lys-2Arg and Lys-2Lys dendrimers is difficult to distinguish. Thus, the difference in the mobility of the side groups CH_2-N in spacers of these similar dendrimers makes it possible to detect and distinguish them in aqueous solution experimentally by NMR..

Acknowledgements

This work is supported by the Russian Science Foundation (grants No. 19-13-00087). The research is carried out using the equipment of the shared research facilities of HPC computing resources at Lomonosov Moscow State University [37] and Computer Resources Center of Saint Petersburg State University.

References

1. Denkewalter R.G., Kolc J., Lukasavage W.J., US Patent, 1983, № 4410688.
2. Neelov, I., Markelov D., Falkovich S.G., Paci E., Darinskii A., Tenhu H., Dendrimers in Biomedical Applications, (London: RSC) 2013, 99-114.
3. S. Falkovich, D. Markelov, I. Neelov, A. Darinskii. J. Chem. Phys. 2013, 139, 064903.
4. Neelov, I. M., Markelov D.A, Falkovich S.G., Darinskii A, Polym.Sci., 2013, 55, 154.

5. Sheveleva N.N., Markelov D.A., Vovk M.A., Tarasenko I.I, Neelov I.M., E.Lähderanta, 2019, RSC Adv. 9, 18018.
6. Sheveleva N.N., Markelov D.A., Vovk M.A. Mikhailova, M.E., Tarasenko I.I, Neelov I.M., E.Lähderant. Scientific Reports, 2018, 8, 8916
7. Sheveleva N.N., Markelov D.A., Vovk M.A., Tarasenko I.I, Mikhailova M.E., Neelov I.M., 2019, Molecules, 24, 2481
8. M. Gorzkiewicz,, A.Konopka, A.Janaszewska, A., I.I.Tarasenko, V.V.Bezrodnyi. I.M. Neelov, B.Klajnert, Int. J. Mol. Sci., 2020, 21 (9), 3138.
9. M.Gorzkiewicz, O.Kopec, A.Janaszevska, I.I.Tarasenko, N.N.Sheveleva, I.M. Neelov, B.Klajnert, Bioorg.Chem. 2020, 95, 103504.
10. Gotlib,Y.Y., Darinskii,A.A., Neelov, I.M., Balabaev, N.K. Macromol.,1980, 13, 602.
11. Neelov I.M., Adolf D.B., Lyulin AV., Davies G.R. J. Chem. Phys., 2002, 117,4030.
12. Darinskii A., Lyulin A., Neelov I., Makromolekulare Chemie - Theory and Simulations (Macromolecular Theory and Simulations), 1993, 2, 523.
13. Zarembo, A., Balabaev, N.K., Neelov, I.M., Darinskii, A.A., PCCP, 2003, 5, 2410.
14. Neelov I.M., Adolf D.B., McLeish T.C.B., Paci E., Biophys. J., 2006, 91, 3579.
15. Neelov I.M., Binder K., Macromolecular Theory and Simulations, 1995, 4, 1063.
16. Gowdy, J., Batchelor, M, Neelov, I, Paci, E. J. Phys. Chem. B, 2017, 121, 9518.
17. Neelov, I.M., Binder, K. Macromol. Theory&Simul/, 1995, 4(1), pp. 119–136
18. Ennari J., Neelov I., Sundholm F., Polymer, 2001, 42, 8043.
19. Ennari J., Neelov I., Sundholm F., Polymer, 2000, 41, 4057.
20. Darinskii A., Gotlib Yu., Lyulin A., Neelov I., Progr. Coll.&Polym.Sci., 1993, 91, 13.
21. Ennari J., Elomaa M., Neelov I., Sundholm F., 2000, Polymer, 41, 985
22. Ennari J., Neelov I., Sundholm F., Comput. Theor. Polym. Sci., 2000, 10, 403. .
23. Darinskii A.,Gotlib Yu., Lyulin A., Neelov I., Vysokomolek. Soed.. ,A 1991, 33, 1211
24. Ennari J., Neelov I., Sundholm F., Polymer, 2000, 41, 2149.
25. Ennari J., Neelov I., Sundholm F., Polymer, 2004, 45, 4171
26. Mazo M.A., Shamaev M.Y., Balabaev N.K., Neelov I.M., PCCP, 2004, 1285.
27. Okrugin B., Ilyash M., Markelov D., Neelov I., Pharmaceutics, 2018, 10, 129.
28. Neelov I.M., Adolf D.B., 2004, J. Phys. Chem. B, 108, 7627.
29. O.V.Shavykin, I.M.Neelov, A.A.Darinskii. PCCP, 2016, 18, 24307
30. Neelov I.M., Adolf D.B., 2003, Macromolecules, 36, 6914.
31. Shavykin O.V., Mikhailov I.V., Darinskii A.A., Neelov I.M., Polym., 2018, 146, 256.
32. Okrugin B.M., Neelov I.M., Leermakers F., Borisov O.V., Polym, 2017, 125, 292.
33. Shavykin O.V., Leermakers F, Neelov I.M., Darinskii A.A, Langmuir, 2018, 34, 1613.
34. Mikhtaniuk, S.E., Bezrodnyi, V.V., Shavykin, O.V., Neelov I.M., Penkova, A.V., Markelov, D.A., Polymers, 2020, 12(8), 1657.
35. Bezrodnyi, V.V., Shavykin, O.V., Mikhtaniuk, S.E., Neelov I.M., Sheveleva, N.N., Markelov, D.A., Int. J. Mol. Sci., 2020, 21(24), 1–22, 9749.
36. Shavykin, O.V., Neelov, I.M., Borisov, O.V., Darinskii, A.A., Leermakers, F.A.M.,Macromolecules, 2020, 53(17), pp. 7298–7311.
37. Sadovnichy, V.; Tikhonravov, A.; Voevodin, V.; Opanasenko, V. "Lomonosov": Supercomputing at Moscow State University. In Contemporary High Performance Computing: From Petascale toward Exascale; Chapman and Hall/CRC: Boca Raton, FL, USA, 2013; pp. 283–307.

Novel lysine-based peptide dendrimers modeled by the self-consistent field approach

Valeriy V. Bezrodnyi[1,2], Oleg V. Shavykin[1,2], Igor Neelov[1,2]

[1]St. Petersburg State University, 7/9 Universitetskaya nab., 199034 St. Petersburg, Russia
[2]St. Petersburg National Research University of Information Technologies, Mechanics and Optics (ITMO University), Kronverkskiy pr. 49, 197101 St. Petersburg, Russia
E-mail: v.v.bezrodniy@mail.ru, kupala-89@mail.ru

Introduction

Lysine and peptide dendrimers [1-4] were tested for a long time for applications in drug and gene delivery [5-11]. Computer simulation of these systems were performed by molecular dynamics and Brownian dynamics simulation [2-4, 7-8, 12-18]. Numerical self-consistent field (SCF) approach was applied to them also [19-21].

The novel dendrimers were modeled using the numerical self-consistent field method. A model of united atoms used earlier for linear polymers and peptides [22-37] showed good agreement with our recent results on full atomic simulation of the same peptide dendrimers using molecular dynamics simulation [7, 8].

The united atom model of novel peptide dendrimers

Self-consistent field approach and the set of Flory parameters for united atoms, which were successfully applied by us earlier for SCF study of non-charged and charged lysine dendrimers [19, 21] was used. The size of lattice corresponds the average bond length between monomer beads in the Amber force-field. We consider four model dendrimers: with Lys-2Ala, Lys-2Gly, Lys-LysAla and Lys-2Lys repeat units similar to dendrimer studied by us earlier in MD simulation using full atomic models [7-8].

The structure of novel peptide dendrimers

The dependencies of the radius of gyration of the dendrimers at the salt concentration are shown in the figure 1a. The salt dependencies for core-to-end distance also estimated (Figure 1b).

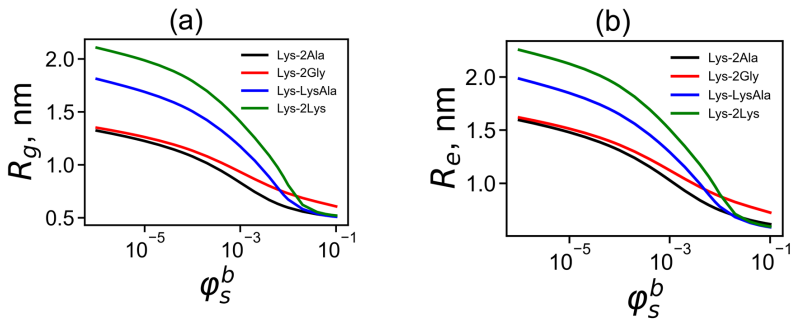

Figure 1. The salt dependencies for (a) gyration radius R_g (b) the core-to-end distance R_e

Table 1. The gyration radius R_g (nm), the core-to-end distance R_e (nm) in a salt-free solution

Term	R_g [nm]	R_e [nm]
Lys-2Ala	1.28	1.60
Lys-2Gly	1.35	1.62
Lys-LysAla	1.81	1.98
Lys-2Lys	2.11	2.25

The average sizes (the radius of gyration R_g and the core-to-end distance R_e) for four dendrimers in case of salt-free solution are shown in the Table 1. These values are in good agreement with molecular dynamic simulations of similar dendrimers on full atomic models [7-8].

Acknowledgements

This work is supported by the Russian Science Foundation (grants No. 19-13-00087). The research is carried out using the equipment of the shared research facilities of HPC computing resources at Lomonosov Moscow State University [2].

References

1. Denkewalter R.G., Kolc J., Lukasavage W.J., US Patent, 1983, № 4410688.
2. Neelov, I. M., Markelov D.A, Falkovich S.G., Ilyash M.Y., Okrugin B.M., Darinskii A.A., Polymer Science, 2013, 55, 154.
3. S. Falkovich, D. Markelov, I. Neelov, and A. Darinskii. J. Chem. Phys. 2013, 139, 064903.
4. Neelov, I., Markelov D., Falkovich S.G., Paci E., Darinskii A., Tenhu H., Dendrimers in Biomedical Applications, (London: RSC) 2013, 99-114.
5. M.Gorzkiewicz, O.Kopec, A.Janaszevska, I.I.Tarasenko, N.N.Sheveleva, I.M. Neelov, B.Klajnert, Bioorg.Chem. 2020, 95, 103504.
6. M. Gorzkiewicz,, A.Konopka, A.Janaszewska, A., I.I.Tarasenko, V.V.Bezrodnyi. I.M. Neelov, B.Klajnert, Int. J. Mol. Sci., 2020, 21 (9), 3138.
7. Mikhtaniuk, S.E., Bezrodnyi, V.V., Shavykin, O.V., Neelov I.M., Penkova, A.V., Markelov, D.A., Polymers, 2020, 12(8), 1657
8. Bezrodnyi, V.V., Shavykin, O.V., Mikhtaniuk, S.E., Neelov I.M., Sheveleva, N.N., Markelov, D.A., International Journal of Molecular Sciences, 2020, 21, 9749, 1–22.
9. Sheveleva N.N., Markelov D.A., Vovk M.A. Mikhailova, M.E., Tarasenko I.I, Neelov I.M., E.Lähderant. Scientific Reports, 2018, 8, 8916
10. Sheveleva N.N., Markelov D.A., Vovk M.A., Tarasenko I.I, Neelov I.M., E.Lähderanta, 2019, RSC Adv. 9, 18018.
11. Sheveleva N.N., Markelov D.A., Vovk M.A., Tarasenko I.I, Mikhailova M.E., Neelov I.M., 2019, Molecules, 24, 2481
12. Mazo M.A., Shamaev M.Y., Balabaev N.K., Darinskii A.A., Neelov I.M., Physical Chemistry Chemical Physics, 2004, 1285.
13. Okrugin B., Ilyash M., Markelov D., Neelov I., Pharmaceutics, 2018, 10, 129.
14. Neelov I.M., Adolf D.B., Macromolecules, 2003, 36, 6914.
15. Neelov I.M., Adolf D.B., J. Phys. Chem. B, 2004, 108, 7627.
16. Markelov D.A., Falkovich S.G.,, Neelov, I. M., et al, PCCP, 2015, 17, 3214
17. O.V.Shavykin, I.M.Neelov, A.A.Darinskii. PCCP, 2016, 18, 24307
18. Shavykin O.V., Mikhailov I.V., Darinskii A.A., Neelov I.M., Leermakers F.A.M., Polymer, 2018,146, 256.

19. Okrugin B.M., Neelov I.M., Leermakers F., Borisov O.V., Polymer, 2017, 125, 292.
20. Shavykin O.V., Leermakers F., Neelov I.M., Darinskii A.A, Langmuir, 2018,34, 1613.
21. Shavykin, O.V., Neelov, I.M., Borisov, O.V., Darinskii, A.A., Leermakers, F.A.M., Macromolecules, 2020, 53(17), pp. 7298–7311
22. Gotlib, Y.Y., Darinskii, A.A., Neelov, I.M., Balabaev, N.K. Macromolecules, 1980, 13(3), 602–608
23. Darinskii A., Lyulin A., Neelov I., Makromolekulare Chemie - Theory and Simulations (Macromolecular Theory and Simulations), 1993, 2, 523.
24. Neelov I.M., Adolf D.B., Lyulin AV., Davies G.R. J. Chem. Phys., 2002, 117,4030.
25. Zarembo, A., Balabaev, N.K., Neelov, I.M., Sundholm, Darinskii, A.A., , F. PCCP, 2003, 5(11), 2410–2416
26. Neelov I.M., Adolf D.B., McLeish T.C.B., Paci E., Biophys. J., 2006, 91, 3579.
27. Gowdy, J., Batchelor, M, Neelov, I, Paci, E. J. Phys. Chem. B, 2017, 121, 9518.
28. Neelov I.M., Binder K., Macromolecular Theory and Simulations, 1995, 4, 1063.
29. Neelov, I.M., Binder, K. Macromol. Theory&Simul/, 1995, 4(1), 119–136
30. Ennari J., Neelov I., Sundholm F., Polymer, 2000, 41, 4057.
31. Ennari J., Neelov I., Sundholm F., Polymer, 2001, 42, 8043
32. Darinskii A., Gotlib Yu., Lukyanov M., Lyulin A., Neelov I., Progress in Colloid & Polymer Science, 1993, 91, 13.
33. Ennari J., Neelov I., Sundholm F., Comput. Theor. Polym. Sci., 2000, 10, 403.
34. Ennari J., Elomaa M., Neelov I., Sundholm F., 2000, Polymer, 41, 985.
35. Darinskii A., Gotlib Yu., Lyulin A., Neelov I., Vysokomolek. Soed.. Ser,A 1991, 33, 1211 (translation to English: Polymer Science, 33,1116).
36. Ennari J., Neelov I., Sundholm F., Polymer, 2004, 45, 4171
37. Ennari J., Neelov I., Sundholm F., Polymer, 2000, 41, 2149.
38. Sadovnichy, V.; Tikhonravov, A.; Voevodin, V.; Opanasenko, V. "Lomonosov": Supercomputing at Moscow State University. In Contemporary High Performance Computing: From Petascale toward Exascale; Chapman and Hall/CRC: Boca Raton, FL, USA, 2013; pp. 283–307.

The classification of residual bound water fractions in rehydrated phospholipid lyophilizates

A. Bogdał[1], K. Kubat[1], M. Jemioła-Rzemińska[2], K. Strzałka[2] and H. Harańczyk[1]

[1]Institute of Physics, and [2]Faculty of Biochemistry, Biophysics and Biotechnology; Jagiellonian University, Cracow, Poland

The cells and organelles are surrounded by a cell membrane. The membrane structure is based on a lipid bilayer in a liquid crystal laminar phase L_α [1]. Multilayer liposomes are models of natural biological membranes. They are well suited for studying the molecular structure and dynamics of membrane lipids [2, 3]. For these research as a biological membrane model, we have selected synthetic phospholipids such as DPPC, DOPC. The DOPC model biological membrane is built from the glycerol backbone to which two 18-carbon oleic acid chains are attached, and a hydrophilic head containing orthophosphate and choline. The DPPC molecule differs from the previously analyzed type of hydrophobic part, which consists of two chains of palmitic acid. The phase transition temperature for these lipids is respectively: for DPPC about 41°C, and about -15 °C for DOPC. The unsaturated bonds cause lateral torsion of hydrocarbon chains, leading to a reduction in the density packing of biological membrane.

Multilayer liposomes were prepared by using the thin film method, which is a basic method for preparing multilayer liposomes MLV. Then the material was frozen at -80^0C for about 2 hours under atmospheric pressure. Freeze drying lasted 3 days and included ice sublimation at 0.01 mbar pressure and -60^0C temperature. Samples were prepared immediately after freeze-drying without incubation. Freeze drying is a process practically for food preservation in food industry.

The dehydration courses were performed for DPPC and for DOPC at 100% relative humidity. ^{1}H-NMR spectra were collected on Bruker Avance III 300, Bruker Biospin, spectrometer (transmitter power 400 W; pulse length $\pi/2 = 2.2$ μs; bandwidths 300 kHz). All measurements are made at room temperature.

The hydration process of multilayer DOPC liposomes is different from the system consisting of DPPC. The adopted procedure may result in a different form of external surfaces, which make local structures more vulnerable to the penetration of water molecules deposited from the steam. The different lyotropic liquid crystalline phase for DOPC may also be an important factor, while for DPPC it is the $L_{\beta'}$ gel below major phase transition. ^{1}H-NMR spectra were used to quantify the molecular dynamics of residual water bound for gas phase rehydration of multilayer liposome lyophilisate of DPPC and of DOPC. The spectra after decomposition showed differences between the two systems. For both lipids the ^{1}H-NMR spectra are superpositions of one Gaussian component, S_1, coming from immobilized protons of solid matrix of liposomes and one or two Lorentzian components, L_1, L_2, coming from mobile protons, most likely coming from different bound water fractions, as their signal linearly increases with the increasing hydration level.

The signal from protons of tightly bound, and of loosely-bound water may be easily distinguished. Our results suggest that loosely bound water fraction is not uniform. Although does not much differ in mobility, is most likely localized in several isolated sites differentiated either by chemical shifts or by sizes of the compartments.

References

1. H. Harańczyk, E. Baran, P. Nowak, M. Florek-Wojciechowska, A. Leja, D. Zalitacz, K. Strzałka, “Non-cooperative immobilization of residual water bound in lyophilized photosynthetic lamellae”, *Cellular & Molecular Biology Letters*, **20**, 5 (2015), 717-735.

2. D. Augustyńska, M. Jemioła-Rzemińska, K. Burda, K. Strzałka, “Influence of polar and nonpolar carotenoids on structural and adhesive properties of model membranes”, *Chemico-Biological Interactions*, **239** (2015), 19–25.
3. H. Harańczyk, J. Czak, P. Nowak, J. Nizioł, “Initial phases of DNA rehydration by NMR and sorption isotherm”, *Acta Phys. Polon,* **A117** (2010), 397-402.

Magnon quantization in the magnetic field gradient

Yu. M. Bunkov[1], K. Dunichev[2], T. R. Safin[2] and M. S. Tagirov[2,3]

[1]Russian quantum center, Moscow, 143025, Russian Federation
[2]Kazan Federal University, Kazan, 420008, Russian Federation
[3]Tatarstan Academy of Sciences, Kazan, 420111, Russian Federation

The report is devoted to the study of two different coherent quantum phenomena of magnonic bosons: Bose-Einstein condensation (mBEC) and Superfluid State of Magnons (SSM). What is the difference between them? Magnon BEC is a quantum phenomenon determined by local density of bosonic quasiparticles. The superfluid state of magnons is a long-range coherent quantum state characterized by the rigidity of the order parameter. This is similar to the states of mass superfluidity and superconductivity. In this state the deflected magnetization can coherently precess even in a strongly inhomogeneous magnetic field. The magnon superflow restore the coherence of SSM after a perturbation. The critical Landau velocity of the coherent magnon flow is determined by an energy gap arising from the repulsion of magnons. In this report the mechanism of SSM formation will be described in detail.

Computer simulation of ionic liquid $[C_{12}\text{-Im-}C_{12}]^+[BF4]^-$ in smectic-A phase

Anna A. Butyugina[1], Andrei V. Komolkin[1], Sergey V. Dvinskikh[2,3]

[1]Faculty of Physics, Saint Petersburg State University, Saint Petersburg, 199034, Russia
[2]Department of Chemistry, KTH Royal Institute of Technology, SE-10044 Stockholm, Sweden
[3]Laboratory of Biomolecular NMR, Saint Petersburg State University, Saint Petersburg, 199034, Russia
E-mail: st068699@student.spbu.ru

Introduction

Currently, ionic liquids (IL) containing an imidazole ring are used as electrolytes for fuel cells, as stabilizers for nanoparticles [1, 2].

As a representative of imidazolium ionic liquids, 1,3-di-n-dodecyl-imidazolium tetrafluoroborate ($[C_{12}\text{-Im-}C_{12}]^+[BF_4]^-$) is a testing ground for both experimental research and computer simulation of ionic liquids. For example, it was used to study the properties of long-alkyl-chain-derivatized imidazolium salts and ionic liquid crystals [3]. Also, the model of this IL was used to study the effect of a systematic change in the length of the alkyl chain and the behavior of anions [4]. Due to the long alkyl chains $[C_{12}\text{-Im-}C_{12}]^+[BF_4]^-$ can exhibit the properties of liquid crystals, which is why this liquid was chosen for the study. Temperature range of the smectic-A phase is 49.9-69.9 °C.

The purpose of this work is to study the ionic liquid $[C_{12}\text{-Im-}C_{12}]^+[BF_4]^-$ in liquid crystalline state using the method of quantum chemistry and molecular dynamics. This method is one of the molecular systems modeling methods, successfully used to study the physicochemical properties of the condensed state of matter – isotropic liquids and solutions, liquid crystals [5].

Computer simulation

It was decided to start modeling the initial system by modeling $[C_{12}\text{-Im-}C_{12}]^+[BF_4]^-$ in the freely distributed program Jmol [6] (Fig. 1). To calculate the charges in the system, a simulation was carried out by the method of quantum chemistry in Gaussian 16. Two models were used: the Hartree–Fock method with standard basis functions 6-31++G** and the coupled clusters method with basis functions cc-pVDZ.

Calculations showed that in the first system the total charge on the ion of the $[BF_4]^-$ ion is $-0.9|e^-|$. And in the system calculated using the basis function cc-pVDZ, it is $-0.88|e^-|$. The results obtained agree with the data used in [7], in its models the ion was also charged with a non-unit charge.

Then, using the AKMD program, we simulated 330 ion pairs $[C_{12}\text{-Im-}C_{12}]^+[BF_4]^-$ in a $65 \times 65 \times 65$ Å^3 cell. The report will discuss the parameters of the system, such as the diffusion coefficient, the distribution of cations around the $[BF_4]^-$ ion in the ionic liquid, and the conformation of aliphatic chains.

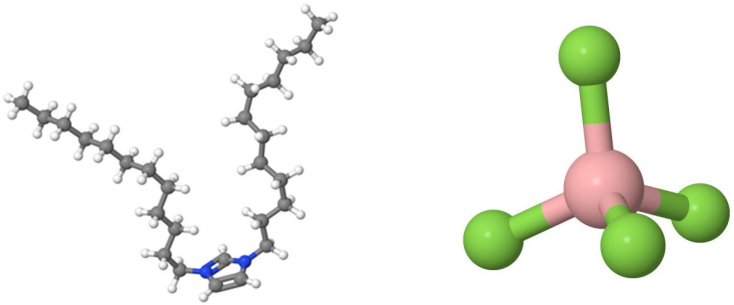

Figure 1. Cation 1,3-di-n-dodecyl-imidazolium and anion $[BF4]^-$

Acknowledgment

The authors thank the science park of St. Petersburg State University for providing the equipment for the experiment.

References

1. Fabio Bellina and others, 'Synthesis and Properties of Glycerylimidazolium Based Ionic Liquids: A Promising Class of Task-Specific Ionic Liquids', Green Chemistry, 11.5 (2009) https://doi.org/10.1039/b821927c.
2. Rondla Rohini and others, 'Symmetrical 1, 3-Dialkylimidazolium Based Ionic Liquid Crystals', Journal of the Chinese Chemical Society, 60.7 (2013) https://doi.org/10.1002/jccs.201200598.
3. Xinjiao Wang and others, 'Solid-State Structures of Double-Long-Chain Imidazolium Ionic Liquids: Influence of Anion Shape on Cation Geometry and Crystal Packing', Crystal Growth and Design, 11.5 (2011) https://doi.org/10.1021/cg200169u
4. Kwang Ming Lee, Ching Kuan Lee, and Ivan J.B. Lin, 'First Example of Interdigitated U-Shape Benzimidazolium Ionic Liquid Crystals', Chemical Communications, 9, 1997 https://doi.org/10.1039/a608517b.
5. Комолкин А.В., Шеляпина М.Г. Метод молекулярной динамики: Учеб.-метод. пособие — Спб.: Изд-во «Соло», 2007. - 72с., ил.
6. Jmol: an open-source browser-based HTML5 viewer and stand-alone Java viewer for chemical structures in 3D. URL: http://jmol.sourceforge.net/ (accessed 22.09.2020).
7. Jones de Andrade, Elvis S. Bo1es, and Hubert Stassen. Computational Study of Room Temperature Molten Salts Composed by 1-Alkyl-3- methylimidazolium Cations Force-Field Proposal and Validation. J. Phys. Chem. B 2002, 106, 13344-13351, DOI: 10.1021/jp0216629.

Chiral carbon bearing the hydrogen: a porphyrin and the tetrapyrroles

Nina Djapic

University of Novi Sad, Technical Faculty "Mihajlo Pupin", Zrenjanin, Serbia
E-mail: nidjapic@gmail.com

Introduction

The assumption was that one chlorophyll catabolic pathway is (Fig. 1):

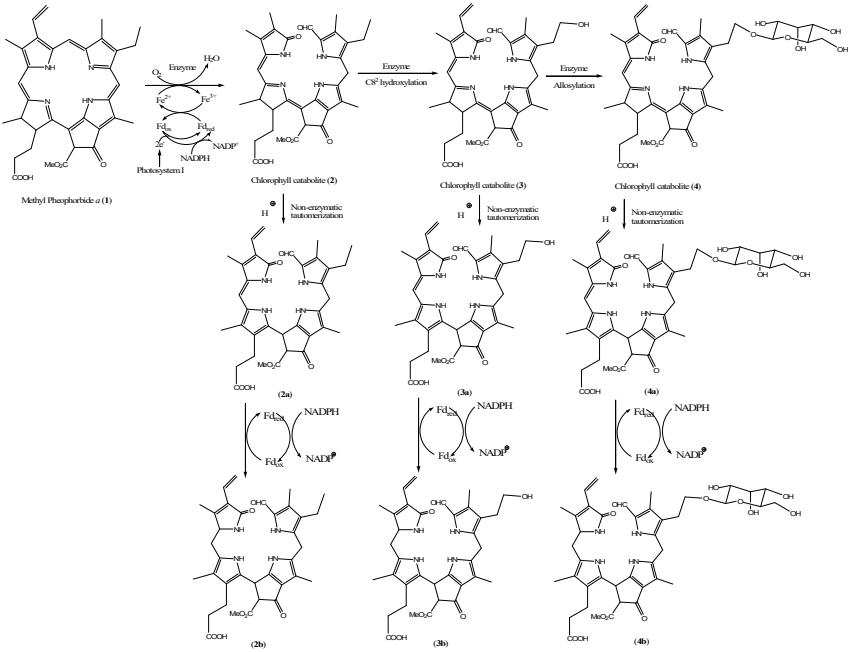

Figure 1. One chlorophyll catabolic pathway

The coupling constants, for the hydrogen attached to the chiral carbon, were observed in a porphyrin and the tetrapyrroles. The porphyrin observed was the methyl pheophorbide *a* (1) with three chiral carbons: 13^2, 17 and 18. The tetrapyrroles observed were chlorophyll catabolites: 3, 3a, 3b and 4b. The chlorophyll catabolite 3 has three chiral carbons: 13^2, 17 and 18. The chlorophyll catabolite 3a has two chiral carbons: 13^2 and 15. The chlorophyll catabolite 3b has three chiral carbons: 1, 13^2 and 15. The chlorophyll catabolite 4b has eight chiral carbons: 1, 13^2, 15, 1', 2', 3', 4' and 5'.

Proton-proton coupling constants at chiral center

The proton at 13^2 position exchange with deuterium in deuterated solvents. Trifluoroacetic acid was used during chlorophyll catabolites isolation and purification. The solvent used for dissolving chlorophyll catabolites and recording NMR spectra was deuterated methanol. The H13^2 proton in deuterated methanol acidified with trifluoroacetic acid undergoes keto-enol tautomerization and is exchanged with deuterium. Proton signal shift and coupling values are depicted in Table 1, 2, 3, 4 and 5.

*Table 1. ^{1}H assignments and proton-proton coupling constants of **1** in $CDCl_3$ (360 MHz)*

Position	δ(^{1}H)	J(HH) [Hz]
13^2	6.27	-
17	4.48	13.7, 7.8, 0.9
18	4.22	8.6, 2.3

*Table 2. ^{1}H assignments and proton-proton coupling constants of **3** in CD_3OD (500 MHz)*

Position	δ(^{1}H)	J(HH) [Hz]
13^2	unrevealed	Enol form
17	3.54	6.9, 1.5
18	2.70-2.85	unrevealed

*Table 3. ^{1}H assignments and proton-proton coupling constants of **3a** in CD_3OD (500 MHz)*

Position	δ(^{1}H)	J(HH) [Hz]
13^2	unrevealed	Enol form
15	Signal being located under residual HDO signal	unrevealed

*Table 4. ^{1}H assignments and proton-proton coupling constants of **3b** in CD_3OD (500 MHz)*

Position	δ(^{1}H)	J(HH) [Hz]
1	4.0	8.2, 5.2
13^2	3.88	4.2
15	Signal being located under residual HDO signal	unrevealed

*Table 5. ^{1}H assignments and proton-proton coupling constants of **4b** in CD_3OD (500 MHz)*

Position	δ(^{1}H)	J(HH) [Hz]
1	4.00	8.4, 4.6
13^2	3.78	3.6
15	Signal being located under residual HDO signal	unrevealed
1’	4.20	7.8
2’	3.16	7.7, 9.1
3’	3.24	9.1, 5.7
4’	3.63	5.6, 11.7
5’	3.84	11.7, 2.6, 4.3

The constants were revealed. The reveal spins up to the ancient Greek mythology [1]. Kat’ exochen, nothing new.

Reference

1. H. Siemiradzki. Phryne at the Poseidonia in Eleusis. 1889.

The application of bulk and surface modifications for sodium alginate membranes for enhanced pervaporation dehydration

Mariia E. Dmitrenko, Vladislav P. Liamin, Anastasia V. Penkova

St. Petersburg State University, 7/9 Universitetskaya nab., St. Petersburg 199034, Russia
E-mail: m.dmitrienko@spbu.ru

Introduction

Nowadays, membrane technologies related to the sustainable processes due to their characteristics (environmentally friendly, energy efficient, compact equipment) are actively developed. One of the promising membrane processes for separation of liquid mixtures of low molecular weight substances is pervaporation, which is effectively applied for the separation of azeotropic and isomer mixtures, close-boiling and thermally unstable substances, and, in particular, for the dehydration. The rapid development of pervaporation requires the significant improvement of the properties for already existing polymeric membranes. This may be easily achieved by the application of bulk and surface modifications of well-known polymer.

Results

The aim of the work was to develop novel green high-performance membranes based on sodium alginate (SA) with improved characteristics for pervaporation dehydration by bulk and surface modifications. Water-soluble fullerene derivatives (fullerenol and fullerene derivative with L-arginine) were used as modifiers for the bulk modification of sodium alginate matrix. Surface modification of developed SA membranes was carried out by the layer-by-layer assembly for the deposition of nanosized polyelectrolyte layers. The structural features and physicochemical properties of the composites and membranes was studied by various analysis methods: FTIR and NMR spectroscopies, scanning electron (SEM) and atomic force (AFM) microscopies, thermogravimetric analysis, measurements of contact angle and swelling experiments. Transport properties of the obtained membranes were evaluated in pervaporation dehydration of isopropanol in a wide concentration range. It was demonstrated that the combination of both bulk and surface modifications for SA membranes significantly improved transport characteristics.

Acknowledgements

This work was supported by Russian Science Foundation [project No 19-73-00105]. The experimental work was facilitated by equipment from the Resource Centers for Nanotechnology, Magnetic Resonance, X-ray Diffraction Studies, Thermogravimetric and Calorimetric Research Centre, Chemical Analysis and Materials Research Centre, Cryogenic Department and Centre "Nanofabrication of Photoactive Materials (Nanophotonics)" at the St. Peters-burg State University.

The Brownian dynamics and numerical self-consistent field simulations of the dendrigraft nanocontainers

Emil I. Fatullaev, Oleg V. Shavykin[1,2], Anatoly A. Darinskii[1,3], Igor M. Neelov[1,2]

[1]St. Petersburg National Research University of Information Technologies, Mechanics and Optics (ITMO University), Kronverkskiy pr. 49, 197101 St. Petersburg, Russia
[2]St. Petersburg State University, 7/9 Universitetskaya nab., 199034 St. Petersburg, Russia
[3]Institute of Macromolecular Compounds, Russian Academy of Sciences, Bolshoi Prospect 31, V.O., St. Petersburg 199004, Russia
E-mail: ximik53@yandex.ru, kupala-89@mail.ru

Introduction

Dendrimer and especially lysine and peptide dendrimers [1-4] are good candidates for use as nanocontainers [5-11] for drug and gene delivery. Due to this reason they were intensively studied during last years using molecular dynamics (MD) and Brownian dynamics (BD) simulation [2-4, 7-8, 12-18] as well as using theoretical self-consistent field (SCF) approaches [19-21]. But synthesis of dendrigrafts is essentially cheaper. That is why we study single dendrigraft molecules of different generation G in dilute solution by the Brownian dynamics method (BD, neutral molecule) and by the numerical self-consistent field (SCF) approach (charged molecule). In both cases a coarse-grained dendrigraft model with different spacer lengths and different generation numbers was used.

The Brownian dynamics simulation

We applied the same simulation procedures used as in our previous works on MD and BD simulation of polymers [22-37]. The dendrigraft have the molecular topology close to molecular brushes. However, the dendrigraft is rather short brush (with about 8 branched side chains) attached to main chain and due to this reason it can have shape close to spherical. Thus the spatial structure of dendrigraft could be similar to that of dendrimer [2]. We tested this assumption over a wide range of spacer lengths and generation numbers and found that the dendrigaft indeed has an almost spherical shape (see, Figure 1a).

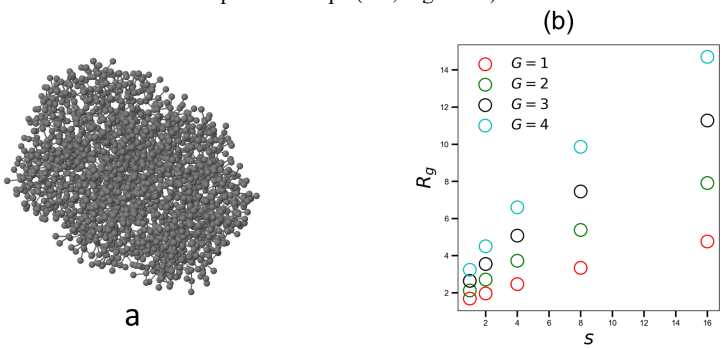

Figure 1. (a) The snapshot of dendrigraft with generation number G = 8 and spacer length s=1;
(b) the gyration radius for different generation numbers as function of spacer length

The radius of gyration R_g was used as a characteristic size of dendrigraft nanocontainers. The Figure 1b demonstrates dependences of R_g (for generation number G = 1, 2, 3, 4) on spacer length *s*.

The self-consistent field approach

The calculation of the electrostatic interactions using Brownian dynamics is very time consuming. This is why the numerical self-consistent (SCF) field approach is a good choice for simulation charged systems [19-21]. We used this approach to study charged dendrigrafts in solution. Two different dielectric constant values were taken for an aqueous solution (80.3) and for methanol (33.1).

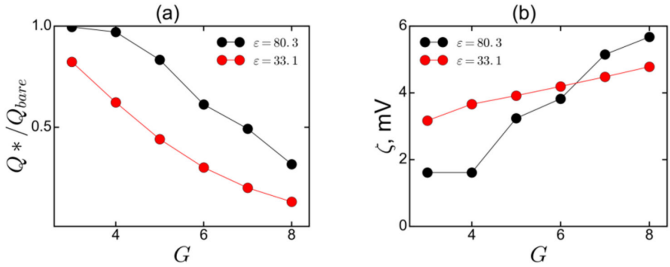

Figure 2. (a) Relative charge of dendrigraft in low salt mode as a function of the number of generations; (add comparison with theory) (b) dependence of zeta potential on the number of generations. Each graph contains data for two media – water and methyl alcohol

In Figure 2a the relative charge of denrigraft nanononteiners of different generations G is depicted. The relative charge drops with generation number. The relative charge smaller in methanol solution, than in case of water solution. The dependence of zeta-potential on G has a dependence close to linear (see, Figure 2b) but the slope of this dependence is greater in water than in methanol. Due to this reason the zeta-potential of dendrigraft in methanol is greater than in water for small generations G and smaller at large G.

Acknowledgements

This work was supported by RFBR grant 20-53-12036. The research is carried out using the equipment of the shared research facilities of HPC computing resources at Lomonosov Moscow State University [38].

References

1. Denkewalter R.G., Kolc J., Lukasavage W.J., US Patent, 1983, № 4410688.
2. Neelov, I. M., Markelov D.A, Falkovich S.G., Ilyash M.Y., Okrugin B.M., Darinskii A.A., Polymer Science, 2013, 55, 154.
3. S. Falkovich, D. Markelov, I. Neelov, and A. Darinskii. J. Chem. Phys. 2013, 139, 064903.
4. Neelov, I., Markelov D., Falkovich S.G., Paci E., Darinskii A., Tenhu H., Dendrimers in Biomedical Applications, (London: RSC) 2013, 99-114.
5. M.Gorzkiewicz, O.Kopec, A.Janaszevska, I.I.Tarasenko, N.N.Sheveleva, I.M. Neelov, B.Klajnert, Bioorg.Chem. 2020, 95, 103504.
6. M. Gorzkiewicz,, A.Konopka, A.Janaszewska, A., I.I.Tarasenko, V.V.Bezrodnyi. I.M. Neelov, B.Klajnert, Int. J. Mol. Sci., 2020, 21 (9), 3138.
7. Mikhtaniuk, S.E., Bezrodnyi, V.V., Shavykin, O.V., Neelov I.M., Penkova, A.V., Markelov, D.A., Polymers, 2020, 12(8), 1657
8. Bezrodnyi, V.V., Shavykin, O.V., Mikhtaniuk, S.E., Neelov I.M., Sheveleva, N.N., Markelov, D.A., International Journal of Molecular Sciences, 2020, 21, 9749, 1–22.
9. Sheveleva N.N., Markelov D.A., Vovk M.A. Mikhailova, M.E., Tarasenko I.I, Neelov I.M., E.Lähderant. Scientific Reports, 2018, 8, 8916

10. Sheveleva N.N., Markelov D.A., Vovk M.A., Tarasenko I.I, Neelov I.M., E.Lähderanta, 2019, RSC Adv. 9, 18018.
11. Sheveleva N.N., Markelov D.A., Vovk M.A., Tarasenko I.I, Mikhailova M.E., Neelov I.M., 2019, Molecules, 24, 2481
12. Mazo M.A., Shamaev M.Y., Balabaev N.K., Darinskii A.A., Neelov I.M., Physical Chemistry Chemical Physics, 2004, 1285.
13. Okrugin B., Ilyash M., Markelov D., Neelov I., Pharmaceutics, 2018, 10, 129.
14. Neelov I.M., Adolf D.B., Macromolecules, 2003, 36, 6914.
15. Neelov I.M., Adolf D.B., J. Phys. Chem. B, 2004, 108, 7627.
16. Markelov D.A., Falkovich S.G.,, Neelov, I. M., et al, PCCP, 2015, 17, 3214
17. O.V.Shavykin, I.M.Neelov, A.A.Darinskii. PCCP, 2016, 18, 24307
18. Shavykin O.V., Mikhailov I.V., Darinskii A.A., Neelov I.M., Leermakers F.A.M., Polymer, 2018,146, 256.
19. Okrugin B.M., Neelov I.M., Leermakers F., Borisov O.V., Polymer, 2017, 125, 292.
20. Shavykin O.V., Leermakers F., Neelov I.M., Darinskii A.A, Langmuir, 2018,34, 1613.
21. Shavykin, O.V., Neelov, I.M., Borisov, O.V., Darinskii, A.A., Leermakers, F.A.M.,Macromolecules, 2020, 53(17), pp. 7298–7311
22. Gotlib, Y.Y., Darinskii, A.A., Neelov, I.M., Balabaev, N.K. Macromolecules, 1980, 13(3), 602–608
23. Darinskii A., Lyulin A., Neelov I., Makromolekulare Chemie - Theory and Simulations (Macromolecular Theory and Simulations), 1993, 2, 523.
24. Neelov I.M., Adolf D.B., Lyulin AV., Davies G.R. J. Chem. Phys., 2002, 117,4030.
25. Zarembo, A., Balabaev, N.K., Neelov, I.M., Sundholm, Darinskii, A.A., , F. PCCP, 2003, 5(11), 2410–2416
26. Neelov I.M., Adolf D.B., McLeish T.C.B., Paci E., Biophys. J., 2006, 91, 3579.
27. Gowdy, J., Batchelor, M, Neelov, I, Paci, E. J. Phys. Chem. B, 2017, 121, 9518.
28. Neelov I.M., Binder K., Macromolecular Theory and Simulations, 1995, 4, 1063.
29. Neelov, I.M., Binder, K. Macromol. Theory&Simul/, 1995, 4(1), 119–136
30. Ennari J., Neelov I., Sundholm F., Polymer, 2000, 41, 4057.
31. Ennari J., Neelov I., Sundholm F., Polymer, 2001, 42, 8043
32. Darinskii A., Gotlib Yu., Lukyanov M., Lyulin A., Neelov I., Progress in Colloid & Polymer Science, 1993, 91, 13.
33. Ennari J., Neelov I., Sundholm F., Comput. Theor. Polym. Sci., 2000, 10, 403.
34. Ennari J., Elomaa M., Neelov I., Sundholm F., 2000, Polymer, 41, 985.
35. Darinskii A., Gotlib Yu., Lyulin A., Neelov I., Vysokomolek. Soed.. Ser,A 1991, 33, 1211 (translation to English: Polymer Science, 33,1116).
36. Ennari J., Neelov I., Sundholm F., Polymer, 2004, 45, 4171
37. Ennari J., Neelov I., Sundholm F., Polymer, 2000, 41, 2149.
38. Sadovnichy, V.; Tikhonravov, A.; Voevodin, V.; Opanasenko, V. “Lomonosov”: Supercomputing at Moscow State University. In Contemporary High Performance Computing: From Petascale toward Exascale; Chapman and Hall/CRC: Boca Raton, FL, USA, 2013; pp. 283–307.

EPR study and DFT-assisted identification of radicals in γ-irradiated calcium gluconate

A. R. Gafarova, G. G. Gumarov, M. M. Bakirov, R. B. Zaripov, V. Yu. Petukhov

Zavoisky Physical-Technical Institute, Kazan, Russian Federation
E-mail: albina-gafarova@mail.ru

Calcium gluconate is widely used in the chemical and food industries, it is used as a drug for the treatment of diseases associated with a lack of calcium in the body. Also, interest in the study of this compound is high in connection with the development of a mechanically activated modified nanodispersed amorphous form of calcium gluconate (MACG), the treatment efficiency of which is much higher. It is assumed that an increase in the bioavailability of the drug may be associated with a change in the conformation of the calcium gluconate (GC) molecule as a result of the rupture of hydrogen bonds and the separation of the coordination water from the GC molecule [1-4]. Given the high importance of calcium gluconate for industrial and medical applications, it is surprising that its structure has remained unexplored for a long time.

This may be because the traditional method of slowly cooling an aqueous solution produces very fine needles with correspondingly weak X-ray diffraction. Thicker crystals, providing good data quality on a laboratory diffractometer, were obtained by V. Bugris et al. using the hanging drop method and systematically optimizing crystal growth conditions. A single crystal with dimensions of 0.05mm x 0.02mm x 0.01mm was investigated using synchrotron radiation [5].

However, mechanical activation is often accompanied by amorphization, which makes it impossible to use diffraction methods. In this regard, it becomes necessary to use alternative research methods, in particular, this work considers the possibility of using the EPR method to determine the conformation of calcium gluconate. Since the original GC does not have an EPR signal, to obtain information about the system, it is possible to introduce artificial defects into it; for this, we used ionizing radiation in our work. Earlier, we showed the possibility of determining the conformational structure of gluconic acid salts by creating paramagnetic centers in them by irradiation with gamma quanta. Using different radiation doses, and applying EPR spectroscopy in the X- and Q- bands, it turned out to be possible to decompose the observed spectra into components. In addition, comparing the obtained parameters of hyperfine interaction with the structure of calcium gluconate, the obtained components were compared with quite definite positions in the structure of the molecule. However, in this case, one has to make simplifying assumptions, for example, about the isotropy of the g factor and HFI parameters. In this respect, the method for calculating the parameters of the EPR spectrum using quantum chemical methods is more attractive, which was the purpose of this work.

The starting material was a laboratory calcium gluconate powder manufactured by Sigma Aldrich. The samples were preliminarily irradiated with photons on a Rokus gamma-therapeutic apparatus with a Co^{60} source with an average energy of 1.25 MeV. The resulting radiation doses were 400, 600, 800 and 1000 Gy. EPR spectra were obtained at room temperature on an EMX Plus spectrometer at 9.3 GHz in the X-band and on an Elexsys E680 spectrometer (36 GHz) in the Q-band at various powers.

Using the V. Bugris X-ray diffraction data, we built a model of the GC molecule in the Avogadro program. This program was used to generate input files for the ORCA quantum chemical program. An internal coordinate system was used, which is convenient for setting the optimization conditions. Because it is assumed that irradiation with gamma quanta leads to the rupture of the C-H bond; hydrogen atoms in the structure of the calcium gluconate molecule, bound directly to the carbon atom, were successively removed. For each case, a quantum

chemical calculation was performed. Since the breaking of the bond leads to a change in the position of the corresponding carbon atom, optimization was carried out. For the calculation, the density functional theory (DFT) method was used, namely the unrestricted Kohn-Sham method. Meta-GGA functional (TPSS) and cc-pVDZ basis were used. The parameters of HFC and g-factor obtained as a result of the quantum-chemical calculation were used to decompose the experimental EPR spectra using the EasySpin software.

The result of the decomposition of the EPR spectrum in the X-band of the GC sample irradiated with a dose of 1000 Gy is shown in Figure 1.

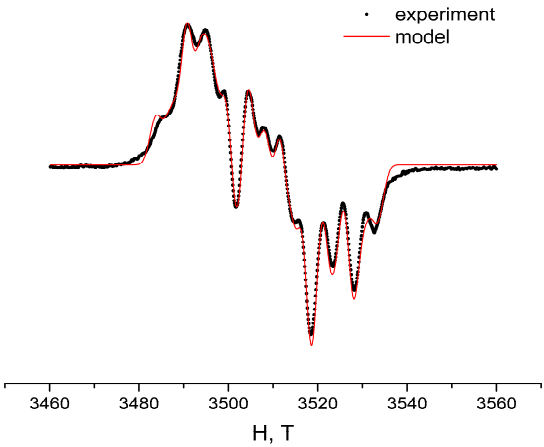

Figure 1. Spectrum of calcium gluconate irradiated with a dose of 1000 Gy (experiment) and the result of a quantum-chemical calculation on ORCA with fit in EasySpin (model)

The components used were the EPR spectra of radicals located on the C3 and C5 atoms of the first structure and two radicals located on C3 in the second structure of calcium gluconate indicated in the work of V. Bugris et al. It is noteworthy that the calculated EPR spectrum of the radical on C4 in the first GC structure exhibits significantly higher HFC parameters than is observed experimentally. Thus, this corresponds to our earlier results [6].

It should be noted that the parameters of the EPR spectra components (HFI and g factors) calculated in the ORCA program turned out to be anisotropic. In this case, the spectral parameters calculated in the ORCA program as a result of fitting in the EasySpin program change insignificantly, which indicates the correctness of the used methods of quantum-chemical calculation. The parameters of the HFI and g factor of the components obtained in the Q-band are also in good agreement with the results obtained in the X-band.

We also calculated the dependence of the isotropic HFI on the torsion angle H11-C6-C5-C4 (Fig. 2). Such a dependence for calcium gluconate obeys the $\cos^2\theta$ law with good accuracy, that is, it corresponds to the McConell ratio [7].

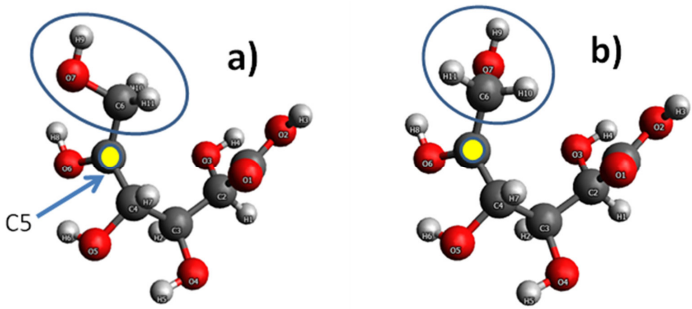

Figure 2. Changing the position of the tail of the calcium gluconate molecule as a result of rotation along the C5-C6 bond (torsion angle): a) initial position, b) rotation by 90 degrees. The position of the radical is shown by an arrow

Thus, the quantum-chemical calculation using the DFT method makes it possible to correctly describe the observed EPR spectrum of calcium gluconate irradiated with gamma quanta. The torsion angles obtained from the EPR data are consistent with the X-ray diffraction data reported in a recent paper by [5]. In addition, the calculated values of the hyperfine splitting of the radical at the C4 carbon atom turned out to be much higher than those observed by us experimentally. Thus, this confirms our earlier conclusion about the absence of a radical on the C4 atom.

Acknowledgments

G. A. R. and P. V. Yu. thank RFBR (Project Nr. 20-33-90201) for supporting of this research activity. G.G.G., B.M.M. and Z.R.B are thankful to the Government assignment for FRC Kazan Scientific Center of RAS (Reg. Nr. AAAA-A18-118030690040-8) for supporting EPR study.

References

1. D. S. Rybin, G. N. Konygin, V. E. Porsev, et al E. P. Elsukov, M. A. Eremina, D. R. Sharafutdinova, G. G. Gumarov, V. Yu. Petukhov, O. I. Gnezdilov, M. M. Akhmetov, K. M. Salikhov, V.V. Boldyrev, Chemical Physics and Mesoscopy. 15, No. 3. 429 (2013).
2. G. N. Konygin, F. Z. Gilmutdinov, S. G. Bystrov, O. V. Karban, G. A. Dorofeev, E. P. Elsukov, A. A. Shakov, N. S. Strelkov, E. P. Tyulkin, V. V. Pozdeev, S. B. Shishkin, P. N. Maksimov, A. N. Filippov, V. V. Korepanova, Chemistry for sustainable development. 13 No. 2. 249 (2005).
3. G. G. Gumarov, V. Yu. Petukhov, G. N. Konygin, D. S. Rybin, E. P. Zheglov, Almanac of Clinical Medicine. No. 17-2. 47 (2008).
4. N. S. Strelkov, G. N. Konygin, D. S.Rybin, V. V.Pozdeev, N. A.Kiryanov, O. V. Yakovenko, P. N. Maximov, E. P. Elsukov, Yu. I. Efremov, D. R. Sharafutdinova, V. Yu. Petukhov, G. G. Gumarov, Almanac of Clinical Medicine. No. 17-2. 366 (2008)
5. V. Bugris, Cs. Dudas, B. Kutus, V. Harmat, K. Csanko, S. Brockhauser, I. Palinko, P.Turner, P. Sipos, Acta Cryst (2018) https://doi.org/10.1107/S2052520618013720
6. A.R Gafarova, G.G. Gumarov, I.A. Goenko, M.M. Bakirov, R.B. Zaripov, V.Yu. Petukhov., Modern development of magnetic resonance 129 (2018)
7. C. Hellert, H. M. Mcconnell, J Chem Phys 32, 1535 (1960).

Primary echo signals in flexible polymers with isolated three-spin groups

Irina Yu. Golubeva[1], Grigorii E. Karnaukh, Tatiana P. Kulagina[2]

[1]Facultyof fundamental physical and chemical engineering, Moscow state University, Moscow, Russia,
[2]Institute of problems of chemical physics RAS, 142432, Chernogolovka, Russia
E-mail: tan@icp.ac.ru

Introduction

Based on the previously developed theory of free induction decay and primary echo [1], a theory of primary echo in flexible polymers with isolated groups of three spins with arbitrary dipole-dipole interaction (DDI) constants is proposed. The possibility of using the general theory of spin echoes in multi-spin systems [2] is shown. A method for estimating the influence of temperature on the shape of a line from the integral signal intensity is proposed. It is shown that when the temperature increases, the difference in the influence of the same or arbitrary constants of DDI is not observed.

The method of calculating the signal

The proposed theory allows us to characterize the primary echo $A(t,\tau)$ and the shape of the line $F(\omega)$ in polymers containing selected three-spin groups

FID in linear polymers with free ends are calculated in the Anderson-Weight model with corresponding correlation functions of molecular motions $k_i(\tau)$:

$$G_i(t) = \exp\left(-\omega_{loc}^2 \int_0^t (t-\tau) k_i(\tau) d\tau\right), i = 1,2 \quad (1)$$

where ω_{loc} – the average local field created on any spin by both the spins belonging to the selected segment and all other spins in the chain.

For chains with entanglements with FID has the form [2]:

$$G_r(t) = G_1(t) G_2(t) G_{3c}(t), \quad (2)$$

where $G_{3c}(t) = \int_1^N \int_0^{\pi/2} g(N,\theta,t) P(N)\, dcos\theta\, dN$ and takes into account the movement of the chain as a whole due to the correlation function $k_3(\theta, N) = \left(3cos^2\theta - 1\right)^2 lnN\ N^{-2}$.

In a linear polymer containing isolated three-spin groups, FID is expressed by the following formula:

$$G(t) = G_3(t) G_r(t), \quad (3)$$

where $G_3(t)$ – FID in the three-spin system ½ [1].

The SE expression looks similar for the entire spin system:

$$A(t,\tau) = A_3(t,\tau) A_r(t,\tau) \quad (4)$$

where $A_r(t,\tau)$- the primary echo signal in polymers [2], which is associated with the free induction decay $G_r(t)$:

$$A_r(t,\tau) = \frac{G_r(t)^2 G_r(\tau)^2}{G_r(t+\tau)}$$

Results and discussion

In the course of this work, the primary echo formula was obtained in linear polymers containing isolated three-spin groups, and the free-induction decay and solid-echo signals were modeled in linear polymers with a three-spin group½.

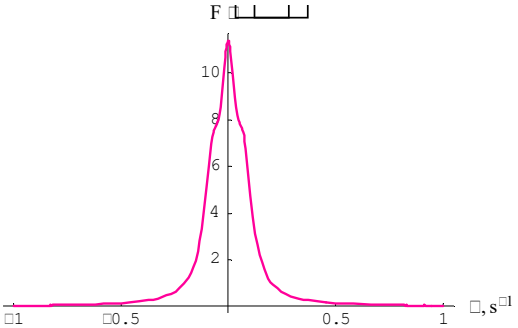

Figure 1. The line shape with the same constants DDI (weak influence)

$N_0 = 20, \alpha = 0{,}05, \omega_{loc} = 0.01c^{-1},\ \tau_c = 0{,}04c, b = 5 \bullet 10^{-4}c$

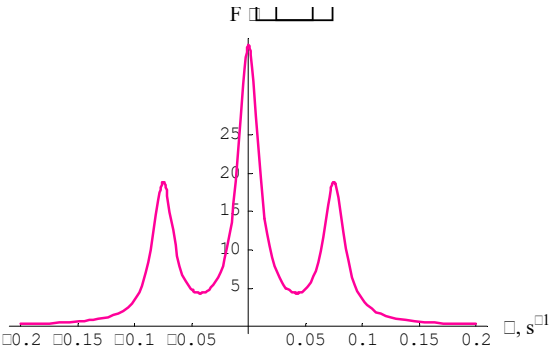

Figure1. The line shape with the same constants DDI (strong influence)

$N_0 = 20, \alpha = 0{,}05, \omega_{loc} = 0.01c^{-1}, \tau_c = 0{,}01\ c, b = 5 \bullet 10^{-4}c$

Acknowlegment

The work was carried out on the topic of the state assignment of the Ministry of Science and Higher Education No. 0089-2014-0021

References

1. T.P. Kulagina, G.E. Karnaukh, I.Yu. Golubeva // *Applied Magnetic Resonance* 51 (2), p.155-163 (2020), DOI: 10.1007/s00723-019-01172-2
2. Kulagina T. P., Karnaukh G. E., Kuzina A. N., Smirnov L. P. // *Russian Journal of Phys. Chem. B.* **7,** 170-176 (2013).

Modern capabilities of NMR magnetometry

A. V. Ievlev[1], I. E. Starikov[2]

[1]Department of Nuclear Physics Research Methods, Saint Petersburg State University, 199034, 7/9 Universitetskaya nab., Saint Petersburg, Russia
[2]Geodezicheskie Pribory Co. LTD, Surveying Instruments and Software, 197101, 16 Bolshaya Monetnaya str., Saint Petersburg, Russia
E-mail: a.ievlev@spbu.ru

Introduction

Magnetic prospecting using NMR magnetometers has been carried out for a long time, so much so that it has already entered the standard research methods of geophysics. Due to the fact that NMR methods have numerous applications in physics, chemistry, medicine, archeology, geology, they can also be used in industry. Just one of such applications will be discussed in this work. Magnetic reconnaissance in archeology allows traces of human economic activity to be traced, by the contrast of the magnetic properties of materials used by humans in construction, everyday life, art and others. However, if you think about it, what is the difference between human economic activity in the modern world and in the past history? The first answer suggests itself it is materials, and this is true, but in general, a person is still inclined to create and change the environment to suit his needs. As in the ancient world, viaducts for water supply were built, so now people tend to lay various engineering communications: water supply, gas and oil pipelines, laying power electrical cables, power lines and much more.

Experimental section

In this work, we tried to reflect the new possibilities of NMR magnetometry, primarily due to the increased accuracy of determining the coordinates. At the dawn of the use of NMR magnetometers in archeology, researchers were forced to carry out all research, making a time-consuming coordinate division of the site and topogeodetic binding to some landmarks on the ground. The accuracy of such a coordinate reference left much to be desired, and further determination of the coordinates of the anomaly found on a magnetic map gave a strong error when searching for this anomaly on the ground. Modern quantum NMR magnetometers have the ability to receive the coordinates of the point of measurement of the magnetic field from external GPS receivers. Such receivers allow you to determine the coordinate of a point on the ground using satellite measurement methods, and in some models such receivers are already built-in. We used a POS-2 two-sensor optically pumped quantum NMR magnetometer-gradiometer in our research. POS-2 is a keyboardless, port-controlled, precision measuring instrument of the cyclic type, based on the principle of dynamic polarization of nuclei (Overhauser effect). The sensor is designed to measure the modulus of induction of the Earth's magnetic field in the range of 20,000-100,000 nT. The POS-2 sensor system can be used with various information gathering systems, comes with the DLPOS system. The first figure shows an example of interaction with a typical Garmin semi-professional navigator.

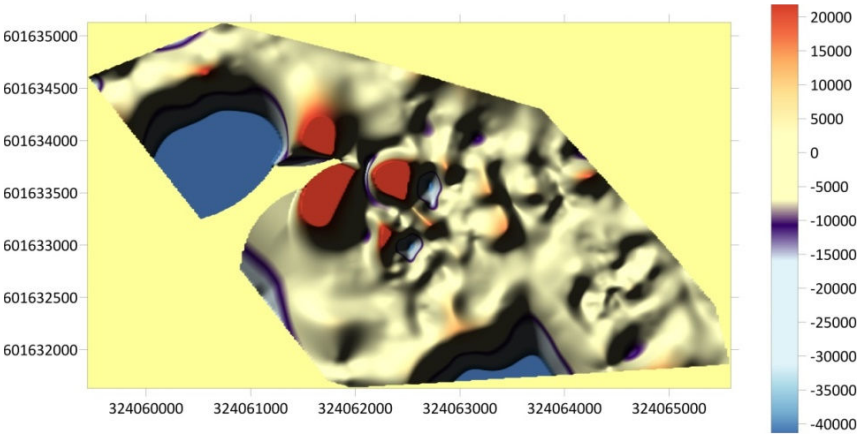

Figure 1. Previous survey using Garmin semi-professional navigator

The accuracy of determining the coordinates of such devices is measured in meters, so in the future it was decided to use receivers of the geodetic accuracy class. The second figure shows an example of how the gradiometer interacts with the Sokkia GRX3 receiver. This professional receiver provides measurement accuracy of up to 5 mm in real time, operates in the field at temperatures from -40 ° C to + 65 ° C, and has an IP67 degree of protection against the external environment [1]. As you can see from the brief description, the accuracy of determining the coordinates has increased to centimeter scale, moreover, there is immediately a binding to geographic coordinates. Table 1 shows an example of the data format unloaded from the magnetometer; these data confirm the correctness of the transmission of coordinates from the GPS receiver. Coordinates are transmitted by reading periodic NMEA messages from the receiver.

Table 1. This is an example of the output data from a magnetometer

FIELD(pT)	LINE(LON)	POINT(LAT)	GRAD(pT)	Grad(mkT)
48310988	301939289	601089300	-2615666	-2.615666
52737411	301939249	601089310	363621	0.363621
43758159	301939226	601089340	-5623157	-5.623157
44951563	301939193	601089360	-4828843	-4.828843
55590987	301939149	601089380	2275701	2.275701
32137548	301939099	601089410	-13339668	-13.339668
42262153	301939040	601089420	-6523166	-6.523166
48316509	301939003	601089450	-2521935	-2.521935
44631243	301938970	601089470	-4969556	-4.969556
43521665	301938924	601089450	-6031571	-6.031571
43521665	301938947	601089430	-6041445	-6.041445
48770774	301938983	601089390	-2278862	-2.278862

Results

The main result of this work is the possibility of interaction of two rather complex measuring devices in a single measuring complex, which makes it possible not to waste the researcher's time on creating a coordinate grid and it's binding to the terrain.

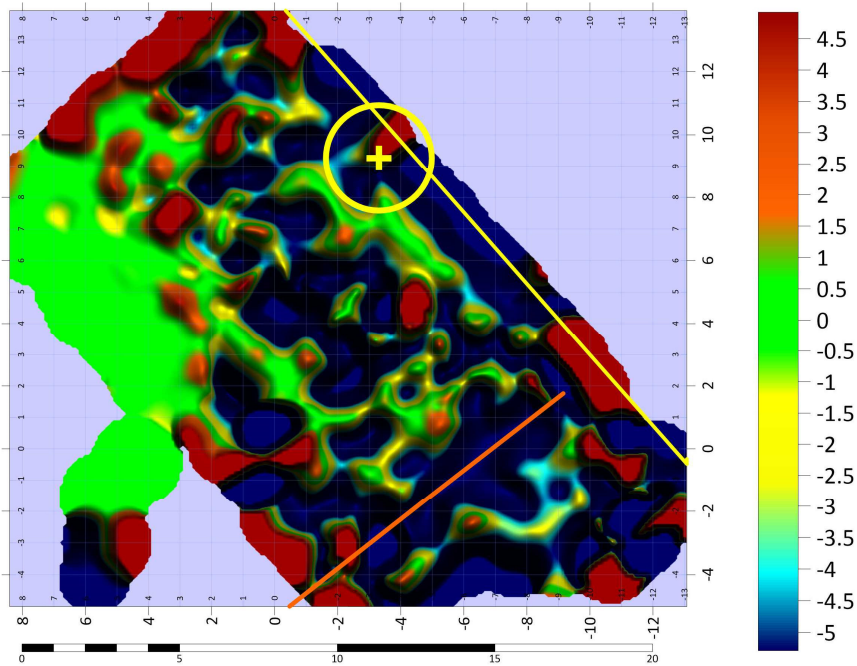

Figure 2. Map of gradient Earth magnetic field, mkT

Acknowledgements

Scientific researches were performed at the "Magnetic Resonance Research Centre" of Research park of St. Petersburg State University.

References

1. Sokkia Corporation, GCX3 GNSS Receiver Operator's Manual. 1023998-01 Rev A 07/© 2018. Topcon Positioning Systems, Inc.

^{1}H-NMR spectroscopy and relaxometry studies of hydration from gaseous phase of foliose lichenized fungi: *Roccellina nigricans* from Atacama Desert region Chañaral

D. Jakubiec[1], K. Kubat[1], A. Andrzejowska[1], M. A. Olech[3,4], A. Casanova-Katny[2], K. Strzałka[5,6] and H. Harańczyk[1]

[1]*Institute of Physics, Jagiellonian University, ul. Prof. Stanisława Łojasiewicza 11, 30-348 Kraków, Poland*
[2]*Faculty of Natural Resources, Catholic University of Temuco, Chile*
[3]*Institute of Botany, Jagiellonian University, ul. Kopernika 27, 31-501 Kraków, Poland*
[4]*Institute of Biochemistry and Biophysics, Polish Academy of Sciences, ul. Pawińskiego 5a, 02-106 Warsaw, Poland*
[5]*Malopolska Centre of Biotechnology, Jagiellonian University,ul. Gronostajowa 7A, 30-387 Kraków, Poland*
[6]*Faculty of Biochemistry, Biophysics and Biotechnology, Jagiellonian University, ul. Gronostajowa 7A, 30-387 Kraków, Poland*
E-mail: daniel.jakubiec@doctoral.uj.edu.pl

Introduction

Lichens may survive the extreme environmental conditions such as very low temperatures and long periods of drought typical for Antarctic regions. Similar organisms can be found in regions of extreme dehydration and high temperatures like Atacama Desert. ^{1}H-NMR may yield a thorough insight in molecular mechanisms of their resistance. The understanding of the molecular mechanisms of freezing resistance requires a knowledge on water mobility for different steps of hydration level.

Materials and methods

The hydration of the extremely dehydrated lichenized fungi (*Roccellina nigricans*) from the Atacama Desert was studied. Relaxometry and ^{1}H-NMR spectroscopy were used, as well as sorption isotherm analysis - methods allowing to monitor the molecular dynamics of bound water in order to distinguish several fractions of water present in a living cryptobiotic organism (in a dehydrated lichenized fungus). The sorption isotherm has a sigmoidal shape and is well fitted using Dent's model ($\Delta M/m_0 = 0{,}029 \pm 0{,}004$). For the dehydrated thallus of *R. nigricans*, the course of gas phase hydration shows the sequential bonding of a very tightly bound water fraction, tightly bound water, and finally loosely bound water. The rehydration process is faster for *R. nigricans*, a desert lichen fungus species, compared to Antarctic species from more humid polar region, reflecting the availability of water in the environment. For *R. nigricans*, the ^{1}H-NMR spectra make it possible to distinguish two bound water signals, namely the signal from loosely bound water, and the signal from tightly bound water. In the ^{1}H-NMR spectra a chemical shift between lines can be seen. The relaxation times make it possible to distinguish two signals from loosely bound water and from tightly bound water for the two lowest hydration levels and three signals for higher hydration level where a second signal appears from the loosely bound water layer. The hydration dependency of ^{1}H-NMR signal is described by a linear function, which indicates the absence of a water-soluble solid fraction for *R. nigricans*. This feature was not observed in other lichen species from Atacama desert (*Niebla tigrina*) or in Antarctic ones (*Umbilicaria Antarctica*) where the water-soluble solid fraction is occurs.

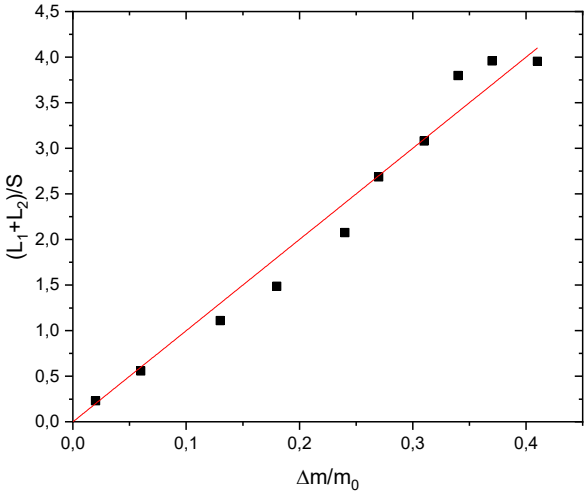

Figure 1. ^{1}H-NMR amplitude dependence of the liquid signal expressed in units of a solid signal for the free induction decay as a function of hydration for the thallus of the lichen Roccellina nigricans

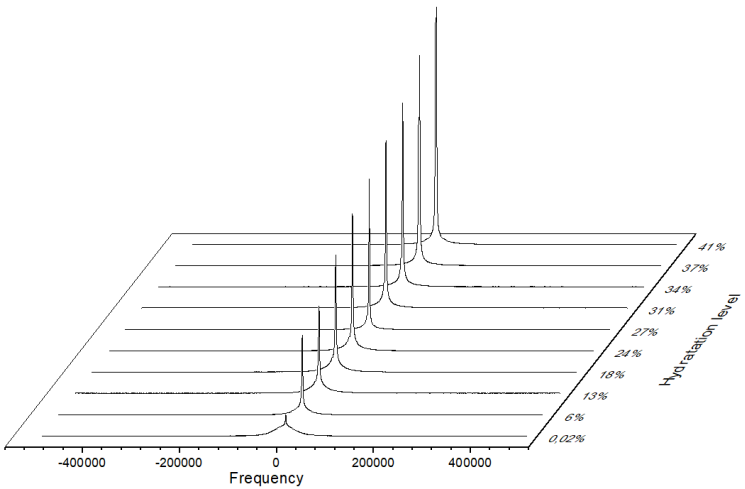

Figure 2. ^{1}H-NMR spectra for Roccellina nigricans lichen thallus ordered according to hydration level

Acknowledgments

The research was carried out as a part of Chile grant from INACH (Instituto Antártico Chileno, Ministerio de Relaciones Exteriores, Chile): Sistema de Proyectos INACH, RT_27_16; Concurso: Título: XXII Concurso National de Proyectos de Investigación Científica y Tecnológica, Antártica, 2016, Project: "Ecophysiology of Antarctic and Atacama desert lichens: freezing and deep dehydration mechanism under natural conditions and under passive warming experiments", supervisor: Investigador Principal prof. Angélica Casanova-Katny, Universidad Católica de Temuco, Temuco, Chile.

References

1. H. Harańczyk, K. Strzałka, K. Kubat, A. Andrzejowska, M. Olech, D. Jakubiec, P. Kijak, and A. Casanova-Katny, 2021. "A comparative analysis of gaseous phase hydration properties of foliose lichenized fungi: *Niebla tigrina* Follman from Atacama Desert and *Umbilicaria antarctica* Frey & I. M. Lamb from Robert Island, Southern Shetlands", submitted to Extremophiles.
2. H. Harańczyk, A. Casanova-Katny, M. Olech, K. Strzałka, 2017. "Dehydration and Freezing Resistance of Lichenized Fungi". Springer Nature Singapore Pte Ltd., Plant Adaptation Strategies in Changing Environment, https://doi.org/10.1007/978-981-10-6744-0_3;
3. Robert M. Silverstein, Francis X. Webster, David J. Kiemle, David L. Bryce, "Spectrometric Identification of Organic Compounds", 8th Edition, (2014) ISBN: 978-0-470-61637-6

Direct exchange of identical quantum objects with a finite number of eigenstates

Grigorii E. Karnaukh

Institute of Problems of Chemical Physics RAS, Semenov prospec 1t, Chernogolovka, Moscow region, 142432, Russia
E-mail: karnauh@chgnet.ru

Introduction

The paper describes how and under what conditions the exchange interaction produces a direct exchange of a pair of identical quantum objects (IQO) with a finite number of eigenstates, including spins.

In a study [1] of the nuclear spins exchange had been shown, that in order to the exchange interaction might produce an exchange of spins, the spin system must have at least one pair of mutually indistinguishable spins (IQO). That is, there are IQO, which during the transfer to a new location would be the same as at the old location, and they would not feel the difference between the old and new locations. There are two types of exchanges: the exchange of states and the packet of exchanges of IQO in specific states. The packet is determined by the eigenstates of the interaction Hamiltonian. Therefore, the exchange of IQO, for all parts of the packet, can be described as an exchange of states.

The exchange operator of a pair IQO with the number of states *m*

Projectors onto the spaces of even and odd states of the pair (1, 2) are:

$$\hat{P}_{12}^{e}=\frac{m+1}{2m}+\hat{O}_{12} \text{ and } \hat{P}_{12}^{o}=\frac{m-1}{2m}-\hat{O}_{12}\text{, where } Tr\hat{O}_{12}=0\,.$$

The exchange operator is

$$\hat{E}x_{12}=\hat{P}_{12}^{e}-\hat{P}_{12}^{o}=\frac{1}{m}+2\hat{O}_{12}=\sum_{l=1}^{m}\hat{P}_{ll}^{1}\hat{P}_{ll}^{2}+\sum_{1\le k<l\le m}\left(\hat{P}_{lk}^{1}\hat{P}_{kl}^{2}+\hat{P}_{kl}^{1}\hat{P}_{lk}^{2}\right) \tag{1}$$

and acts as follows:

$$\hat{E}x_{12}\left|\beta\right\rangle_{2}=\left|\beta\right\rangle_{1},\ \hat{E}x_{12}\left|\alpha\right\rangle_{1}=\left|\alpha\right\rangle_{2}$$

There $\left|\alpha\right\rangle$ and $\left|\beta\right\rangle$ are arbitrary states.

Exchange evolution operator

The exchange evolution operator on a segment $\left[0,\frac{\pi}{2}\right]$ with a positive exchange J_{12} integral [1] is:

$$\hat{U}_{12}(t)=\cos\frac{\hbar J_{12}t}{2}+\sin\frac{\hbar J_{12}t}{2}\hat{E}x_{12} \tag{2}$$

$$\hat{U}_{12}(t)\left|\alpha\right\rangle_{1}=\cos\frac{\hbar J_{12}t}{2}\left|\alpha\right\rangle_{1}+\sin\frac{\hbar J_{12}t}{2}\left|\alpha\right\rangle_{2}\quad \hat{U}_{12}(t)\left|\beta\right\rangle_{2}=\cos\frac{\hbar J_{12}t}{2}\left|\beta\right\rangle_{2}+\sin\frac{\hbar J_{12}t}{2}\left|\beta\right\rangle_{1} \tag{3}$$

$$cos\frac{\hbar J_{12}t}{2}\left|\alpha\right\rangle_{1}+\sin\frac{\hbar J_{12}t}{2}\left|\beta\right\rangle_{1};\quad cos\frac{\hbar J_{12}t}{2}\left|\beta\right\rangle_{2}+\sin\frac{\hbar J_{12}t}{2}\left|\alpha\right\rangle_{2} \tag{4}$$

Formula (4) shows that IQO exists in the time during exchange

$$\hat{U}_{12}(t)|\alpha\rangle_1 = \cos\frac{\hbar J_{12}t}{2}|\alpha\rangle_1 + \sin\frac{\hbar J_{12}t}{2}|\alpha\rangle_2 \Rightarrow \left(\cos\frac{\hbar J_{12}t}{2} + \sin\frac{\hbar J_{12}t}{2}\right)|\alpha\rangle$$
$$\left(\cos\frac{\hbar J_{12}t}{2} + \sin\frac{\hbar J_{12}t}{2}\right)^2 = 1 + \sin\hbar J_{12}t = \exp\left[-\frac{\Delta}{kT}\right] \Rightarrow \Delta = -kT\ln\left(1+\sin\hbar J_{12}t\right) \quad (5)$$

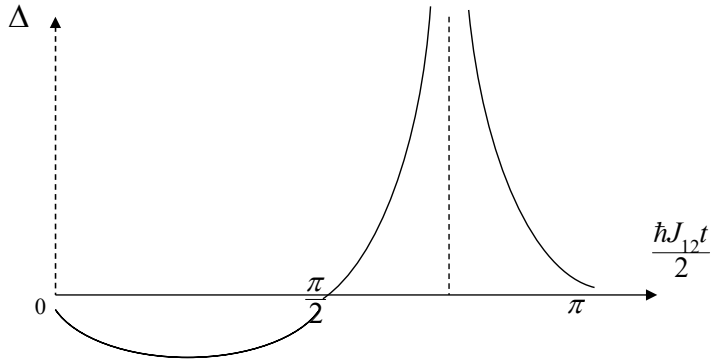

Figure 1

The function graph $\Delta\left(\frac{\hbar J_{12}t}{2}\right)$ shows that first there is a potential hole, depth $kT\ln 2$.

Further, a potential barrier arises. Therefore, the exchange takes place in portions (exchange quantum). The coefficients change after each portion (2). That is, the exchange evolution operator undergoes a phase transition and has four phases.

Table of coefficients

$J>0$	$J<0$
$\left[2k\pi, 2k\pi+\frac{\pi}{2}\right]\left(\cos\frac{Jt}{2}, \sin\frac{Jt}{2}\right);$	$\left[2k\pi+\frac{\pi}{2}, 2k\pi\right]\left(\sin\frac{Jt}{2}, \cos\frac{Jt}{2}\right)$
$\left[2k\pi+\frac{\pi}{2}, 2k\pi+\pi\right]\left(\sin\frac{Jt}{2}, -\cos\frac{Jt}{2}\right);$	$\left[2k\pi+\pi, 2k\pi+\frac{\pi}{2}\right]\left(-\cos\frac{Jt}{2}, \sin\frac{Jt}{2}\right)$
$\left[2k\pi+\pi, 2k\pi+\frac{3\pi}{2}\right]\left(-\cos\frac{Jt}{2}, -\sin\frac{Jt}{2}\right);$	$\left[2k\pi+\frac{3\pi}{2}, 2k\pi+\pi\right]\left(-\sin\frac{Jt}{2}, -\cos\frac{Jt}{2}\right)$
$\left[2k\pi+\frac{3\pi}{2}, 2k\pi+2\pi\right]\left(-\sin\frac{Jt}{2}, \cos\frac{Jt}{2}\right);$	$\left[2k\pi+2\pi, 2k\pi+\frac{3\pi}{2}\right]\left(\cos\frac{Jt}{2}, -\sin\frac{Jt}{2}\right)$

Exchange spin wave

$$\downarrow\uparrow\uparrow\uparrow\uparrow \ldots \rightarrow \uparrow\downarrow\uparrow\uparrow\uparrow \ldots \rightarrow \uparrow\uparrow\downarrow\uparrow\uparrow \ldots \rightarrow \uparrow\uparrow\uparrow\downarrow\uparrow \ldots \rightarrow \uparrow\uparrow\uparrow\uparrow\downarrow \ldots \rightarrow \ldots$$

$$\begin{pmatrix} \cos\left(\frac{J_{12}t}{2}\right)\downarrow_1 + \sin\left(\frac{J_{12}t}{2}\right)\downarrow_2 \\ \cos\left(\frac{J_{12}t}{2}\right)\uparrow_2 + \sin\left(\frac{J_{12}t}{2}\right)\uparrow_1 \end{pmatrix} \rightarrow \begin{pmatrix} -\cos\left(\frac{J_{23}t}{2}\right)\downarrow_2 + \sin\left(\frac{J_{23}t}{2}\right)\downarrow_3 \\ -\cos\left(\frac{J_{23}t}{2}\right)\uparrow_3 + \sin\left(\frac{J_{23}t}{2}\right)\uparrow_2 \end{pmatrix} \rightarrow$$

$$\begin{pmatrix} -\cos\left(\frac{J_{34}t}{2}\right)\downarrow_3 - \sin\left(\frac{J_{34}t}{2}\right)\downarrow_4 \\ -\cos\left(\frac{J_{34}t}{2}\right)\uparrow_4 - \sin\left(\frac{J_{34}t}{2}\right)\uparrow_3 \end{pmatrix} \rightarrow \begin{pmatrix} \cos\left(\frac{J_{45}t}{2}\right)\downarrow_4 - \sin\left(\frac{J_{45}t}{2}\right)\downarrow_5 \\ \cos\left(\frac{J_{45}t}{2}\right)\uparrow_5 - \sin\left(\frac{J_{45}t}{2}\right)\uparrow_4 \end{pmatrix} \rightarrow \ldots$$

Conclusions

The elementary exchange base is exchange of pair. The exchange of a pair consists of two transfers: to and back (3). The exchange operator for the IQO pair is obtained (1). It is shown that the operator of the exchange evolution of a pair IQO (2) is a strip of four phases, which are specified by a parameter $\frac{\hbar J_{kl} t}{2}$. The fulfillment of mutual indiscernibility leads to the fact that spins located in different fields cannot participate in one exchange spin wave.

Acknowledgements

This work is performed on the theme of the state task № AAAA-A19-119071190017-7.

References

1. G.E.Karnaukh. – Collection of articles of the XXIII-rd All-Russian conference "Structure and dynamics of molecular systems". 177-185 (2016).

The distribution of electron density in orpiment. Crystalline and amorphous phases

D. Kitanin, A. Nazarova, V. Ivanov, Y. Shaikhutdinov, A. Pogoreltsev

Kazan State Power Engineering University, 420066, Kazan, Russia
E-mails: apogoreltsev@rambler.ru, zak7235@mail.ru

Introduction

The As_2S_3 orpiment belongs to the class of chalcogenide semiconductors. The amorphous phase is quite simply obtained artificially by fusing stoichiometric amounts of As and S. Samples of natural origin, on the contrary, as a rule, have a crystalline structure. Orpiment is widely used in modern technologies – in the manufacture of solar cells, optical memory devices, etc.

Research results

In this work, we studied the electron density distribution maps for the crystalline and amorphous phases of the orpiment. The experimentally obtained ^{75}As NQR frequencies [1, 2] were used as a basis for estimating the electric field gradients (EFG). Estimates of the EFG on copper nuclei were performed within the framework of the self-consistent limited Hartree-Fock open-shell method (SCF-LCAO-ROHF) in various modes [3]. Figures 1 and 2 show maps electron density distributions for crystalline and amorphous states, respectively. On all contour maps, small circles on the communication lines are critical points (3, -1). Isolines on the electron density distribution map were plotted with a variable step: 0.0 0.001 0.002 0.004 0.008 0.02 0.04 0.08….-0.001 -0.002 -0.004 -0.008 -0.02 -0.04 -0.08…. (e / Bohr^3). The lines crossing at points (3, -1) the communication lines are the surfaces of the zero flux of the electron density gradient vector and define the basin of each atom.

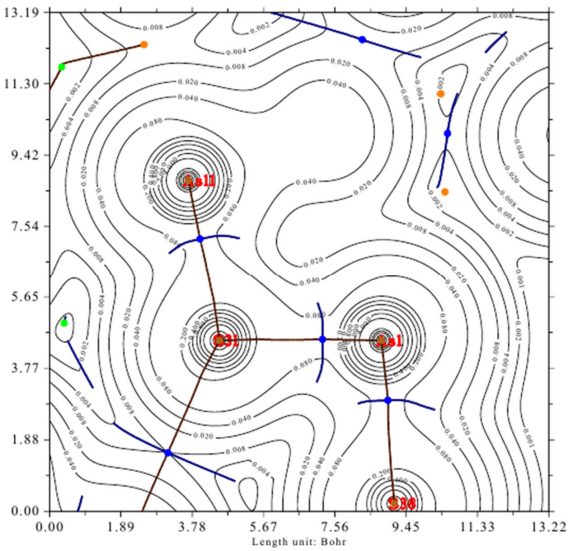

Figure 1. Map of electron density distribution for planes 21-31-11. Crystalline phase

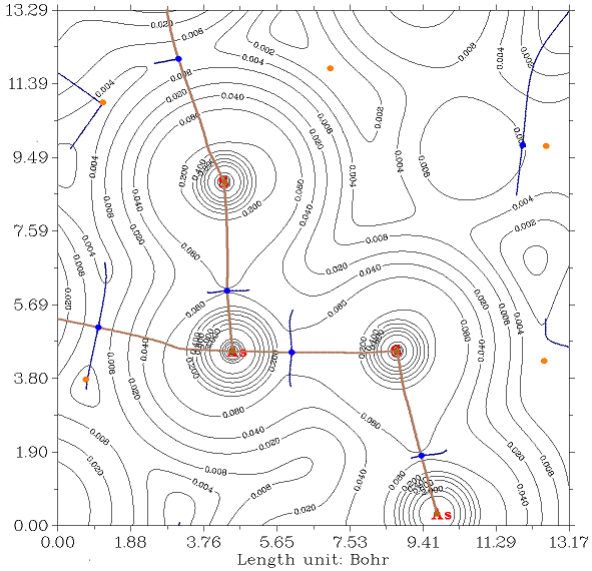

Figure 2. Map of electron density distribution for plane 21-31-11. Amorphous phase

As can be seen from these figures, there is a significant difference in the distribution of the electron density for the crystalline and amorphous states. In particular, in the crystalline state, there is a general isoline at the 0.08 e / Bohr^3 level, covering the entire As-S-As-S chain.

In our opinion, the observed difference in the distribution of electron density for the crystalline and amorphous phases is associated, first of all, with the fact that in the amorphous phase the exchange-correlation effects no longer play such a decisive role as for the crystalline phase.

References

1. Penkov I. N., Safin I. A. // Physics of the solid state, V. 6, No. 8, C. 1264 (1964)
2. P. Craig Taylor // Z. Naturforsch. 51a, 603-610 (1996)
3. A. A. Granovsky. Firefly version 7.1.G, http://clasic.chem.msu.su/gran/firefly/index.html

Investigation of the molecular mobility of the ionic liquid BmpyrrNTF2 by NMR methods

Olga A. Kokh[1], Vladimir V. Matveev[1], Alexander V. Ievlev[1], Konstantin V. Tyutyukin[1], Luis M. Varela[2]

[1]Department of Nuclear Physics Research Methods, Saint Petersburg State University, 199034, 7/9 Universitetskaya nab., Saint Petersburg, Russia
[2]Grupo de Nanomateriais e Materia Branda, Departamento de Fisica da Materia Condensada, Universidade de Santiago de Compostela, Campus Vida s/n E-15782, Santiago de Compostela, Spain
E-mail: st085087@student.spbu.ru

Introduction

Ionic liquids exhibit a unique combination of physicochemical properties that make them ideal candidates for electrolyte applications. Salt solutions containing the TFSI anion are typical and/or promising electrolytes for supercapacitors and lithium batteries. The aim of this work was to test the mobility of counterions (and the solvent if any) in order to compare the diffusion of ions and the physicochemical, in particular the electrically conductive properties of the above systems.

Samples studied

In this work 1-Butyl-1-methylpyrrolidinium bis (trifluoromethylsulfonyl) (Fig. 1) with addition of lithium ions with a concentration of 0.1 mol and 1.5 mol was studied by NMR methods on the Bruker Avance III NMR spectrometer 500 MHz.

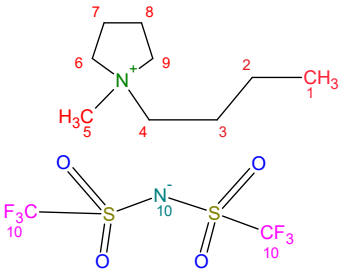

Figure 1. BmpyrrNTF2 chemical formula

During the study of the samples, measurements of the relaxation rates and diffusion coefficients were carried out at various temperatures in the range from 243 to 333 Kelvin. These measurements were carried out on several nuclei: 1H, 13C, 7Li, 19F. The research results will be presented at the report during the conference.

Acknowledgements

Thanks to the staff of Center for Magnetic Resonance of Research Park of St. Petersburg State University for fast and high-quality measurements.

References

1. V.V. Matveev et al. PCCP. 2014, 16. 10480-10484.
2. V.V. Matveev et al. Magn. Reson. Chem., 2018, 56. 140-143.
3. V.V. Matveev et al., J. Mol. Liq., Vol. 278, 2019, pp. 239-246.

The study of non-covalent interactions in complexes of CH_3Br by quantum-chemical calculations

Mikhail Kostin[1], Peter Tolstoy[2], Sona Melikova[1]

[1]Faculty of Physics, Saint-Petersburg State University
[2]Institute of Chemistry, Saint-Petersburg State University
E-mail: kostin-micha@mail.ru

Introduction

The anesthetic effect of the safest inhalation anesthetics (for example halothane, enflurane, isoflurane) appears to be due to non-covalent interactions between the anesthetic molecules and target molecules. The most likely target for halothane is the gamma-aminobutyric acid receptor ($GABA_A$). Determining the binding process of an anesthetic molecule and a target molecule is difficult task. Most anesthetic molecules contain two types of groups that are most likely to be involved in the formation of non-covalent interactions. Such groups are the C–H group and the C–Hal groups, where Hal is a halogen atom (Cl, Br, F for halothane). The C–H group can be involved in hydrogen bonding to the target molecule. When considering the electron density around the halogen atom in the C-Hal group, several features can be distinguished (on example of CH_3Br molecule in Fig. 1). There is a so-called sigma-hole in the electron density distribution (which makes it possible to form a halogen bond), as well as around the halogen atom there is a circular region of increased electron density (this makes it possible to form a bond in which a halogen atom can be an electron density donor). The C-Hal group can provide a possibility for the formation of both halogen and hydrogen bonds. The strongest non-covalent bond with the C–Hal group in complexes formed by halothane is the halogen bond with the bromine atom [1].

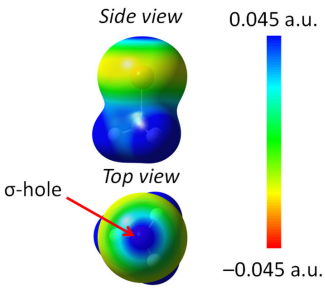

Figure 1. Distribution of electrostatic potential (in a.u.) on the isosurface of electron density

Aims

We studied the formation of complexes of halothane and target molecules involving C–Hal group on the example of model compounds (Fig. 2). The main goal of our work is to determine the number of hydrogen and halogen bonds that CH_3Br molecule can form with target molecules (HF and Cl_2) and to study properties of these bonds. In the first part of this work, we investigated CH_3Br complexes with one or more hydrogen bonds (target molecule is HF) and one or more halogen bonds (target molecule is Cl_2). In the second part, we studied changes in the properties of halogen and hydrogen bonds in the same complexes when the sigma-hole on the bromine atom is involved in the formation of additional halogen bond with the fluorine anion (F^-).

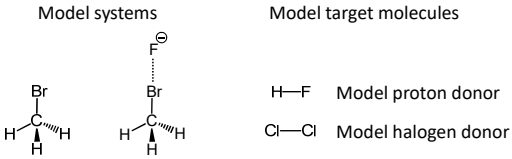

Figure 2. The set of studied molecules that contain C–Hal group

Results

We obtained the optimized geometries of complexes formed by CH_3Br and $CH_3Br\cdots F^-$ with one, two, and three hydrogen bonds, or with one or several (up to 5) halogen bonds. Anticooperativity effects are observed on the length of non-covalent bond, the strength of each bond, and on spectral characteristics (chemical shifts, vibration frequencies). Changes in these parameters determined for each complexes with an additional bond formed by CH_3Br and F^-. The maximum number of non-covalent bonds is explained by the anisotropy of the electron density distribution around the halogen atom and the redistribution of the electron density during the formation of each new bond.

Acknowledgements

This work was supported by RFBR grant 20-03-00536.

References

1. W. Zierkiewicz, R. Wieczorek, P. Hobza and D. Michalska, *Phys. Chem. Chem. Phys.*, **2011**, 13, 5105–5113.

Hydration properties of tadalafil preparations in the matrix of the soluplus polymer

K. Kubat[1], A. Krupa[2], A. Bogdał[1] and H. Harańczyk[1]

[1]Institute of Physics, Jagiellonian University, ul. Łojasiewicza 11, 30-348 Kraków, Poland
[2]Institute of Pharmacology, Collegium Medicum of Jagiellonian University, ul. Medyczna 9, 30-688 Kraków, Poland
E-mail: karol.kubat@doctoral.uj.edu.pl

The effectivity and bioactivity of a drug may change with the increase of residual water content in the tablet. Water vapor sorption level is a measure of the hydrophilicity of a system. Residual water associated with drugs can affect their powder bulk density, physicochemical stability, powder flow, dissolution rate, and compactibility [1-3]. A detailed characterization of the impact that moisture may have on drug properties was reviewed by Sacchetti [4] or by Newman [5]. However, the assessment of water level in raw materials as well as in final products is not limited to drugs. In biophysics, it can be used to analyse not only water content but also to distinguish mobility of water layers bound to the sample by analysing ^{1}H-NMR spectra, and searching for different relaxation times of water protons. It can be helpful to understand the absorption process for an individual compound [6].

For the tests carried out as part of These Author dissertation, samples containing 100% polymer (Soluplus) and active substance (Tadalafil) as well as mixtures containing 10 wt%, 50 wt% of the drug mixed in a ball mixing process for different centrifugation speeds, and different mixing times were used. The obtained samples were examined during two series of ^{1}H-NMR measurements at hydration from the gaseous phase above the water surface (100% relative humidity).

Unexpected phase changes initiated by the sorption of water are one of major problems in the development of solid dispersions that limit their practical use. In our study, a model of multilayer moisture sorption was proposed to explain the mechanism of moisture sorption in binary solid dispersions composed of poorly soluble drug-tadalafil and amorphous, hygroscopic polymer-Soluplus. These results were already published [7]. In the near future, it is planned to measure the behavior of samples of Tadalafil: Soluplus systems depending from different rpm at the 1h mixing time.

References

1. C. Ahlenck, G. Zografi, The molecular basis of moisture effects on the physical and chemical stability of drugs in the solid state, Int. J. Pham. 62 (1990) 87-95.
2. M.C. Paisana, M.A. Wahl, J.F. Pinto, Effects of polymers in moisture sorption and physical stability of polymorphic olanzapine, Eur. J. Pharm. Sci. 97 (2017) 257-268.
3. M.C. Paisana, M.A. Wahl, J.F. Pinto, Role of moisture on the physical stability of polymorphic olanzapine, Int. J. Pharm. 509 (2016) 135-149.
4. M. Sacchetti, Thermodynamics of water-solid interactions in crystalline and amorphous pharmaceutical materials, J. Pharm. Sci. 103 (2014) 2772-2783.
5. A.W. Newman, S.M. Reutzel-Edens, G. Zografi, Characterization of the “hygroscopic” properties of active pharmaceutical ingredients. J. Pharm. Sci. 97 (2008) 1047-1059.
6. Harańczyk H., *On water in extremely dry biological systems*, Wyd. UJ, Kraków 2003.
7. P. Nowak, A. Krupa, K. Kubat, et all., *Water vapour sorption in tadalafil-Soluplus co-milled amorphous solid dispersions*, Powder Technology 346 (2019) 383-384

Peculiarities of processing and analysis of NMR spectra of liquids with a low abundance of studied nuclei in the Earth magnetic field

P. Kupriyanov[1], V. Kirilenko[2], V. Chizhik[1]

[1]Saint-Petersburg State University
[2]"Vorobyovy Gory" Technical Education Centre, Moscow, Russia
E-mail: p.kupriyanov@spbu.ru

Introduction

J-coupling constants are the only data that can be extracted from an NMR spectrum in the Earth magnetic field. Is it enough to identify a liquid? As far as phosphorus- and fluorine-containing liquids are concerned, NMR makes it possible to distinguish liquids quite well. A single scan is sufficient to obtain NMR spectra of these liquids because the ^{19}F and ^{31}P isotopes have the high abundance. Besides, fluorine-containing liquids have spectral lines at the NMR frequency of fluorine (in addition to proton lines). Identification of organic liquids where protons can only interact with the ^{13}C nuclei is significantly more challenging (the ^{13}C natural abundance is about 1%). For a portable device, the signal accumulation is necessary to increase the signal-to-noise ratio. The influence of fluctuations in the Earth field can be eliminated [1], and a set of software algorithms is used to determine the interaction constant value that accurately characterizes a liquid (see Fig. 1).

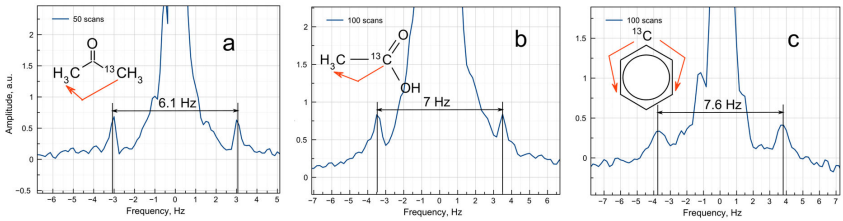

Figure 1. The proton NMR-spectra in the Earth magnetic field of acetone (a), acetic acid (b), and benzene (c) with different J-coupling constants

Preliminary processing

The main difficulty in determining the constant *J* accurately is the lack of resolution of NMR spectra. The spectral line can be clearly seen, but sometimes there are not enough points to determine its peak frequency. By simply adding zeros, additional oscillations are produced along the spectrum, hiding smaller lines of proton-carbon interactions (see Fig. 2). The sharp edge at the end of the signal is the reason for this. In such cases, apodization is used, which includes the multiplication of each signal by a descending curve (see Fig. 3).

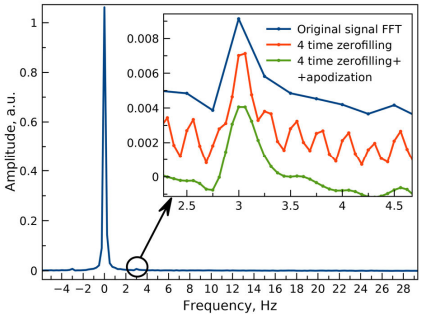

Figure 2. Acetone NMR spectrum in the Earth field (blue). The line masking after zero filling (red), the same zero filling after apodization (green)

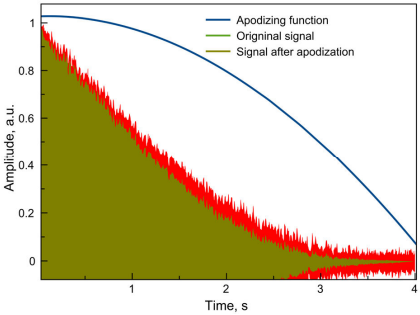

Figure 3. Original signal (red). Signal apodization (green) and apodizing function (blue)

Fourier Transform

In the case of NMR signals in the Earth magnetic field, problems arise when raw traditional mathematical transformations are used. It is not possible to start recording a signal immediately after the excitation pulse. It takes time, called dead time, for the transient process to decay in a receiving circuit. During the dead time, the initial part of the NMR signal is lost and shifts out of phase, resulting in the distortions of the spectrum. In most cases, the simple phase de-shift is not enough. It produces artifacts that may confuse a researcher. A good example is the spectrum of trimethyl phosphate, in which a "roughness" appears between the strong lines (see Fig. 4). The loss of the initial part of the signal also leads to a global phase change, which reveals an uneven distortion of the spectral lines that significantly differ in frequency, especially in fluorine-containing liquid spectra, where it is impossible to align the proton and fluorine lines simultaneously (see Fig. 5). This problem can be solved by adding zeros at the beginning of the signal, filling in the dead time, and it is also necessary to use apodization to avoid the appearance of fluctuations in the spectrum.

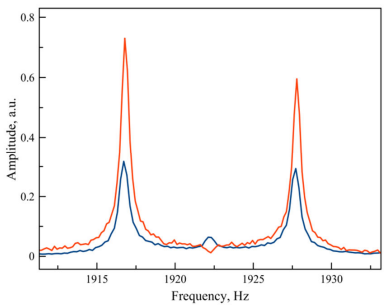

Figure 4. Trimethyl phosphate NMR spectra in the Earth field with different dead time after excitation

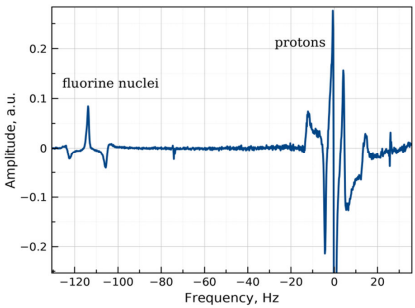

Figure 5. 2,2,2-trifluoroethanol NMR spectra in the Earth field

Signal accumulation

It is worth noting that we consider not the signal accumulation, but the spectrum accumulation, as it is more reasonable in the case of a signal with a floating frequency. Once the Larmor frequency is known, it is possible to perform a quadrature detection for each signal of a series. In this case, the NMR frequency in the spectrum will coincide with the zero frequency. Moreover, the shift in the spectrum due to fluctuations in the Earth magnetic field (see Fig. 6) is now out of our concern.

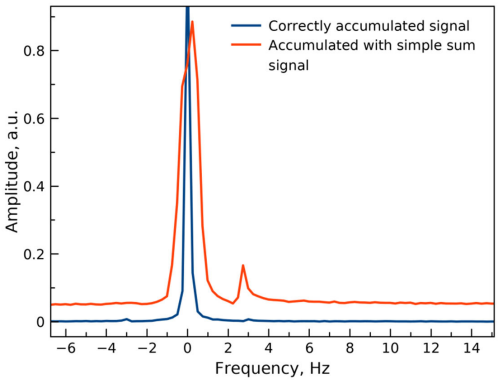

Figure 6. NMR spectrum of acetone in the Earth's field: Spectrum accumulation with frequency fluctuation compensation (blue) and FFT of the sum of the original signals (red)

Analysis

The practical goal of the NMR-spectra analysis is to determine a molecule structure based on the data obtained. Two approaches can be distinguished for this:

1. Analytical – to mathematically find the molecule that produces the most similar spectrum to the one being observed, based on the available data and the shape of the spectrum;
2. Accumulative – based on the extraction of a number of parameters and distinctive features of the spectrum in numerical form and their subsequent comparison with a pre-collected database of known chemical substances.

The analytical approach is slow and not universal. The accumulative method can be presented in two versions depending on the conditions:

1. The algorithm consists of accumulating a database of sets of scalar parameters for all the known molecules and is best suited for cases with a large variety of dissimilar (in terms of spectra) molecules. The following parameters are allocated for further recognition: the number of detected peaks pairs, an array of frequencies consisting of modulo sorted locations of the detected *J*-coupling peaks, and an array of ratios of their amplitudes to the amplitude of the main spectral line. The resulting array is stored in a database and associated with the name of the molecule. Then, after a sufficient molecule database is accumulated, a support vector machine model is trained and used for the recognition of an unknown molecule.
2. The second approach may be applied in case of poor-quality recordings or when there is a large number of similar molecules. A mask window should be selected around each peak found so that its edges contain the local minima. This method saves the following parameters to the database for each peak: left and right positions of the selected window k and the ratio of the maximum amplitude within the window to the amplitude of the main spectral line. This set of parameters is also associated with the observed molecule. If data from another recording of

a similar molecule is added, the previously recorded data should be overwritten as the average between them and the new data. To identify a previously unknown molecule, all previously recorded masks must be enumerated and a molecule is selected as the result of recognition such that the Euclidean distance between the data in the database and the data obtained after applying the mask is minimal (k-nearest neighbors for $k = 1$).

The developed algorithms [2] were successfully tested on the task of molecule recognition. The system has been tested as supplementary software for a currently developing spectrometer and may be used for any such device. The resulting software system is optimized for business purposes, providing a fully automatic full-cycle processing and analysis functionality (see Fig. 7).

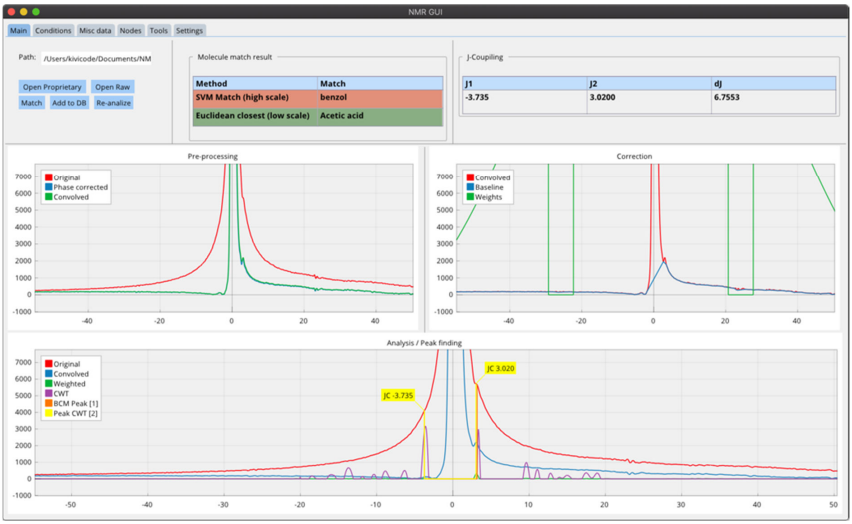

Figure 7. An example of processing of acetic acid via the developed software system

References

1. V. Chizhik, P. Kupriyanov. Device for recording nuclear magnetic resonance spectra in the Earth magnetic field. Eurasian patent №034623, 2020, available at: http://www.eapatis.com/Data/EATXT/eapo2020/PDF/034623.pdf
2. V. D. Kirilenko. Software package for the analysis of spectra of substances for low-field low resolution NMR spectrometers, 2021, available at: https://www.researchgate.net/publication/349773520_Software_package_for_the_analysis_of_spectra_of_substances_for_low-field_low_resolution_NMR_spectrometers

Development and characterization of novel pervaporation membranes based on sodium alginate modified by FeBTC

Anna I. Kuzminova, Anastasia V. Penkova

St. Petersburg State University, St. Petersburg, 199034 Russia
E-mail: ai.kuzminova@mail.ru

Introduction

Pervaporation is a promising method for the separation of liquids in the bioprocessing, petrochemical and pharmaceutical industries. This method allows to separate closely boiling and thermally unstable components, as well as azeotropic mixtures and mixtures of isomers. Pervaporation is an environmentally-friendly method of separation, for its implementation does not require expensive equipment and high energy consumption. The rapid development of pervaporation requires the search for new high-performance membrane materials with desired properties. Currently, the improvement of the transport properties of polymer pervaporation membranes occurs due to the creation of mixed matrix membranes (MMMs), by modifying the polymer matrix with an inorganic and/or organic filler.

In the present work the novel green membranes based on biopolymer sodium alginate (SA) were prepared by introducing the metal-organic frameworks FeBTC into the SA matrix. The improvement of the transport properties of the membranes based on SA modified by FeBTC was expected due to the porous structure, hydrophilic/hydrophobic properties, excellent chemical stability of the FeBTC. The structural and physicochemical properties of the developed SA-FeBTC membranes were studied by spectroscopic techniques (nuclear magnetic resonance (NMR) and Fourier-transform infrared spectroscopy (FTIR)), microscopic methods (scanning electron microscopy (SEM) and atomic force microscopy (AFM)), thermogravimetric analysis (TGA), and swelling experiments. Transport properties of developed SA-FeBTC membranes were studied in the pervaporation of water-isopropanol mixtures at 22 °C.

Acknowledgements

The reported study was funded by RFBR, project number 19-38-90008. The experimental work of this study was facilitated by the equipment from the Resource Centre of Geomodel, Chemical Analysis and Materials Research Centre, Centre for X-ray Diffraction Methods, Magnetic Resonance Research Centre, Centre for Innovative Technologies of Composite Nanomaterials, Nanophotonics Centre, Cryogenic department, Thermogravimetric and Calorimetric Research Centre and the Interdisciplinary Resource Centre for Nanotechnology at the St. Petersburg State University.

The basic physics of ASL perfusion and its applications in neuroimaging: a review

Anna Y. Lavrova[1], M. A. Zubkov[2], V. M. Cheremisin[1]

[1]Faculty of General Medicine, Department of oncology with a course of Radiation diagnostics and Radiotherapy, Saint Petersburg State University, Saint Petersburg, Russia
[2]Department of Physics and Engineering, Saint Petersburg National Research University of Information Technologies, Mechanics and Optics, Saint Petersburg, Russia
E-mail: lavrova.anya@gmail.com

Introduction

Arterial spin labeling (ASL) is an MR technique that does not require extrinsic administration of contrast media. Instead, spins of flowing arterial blood are labeled as intrinsic contrast agent. Although the ASL principle was discovered in the early 1990s and was used in MR systems with low field strength, modern high-field MR scanners with improved signal-to-noise ratio (SNR) and state-of-the-art pulse sequences and multichannel coils have opened up opportunities for widespread use of ASL in neurological and mental diseases. The most important parameter of ASL is Cerebral Blood Flow (CBF).

Purpose

To explain the basic physics of arterial spin labeling (ASL) perfusion and to point out opportunities for its use in daily clinical practice.

Findings

There are 4 main techniques to achieve ASL perfusion: pulsed (PASL), continuous (CASL), pseudo-continuous (PCASL), velocity-selective (VS-ASL).

PASL uses short (5-2 millisecond) radiofrequency (RF) pulses to label a thick slab of arterial blood spins at a single instance in time proximal to the scanning region, and the imaging is performed after a time long enough for that spatially labeled blood to reach the tissue in the region of interest. After labeling, a post-labeling delay is required, during which tagged blood moves into the scanning region, losing some of its labels due to longitudinal T1 relaxation.

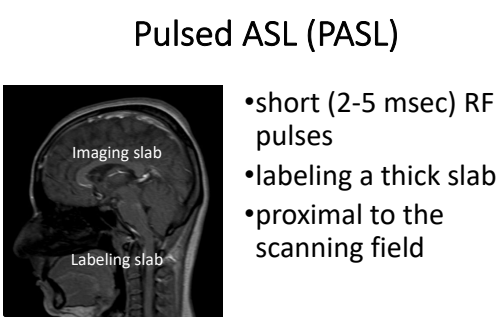

Figure 1. PASL technique

CASL uses long and continuous RF pulses (1–2 seconds) and the supplying blood is continuously labeled below the imaging slab through flow-driven adiabatic inversion until the tissue magnetization reaches a steady state. The limitation of this technique is the necessity of continuous RF transmitting hardware, which is mostly unavailable in commercial MR scanners.

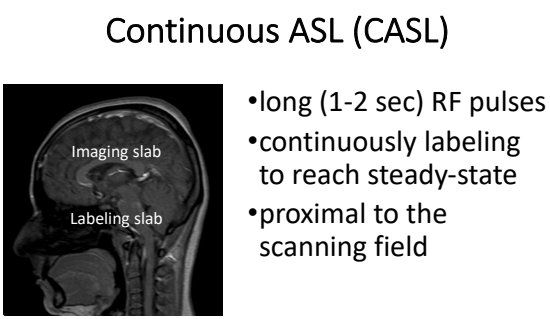

Figure 2. CASL technique

PCASL uses a long (1-2 seconds) series of short (1millisecond) RF pulses together with a strong slice-selection gradient, which is designed to invert inflowing blood into adiabatic and pseudo steady-state manner without a need of specific hardware. Currently, this technique is accepted and commonly used in clinical practice.

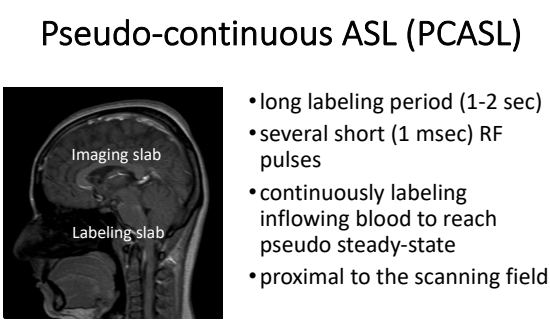

Figure 3. PCASL technique

VS-ASL tags blood based on velocity, not spatial location. Crusher gradients are used to saturate spins flowing faster than a chosen cutoff velocity, thus allowing the labeling of slower blood flows. This technique is still in development and requires further validation for clinical use.

Velocity-selective ASL (VS-ASL)

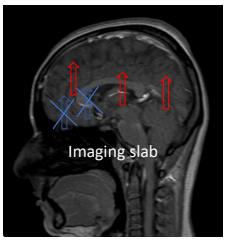

- labels blood which moves faster than cutoff value
- requires optimal cutoff velocity
- for local perfusion measurements (e.g. stroke)

Figure 4. VS-ASL technique

Recommended imaging parameters

CASL/PCASL:

- Labeling duration ≈ 1500-2000 ms
- Labeling $B_1 \approx 1.5$ μT
- Average Labeling Gradient ≈ 1 mT/m (10 mT/m if selective labeling)
- Post-Label delay > Arterial transfer time (1500-2000 ms)

PASL:

- TI ≈ 1500-2000 ms
- TI_1 ≈ 800 ms (for tagged bolus tail removal)
- Labeling Slice thickness ≈ 15-20 c

Image acquisition techniques

3D EPI (most common)	3D GRASE (most efficient)	3D RARE (highest SNR)
Fast	Good coverage	Short TE
Susceptible to artifacts	Less artifacts	Good coverage

Artifacts

- motion artifacts (e.g., head movements, breathing)
- susceptibility (e.g., postsurgical sites, hemorrhage, calcifications, paranasal sinuses)

Clinical applications of ASL perfusion

In dementia, the ASL hypoperfusion pattern closely matches the areas of hypometabolism on positron emission tomography (PET) due to the connection of perfusion and metabolism in the brain, which suggests the use of ASL as an alternative for high-cost and invasive PET. In a stroke, ASL can be used to assess perfusion both in the acute and the chronic phase. In arteriovenous malformations and dural arteriovenous fistulas, ASL is sensitive to detect even small (> 2 cm) shunts. In epilepsy, ASL can be used to assess the epileptogenic focus, both in the peri- and interictal period. In neoplasms, ASL is of particular interest in cases in which gadolinium-based perfusion is contraindicated (e.g., allergy, kidney insufficiency) and promise to differentiate tumor progression from radiation necrosis.

Conclusion

ASL is a promising MR technique that could challenge established “gold-standard” methods. In neurovascular diseases, ASL is an alternative tool for CT and bolus tracking MRI for studying the mechanisms and predicting the outcome of stroke. Also, a strong correlation was found between ASL and DSC perfusion in brain tumors investigation. ASL is especially

important as a non-invasive MR-modality in pediatric patients, as it minimizes exposure to ionizing radiation and traumatic venous cannulation.

References

1. Pollock J. M. et al. Arterial spin-labeled MR perfusion imaging: clinical applications // Magnetic resonance imaging clinics of North America. – 2009. – V. 17. – №. 2. – Pp. 315-338.
2. Haller S. et al. Arterial spin labeling perfusion of the brain: emerging clinical applications // Radiology. – 2016. – V. 281. – №. 2. – Pp. 337-356.
3. Alsop D. C. et al. Recommended implementation of arterial spin-labeled perfusion MRI for clinical applications: A consensus of the ISMRM perfusion study group and the European consortium for ASL in dementia // Magnetic resonance in medicine. – 2015. – V. 73. – №. 1. – Pp. 102-116.

^{14}N Quadrupole Coupling Constants calculation in some compounds with amino groups

S. Mamadazizov[1,2], G. V. Mozzhukhin[3], G. S. Kupriyanova[2]

[1]School of Arts and Sciences, University of Central Asia, 736000, Khorog, Tajikistan
[2]Baltic Federal University by Immanuel Kant, 236041 Kaliningrad, Russian Federation
[3]Gebze Technical University, 41400 Gebze/Kocaeli, Turkey.
E-mail: sultonazar.mamadazizov@mail.ru
https://ucentralasia.org

Introduction

Quadrupole Coupling Constant (QCC) is an important parameter both for Nuclear Magnetic Resonance (NMR) and Nuclear Quadrupole Resonance (NQR) spectroscopy, which is defined by the interaction of the nuclear electric quadrupole moment eQ with Electric Field Gradient (EFG). QCC determines the resonance frequencies for NQR. In case of NMR quadrupole interaction is the main relaxation mechanism [1].

QCC of the following compounds was calculated by the means of Density Functional Theory: acetamide, glycine, nitromethane, urea. QCC and asymmetry parameter η for ^{14}N could be computed with high accuracy if the local environment of the atoms is reproduced properly [2].

Computational method

Computation of the ^{14}N NQR parameters were performed in the package GAUSSIA09[3]. In [4] was shown that B3PW91 method is a good choice for this task. Comparative analysis of different basis set results will be provided elsewhere. Clusters for the acetamide, glycine, nitromethane, urea were prepared based on structural data in [5-8]. Calculation with a number of possible basis sets were conducted, in order, to select an optimal for the purposes of this paper. The provided data was computed with the basis set 6-311++g.

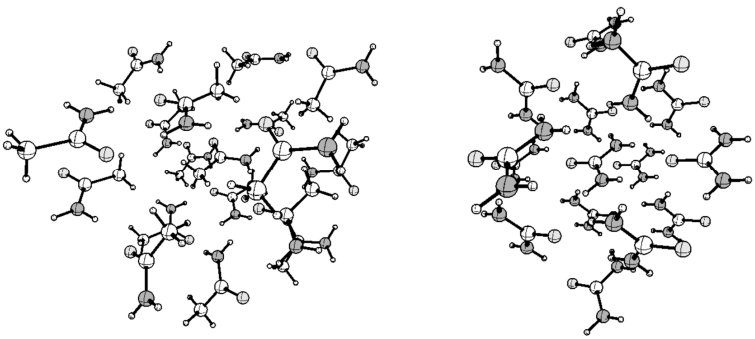

Figure 1. Computational clusters for acetamide (on the left) and urea (on the right)

Results and discussion

Computed ^{14}N QCC and asymmetry parameters provided in table 1. Calculated data are very close to experimental one. In case of Glycine difference between experimental and theoretical QCC is 9.18 %. The results of Urea are more accurate. The difference is only in 51 kHz, which is about 1.4 %. For acetamide there is no experimental data, but since the results for the known compound glycine and urea are close, we can assume that these computations are trustworthy. In [9] calculated QCC for different linear clusters in the range 3.57 – 4.49 MHz.

But in case of linear cluster the impact of the amino group of a single neighbor is considered, while the cluster that were used in this work allows to reproduce all the neighbors, which results in more accurate EFG tensor. Since the EFG tensor is very sensitive to local environment of the atom.

Table 1. Calculated ^{14}N QCC and asymmetry parameter η

Compound	η	QCC, MHz
Acetamide	0.47	3.102
Glycine	0.29	1.544
Nitromethane	0.6	1.287
Urea	0.54	3.751

Conclusion

Clusters with reproduced local environment for target ^{14}N were used to calculate the QCC and asymmetry parameter of several compounds. The results of Urea and Glycine in a good compliance with experimental data, which proves that the results for left materials are also close to the experimental data.

Acknowledgements

Authors acknowledge support by the Department of Mathematics and Natural Science, SAS, University of Central Asia.

References

1. M. Witanovski, Nitrogen NMR. Spectroscopy, Pure and Applied Chemistry 37 (1974) 225-233.
2. Mamadazizov, Sultonazar, et al. "New assignment of 14N NQR spectral lines for tetrazoles derivatives." Chemical Physics 506 (2018): 52-60.
3. D.J.F.M.J. Frisch, G.W. Trucks, H.B. Schlegel, G.E. Scuseria, M.A. Robb, J.R. Cheeseman, G. Scalmani, V. Barone, G.A. Petersson, H. Nakatsuji, X. Li, M. Caricato, A. Marenich, J. Bloino, B.G. Janesko, R. Gomperts, B. Mennucci, H.P. Hratchian, J.V. Ort, Gaussian, Revision D.01, Gaussian Inc, Wallingford CT, 2016.
4. Bailey, William C. "DFT and HF–DFT calculations of 14N quadrupole coupling constants in molecules." Chemical Physics 252.1-2 (2000): 57-66.
5. J.W.Bats, M.C.Haberecht, M.Wagner CCDC 225718: Experimental Crystal Structure Determination, 2004, DOI: 10.5517/cc7kw7w
6. T.N.Drebushchak, E.V.Boldyreva, E.S.Shutova, Acta Crystallographica Section E: Structure Reports Online, 2002, 58, o634
7. Trevino, S. F., E. Prince, and C. R. Hubbard. "Refinement of the structure of solid nitromethane." The Journal of Chemical Physics 73.6 (1980): 2996-3000.
8. V.Nikolic, M.Stankovic, L.Nikolic, D.Cvetkovic, A.Kapor, M.Cakic, Chemical Industry and Chemical Engineering Quarterly, 2005, 1, 69
9. Esrafili, Mehdi D., Hadi Behzadi, and Nasser L. Hadipour. "Theoretical study of N–H⋯ O hydrogen bonding properties and cooperativity effects in linear acetamide clusters." Theoretical Chemistry Accounts 121.3 (2008): 135-146.

Evaluation of the dynamic viscosity in protein solutions applying Nuclear Magnetic Relaxation

Yulianela Mengana Torres[1], Manuel A. Lores Guevara[1], Juan. C. García Naranjo[1], Beatriz T. Ricardo Ferro[1], Yamirka Alonso Geli[1], Edalis Guerrero Piña[2], Yomaidis Araujo Durán[3], Lidia C. Suárez Beyries[3], Inocente C. Rodríguez Reyes[3], Samuel Jorge Rosales Rodriguez[3]

[1]Centro de Biofísica Médica, Universidad de Oriente, Patricio Lumumba S/N. CP: 90500. Santiago de Cuba. Cuba.
[2]Departamento Física, Facultad de Ciencias Naturales y Exactas, Universidad de Oriente, Patricio Lumumba S/N. CP: 90500. Santiago de Cuba. Cuba.
[3]Hospital General "Dr. Juan Bruno Zayas Alfonso", Carretera del Caney S/N. Santiago de Cuba. Cuba.

A Nuclear Magnetic Relaxation method to determine the dynamic viscosity in samples of hemoglobin (Hb) solution and blood serum is presented. The approach is based on the inverse relationship between this physical parameter and the magnetic relaxation time proton spin-spin (T_2). Carr-Purcell-Meiboon-Gill pulse sequence was employed to determine the relaxation time T_2 in a Tecmag Magnetic Resonance console coupled to a homogeneous magnet of 0,1 T. The obtained dynamic viscosity values of Hb solution (12,82 ± 3,35 mPas) statistically coincide with those reported in the literature and those obtained with the reference method (11,19 ± 2,02 mPas) with 95% reliability. For blood serum the values obtained (1,28 ± 0,06 mPas) statistically coincide with the reference method (1,32 ± 0,05 mPas) with 95% reliability.

The structural and dynamic characteristics of Lys2Gly and Lys2Lys peptide dendrimers. The molecular dynamics simulation at different temperatures

Sofia E. Mikhtaniuk[1,2], Valeriy V. Bezrodnyi[1,2], Oleg V. Shavykin[1,2], Igor M. Neelov[1,2], Nadezhda N. Sheveleva[2], Denis A. Markelov[2]

[1]St. Petersburg National Research University of Information Technologies, Mechanics and Optics (ITMO University), Kronverkskiy pr. 49, 197101 St. Petersburg, Russia
[2]St. Petersburg State University, 7/9 Universitetskaya nab.,199034 St. Petersburg, Russia
E-mail: mikhtanyuk@mail.ru

Introduction

Recently, several new peptide dendrimers have been synthesized, studied by NMR [1-3] and tested as gene delivery vehicles [4-5]. These dendrimers differ from usual lysine dendrimers [6-9] by insertion of various double residues (2Gly, 2Lys or others) between each pair of neighbouring lysine branching points. All these dendrimers have the same AlaLys core, same branched backbone, same charged (+2) terminal Lys groups but different side groups in dipeptides in their spacers. If you insert small neutral 2Gly spacers or large charged (+2) 2Lys spacers their repeating units will be Lys2Gly and Lys2Lys (where first Lys is neutral branched Lys residue). We applied the molecular dynamics (MD) simulations method to study the structural and dynamic characteristics of such dendrimers in water with explicit counterion in the wide interval of temperatures (from 280 to 340 K). The details of MD method [10] and structures of united atoms and full atomic models used for linear polymers [10-17], polyelectrolytes [18-25] and branched polymers [26-36] were described by us earlier.

The structural characteristics

We have shown that the size (see, the Figure 1a) and internal structure of both dendrimers practically do not depend on temperature. The Lys-2Lys dendrimer has a larger bare charge and therefore its spacers are more elongated than for Lys-2Gly. It leads to a few effects: Lys-2Lys have the larger size, the smaller fluctuations and lower internal density in comparison with the Lys-2Gly dendrimer.

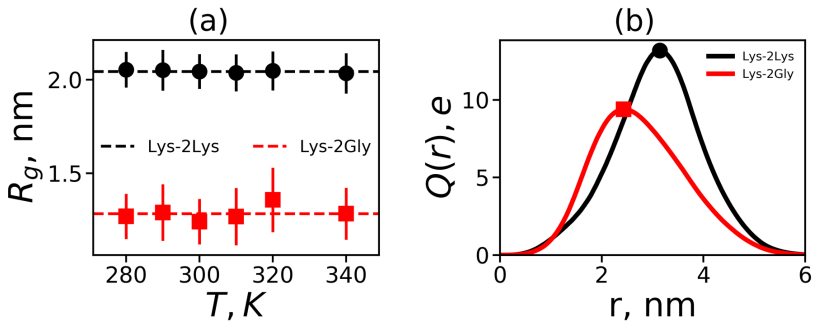

Figure 1. (a) The mean square gyration radius as function of temperature; (b) The radial distribution of the cumulative charge for both dendrimers

The Lys-2Lys denrimer contains more water and counterion molecules in its interior. The Figures 1b demonstrates the cumulative charge distributions for both dendrimers. The larger surface of the Lys-2Lys dendrimer leads to greater surface charge density and lower zeta-potential of this dendrimer.

The dynamic properties

We have shown that the Lys-2Lys dendrimer rotates more slowly than Lys-2Gly. The terminal CH_2 groups in both dendrimers move faster than the inner CH_2 groups. The calculated temperature dependencies of the spin-lattice relaxation times of these groups for both dendrimers are in a good agreement with the experimental results obtained by NMR (see Figure 2).

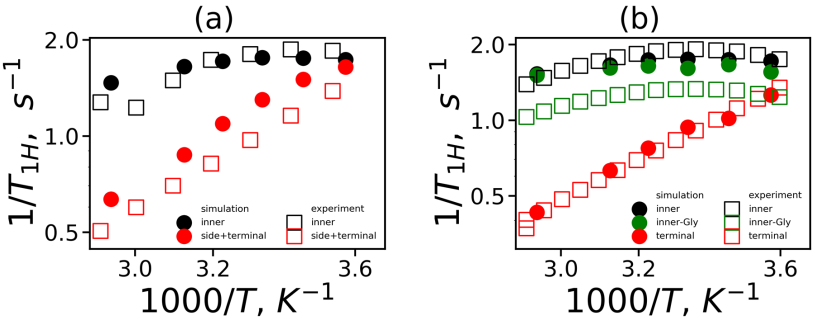

Figure 2. The spin-lattice ^1H NMR relaxation rate $1/T_{1H}$ at the fixed frequency $\omega_H/2\pi$ = 400 MHz as a function of inverse temperature 1000/T for (a) Lys-2Lys and (b) Lys-2Gly dendrimers calculated from MD simulation and NMR experiments [1]

The local orientational mobility of the CH_2(-N) groups in inner and terminal segments in Lys-2Lys are close to local orientational mobility of that groups in Lys-2Gly. It has been shown that the mobility of terminal groups is essentially larger than the mobility of inner groups.

Acknowledgements

This work is supported by the Russian Foundation for Basic Research (grants No. 2019-03-00715). The research is carried out using the equipment of the shared research facilities of HPC computing resources at Lomonosov Moscow State University [37] and Computer Resources Center of Saint Petersburg State University.

References

1. Sheveleva N.N., Markelov D.A., Vovk M.A. Mikhailova, M.E., Tarasenko I.I, Neelov I.M., E.Lähderant. Scientific Reports, 2018, 8, 8916
2. Sheveleva N.N., Markelov D.A., Vovk M.A., Tarasenko I.I, Neelov I.M., E.Lähderanta, 2019, RSC Adv. 9, 18018.
3. Sheveleva N.N., Markelov D.A., Vovk M.A., Tarasenko I.I, Mikhailova M.E., Neelov I.M., 2019, Molecules, 24, 2481
4. M.Gorzkiewicz, O.Kopec, A.Janaszevska, I.I.Tarasenko, N.N.Sheveleva, I.M. Neelov, B.Klajnert, Bioorg.Chem. 2020, 95, 103504.
5. M. Gorzkiewicz,, A.Konopka, A.Janaszewska, A., I.I.Tarasenko, V.V.Bezrodnyi. I.M. Neelov, B.Klajnert, Int. J. Mol. Sci., 2020, 21 (9), 3138.
6. Denkewalter R.G., Kolc J., Lukasavage W.J., US Patent, 1983, № 4410688.
7. Neelov, I. M., Markelov D.A, Falkovich S.G., Ilyash M.Y., Okrugin B.M., Darinskii A.A., Polymer Science, 2013, 55, 154.
8. S. Falkovich, D. Markelov, I. Neelov, and A. Darinskii. J. Chem. Phys. 2013, 139, 064903.

9. Neelov, I., Markelov D., Falkovich S.G., Paci E., Darinskii A., Tenhu H., Dendrimers in Biomedical Applications, (London: RSC) 2013, 99-114.
10. Gotlib, Y.Y., Darinskii, A.A., Neelov, I.M., Balabaev, N.K. Macromolecules, 1980, 13(3), pp. 602–608
11. Darinskii A., Lyulin A., Neelov I., Makromolekulare Chemie - Theory and Simulations (Macromolecular Theory and Simulations), 1993, 2, 523.
12. Neelov I.M., Adolf D.B., Lyulin AV., Davies G.R. J. Chem. Phys., 2002, 117,4030.
13. Zarembo, A., Balabaev, N.K., Neelov, I.M., Sundholm, Darinskii, A.A., , F. PCCP, 2003, 5(11), 2410–2416
14. Neelov I.M., Adolf D.B., McLeish T.C.B., Paci E., Biophys. J., 2006, 91, 3579.
15. Gowdy, J., Batchelor, M, Neelov, I, Paci, E. J. Phys. Chem. B, 2017, 121, 9518.
16. Neelov I.M., Binder K., Macromolecular Theory and Simulations, 1995, 4, 1063.
17. Neelov, I.M., Binder, K. Macromol. Theory&Simul/, 1995, 4(1), pp. 119–136
18. Ennari J., Neelov I., Sundholm F., Polymer, 2000, 41, 4057.
19. Ennari J., Neelov I., Sundholm F., Polymer, 2001, 42, 8043
20. Darinskii A., Gotlib Yu., Lukyanov M., Lyulin A., Neelov I., Progress in Colloid & Polymer Science, 1993, 91, 13.
21. Ennari J., Neelov I., Sundholm F., Comput. Theor. Polym. Sci., 2000, 10, 403.
22. Ennari J., Elomaa M., Neelov I., Sundholm F., 2000, Polymer, 41, 985.
23. Darinskii A., Gotlib Yu., Lyulin A., Neelov I., Vysokomolek. Soed.. Ser,A 1991, 33, 1211 (translation to English: Polymer Science, 33,1116).
24. Ennari J., Neelov I., Sundholm F., Polymer, 2004, 45, 4171
25. Ennari J., Neelov I., Sundholm F., Polymer, 2000, 41, 2149.
26. Mazo M.A., Shamaev M.Y., Balabaev N.K., Darinskii A.A., Neelov I.M., Physical Chemistry Chemical Physics, 2004, 1285.
27. Okrugin B., Ilyash M., Markelov D., Neelov I., Pharmaceutics, 2018, 10, 129.
28. Neelov I.M., Adolf D.B., 2003, Macromolecules, 36, 6914.
29. Neelov I.M., Adolf D.B., 2004, J. Phys. Chem. B, 108, 7627.
30. O.V.Shavykin, I.M.Neelov, A.A.Darinskii. PCCP, 2016, 18, 24307
31. Shavykin O.V., Mikhailov I.V., Darinskii A.A., Neelov I.M., Leermakers F.A.M., Polymer, 2018,146, 256.
32. Okrugin B.M., Neelov I.M., Leermakers F.A.M., Borisov O.V., Polymer, 2017, 125, 292.
33. Shavykin O.V., Leermakers F.A.M., Neelov I.M., Darinskii A.A., Langmuir, 2018, 34, 1613.
34. Mikhtaniuk, S.E., Bezrodnyi, V.V., Shavykin, O.V., Neelov I.M., Penkova, A.V., Markelov, D.A., Polymers,2020,12(8),1657
35. Shavykin, O.V., Neelov, I.M., Borisov, O.V., Darinskii, A.A., Leermakers, F.A.M.,Macromolecules, 2020, 53(17), pp. 7298–7311
36. Bezrodnyi, V.V., Shavykin, O.V., Mikhtaniuk, S.E., Neelov I.M., Sheveleva, N.N., Markelov, D.A., International Journal of Molecular Sciences, 2020, 21(24), 1–22, 9749
37. Sadovnichy, V.; Tikhonravov, A.; Voevodin, V.; Opanasenko, V. "Lomonosov": Supercomputing at Moscow State University. In Contemporary High Performance Computing: From Petascale toward Exascale; Chapman and Hall/CRC: Boca Raton, FL, USA, 2013; pp. 283–307.

The self-assembly of the amphiphilic molecules consisting of polylysine dendrons with the single and double hydrophobic tails

Sofia E. Mikhtaniuk[1,2], Emil I. Fatullaev[1], Oleg V. Shavykin[1,2], Anatoly A. Darinskii[1,3], Christian Holm[4], Igor M. Neelov[1,2]

[1]St. Petersburg National Research University of Information Technologies, Mechanics and Optics (ITMO University), Kronverkskiy pr. 49, 197101 St. Petersburg, Russia
[2]St. Petersburg State University, 7/9 Universitetskaya nab., 199034 St. Petersburg, Russia
[3]Institute of Macromolecular Compounds RAS, Bolshoy pr.V.O. 31, St. Petersburg, Russia
[4]Universität Stuttgart, Allmandring 3, 70569 Stuttgart, Germany
E-mail: mikhtanyuk@mail.ru

Introduction

Branched polymers including dendrimers and dendrigrafts [1-4] are used for drug and gene delivery [5-11]. These systems were studied theoretically using molecular and Brownian dynamics simulation [2-4, 7-8, 12-18] and numerical self-consistent field approach [19-21]. Liposomes and spherical micelles are other carriers for drug and gene delivery. We used earlier self-consistent field (SCF) method to consider the formation of spherical micelles based on hybrid molecules consisting of one lysine dendron and one hydrophobic tail [21] similar to that studied experimentally [22]. In the current work, we consider the case of similar hybrid molecules but with two hydrophobic tails.

The model and method

The schematic model of hybrid surfactants is shown on Figure 1. The self-consistent field approach was applied to calculate the equilibrium micelle properties.

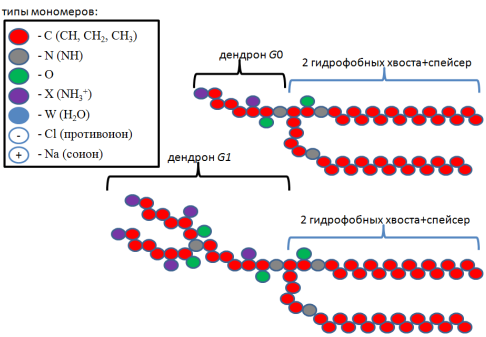

Figure 1. The united atom model of surfactant molecules based on a dendron of 0-th and 1-st generations with two hydrophobic tails. The two tails are connected through a lysine spacer. The colors indicate the types of monomers used

To determine the local structure, we made numerical calculation in the Grand canonical ensemble. We calculated also the radial distribution functions of the density of micelle relative to its center of mass, corresponding to the equilibrium state of micelles.

The equilibrium properties of micelles

The Figure 2a shows the dependences of the aggregation numbers on the salt concentration for hybrid molecules with two tails.

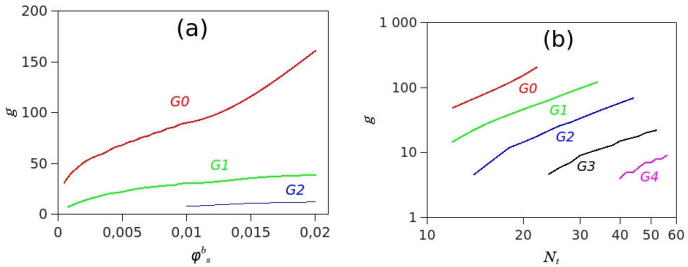

Figure 2. The aggregation number for different generation number G as functions of: (a) salt concentration (at fixed total length of both hydrophobic tails is equal to 16) and (b) total length of hydrophobic tails (at fixed salt volume fraction 0.01)

The aggregation number over a wide range of total tail length are depicted on Figure 2b. It can be seen that the formation of micelles for hybrid molecules with dendrons of generation G=0-4 and two hydrophobic tails is possible but in the case of G>2 it requires rather long tails.

Acknowledgements

This work was supported by RFBR grant 20-53-12036. The research is carried out using the equipment of the shared research facilities of HPC computing resources at Lomonosov Moscow State University [23].

References

1. Denkewalter R.G., Kolc J., Lukasavage W.J., US Patent, 1983, № 4410688.
2. Neelov, I. M., Markelov D.A, Falkovich S.G., Ilyash M.Y., Okrugin B.M., Darinskii A.A., Polymer Science, 2013, 55, 154.
3. S. Falkovich, D. Markelov, I. Neelov, and A. Darinskii. J. Chem. Phys. 2013, 139, 064903.
4. Neelov, I., Markelov D., Falkovich S.G., Paci E., Darinskii A., Tenhu H., Dendrimers in Biomedical Applications, (London: RSC) 2013, 99-114.
5. Gorzkiewicz M., Kopec O., Janaszevska A., Tarasenko I.I., Sheveleva, N.N., Neelov I.M., Klajnert B., Bioorg.Chem. 2020, 95, 103504.
6. Gorzkiewicz M., Konopka A., Janaszevska A., Tarasenko I.I., Bezrodnyi V.V., Neelov I.M., Klajnert B., Int. J. Mol. Sci., 2020, 21 (9), 3138.
7. Mikhtaniuk, S.E., Bezrodnyi, V.V., Shavykin, O.V., Neelov I.M., Penkova, A.V., Markelov, D.A., Polymers, 2020, 12(8), 1657.
8. Bezrodnyi, V.V., Shavykin, O.V., Mikhtaniuk, S.E., Neelov I.M., Sheveleva, N.N., Markelov, D.A., International Journal of Molecular Sciences, 2020, 21, 9749, 1–22.
9. Sheveleva N.N., Markelov D.A., Vovk M.A. Mikhailova, M.E., Tarasenko I.I, Neelov I.M., E.Lähderant. Scientific Reports, 2018, 8, 8916.
10. Sheveleva N.N., Markelov D.A., Vovk M.A., Tarasenko I.I, Neelov I.M., E.Lähderanta, 2019, RSC Adv. 9, 18018.
11. Sheveleva N.N., Markelov D.A., Vovk M.A., Tarasenko I.I, Mikhailova M.E., Neelov I.M., 2019, Molecules, 24, 2481.
12. Mazo M.A., Shamaev M.Y., Balabaev N.K., Darinskii A.A., Neelov I.M., Physical Chemistry Chemical Physics, 2004, 1285.
13. Okrugin B., Ilyash M., Markelov D., Neelov I., Pharmaceutics, 2018, 10, 129.
14. Neelov I.M., Adolf D.B., Macromolecules, 2003, 36, 6914.
15. Neelov I.M., Adolf D.B., J. Phys. Chem. B, 2004, 108, 7627.

16. Markelov D.A., Falkovich S.G.,, Neelov, I. M., et al, PCCP, 2015, 17, 3214.
17. Shavykin, .O.V. I.M.Neelov, A.A.Darinskii. PCCP, 2016, 18, 24307.
18. Shavykin O.V., Mikhailov I.V., Darinskii A.A., Neelov I.M., Leermakers F.A.M., Polymer, 2018,146, 256.
19. Okrugin B.M., Neelov I.M., Leermakers F., Borisov O.V., Polymer, 2017, 125, 292.
20. Shavykin, O.V., Neelov, I.M., Borisov, O.V., Darinskii, A.A., Leermakers, F.A.M., Macromolecules, 2020, 53(17), pp. 7298–7311.
21. Shavykin O.V., Leermakers F., Neelov I.M., Darinskii A.A, Langmuir, 2018,34, 1613
22. Mirsharghi, S., Knudsen, K. D., Bagherifam, S., Nystrom, B., Boas, U. New J. Chem. 2016, 40, 3597−3611.
23. Sadovnichy, V.; Tikhonravov, A.; Voevodin, V.; Opanasenko, V. “Lomonosov”: Supercomputing at Moscow State University. In Contemporary High Performance Computing: From Petascale toward Exascale; Chapman and Hall/CRC: Boca Raton, FL, USA, 2013; pp. 283–307.

Determination of the magnetic moments of the ^{6}Li and ^{7}Li nuclei using a spectrometer that registers simultaneous signals from two types of nuclei

Yuriy I. Neronov, Anton N. Pronin, Nikolay N. Seregin

Mendeleyev Institute for metrology, St. Petersburg, Moskovsky pr. 19, Russia
E-mail: yineronov@mail.ru

Introduction

The interaction of protons and neutrons inside the nucleus has a rather complex tensor character and searches for a theoretical description of the magnetic moments of nuclei have continued for many decades. To date, theoretical studies allow theorists to calculate the magnetic moments of ^{6}Li and ^{7}Li, but with a deviation from the experiment by several percent. Experimental work on the precision determination of magnetic and quadrupole moments of nuclei is the basis for testing new theoretical models that are designed to more accurately describe the non-trivial features of the structure of nuclear matter.

Accumulation of spectra and processing of experimental data

In this work, we studied the capabilities of an NMR spectrometer with simultaneous twochannel recording of signals from two types of nuclei. This mode is not available on serial spectrometers, where a transition to another core requires a break to adjust the frequency of the receiving circuit, at which, as a rule, the temperature of the sample changes. The recorded signals from the nuclei studied by us differed in intensity by two orders of magnitude. Therefore, the ampoules were placed in a receiving inductance specially made by the author, which was optimally tuned to a weaker signal.

To register the second signal, an additional small inductance was used, which, according to the equivalent circuit, turned out to be parallel to the main one. An electromagnet with a field of 2.14 T was used, which was previously used for precision determination of the magnetic moments of the nuclei of deuterium, tritium, and ^{3}He [1-4]. The AD9958 integrated circuit was used to form two reference frequencies close to the resonances of the studied pair of nuclei. The studied solutions were prepared by weighing lithium chloride salts LiCl, or lithium hydroxide mono-hydrate LiOH*H_2O and distilled water. Signals were recorded from standard 5 millimeter ampoules with rotation. To control the temperature, we used two DS18B20 digital sensors from Dallas Semiconductor. In the first part of the experiment, the ratio of the resonance frequencies f(^{7}Li)/f(^{6}Li) was determined, in the second part, the ratio of the frequencies f(H_2O)/f(^{7}Li). The ratios of magnetic moments are calculated by the formulas:

$$\mu(^7\text{Li})/\mu(^6\text{Li}) = [f(^7\text{Li})/f(^6\text{Li})]\times[S(^7\text{Li})/S(^6\text{Li})]\times\{1 + [\sigma(^7\text{Li}) - \sigma(^6\text{Li})]\} \quad (1)$$

$$\mu_p/\mu(^7\text{Li}) = [f(H_2O)/f(^7\text{Li})]\times[S_p/S(^7\text{Li})]\times\{1 + [\sigma(H_2O) - \sigma(^7\text{Li})]\}, \quad (2)$$

where the spin ratio is a strictly quantized quantity: $S(^7\text{Li})/S(^6\text{Li}) = 3/2$; $S_p/S(^7\text{Li}) = 1/3$. The ^{6}Li and ^{7}Li ions have the same electron shell and have a similar effect from the nearest water molecules. The correction for the isotopic shift for the difference $\sigma(^7\text{Li}) - \sigma(^6\text{Li})$ when compared with other similar calculations shows that, due to the difference in the amplitudes of the oscillations of the ions, due to the difference in their masses (17%), when estimated from above, they should not exceed 10^{-9}.

Therefore, the experimental determination of the ratio of the magnetic moments of ^{6}Li and ^{7}Li nuclei in aqueous solutions can be several orders of magnitude more accurate than the accuracy of determination of the magnetic moments themselves. Proton screening in water is known from [5]: $\sigma(H_2O) = 25680\ (2.5) \times 10^{-9}$ for 25.0 °C , and screening of lithium ions in water was estimated theoretically in [6]: $\sigma(^7\text{Li}) = 90.89\ (300) \times 10^{-6}$.

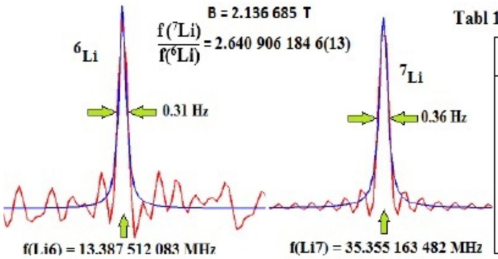

Tabl 1. Comparison of the results of diffrent authors

f(7Li)/f(6Li)	Error, δ	Reference
2.640 906 6(17)	6.4 × 10^-7	[9]
2.640 907 9(13)	4.9 × 10^-7	[10]
2.640 908 0(25)	9.5 × 10^-7	[11]
2.640 905 81(19)	7.2 × 10^-8	[12]
2.640 906 190 9(77)	2.9 × 10^-9	[7]
2.640 906 184 6(13)	4.9 × 10^-10	This work

Figure 1. Signal spectra from ^{6}Li and ^{7}Li nuclei, simultaneously accumulated and results comparison table

Figure 1 shows typical paired spectra obtained from ^{6}Li and ^{7}Li nuclei and which were used to calculate the averaged data (bottom row of table 1). The table above shows that interest in a more accurate determination of the magnetic moments of nuclei ^{6}Li and ^{7}Li lasts from 1968 to 2018. In the regime of simultaneous recording of the resonance frequencies of the ^{6}Li and ^{7}Li nuclei, we did not notice the dependence of the ratio $f(^{7}Li)/f(^{6}Li)$ on the temperature and concentration of the solution. This once again confirms that the difference $\sigma(^{7}Li) - \sigma(^{6}Li)$ can affect the result in no more than the ninth digit.

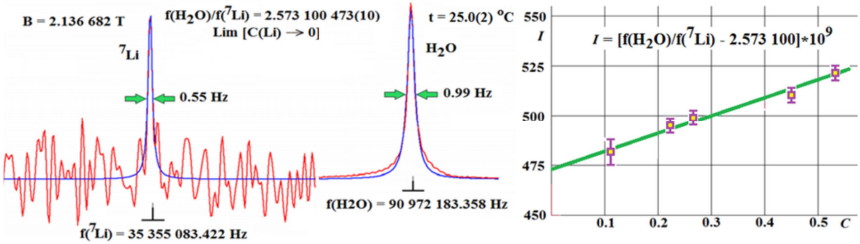

Figure 2. A typical pair of spectra obtained from protons of water and ^{7}Li nuclei and a graph for determining the ratio of resonance frequencies for the endless dissolution of LiOHH_2O salt in water: along the horizontal axis is the salt concentration in g/100 g (H_2O)*

However, the signal from the protons (deuterons) of water substantially depends on temperature. The technique we used allowed us to reduce the error due to the control of the sample temperature with an error of +/- 0.2 °C.

Results and Discussion

The formula (1,2) and new experimental results: $f(^{7}Li)/f(^{6}Li) = 2.640\ 906\ 1846(13)$ and $f(H_2O)/f(^{7}Li)_{C\to 0} = 2.573\ 100\ 473(10)$ for 25.0 °C; allow us to calculate the magnetic moments of ^{6}Li and ^{7}Li nuclei in units of nuclear magneton's:

$$\mu(^{6}Li) = 0.822\ 0454(25)\ \mu_N \text{ and } \mu(^{7}Li) = 3.256\ 4171(98)\ \mu_N \quad (3)$$

These data are in good agreement with the data of previous experimental studies [7]. Unfortunately, it is not possible to implement fully more accurate measurements in this case. The total error is determined by the uncertainty of calculating the screening of lithium ions in water [6]: $\sigma(^{7}Li) = 90.89\ (300) \times 10^{-6}$.

If we confine ourselves to only the lightest nuclei, then a comparison of the experimental data on their magnetic and quadrupole moments will allow us to unambiguously represent

the structure of these nuclei, but only in a first approximation. In particular, the magnetic and quadrupole moments of ^{6}Li and ^{7}Li nuclei unambiguously indicate that the structure of these nuclei mainly consists of two clusters. Moreover, the central cluster is the ^{4}He nucleus (spinless α-particle as the most stable nucleus of four nucleons), and the second cluster is either the deuterium nucleus [$\mu(^{2}D) = 0.8574382311(48)\ \mu_N$] or the tritium nucleus [$\mu(^{3}T) = 2.978962460(14)\ \mu_N$]. The intensity of interaction of these two clusters provides an orbital contribution to the magnetic (3) and quadrupole moment. However, the interaction of the two clusters is so limited that it allows the light cluster to retain mainly its magnetic (and quadrupole) characteristics. The positive quadrupole moment of the light cluster (deuteron) minimizes the contribution of the negative orbital quadrupole moment to lithium-6 nuclei.

The theoretical work [13] presents the results of calculations of these constants: $\mu(^{6}Li)_{theor} = 0.832\ \mu_N$ and $\mu(^{7}Li)_{theor} = 3.036\ \mu_N$. As you can see, the deviation from the experimental result is: +1.6 % for lithium-6 and -7.3 % for lithium-7 nuclei.

References

1. Yu. I. Neronov, Aleksandrov V.S.; «Measurement of the nuclear magnetic moment of tritium to nine-digit accuracy»; JETP Letters. V. 94. № 6. pp. 418-421 (2011).
2. S.G. Karshenboim, Ivanov V.G., Neronov Yu. I., et. al.; «A new determination of the proton-to-deuteron ratio of magnetic moments» Canadian Journal of Physics, V. 83. № 4. pp. 405-412 (2005).
3. A.A. Anselm, Neronov Yu. I.; «Restrictions on the existence of spin-spin coupling of nonelectromagnetic origin in experiments on the measurement of the gyromagnetic ratios of the proton and deuteron». Soviet Physics - JETP. V. 61. № 6. pp. 1946-1949 (1985).
4. Yu. I. Neronov, Seregin N.N.; «High-precision evaluation of the magnetic moment of the helion», JETP. V. 115. № 5. pp. 777-781 (2012).
5. Yu. I. Neronov, Seregin N.N.; «Precision determination of the difference in shielding by protons in water and hydrogen and an estimate of the absolute shielding by protons in water». Metrologia.V. 51. № 1. pp. 54-60 (2014).
6. A. Antušek; Kedziera D.; Kaczmarek-Kedziera A.; M. Jaszunski; Chem. Phys. Lett. V.532, pp. 1–8 (2012).
7. W. Makulski; Magnetochemistry, V. 4, pp. 9, (2018).
8. Yu. I. Neronov, «Determination of the temperature dependence of the shielding of water protons and a method for estimating the temperature of living tissues»; Measurement Techniques.V. 60. № 1. pp. 96-102. (2017).
9. O. Lutz, Nanurforsdi, V. 23 a, pp. 1202-1209 (1968).
10. A. Beckmann, et. al., Z. Physik V. 270, pp. 173-189 (1974).
11. D. Borremans, et. al., Phys. Rev. V. C72, 044309 (2005).
12. R. Harris, et. al., Pure Appl. Chem., V. 80, pp. 59-84 (2008).
13. Cockrell, R.C. Ab Initio Nuclear Structure Calculations for Light Nuclei,Ph. D Thesis, Iowa State University, Ames, IA, USA, 30 January (2012).

NMR spectra of potassium-39 nuclei in aqueous solutions and determination of the magnetic moment of the ^{39}K nucleus

Yu. I. Neronov, A. N. Pronin, N. N. Seregin

D. I. Mendeleev All-Russian Research Institute of Metrology,
190005 Saint Petersburg, Russia
E-mail: yineronov@mail.ru

Introduction

Potassium ions are of particular importance for the functioning of living organisms. The features of the passage of potassium ions through the cell membrane ensure the presence of a negative potential inside the cell and this potential allows you to realize the most important mechanisms of cellular life. The precision estimation of the magnetic moment of the potassium nucleus $\mu(^{39}K)$ allows for the formation of a scale of chemical shifts, which is of interest for the development of local spectral studies on $^{39}K^+$ nuclei in the tissues of a living organism using medical MR tomographs. Estimates of the chemical shift, concentration, and relaxation properties of intracellular and extracellular $^{39}K^+$ ions provide valuable information about the norm and pathology of living body tissues.

The frequency of the NMR signal from the $^{39}K^+$ ions of an aqueous solution can be used for the precision determination of $\mu(^{39}K)$, if the field is determined with the required high accuracy. The precision estimation of the magnetic field is also determined by recording the frequency of the NMR signal, and from water protons and using the fundamental physical constants [1]: μ_p – the magnetic moment of the proton and $\sigma(H_2O)$ – the proton shielding in water [2].

$$\mu(^{39}K) = \mu_p \times [f(^{39}K)/f(H_2O)] \times [I(^{39}K)/I_p] \times \{[1 - \sigma(H_2O)]/[1 - \sigma(^{39}K^+)]\}, \quad (1)$$

where the ratio of nuclear spins is a strictly quantized quantity: $I(^{39}K)/Ip = 3$; $f(^{39}K)/f(H_2O)$ is the ratio of the resonance frequencies at extremely low concentrations of potassium salts in water; s $\sigma(^{39}K^+)$ is the shielding of potassium nuclei. If you accumulate the signals from the protons of water and potassium ions at the same time, it can significantly minimize random and systematic errors.

In this work, an electromagnet with a field of 2.14 T was used as the instrument basis of the spectrometer, which was previously used [3] to determine the magnetic moment and isotopic shifts of tritium nuclei. At low concentrations of KCl and KNO_3 in water, the signal from protons is three to four orders of magnitude more intense than the signal from $^{39}K^+$ nuclei.

Therefore, the receiving inductance of the spectrometer with the maximum Q-factor was used for the frequency $f(^{39}K) \approx 4.244$ MHz, which contained 40 turns for the greatest gain of the weaker signal. The signal from the protons $f_p \approx 90.97$ MHz was recorded by the same receiving inductance as the signals from $^{39}K^+$. For this purpose, the matching module used an additional small inductance, which contained three turns.

The spectrometer used the AD9958 integrated circuit (a two-channel frequency synthesizer) to generate two reference frequencies close to the resonant frequencies of the studied pair of dissimilar nuclei: f_{op}=90 973 815.92 Hz; f_{oK}=4 244 461.06 Hz. The magnetic field of the spectrometer was equal to $B \approx 2.136\ 753$ T, at which the resonant frequencies of protons and potassium nuclei Δf_p and $\Delta f(^{39}K^+)$ registered after amplification and conversion exceeded the reference frequencies f_{op} and f_{oK} by several hundred Hertz (Fig. 1).

When accumulating a paired numerical array containing the Δf_p and Δf_{oK} frequencies ($^{39}K^+$), the free precession signals from protons and from ^{39}K nuclei were sequentially summed. The intensity of each signal and its shape were monitored by the operator on the monitor during the accumulation of digital data. Mathematical processing of numeric arrays was performed using the software described in [2, 4].

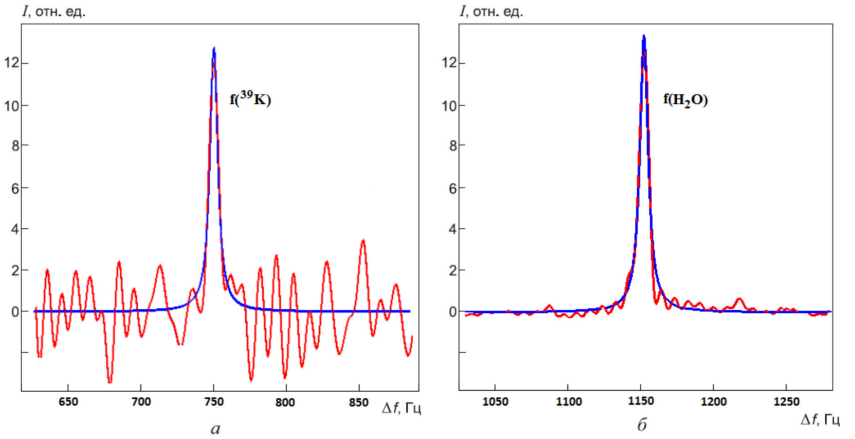

Figure 1. Typical pair spectrum obtained from a 10 mm ampoule with KNO_3 solution in water with simultaneous accumulation of two signals: a-from ^{39}K nuclei and b-from water protons

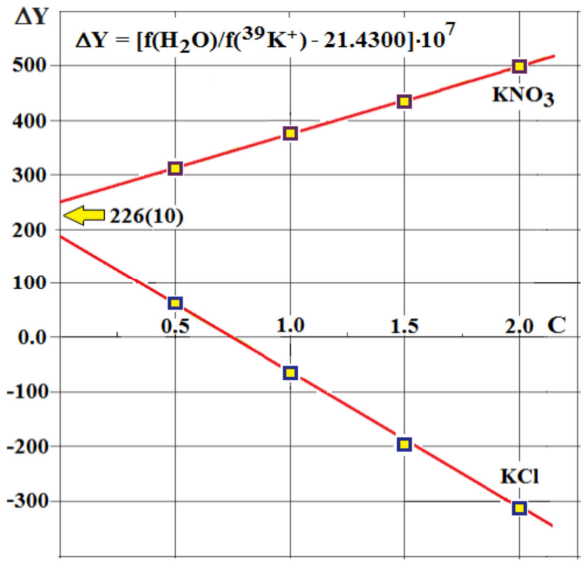

Figure 2. The ratio of the resonance frequency of water protons to the resonance frequency of ^{39}K nuclei, depending on the C – concentration of KCl and KNO_3 in water. Horizontal: C is the concentration of the solution in units of Mol/1 kg of H_2O. Vertical: $\Delta Y = [f(H_2O)/f(^{39}K^+) - 21.4300] \times 10^7$

The following expressions can be used to estimate the resonance frequency of potassium ions:

$$f(^{39}K^+,Cl^-)_{C\to 0} = [\mu(^{39}K)\times B_o/I(^{39}K^+)]\times\{1 - [\sigma(^{39}K^+ + n\times H_2O) - \sigma(Cl^-)_{C\to 0}]\} \quad (2)$$

$$f(^{39}K^{+},NO_3^{-})_{C\to 0} = [\mu(^{39}K)\times B_o/I(^{39}K^{+})]\times\{1 - [\sigma(^{39}K^{+}+n\times H_2O) + \sigma(NO_3^{-})_{C\to 0}]\} \quad (3)$$

where $\sigma(^{39}K^{+}+n\times H_2O)$ – electronic shielding of the nucleus of the ion $^{39}K^{+}$ as internal potassium ion electrons, so the electrons of the water molecules closest associates; n – the number of nearby water molecules; $\sigma(Cl^{-})$ and $\sigma(NO_3^{-})$ – for more averaged shielding of the nucleus of potassium due to the presence of negative ions in the environment. The slopes of the two straight lines (Fig. 2) have different signs and differ twice, respectively, the efficiency of the influence of Cl^{-} and NO_3^{-} ions on the resonance frequency of potassium nuclei differs twice. Given the resulting uncertainty, we can write the equation: $\sigma(NO_3^{-}) = \sigma(Cl^{-})/2$. From this equality and from the solution of the system of equations (2, 3) it follows:

$$[f(H_2O)/f(^{39}K^{+})]_{C\to 0} = 21.4300226(10) \quad (4)$$

The value (4) should be attributed to single $39K^{+}$ ions that are surrounded by water molecules. Expressions (1) and (4) can be applied to determine $\mu(^{39}K)$ based on the fundamental physical constants for pure water [1, 2]. To screen potassium ions, we will use: $\sigma(39K^{+}+n\times H_2O) = (1300.20 \pm 20.0)\times 10^{-6}$ from the work [5]. Then we can calculate: $\mu(^{39}K) = 0.391471(8)/\mu_N$. This result is in good agreement with the data: $\mu(^{39}K) = 0.39147(3)/\mu_N$ of the work [6, 7].

Research for more accurate calculation of the shielding of the ions $\sigma(^{39}K^{+}+n\times H_2O)$ it is hoped will be continued in the direction of assess a more accurate description of the dynamic ion solvation layers by molecular dynamics method and a corresponding calculation of the shielding of the nucleus of an ion based on the approach Hartree – Fock theory and the functional of the total electron density. We present the result of this work without adjusting for the shielding of the potassium ion in water:

$$\mu(^{39}K)\times[1 - \sigma(^{39}K^{+}+n\times H_2O)] = 0.390\ 962\ 111(18)/\mu_N;\ [\ \delta = 4{,}7\times 10^{-8}]; \quad (5)$$

Water is the main component of any complex biological systems. For the study of the norm and pathology of living tissues in NMR spectral studies on potassium nuclei, the value (5) is the most acceptable to use for forming a scale of chemical shifts.

References

1. Mohr P. J., Newell D. B., Taylor B. N.; CODATA recommended values of the fundamental physical constants: 2014; Rev. Mod. Phys., Vol. 88, No. 3, (2016); https://doi:10.1103/RevModPhys.88.035009.
2. Neronov Yu. I., Seregin N.N.; Precision determination of the difference in shielding by protons in water and hydrogen and an estimate of the absolute shielding by protons in water. Metrologia. Vol. 51; № 1; pp. 54-60 (2014); https://doi:10.1088/0026-1394/51/1/54
3. Aleksandrov V.S. and Neronov Yu.I.; Study of the NMR Spectra of Hydrogen Isotopic Analogs and Estimation of the Magnetic Moment of the Triton. JETP Letters, 2011, Vol. 93, No. 6; pp. 305–307; https://doi:10.1134/S0021364011060026.
4. Neronov Yu. I., Simultaneous Determination of the Magnetic Moments of ^{6}Li and ^{7}Li Nuclei Using an NMR Spectrometer; Measurement Techniques, Vol. 63, pp. 667–673 (2020); https://doi.org/10.32446/0368-1025it.2020-9-3-8.
5. Antušek, A.; Kedziera, D.; Kaczmarek-Kedziera, A.; Jaszunski, M.; «Coupled cluster study of NMR shielding of alkali metal ions in water complexes and magnetic moments of alkali metal nuclei». Chem. Phys. Lett. (2012), 532, pp. 1–8; https://doi.org/10.1016/j.cplett.2012.02.03632.
6. CERN, ISOLDE-Collaboration, Nucl. Instrum. Methods Phys. Res. A 325 (1993), pp. 465-474.
7. N.J. Stone; (2014); IAEA Nuclear Data Section; Vienna International Centre; Austria.

Research and development of an information system for optimizing the contrast of a magnetic resonance image

A. V. Nikitina, Yu. V. Bogachev

Department of Physics, Saint-Petersburg Electrotechnical University "LETI",
5, prof. Popov st., Saint-Petersburg, 197376, Russia,
E-mail: nastya_nikitina1996@mail.ru

Introduction

Among the various diagnostic methods of medical imaging, the magnetic resonance imaging (MRI) method is particularly distinguished due to the safety and high information content of the results obtained. For correct diagnosis in MRI, high accuracy and clarity of magnetic resonance (MR) images are required. This means that it is necessary to optimize the parameters of the MRI study to achieve better contrast. Optimizing the contrast of the MR image will improve the quality of the allocated borders of pathological foci when planning operations. Modeling of MR images with different parameters of the scanning mode will allow you to configure these parameters so that the accumulation of a certain paramagnetic substance in the tissue can be detected on the tomogram. This will allow you to diagnose many diseases at an early stage. In this paper, we have developed an information system for optimizing the contrast of MR images, which allows us to model MR images with different parameters of MRI scanning.

Information system

An information system was developed to optimize the contrast of MR images. This system consists of three main blocks. The first block is the database management block. With this block, the user can interact with the data of patients, if they have the appropriate access. The second block is a specialized imaging unit for Dicom Viewer tomograms [1, 2]. Using this block, the user can view and process tomograms without using third-party software for further use in the contrast optimization block. The third block is the contrast optimization block. This unit allows you to select the optimal parameters for a specific MRI study and solves such problems as: selecting the pulse sequence [3-7] and determining its parameters, selecting contrasting agents and determining their desired concentration. In addition, this block allows you to simulate a preliminary MR image with the selected parameters.

A contrast optimization block was developed to evaluate changes in the contrast of the MR image under various conditions and scanning modes. The main window of the developed block is shown in fig. 1.

In this block, the user selects the pulse sequence, sets its parameters, and selects contrast agents. For the set conditions, the block implements preliminary modeling of the MR image for the selected organ, and plots the signal intensity dependence on each parameter of the selected sequence for different concentrations of contrast agents. When you change the parameters in the program, the graphs and the results of the preliminary simulation are dynamically changed. After selecting the optimal parameter values, the user can perform a secondary simulation of the MR image in which the real tomogram will be segmented into areas whose intensity will change depending on the selected conditions.

The developed functionality allows you to select the parameters of MRI research for each specific case.

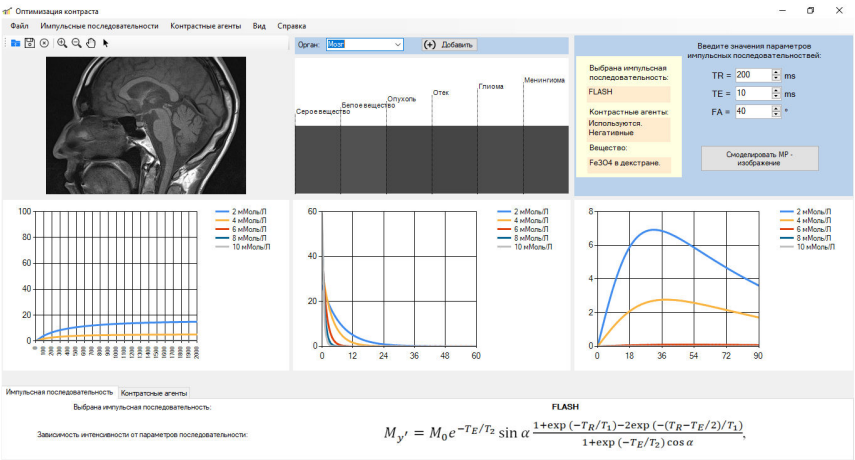

Figure 1. Main window of the contrast optimization block

Conclusion

The information system developed in the framework of this work for optimizing the contrast of MR images has wide functionality and allows you to:

1) speed up the MRI study by pre-optimizing the parameters of radio frequency sequences;

2) evaluate the change in the contrast of tomograms in MRI studies when varying the parameters of the scanning mode and using different contrasting agents;

3) determine the necessary concentration of contrast agents to achieve a certain contrast, which will reduce the harm to the patient's body by minimizing the administered contrast agents.

References

1. D. Haak, C. Page, T. M. Deserno, “A Survey of Dicom Viewer Software to Integrate Clinical Research and Medical Imaging”, J Digit Imaging, 2016, pp. 206–215
2. T. Hacklander, H. Mertens. “Virtual MRI: A PC-based Simulation of a Clinical MR Scanner”, Academic Radiology, vol 12, No 1, January 2005, pp. 85-96.
3. V. Kuperman “Magnetic resonance imaging physical principles and applications”, University of Maryland College Park, Maryland, Academic Press, 2000. 197 p.
4. M. A. Bernstein, K. F. King, X. J. Zhou, “Handbook of MRI Pulse Sequences”, Elsevier Academic Press, 2004, 1017 p.
5. S. Wu, Z. Zhu, Y. Kong, et al. “Assessment of cerebral iron content in patients with Parkinson's disease by the susceptibility-weighted MRI”, Eur Rev Med Pharmacol Sci. 2014; vol. 18, pp. 2605-2613.
6. S. Assis-Hassid, B. J. Grosz, E. Zimlichman, R. Rozenblum, D.W. Bates, “Assessing HER use during hospital morning rounds: A multi-faceted study”, PLoSONE vol. 14(2), 2019.
7. M. Wyss, I. Dobrev, J. H. Sim, et. al “Acoustic noise reduction in MRI based on pulse sequence optimization: Analysis of sound characteristics and impact on sequence parameters”, ESR, Poster No. C-2186, 2018, pp. 1-14.

Nuclear Overhauser effect in determination the geometric configuration of the *N'*-substituted hydrazone methylpyruvate

V. V. Pelipko, R. I. Baichurin, I. S. Adyukov, K. A. Gomonov, S. V. Makarenko

Herzen State Pedagogical University of Russia, Department of Organic Chemistry, Center of collective use at the Faculty of Chemistry "Instrumental methods for the study of nitro compounds, coordination, biologically active substances and nanostructured substances" 48 Moyka River Embankment, Saint Petersburg 191186, Russia
E-mail: kohrgpu@yandex.ru
http://kohrgpu.ru, http://ckpo.herzen.spb.ru/?page=organic-chemistry

Alkyl 3-nitroacrylates are highly active substrates in the *aza*-Michael reaction [1-3]. This opens up perspectives for the preparation of original N'-substituted hydrazones of alkylpyruvates **1** [4].

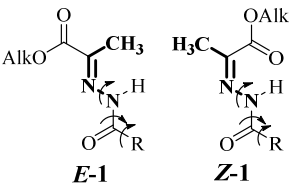

The possibility of existence of compounds **1** in the form of *E*- or *Z*-isomers (C=N bond) and *s-cis*- or *s-trans*-conformational isomers [=N–NH, C(O)–NH, C(O)–R] makes them attractive structures for studying by 1D and 2D NMR spectroscopy methods.

The aim of this work was to study the fine structure of methyl 2-[2-(furan-2-ylcarbonyl) hydrazinylidene]propanoate **2** (Alk = Me, R = furan-2-yl) by NMR spectroscopy including the ^{1}H-^{1}H NOESY experiment.

The presence of one set of signals in the ^{1}H and ^{13}C NMR spectra indicates the existence of hydrazinylidene propanoate **2** as the one configurational isomer (for all the bonds under consideration) in the DMSO-d_6 (Fig. 1).

At the same time, the signals at 6.68-7.95 ppm attract attention, one of which (δ_H 7.60 ppm) appears as a broadened singlet and makes the assignment of the signals of the furan ring protons not so unambiguous (Fig. 1).

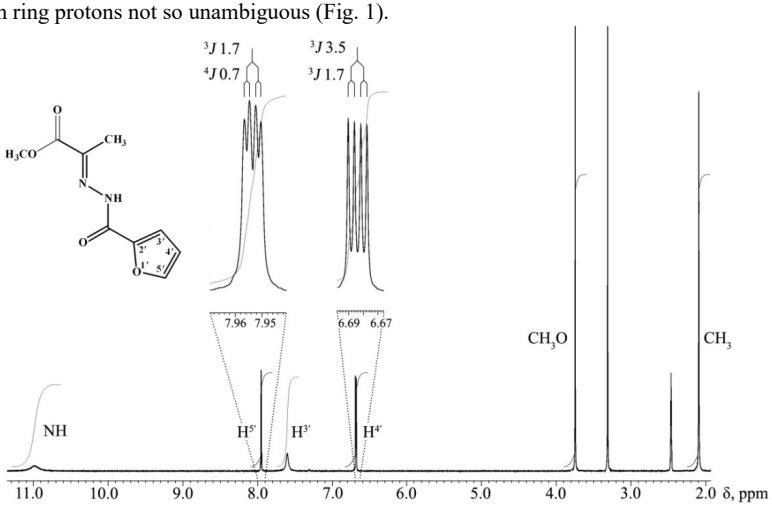

*Figure 1. ^{1}H NMR spectrum of compound **2** (DMSO–d_6)*

According to ^{1}H-^{1}H NOESY experiments obtained with varying mix. time, the NOE correlation [5] in the spectra of compound **2** is demonstrated by the protons of the CH_3 and NH groups, indicating their close position in space, and, consequently, the existence of this compound in a DMSO-d_6 solution in the form of the *E*-isomer (Fig. 2). In addition, the signal of the proton of the NH group forms a cross-peak with the signal at δ_H 7.60 ppm, which allows the latter to be attributed to the proton C$^{3'}$H. The correlations in the ^{1}H-^{1}H NOESY spectrum allows one to assign the *s-trans*-configuration to the =N–NH, C(O)–Fur fragments and the *s-cis*-configuration to the C(O)–NH fragment. An additional confirmation of the *s-cis*-configuration of the C(O)–NH bond is the signal of the C(O) atom at 158 ppm in the ^{13}C NMR spectrum of compound **2**, which is in agreement with the literature data [6-8].

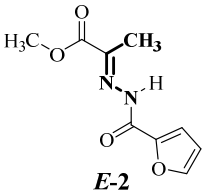

***E*-2**

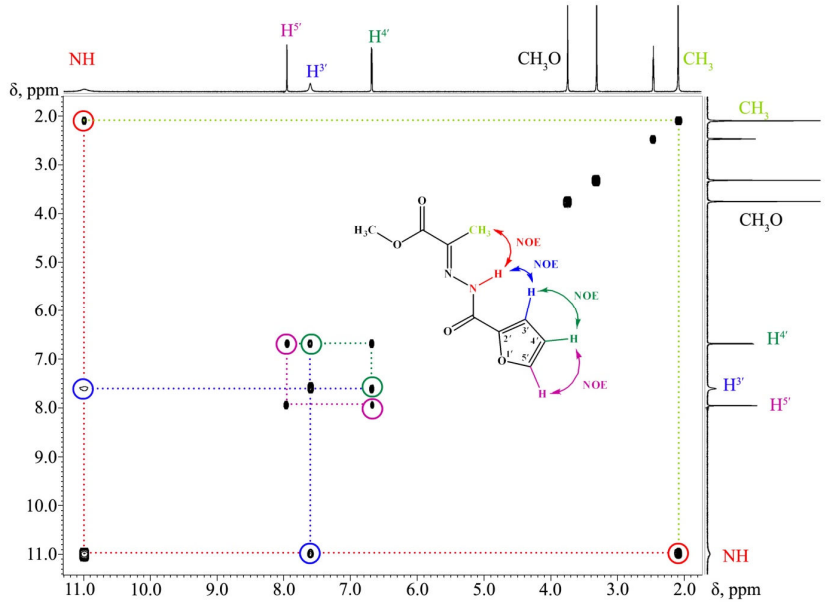

*Figure 2. ^{1}H-^{1}H NOESY spectrum of compound **2** (DMSO–d_6)*

At the same time, the spectrum of ^{1}H-^{1}H NOESY exhibits cross-peaks of the signal of the proton C$^{3'}$H and the singlet at δ_H 6.68 ppm, making it possible to determine its belonging to the proton C$^{4'}$H, while the cross-peak of this signal and the singlet at δ_H 7.95 ppm confirms the belonging of the latter to the proton C$^{5'}$H (Fig. 2).

Signal assignment based on the ^{1}H-^{1}H NOESY spectrum is consistent with the results of ^{1}H-^{1}H dqf-COSY experiments obtained for compound **2** (Fig. 3).

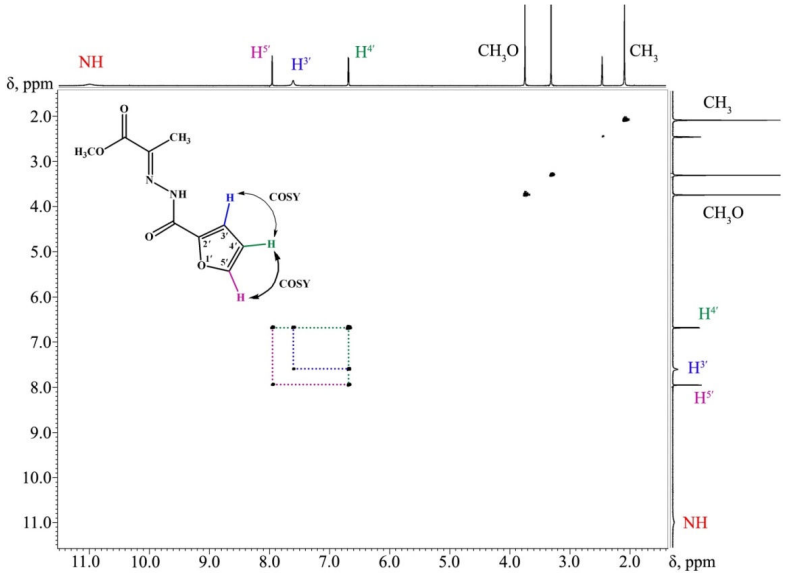

*Figure 3. ^{1}H-^{1}H dqf-COSY spectrum of compound **2** (DMSO–d_6)*

Thus, the fine structure of hydrazinylidene propanoate **2** was determined by ^{1}H-^{1}H NOESY experiment, the *Z*-configuration of the C=N fragment was established, as well as the *s-trans*-configuration of the =N–NH, C(O)–Fur fragments, and the *s-cis*-configuration of the C(O)–NH fragment.

The studies were carried out in the center of collective use at the Faculty of Chemistry of the Herzen State Pedagogical University of Russia on the Jeol ECX-400A spectrometer at 399.78 (^{1}H) and 100.53 (^{13}C) MHz with standard experimental settings. The residual signals of a non-deuterated solvent (for ^{1}H nuclei) or the signals of a deuterated solvent (for ^{13}C nuclei) were used as a standard.

References

1. J. C. Anderson, A. S. Kalogirou, G. J. Tizzard. – *Tetrahedron*, 70, 9337 – 9351 (2014).
2. V. V. Pelipko, I. S. Adyukov, R. I. Baichurin, S. V. Makarenko. – *Rus. J. Gen. Chem.*, 90, 493 – 494 (2020).
3. V. V. Pelipko, R. I. Baichurin, S. V. Makarenko. – *Rus. Chem. Bull.*, 68, 1821-1837 (2019).
4. V. V. Pelipko, I. S. Adyukov, R. I. Baichurin, S. V. Makarenko. – Materialy ochnyh dokladov Mezhdunarodnoj nauchnoj konferencii “Aktual'nye voprosy organicheskoj himii i biotekhnologii”. Ekaterinburg: Izdatel'stvo AMB, 18-21 noyabrya 2020, 408-410.
5. Y. M. Volovenko. Spektroskopiya yadernogo magnitnogo rezonansa dlya himikov. – M.: MBFNP (2011).
6. R. Vaickelioniene, V. Mickevicius. – *Chem. Heterocycl. Compd.*, 42, 753-760 (2006).
7. V. Mickevičius, R. Vaickelionienė, I. Jonuškienė, G. Mikulskienė, K. Kantminienė. – *Monatsh. Chem.*,140, 1513-1522 (2009).
8. K. Anusevičius, I. Jonuškienė, B. Sapijanskaitė, K. Kantminienė, V. Mickevičius. – *Res. Chem. Intermed.*, 42, 6975-6990 (2016).

Mellin-Barnes integral approach for exact evaluation of spin echo signals from fluids with magnetizible grains

M. G. Rudavets

Institute of Problems of Chemical Physics, RAS, Chernogolovka, Moscow region, 142432, Russia

The stimulated echo signals in the proton-carrying fluids with magnetizible grains indicate on the relationship between the echo signals and the internal magnetic field (IMF) correlation function. However, little analytic work reported on the IMF correlator in the random magnetic media prevents interpretation of the experimental data. Herein, we address an explicit relationship between the echo signal from the magnetizible fluids and IMF correlator. The echo signal is represented as the Mellin convolution of the radial and angular functions. Whereas the former involve the radial component of IMF correlator, the angular function comprises the Legendre polynomials of the orders zero, two and four. IMF correlator and the echo signals are evaluated analytically assuming that the magnetizible grains are uniformly dispersed within the spherical cavities of arbitrary radii. When the grains are dispersed in bulk, the analysis allows for incorporation of the correlations between the grains within the Ornstein-Zernike approximation, thus examining the effect of confinement and correlations of the grains on the echo signal. The stimulated echo signals are proved (1) to fall off to the constant value, which is proportional to IMF correlator in the cavity, as the diffusion time proceeds and the echo time is fixed, (2) Have the Gaussian form with respect to the echo time when the diffusion time is fixed. The initial slope of the effective proton propagator along the vertical z-direction, which can be brought out from the data, allows for discrimination whether the grains are free or they correlate. Non-zero slope is characteristic of the correlated grains. The long-range density correlations of the grains result in long rangeness of IMF correlations, which turns out to be inversely proportional to the first power of the spacing between the pair of test points. Finally, the analysis of the calculated spin echo signals under the varied parameters, namely, the radius of the cavity, the average number density, the correlation length of the grains and their diffusivity permits characterization of the spatial and statistical distribution of the grains in the fluids.

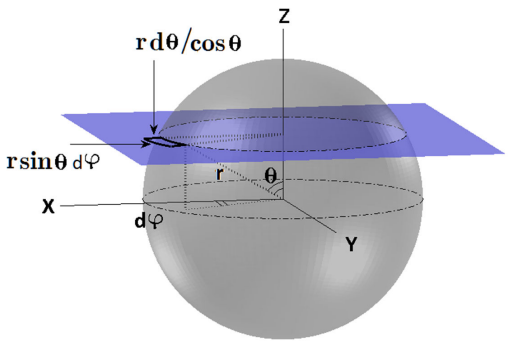

Figure 1. The horizontal plane, which contains the protons contributing to the echo signal $C_{eff}(z,t_d)$*, z-cuts the spherical grain (gray). The differential surface area of the plane reads* $\left(r\sin(\theta)d\varphi\right)\left(rd\theta/\sin\left(\frac{\pi}{2}-\theta\right)\right)$

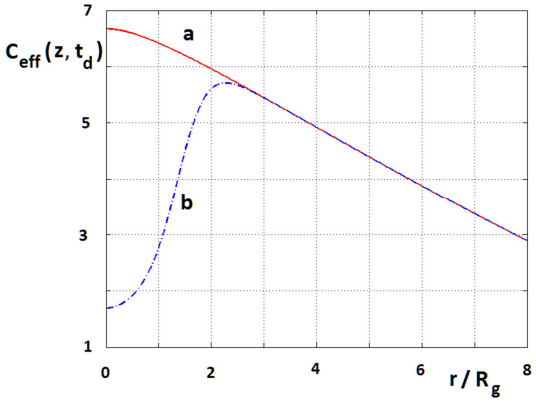

Figure 2. The echo signal, Eq.(...) is shown with respect to the z-coordinate at $t_d = 100$ *ms for the protons that are penetrable (a) and impenetrable (b) into the grains of radius*

References

1. H. Cho and Y.-Q. Song, Phys. Rev. Lett. **100,** 025501 (2008).
2. B. Audoly, P.N. Sen, S. Ryu, and Y. Q. Song, J. Magn. Reson. **164**, 154 (2003).
3. Y.-Q. Song, S. Ryu, and P. N. Sen, Nature (London) **406**,178 (2000).

The spatial structure of SEM1(86-107) peptide in "protein–micelle of dodecylphosphocholine" complex by NMR spectroscopy

Daria A. Sanchugova, Aydar G. Bikmullin, Vladimir V. Klochkov, Dmitriy S. Blokhin

Kazan Federal University, Kremlevskaya Str., 18, 420008 Kazan, Russia
E-mail: dblohin@kpfu.ru

Introduction

About fifteen years ago, in search of sperm factors that modulate HIV infection (the sexually transmitted virus and the causative agent of acquired immunodeficiency syndrome (AIDS)), it was demonstrated that sperm contains amyloid fibrils, which can significantly increase the level of HIV infection [1]. Charged fibrils exacerbate HIV infection neutralizing the characteristic electrostatic repulsion between negatively charged surfaces of HIV virions and target cells, and through direct binding to virions, fibrils simultaneously contribute to the binding of the virus to the cell surface [2]. At present, it is known that sperm amyloid fibrils are formed from small peptide fragments of the proteins PAP (prostatic acid phosphatase), semenogelin 1 (SEM1) and semenogelin 2 (SEM2) [3].

The SEM amyloid precursor protein is two homologous proteins SEM1 and SEM2, which are mainly expressed in the seminal vesicles and form the main component of sperm coagulate. SEM decay rapidly after ejaculation by internal proteases and release a series of short peptide fragments such as SEM1(45–107), SEM2(45–107), SEM1(49–107), SEM2(49–107), SEM1(68–107), SEM2(68–107) and SEM1(86- 107).

The purpose of this job is to investigate, by NMR spectroscopy, the spatial structure of SEM1(86-107) peptide in protein–micelle of dodecylphosphocholine (DPC) complex. DPC micelles were taken as a model of lipid membrane surface [4-6].

Experimental section

Materials

SEM1(86-107) is a peptide of 22 amino acid residues corresponding to 86-107 amino acid residues of the human semenogelin 1 protein. Amino acid sequence of SEM1(86-107) peptide: DLNALHKTTKSQRHLGGSQQLL. The peptide was obtained by solid-phase synthesis by the method described in article Kamalov et.al. [7].

Dodecylphosphocholine for preparation of micelles was purchased from SigmaeAldrich (Milwaukee, WI).

Methods

1D ^{1}H and 2D ^{1}H-^{1}H NMR spectra of SEM1(86-107) (0.9 mM) in aqua solution (H_2O+D_2O/ 90%+10%) with micelle of dodecylphosphocholine (DPC) were carried out on NMR spectrometer 700 MHz (Bruker, AVANCE III-700) equipped with a quadruple resonance (^{1}H, ^{13}C, ^{15}N, ^{31}P) CryoProbe at the temperature 298 K. Data processing was performed using the Bruker Topspin 3.6 software. All spectra were analyzed using the programs NMRFAM-SPARKY [8]. Assignments of hydrogen chemical shifts was made using 2D ^{1}H-^{1}H TOCSY (Total correlation spectroscopy) and 2D ^{1}H-^{1}H ROESY (Rotating frame Overhauser Effect SpectroscopY) [9]. No changes in the ^{1}H NMR spectra of the SEM1(86-107) peptide were observed during all NMR experiments. Based on this, we can suppose that no structural changes of the peptide occurred.

The calculation of the spatial structure was performed using the XPLOR-NIH program [10]. The calculated SEM1(86-107) internuclear distances from 2D ^{1}H-^{1}H ROESY

spectra were used as input parameters. 9 structures with the lowest energies were chosen out of the 1000 calculated structures.

Results and discussions

Assignment of ^{1}H NMR signals was performed using 2D ^{1}H-^{1}H TOCSY and 2D ^{1}H-^{1}H ROESY NMR spectra. The obtained hydrogen chemical shifts of various amino acid residues were compared with the data from the literature [11].

Analyzing ROESY spectrum allowed one to obtain the internuclear distances SEM1(86-107) in "protein–micelle of dodecylphosphocholine" complex. 120 internuclear distances were determined, among which 87 distances within amino acid residues and 33 distances between protons of spatially close amino acid residues (10 distances between protons of NH groups of adjacent amino acid residues, 13 distances between protons of HA and NH groups of adjacent amino acid residues, and 10 distances between protons of other groups).

The estimated internuclear distances of the SEM1(86-107) were used as input parameters for peptide spatial structure calculation using the XPLOR-NH program. Fig. 1A shows an ensemble of 9 SEM1(86-107) structures aligned according to the first part (the backbone (bb) RMSD for Leu87-Lys96: 0.37 ± 0.13 Å).

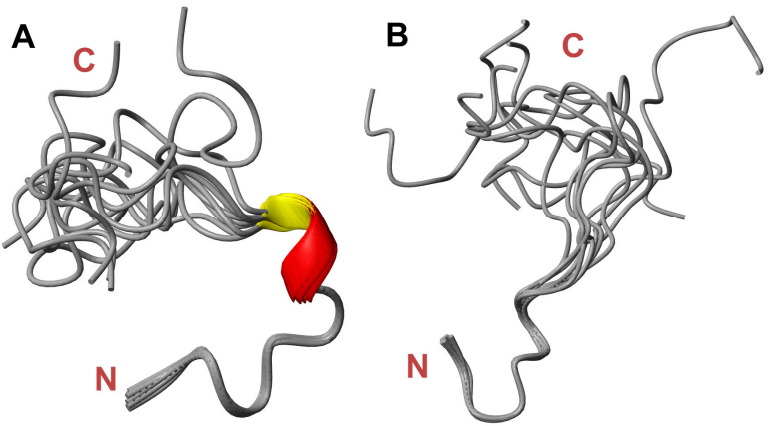

Figure 1. The spatial structure of SEM1(86-107) peptide:A) in "protein–micelle of dodecylphosphocholine", B) in aqua solution, shown as an ensemble of 9 structures

Earlier, we determined the spatial structure of SEM1(86-107) peptide in aqua solution (Fig. 1B) [12]. If we compare the structures, it can be noted that the N-domains of the peptides have good convergence in the ensemble (bb RMSD Leu87-Lys92: for SEM1(86-107) 0.26 ± 0.10 Å; for SEM1(86-107)+DPC 0.18 ± 0.06 Å), in contrast to the C-domain. Both peptides (Fig. 1) are unordered, but SEM1(86-107) with micelle of dodecylphosphocholine has a 3_{10}-helix (Thr94-Ser96). We assume that the presence of DPC micelles as a model of the lipid membrane surface leads to the appearance of a helical region. An increase in the number of helical regions was also observed for PAP(248-286) peptide when studied with lipid membrane models [13].

Based on the above, it can be assumed that when studying semen amyloid peptides, one cannot ignore the effect of lipid membranes on the spatial structure of peptides.

Acknowledgements

This work is supported by the Russian Science Foundation (D.S. Blokhin, project no. 20-73-10034).

References

1. P. Rusert, et al., Quantification of infectious HIV-1 plasma viral load using a boosted in vitro infection protocol. Virology, 2004, Vol. 326(1), P. 113-129.
2. N. R. Roan., et al., The cationic properties of SEVI underlie its ability to enhance human immunodeficiency virus infection. Journal of virology, 2009, Vol. 83, P. 73-80.
3. N. R. Roan, et al., Peptides released by physiological cleavage of semen coagulum proteins form amyloids that enhance HIV infection. Cell Host Microbe, 2011, Vol. 10, P. 541–550.
4. E.Schrank, G. E. Wagner, K. Zangger, Solution NMR Studies of the Orientation of Membrane-Bound Peptides and Proteins by Paramagnetic Probes. Molecules, 2013, Vol. 18, P. 7407-7435.
5. D. E. Warschawski, et al., Choosing membrane mimetics for NMR structural studies of transmembrane proteins. Biochimica et Biophysica Acta, 2011, Vol. 1808, P. 1957-1974.
6. V. Beswick, et al., Dodecylphosphocholine micelles as a membrane-like environment: new results from NMR relaxation and paramagnetic relaxation enhancement analysis. European Biophysics Journal, 1998, Vol. 28(1), P. 48-58.
7. M. I. Kamalov, et al., Syntesis and Characterization of Polyaspartic Acid-Histidine Conjugate as an Analog of Antioxidant Enzymes. Applied Biochemistry and Microbiology, 2019, Vol. 55, P. 474-481.
8. W. Lee, M. Tonelli, J. L. Markley, NMRFAM-SPARKY: enhanced software for biomolecular NMR spectroscopy. Bioinformatics, 2015, Vol. 31(8), P. 1325-1327. https://doi.org/10.1093/bioinformatics/btu830
9. G. S. Rule, T. K. Hitchens, Fundamentals of Protein NMR Spectroscopy. Springer, 2006.
10. C. D. Schwieters, J. J. Kuszewski, G. M. Clore, The Xplor-NIH NMR molecular structure determination package. Journal of Magnetic Resonance, 2003, Vol. 160, P. 65-73. https://doi.org/10.1016/s1090-7807(02)00014-9
11. K. Wuthrich, NMR of proteins and nucleic acids. New York: Wiley-VCH, 1986.
12. D. Sanchugova, et al., The Structure of Fibril-Forming SEM1(86-107) Peptide Increasing the HIV Infectivity. BioNanoScience, 2021. DOI: 10.1007/s12668-020-00822-1
13. Y. H. Lee, A. Ramamoorthy, Semen–derived amyloidogenic peptides – Key players of HIV infection. Protein science, 2018, Vol. 27, P. 1151-1165. DOI: 10.1002/pro.3395.

Optimization of parameters for molecular dynamics modeling of ionic liquid [BMIM][SCN]

A. A. Selivanov, A. V. Ievlev, A. V. Komolkin

Department of Nuclear Physics Research Methods, Saint Petersburg State University, 199034, 7/9 Universitetskaya nab., Saint Petersburg, Russia
E-mail: st068986@student.spbu.ru

Introduction

Recently, ionic liquids (IL) have been increasingly used as components of polymer electrolytes for new current sources. They have several advantages, such as low flammability, low vapor pressure, wide space of thermal, chemical and electrochemical stability, which make it possible to produce more environmentally friendly current sources on the basis of IL.

One of the newest methods of studying IL is Molecular Dynamics Modelling (MDM). This method belongs to a class of computer experiments [1]. It allows observing the behavior of molecules of a substance in liquid phases, their displacements, relative position, conformations, etc. MDM also allows determining the physico-chemical properties of the investigated substances, which can afterwards be compared with a real experiment.

The purpose of this work is to study IL [BMIM][SCN] with the MDM. This IL was selected, because an experimental work was provided to study its physico-chemical properties [2]. The simulation is carried out in GROMACS 2019.4 software package.

Experimental section

To solve this problem models of $BMIM^+$ and SCN^- ions should be built with Jmol or GaussView software package.

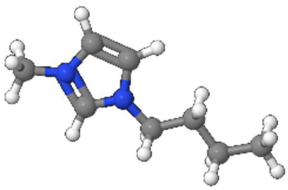

Figure 1. Cation $[BMIM]^+$

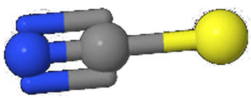

Figure 2. Anion $[SCN]^-$

Then, using the Automated Topology Builder (ATB) service, individual topology files (.itp) were obtained. As we studied these IL in our previous work [3], we decided to optimize our system using Gaussian software package. In this case we have got new charges for every atom for studied IL, since the distribution of charges should strongly influence the physicochemical properties of the modeled molecule, as shown here [4]. Then, we decided to make three different system with different charges: system 1 – system with optimized charges; system 2 – reduce molecules charge by 0,1; system 3 – reduce molecules charge by 0,2.

For the MDM calculation of our system, the following parameters were selected:

- 1000 molecules of IL
- Simulation time – 10 ns
- Simulation step – 2 fs
- Simulation Method: Leap-frog
- NVT ensemble
- Thermostat: Nose – Hoover
- Temperature – 400 K, Initial pressure – 1 atm.
- Force Field – Gromos-54A7

Further, the first 5 nanoseconds were calculated in the NpT ensemble with speed generation according to Maxwell distribution for each system. In these simulations we used V-rescale thermostat and The Berendesen's barostat. The purpose of this calculation is to get our

system “mixed up” and to achieve a certain state of equilibrium from which we could make a “productive” calculation.

After that, the NVT ensemble was set up with Nose-Hoover thermostat and next 10 ns were calculated. NVT ensemble makes it possible to determine dynamic characteristics more accurate, for example, diffusion coefficient.

Density of a box is one of parameters which can prove that the simulation has been provided correctly. It can be obtained by command *gmx density*. For each system we got different densities which are shown in the Fig. 3.

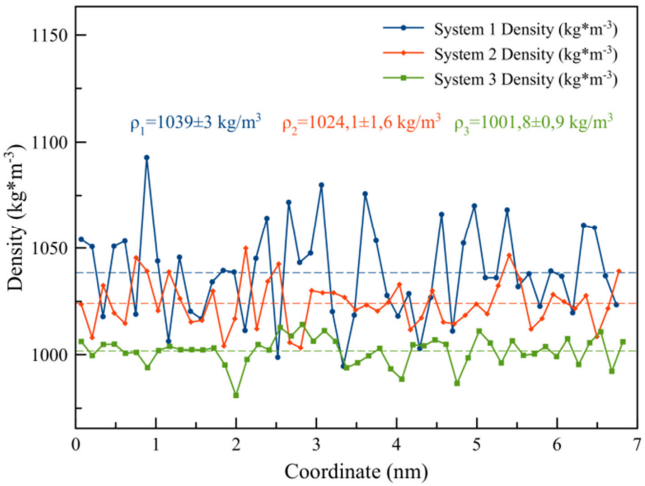

Figure 3. Dependence of the system density on the coordinate for 3 systems

In our previous work [3], the average density of the system was $\rho_{av} = 1079 \pm 9 \frac{kg}{m^3}$. This value was quite close to the experimentally obtained one, which, according to [5], is 1069.7 $\frac{kg}{m^3}$ under normal conditions. In the newest investigation we have following average densities:

$$\rho_1 = 1039 \pm 3 \frac{kg}{m^3};\ \rho_2 = 1024{,}1 \pm 1{,}6 \frac{kg}{m^3};\ \rho_3 = 1001{,}8 \pm 0{,}9 \frac{kg}{m^3}$$

As can be seen, none of the parameters is close to the real one, because experiment took place at 400 K.

To discuss the mobility of molecules, one should determine Mean Square Displacement (MSD) for each ion in each system. The command *gmx msd* can provide it.

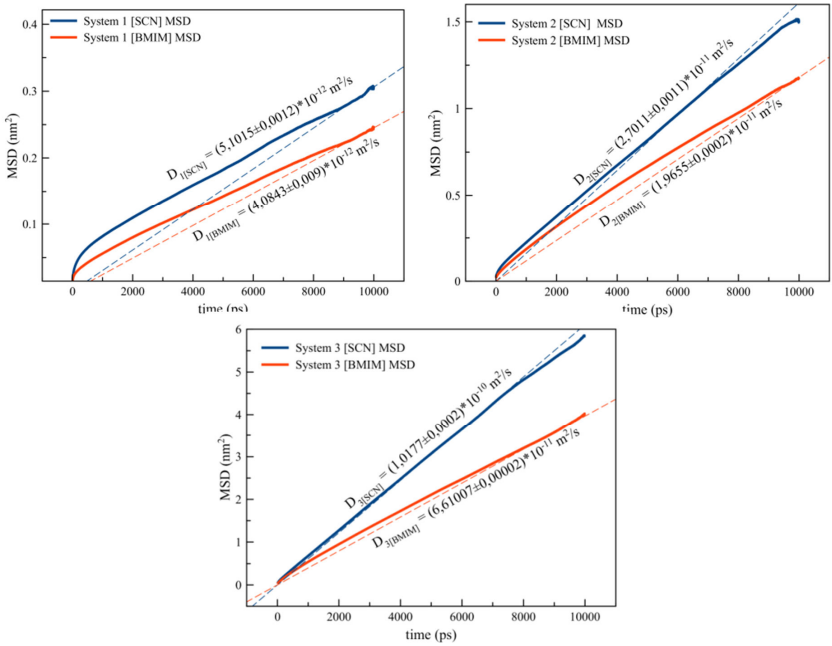

Figure 4. Dependence of the MSD on the time in three systems

Using the Einstein's equality, $D = \lim_{t\to\infty} \langle \|\boldsymbol{r}_i(t) - \boldsymbol{r}_i(0)\|^2 \rangle = 6D_i t$, diffusion coefficients for $BMIM^+$ cation and SCN^- anion can be obtained as in [6]:

Table 1

.	System 1	System 2	System 3
$\mathbf{D_{BMIM}, 10^{-11}\ m^2/s}$	0,40843 ± 0,0009	1,9655 ± 0,0002	6,6101 ± 0,0002
$\mathbf{D_{SCN}, 10^{-11}\ m^2/s}$	0,51015 ± 0,00012	2,7011 ± 0,0011	10,177 ± 0,002

Comparing obtained coefficients with similar ones, which were obtained by NMR-diffometry experiment at temperature 348 K, one can see that diffusion coefficients for 3 are close to real ones:

$$D_{BMIM} = 2{,}39 * 10^{-10}\ \frac{m^2}{s}$$

$$D_{SCN} = 2{,}55 * 10^{-10}\frac{m^2}{s}$$

We don't have information about diffusion coefficients at the temperature of 400 K. The more correct way to compare diffusion of the system is to plot the temperature dependence, which will be provided in our subsequent work.

Acknowledgment

Scientific researches were performed at the "Computing Centre" of Research park of St. Petersburg State University.

References

1. Комолкин А.В., Шеляпина М.Г. Метод молекулярной динамики: Учеб.-метод. пособие — Спб.: Изд-во «Соло», 2007. - 72с., ил.
2. O. Cabeza et al, Synthesis, Microstructure and Volumetry of Novel Metal Thiocyanate Ionic Liquids with BMIM Cation. J. Mol. Liq. 283 (2019) 638-651.
3. Selivanov, A. A., Ievlev, A. V. *Molecular dynamics modeling of ionic liquid [BMIM][SCN].*
4. Yan, T., Burnham, C. J., Del Pópolo, M. G., & Voth, G. A. (2004). Molecular dynamics simulation of ionic liquids: The effect of electronic polarizability. *Journal of Physical Chemistry B*, *108*(32), 11877–11881.
5. Density and Viscosity of Binary Mixtures of Thiocyanate Ionic Liquids + Water as a Function of Temperature, U.Domanska and M.Krolikowska, J Solution Chem. 2012 Sep; 41(8) 1422-1445
6. Khusnutdinova N. R., Markelov D. A. Modeling the system of the carbosilane dendrimer of various generations. 2020. 93–95 p.

The application of nuclear magnetic resonance spectroscopy to the calculation of lignin structure formulas

S. L. Shestakov, Yu. A. Popova, A. Yu. Kozhevnikov

Northern (Arctic) federal university named after M.V. Lomonosov, Severnaya Dvina Emb. 17, Arkhangelsk, Russia; 163002
E-mail: yuliya.popova01@mail.ru

Lignin, in addition to cellulose, is one of the most abundant biopolymers. The abundance of lignin allows its wide industrial using, however, the practical application of lignins and their derivatives are limited because of their complex, branched and randomly crosslinked structure. The determination of lignin structure is one of the actual problems of wood chemistry [1, 2].

According to modern researches and concepts, the main components of lignin are p-coumaryl alcohol, coniferyl alcohol and sinapyl alcohol, based on phenylpropane structure and called monolignols. As a result of combinatorial free radical binding reactions, monolignols transform to p-hydroxyphenyl (H), guaiacyl (G) and syringyl (S) phenylpropane units, and lignin condenses because of generation of different bonds between them (*β*-O-4′, *α*-O-4′, *β*-5′, *β*-1′, 5-5′, 4-O-5′, *β*-*β*′ etc.) [3, 4]. The main tasks in determination of lignin structure are calculations of phenylpropane (C_9) unit elemental composition and amount of bonds of different types between them. The structure of lignin varies depending on the species of wood, the place of growth of the plant and a number of other factors.

The purpose of this research is the determination of semi-empirical formulas of phenylpropane (C_9) units of lignins isolated from different hardwood species. The first stage of the calculation is the determination of the quantitative composition of the elements and is the definition of molecular weight. The elemental composition and distribution of molecular weights of dioxane lignins of selected species are represented in Table 1. The elemental composition was determined using the EuroVector EuroEA-3000 elemental analyzer (CHNS). The molecular weights of the isolated lignins and the degree of their polydispersity were determined by gel permeation chromatography using the LC 20 Prominence HPLC system.

Table 1. Elemental analysis and distribution of molecular weight of hardwood lignins

Family	Sample	Elemental composition, %					Molecular weight, g/mol		
		N	S	C	H	O	M_w	M_n	Mw/Mn
Betulaceae	**Birch**	0	0	59,7	7,8	32,5	4900	2400	2,1
	Hornbeam	0	0	61,1	7,8	31,1	5200	3000	1,8
	Alder	0	0	64,1	8,2	27,7	5800	1800	3,2
Fagaceae	**Oak**	0	0	58,9	7,8	33,3	5700	2100	2,7
	Chestnut	0	0	57,4	7,5	35,1	4400	1300	3,5

The second stage is the calculate hydroxyl and methoxyl groups. The content of hydroxyl and methoxyl groups of lignin was determined with ^{31}P-NMR and ^{13}C-NMR spectroscopy, respectively. NMR spectra were recorded using pulse Bruker AVANCE III NMR spectrometer with an operating frequency for protons of 600MHz equipped with a BBO 600 MHz S3 dual-channel high-resolution broadband sensor. ^{31}P-NMR spectra were registered after phosphitylation of the lignin samples with the special agent 2-chloro-4,4,5,5-tetramethyl-1,3,2-dioxophospholane (TMDP), this method is described in [5]. The internal standards, used for calculation of functional groups content, were endo-N-hydroxy-5-norbornene-2,3-dicarboximide (e-HNDI) for ^{31}P-NMR and trioxane for ^{13}C-NMR. The results of calculations of the content of hydroxyl groups of various types and methoxyl groups in the studied samples are represented in Table 2.

The third stage is combining the obtained data and calculating the structural formula. The analysis of the elemental composition, molecular weight and functional groups allows obtaining the empirical formula of lignins (Table 3). The calculation of the composition of the C_9 unit was carried out according to Zakis, 1987 [6].

Table 2. The content of functional groups of hardwood lignins, mmol/g

Family	Sample	Functional groups					OCH_3
		Aliph	S	G	H	COOH	
Betulaceae	**Birch**	4,74	0,86	0,4	0,03	0,07	6,22
	Hornbeam	3,96	1,11	0,44	0,09	0,1	5,76
	Alder	4,93	0,75	0,64	0,07	0,08	5,85
Fagaceae	**Oak**	4,58	0,84	0,64	-	0,07	3,93
	Chestnut	3,74	0,74	0,49	0,06	0,06	3,1

Table 3. Elemental composition of average C9 unit of hardwood lignins

Family	Sample	Empirical formula	Detailed structural formula of C_9 unit
Betulaceae	**Birch**	$C_{4,35}H_{5,87}O_{1,41}(OCH_3)_{0,62}$	$C_9H_{10,87}O_{1,61}(OCH_3)_{1,29}(OH_{Ph})_{0,32}(OH_{Al})_{0,98}(OOH_{COOH})_{0,006}$
	Hornbeam	$C_{4,51}H_{6,01}O_{1,37}(OCH_3)_{0,58}$	$C_9H_{10,83}O_{1,55}(OCH_3)_{1,15}(OH_{Ph})_{0,38}(OH_{Al})_{0,79}(OOH_{COOH})_{0,008}$
	Alder	$C_{4,75}H_{6,39}O_{1,15}(OCH_3)_{0,58}$	$C_9H_{10,85}O_{0,91}(OCH_3)_{1,10}(OH_{Ph})_{0,32}(OH_{Al})_{0,93}(OOH_{COOH})_{0,006}$
Fagaceae	**Oak**	$C_{4,51}H_{6,56}O_{1,69}(OCH_3)_{0,39}$	$C_9H_{11,79}O_{2,06}(OCH_3)_{0,78}(OH_{Ph})_{0,38}(OH_{Al})_{0,91}(OOH_{COOH})_{0,005}$
	Chestnut	$C_{4,47}H_{6,51}O_{1,88}(OCH_3)_{0,31}$	$C_9H_{12,00}O_{2,67}(OCH_3)_{0,62}(OH_{Ph})_{0,36}(OH_{Al})_{0,75}(OOH_{COOH})_{0,005}$

We can conclude that NMR spectroscopy allows obtaining the data of chemical composition and structure of lignin fragments. Data obtained by NMR spectroscopy can be used for calculation of chemical semi-empirical formulas of phenylpropane units, which are the main component of lignin. Knowledge about the chemical composition of C_9 units. We used auxiliary methods and one-dimensional nuclear magnetic resonance spectroscopy; we have shown a method for calculating the structural link of the most complex plant polymer – lignin.

Acknowledgements

This work was performed using the instrumentation of Core Facility Center «Arktika» of Northern (Arctic) Federal University under support of the Ministry of education. The reported study was funded by Russian Foundation for Basic Research (RFBR), project number 20-33-90126.

References

1. Schutyser, W.; Renders, T.; Van den Bosch, S.; Koelewijn, S.F.; Beckham, G.T.; Sels, B.F. Chemicals from lignin: An interplay of lignocellulose fractionation, depolymerisation, and upgrading. Chem. Soc. Rev. 2018, 47, 852–908.
2. Doherty, W.O.S.; Mousavioun, P.; Fellows, C.M. Value-adding to cellulosic ethanol: Lignin polymers. Ind. Crops Prod. 2011, 33, 259–276.
3. Ralph, J. Lignins: natural polymers from oxidative coupling of 4-hydroxyphenyl-propanoids / J. Ralph, K. Lundquist, G. Brunow, F. Lu // Phytochemistry Reviews. – 2004. – Vol. 3, N 1-2. – P. 29 – 60.
4. Monteil-Rivera, F. Isolation and characterization of herbaceous lignins for applications in biomaterials / F. Monteil-Rivera, M. Phuong, M. Ye, A. Halasz, J. Hawari // Industrial Crops and Products. – 2013. – Vol. 41. – P. 356 – 364.

5. Shestakov, S.L., Kosyakov, D.S., Kozhevnikov, A.Yu., Ulyanovskiy, N.V., Popova, Yu.A. / The elaboration of NMR analysis of different types of hydroxyl groups in the lignin samples // 2017. Khimiya Rastitel'nogo Syr'ya – 2017. – № 2. – P. 81 – 88.
6. G.F. Zakis, Functional Analysis of Lignins and Their Derivatives, Zinatne, Riga, 1987.

NMR study of structure and inner motion types of $ZnZrF_6 \cdot 6H_2O$ and its dehydration products

Arseny B. Slobodyuk, Nina A. Didenko

Institute of chemistry, FEB RAS, 159, Pr. Stoletiya Vladivostoka, 159, Vladivostok, Russia
E-mail: ampy@ich.dvo.ru

Introduction

To date, structural data have been obtained for a number of crystal hydrates of hexafluoride zirconates with divalent cations ($NiZrF_6 \cdot 6H_2O$, $CuZrF_6 \cdot 4H_2O$, $MnZrF_6 \cdot 5H_2O$). The Zn^{2+} and Ni^{2+} hexafluoride zirconates have most diverse composition of crystal hydrates. For these compounds, it is possible to trace the effect of a change in the hydration number on the structure of the complex anion while the water content n in $MZrF_6 \cdot nH_2O$ compounds varies from 6 to 0. The structures of $MgZrF_6 \cdot nH_2O$ ($n = 2, 5$) compounds and temperature transformation of the NMR spectra of the hydrates were studied in [1]. The dihydrate structure (Fig. 1) can be thought of as a basis one which is modified during the structural transformations at hydration/rehydration processes. The structure is formed by infinite chains in which zirconium dodecahedra ZrF_8^{4-} are linked through edges. The chains are combined into three-dimensional network by the Zr-F-Mg bonds. Mg environment is octahedral, consisting of 4 fluoride ions and two water molecules.

Previously, the structure of crystal hydrates of the composition $ZnZrF_6 \cdot nH_2O$ (n = 6-0) was considered according to vibrational spectroscopy data [2]. This work is aimed at applying the NMR method to establishing the structure of crystalline hydrates of the composition $ZnZrF_6 \cdot nH_2O$ ($n = 6, 5, 4, 2, 0$), determining the presence and types of internal mobility, clarifying the conditions under which coordinated water realizes its protolytic properties. The latter is of interest for obtaining compounds with high proton conductivity, promising for devices in hydrogen energy storage systems.

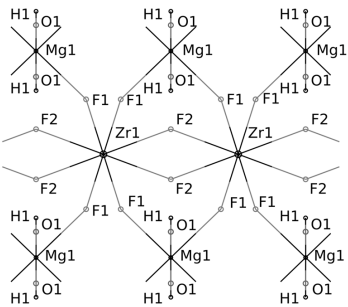

Figure 1. Fragment of the $MgZrF_6 \cdot 2H_2O$ structure

Results and discussion

The ^{19}F NMR spectra of the compound $ZnZrF_6 \cdot 6H_2O$ at temperatures of 200 K and below correspond to a rigid lattice. The shape of the spectrum is due to a combination of the chemical shielding anisotropy (CSA) and dipole-dipole interactions in the octahedral ZrF_6^{2-} anion, which is in good agreement with the calculated ones obtained in [3] with parameters $\Psi = 0.56$; $\beta = 0.2\alpha$. At temperatures of 200–240 K, a rather rapid transformation of the ^{19}F NMR spectrum of $ZnZrF_6 \cdot 6H_2O$ to the Gaussian form takes place, associated with the appearance of isotropic reorientations of the complex anion ZrF_6^{2-}. The activation energy of this

motion, determined from the temperature dependence of the second moment of the ^{19}F NMR spectra, is 0.35 eV.

The ^{1}H NMR spectra of $ZnZrF_6 \cdot 6H_2O$ in the investigated temperature range (150 - 30K) have the form of a fairly well-resolved Pake doublet with a splitting value of $2\alpha = 50.7$ kHz throughout the studied temperature range and correspond to a rigid lattice. No reorientations of $Zn(H_2O)_6^{2-}$ hexaaquacations are evident from the spectra. The interproton distance in a water molecule can be estimated from the splitting and is equal to 1.53 Å.

The ^{19}F NMR spectra of $ZnZrF_6 \cdot 5H_2O$ in the range 150-340 K are represented by an asymmetric two-component line with shape independent on temperature (Fig. 2). The MAS spectrum contains signals with shifts of 7.6, -49.1, and -56.6 ppm. The sum of the integral intensities of the last two signals relates to the intensity of the first one as ~ 2 : 1. Based on the intensity ratio, it is possible to assign the signals to the terminal (-56.6, -49.1 ppm) and bridging (7.6 ppm) fluorine atoms, respectively. Thus, the signal of the terminal atoms split into atoms that bind the anion with zinc and atoms that form hydrogen bonds with water. Lateral lines from sample rotation indicate significant CSA magnitude for all positions of fluorine atoms. Similarly to the case of dihydrates, the signal from the bridging atoms is located in a weak magnetic field.

The ^{19}F MAS NMR spectrum of $MgZrF_6 \cdot 5H_2O$ contains 5 lines (Fig. 2). Lines at -33 and -53 ppm correspond to the impurity of the dihydrate formed during rotation of the sample, while the signals at 11.7, -47, -61 ppm belong to the main phase. It can be concluded that the disposition of the signals is very similar to that observed for $ZnZrF_6 \cdot 5H_2O$.

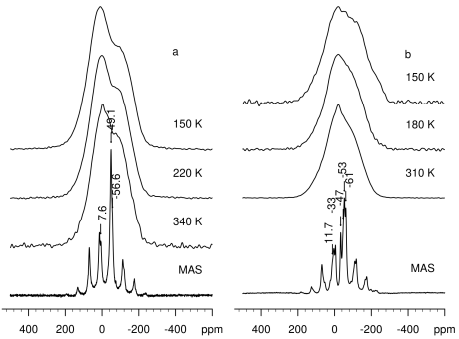

Figure 2. Static and MAS NMR spectra of $ZnZrF_6 \cdot 5H_2O$ (a) and $MgZrF_6 \cdot 5H_2O$ (b)

Of the two pentahydrates only $MgZrF_6 \cdot 5H_2O$ at temperatures below 200 K has the Pake shape of the ^{1}H NMR spectrum. Starting from this temperature, the splitting value begins to decrease and the spectrum transforms to a one-component one. The starting point of the $ZnZrF_6 \cdot 5H_2O$ spectrum transformation is below 135 K. The reason for the narrowing of the spectra is obviously the presence of reorientations of water molecules, which are probably rotations around the OH bond between two stable states, leading to a partial averaging of the tensor of dipole-dipole interactions in a water molecule. The presence of additional intensity in the center of the $MgZrF_6 \cdot 5H_2O$ spectrum at temperatures of 135, 250 - 315 K may also indicate the dissociation of a part of water molecules with the formation of H_3O^- groups.

The static ^{19}F NMR spectra of $ZnZrF_6 \cdot 2H_2O$ and $MgZrF_6 \cdot 2H_2O$ (Fig. 3) differ from that of other studied hydrates. The $ZnZrF_6 \cdot 2H_2O$ spectra practically do not change with temperature while small temperature transformations are observed for $MgZrF_6 \cdot 2H_2O$. The temperature changes can be explained by the presence of motions of water molecules. In the MAS NMR spectra, two signals are observed with CS -30.2 and -48.9 ppm for the first compound and with -32.7 and -52.7 ppm for the second one. The CSA of the positions, the signals of which are

located in a strong magnetic field, is much higher. The ratio of signal intensities, taking into account the spinning sidebands, is 1: 2. Taking into account the intensities and the magnitude of the CSA, estimated from the sidebands, the signals can be assigned, respectively, to the bridging and non-bridging positions in the fluorozirconate chain. The significant asymmetry of the static spectra is due to the large CSA of terminal fluorine atoms. It can be noted that, as in the case of pentahydrates, the effect of the nature of the cation on the magnitude of the magnetic shielding of fluorine is small.

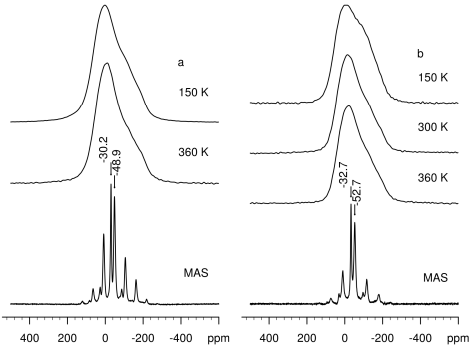

Figure 3. Static and MAS NMR spectra of $ZnZrF_6 \cdot 2H_2O$ (a) and $MgZrF_6 \cdot 2H_2O$ (b)

The ^1H NMR spectrum of the $ZnZrF_6 \cdot 2H_2O$ compound at a temperature of 151 K is a Pake doublet with a splitting of $2\alpha = 57$ kHz, corresponding to immobile water molecules. As the temperature rises, the spectrum transforms. At 200 K the spectral features of the doublet are smoothed out and the splitting decreases, amounting to 50 and 46 kHz, respectively, at 200 and 300 K. The spectra of $MgZrF_6 \cdot 2H_2O$ undergo a similar transformation, however, the temperatures characteristic of its various stages are lowered and the state with immobile water molecules is not observed. The observed change in the shape of the spectrum with temperature can be associated with the motions of water molecules over fixed positions, which lead to a partial averaging of the tensor of dipole-dipole interactions in a water molecule.

The only signal in the ^{19}F MAS NMR spectra $ZnZrF_6$ ($MgZrF_6$) is located at -48 (-47.1) ppm. Averaging of dipole-dipole interactions and CSA as a result of isotropic reorientations of octahedral ZrF_6^{2-} anions up to 420 K is not observed. This may indicate a significant contribution of the covalent component of the Zn-F (Mg-F) bond, which significantly increases the potential barrier to reorientations as compared to compounds containing octahedral anions and alkali or organic cations.

Acknowledgements

This work was supported by the RFBR fund; project no 20-03-00279.

References

1. Gerasimenko, A.V., Gaivoronskaya, K.A., Slobodyuk, A.B. and Didenko, N. A. *Z. Anorg. Allg. Chem.*, 643, 1785–1792 (2017).
2. Voit E.I., Didenko N.A., Gayvoronskaya K.A., Gerasimenko A.V. *Optics and spectroscopy*, 121, 229-240 (2016).
3. E. P. Zeer, V. E. Zobov, O. V. Falaleev, New effects in the NMR of polycrystals (in Russian), “Nauka” Publ., Novosibirsk, 1991.

NMR spectra, structure and ionic motions in the new potassium fluoridooxalate zirconates

A. B. Slobodyuk[1], M. M. Godneva[2]

[1]Institute of chemistry, FEB RAS, 159, Pr. Stoletiya Vladivostoka, 159, Vladivostok, Russia
[2]I. V. Tananaev Institute of Chemistry and Technology of Rare Elements and Mineral Raw Materials, KSC RAS, Apatity
E-mail: ampy@ich.dvo.ru

The known crystallochemical features of mixed-ligand oxalate-fluoride compounds of the transition metals allows one to expect new prospective compounds to be synthesized in the corresponding systems. The combination of the bidentate oxalate bridges with fluorine ligands preferentially occupying the non-bridging positions should result in formation of new framework compounds with spacious channels available to the ionic transport. Compounds with high monovalent metal capacity and low activation energy of its translational mobility are used as electrode materials and solid electrolytes of chemical current sources, in the design of chemical sensors, supercapacitors, and other solid-state electrochemical devices. The structures of many of the fluoridooxalates are, however, unknown as it turned to be difficult to obtain a crystal suitable for XRD structure determination.

Compound $Rb_2Hf_2F_8C_2O_4 \cdot 4H_2O$ is only fluoridooxalatezirconate with known structure [1]. Earlier, the compounds $K_3ZrF_5C_2O_4$, $K_2ZrF_4C_2O_4 \cdot 2H_2O$, $KZrF_3C_2O_4 \cdot 3H_2O$ were synthesized and characterized with powder XRD and IR spectroscopy [2]. This work is aimed towards the determination of their structure using the solid-state NMR spectroscopy.

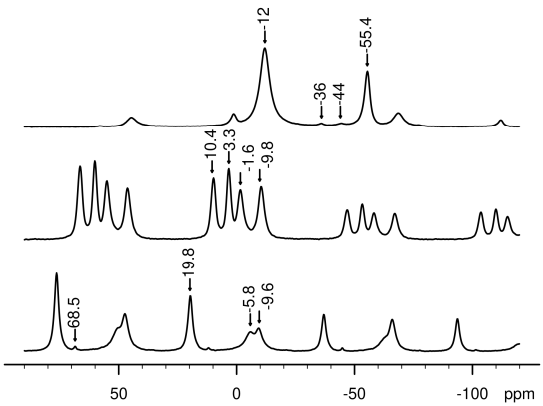

Figure 1. ^{19}F MAS NMR spectra of the fluoridooxalate zirconates $K_3ZrF_5C_2O_4$ (a), $K_2ZrF_4C_2O_4 \cdot 2H_2O$ (b), $KZrF_3C_2O_4 \cdot 3H_2O$ (c). Unlabelled signals are spinning sidebands

In the ^{19}F MAS NMR spectrum of the $K_3ZrF_5C_2O_4$ compound (Fig. 1) two signals near -12 and -55.4 ppm could be attributed to the main phase. Signals near 36 and 44 ppm most probably belong to an admixture. The ratio of integrated intensities of the main phase signals constitutes 74:35 allowing one to interpret signals at -12 and -55.4 ppm as the ones corresponding to 3 and 2 fluorine positions, respectively. On the basis of IR spectroscopy it was concluded that the fluorine occupies only non-bridging positions in the structure. The NMR data make this conclusion doubtful as the observed difference in fluorine shielding is undeniably determined by different structural roles of corresponding positions. Considering known data

of the fluorozirconate ^{19}F NMR, the -55.4 ppm signal should be attributed to the nonbridging signal positions while -12 ppm peak – to the bridging ones.

The shape of the static ^{19}F NMR spectra of $K_3ZrF_5C_2O_4$ at 150 – 220 K is determined by the combination of dipole-dipole interactions and chemical shift anisotropy (Fig. 2a). At higher temperatures the spectrum transforms due to the dynamic processes in the lattice. Considering the fact that two separate peaks are observed in the MAS spectrum, the dynamic process is probably represented by the zirconium polyhedral reorientations around the bridging bonds.

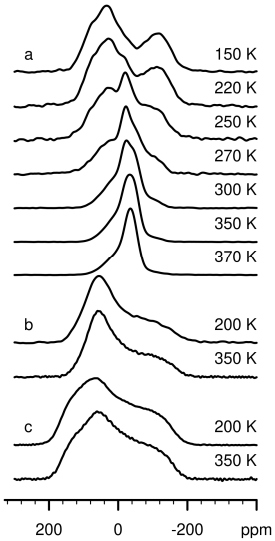

Figure 2. Temperature transformation of the ^{19}F NMR spectra of $K_3ZrF_5C_2O_4$ (a), $K_2ZrF_4C_2O_4 \cdot 2H_2O$ (b) and $KZrF_3C_2O_4 \cdot 3H_2O$ (c)

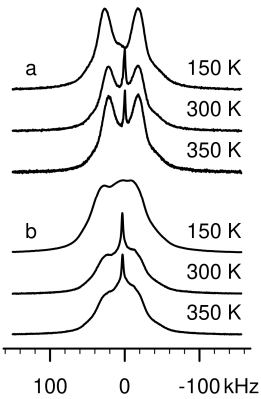

Figure 3. Static ^1H NMR spectra of $K_2ZrF_4C_2O_4 \cdot 2H_2O$ (a) and $KZrF_3C_2O_4 \cdot 3H_2O$ (b) at different temperatures

The ^{19}F MAS NMR spectrum of $K_2ZrF_4C_2O_4 \cdot 2H_2O$ (Fig. 1) contains 4 signals in the chemical shift range characteristic to non-bridging zirconium coordinated fluorine atoms. The shielding anisotropy estimated from the comparison of the intensities of spinning sidebands is equally large for all of the signals and also indicates fluorine occupying the non-bridging positions.

The number of peaks in the ^{19}F MAS NMR spectrum of $KZrF_3C_2O_4 \cdot 3H_2O$ (Fig. 1) corresponds to amount of fluorine in its formula as well. The chemical shifts of signals are 19.8, -5.8 and -9.6 ppm. The spinning sidebands intensity indicates that the chemical shift anisotropy tensor of the first signal has axial anisotropy while for the two other positions it is close to triaxial one. The latter results in the higher intensities of sidebands compared to that of the central signals.

The static ^{19}F NMR spectra of $K_2ZrF_4C_2O_4 \cdot 2H_2O$ and $KZrF_3C_2O_4 \cdot 3H_2O$ are represented by the Blombergen-Rowland functions (Fig. 2). For the former compound the spectrum shape is close to one corresponding to the axially-symmetric CSA tensor. Although three peaks are present in the $KZrF_3C_2O_4 \cdot 3H_2O$ ^{19}F MAS NMR spectrum, the peak chemical shift difference can be considered negligible in the static spectrum scale. It therefore can be

concluded that the spectrum shape of the trihydrate is determined either by overlapping of components with axially-symmetric CSA having different $\delta_\perp$ or of components with triaxial CSA and close eigenvalues.

^{1}H NMR spectra of the studied hydrated are presented by the Pake doublets with an admixture of small narrow component probably corresponding to the sorbed water molecules (Fig. 3). Dipole constants 2α for the di- and trihydrate constitute 52 and 54 kHz, respectively. The interprotonic distances calculated from the dipole constants are 1.51 and 1.49 Å, respectively. The isotropic widening factors (β) are also differ and constitute 16 and 24 kHz. The ^{1}H NMR spectra characteristics point to the presence of the dipole-dipole interaction between protons and the fluorine in the hydrates. The same factor could be responsible for the presence of the central component in the $KZrF_3C_2O_4 \cdot 3H_2O$ spectrum at 150 K. The protons of the structural water molecules sitting in the proximity of the fluorine or absorbed water molecules form a three-spin system.

Obtained ^{19}F MAS NMR data allows one to confirm the formulas obtained by chemical analysis and to make conclusions about the structures of studied compounds. The fluorine is coordinated by zirconium. When the number of ligand atoms (fluorine and oxygen) per one zirconium atom is equal or less than eight, the fluorine occupies only non-bridging positions. A signal corresponding to non-bridging fluorine was observed in spectra of $K_3ZrF_5C_2O_4$ where the corresponding number is equal to 9. Character of temperature transformation of the static ^{19}F NMR spectra of $K_3ZrF_5C_2O_4$ points to the presence of the reorientational motion of the zirconium coordination polyhedra with activation energy of ~ 0.4 eV. It is possible that in this compound a paddle-wheel mechanism of cationic diffusion take place analogously to that was proposed for K_3ZrF_7 – fluorozirconate of a similar composition [3].

Acknowledgements

This work was supported by the RFBR fund; project no 20-03-00279.

References

1. R.L. Davidovich., V. I. Sergienko, Structural chemistry of complex fluorides of titanium (IV), zirconium (IV) and hafnium (IV). (Dal'nauka, Vladivostok, 2016) 176 s (Russ.)
2. Godneva M.M., Rys'kina M.P., Kuznetsov V.Y., Zalkind O.A. Phase formation in the $ZrO(NO_3)_2$-$H_2C_2O_4$-KF-H_2O system at 20°C. Russian journal of inorganic chemistry. 2015. V. 60, No 3. P. 347-354. doi: 10.1134/S0036023615030067.
3. Gaumet V., Latouche C., Avignant D., Dupuis J. *Solid State Ionics*. 1994. V. 74. P. 29-35.

^{1}H high-resolution NMR spectrometry and relaxometry for soybean oil research

Mark Smirnov, Ivan Mershiev, Galina Kupriyanova

Institute of Physics, Mathematics and Information Technology, Immanuel Kant Baltic Federal University, 236041, Kaliningrad, Russia
E-mail: galkupr@yandex.ru
http://kantiana.ru

Introduction

Vegetable oils are an important component of a healthy human diet. An important task is to establish the authenticity of the oil, to determine its quality. Important characteristics such as acidity, iodine number, saturated-to-unsaturated fat ratio are usually determined by chemical and chromatographic methods, many of which are expensive and time-consuming. In recent years, high-resolution ^{1}H, ^{13}C NMR methods have been used to establish the qualitative composition of olive and other vegetable oils of its origin and to identify [1]. NMR relaxation spectroscopy is used to study the degradation of oils. It was found that the content of free fatty acids and polar substances increases with increasing heating time, while T_1 and T_2 relaxation times, decrease, since oil degradation leads to an increase in free fatty acids and polar substances which leads to a decrease in mobility [2]. NMR relaxation techniques can be a promising tool for online oil quality control [3].

The purpose of this work is to determine the qualitative composition of soybean oil samples obtained by various processing methods, such as, for example, extraction and hydrogenation methods, using high-resolution proton NMR and NMR relaxometry. We investigated the question to what extent the relaxation data obtained by high-resolution ^{1}H NMR methods and in a weak magnetic field correlate.

Experiment

^{1}H NMR relaxation experiment in low magnetic field on measuring spin-spin relaxation T_2 of soybean oils were carried out on an NMR-NQR spectrometer Tecmag Apollo. The magnetic field of the permanent magnet in the gap is B = 330 mT. The radio frequency circuit was tuned at a frequency of 13.648 MHz. The Carr-Purcell-Meiboom-Gill (CPMG) sequence was used for the transverse relaxation time T_2 measurements. To process the experimental data, we used the modified RILT script, executed in the MatLab environment [4].

High resolution ^{1}H NMR spectra were obtained on a Varian 400 MHz Premium Shielded instrument with a constant magnetic field of 9 T, operating at a frequency of 400 MHz. A small amount of TMS was added to one of the samples to determine chemical shifts. High-resolution soybean oil spectra were obtained at -2 to 14 ppm spectral width, relaxation delay 1 second, number of scans 8, pulse width 45 °. Relaxation measurements in a strong magnetic field were carried out using inversion-recovery and CPMG methods. The MestreNova program was used to calculate the integrated intensity.

Samples

Three samples of hydrated soybean oil and one sample of extraction soybean, differing in the content of phosphorus and sterol (Table 1) produced by the “Soybean Community” (Kaliningrad), were investigated.

Results and discussion

The spectra of four soybean oil samples were recorded and T_1 and T_2 relaxation times of the functional group protons were determined. Determining the composition of oils is

complicated by the fact that individual signals of different fatty acids, such as linolenic oleic, stearic, and palminic acid, are overlapped.

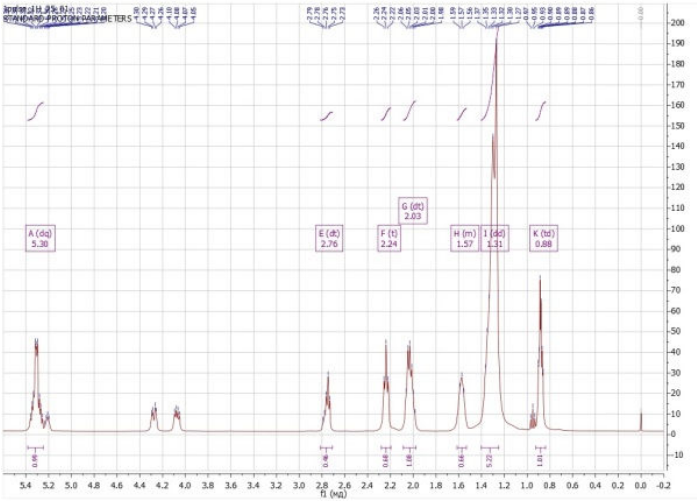

Figure 1. High Resolution Soybean Oil NMR Spectrum

The assignment of signals in ^{1}H NMR spectra was performed by COSY method and using literature data. The spectra of the studied samples differ in integral values and signal intensities. To calculate the proportions of fatty acids, we took into account that the signals of CH3 group methyl protons -CH3 at 0.95 ppm refers to the ring protons of linolenic acid, while the signals of the methyl protons -CH3 at 0.87 ppm refers to the ring protons of all other acids, and the signal at 2.76 ppm refers to the protons CH2-linolic and linolenic acids. Chemometric equations for the composition determination were deduces from analysis of signal assignment in the spectrum and integral signal intensities. The approach proposed in the work [5] was used. Solving the equations made it possible to obtain the relative content of linolenic, linoleic, mono-unsaturated and saturated fatty acid. The results are shown in Table 1.

Table 1. Composition of soybean oils

№ Soybean oil	Linolenic acid (%)	Linoleic acid (%)	Mono-unsaturated fatty acids (%)	Saturated fatty acids (%)
1 extraction	14	37	28	21
2 hydrated	18	45	11	26
3 hydrated	5	41	25	29
4 hydrated	8	48	17	27

In article [1] the following composition of soybean oil was obtained: Linolenic acid – 8%, Linoleic acid – 53%, Unsaturated acids – 21%, Saturated acids – 15,5%.

As you can see, the main differences lie in the percentage of saturated fatty acids, as well as unsaturated acids, while the content of linolenic and linoleic acids in the studied samples practically coincides with the literature data.

It should be noted that the accuracy of determining the composition of the oil is largely determined by the accuracy of determining the integral intensity. To reduce the error, the determination of the integral was performed several times and the average value was chosen.

From Table 1 it can be seen that the composition of the oil changes during processing. The proportion of Linolenic acid decreases and the proportion of Linoleic acid increases.

The results of T_1 and T_2 relaxation measurements are shown in the form of a histogram in Fig. 2. It can be seen that the distribution of T_1 relaxation times is more uniform and changes are weakly expressed, while the distribution of times T_2 is more characteristic and makes it possible to reveal differences in the samples.

It should be noted that the character of the distributions of transverse relaxation times obtained by high-resolution NMR and in a weak magnetic field has a similar character, despite the differences in the values of the relaxation times.

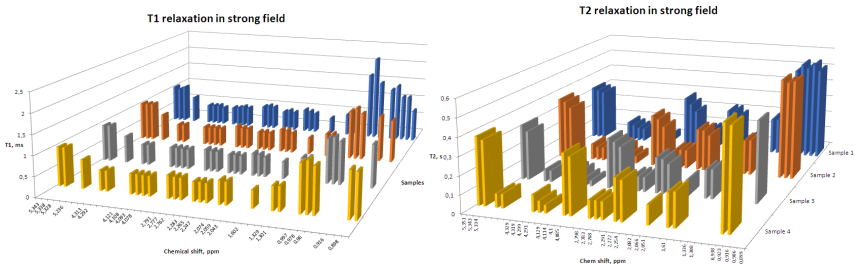

a) *b)*

Figure 2. Distribution of longitudinal T1 (a) and transverse T2 (b) relaxation times of protons

Conclusions

The work revealed the composition of soybean samples obtained with various technological processing. The main changes are related to the percentage of Linolenic and Linoleic acid, as well as mono-unsaturated fatty acids. Analysis of the relaxation data shows that the distribution of relaxation times T2 more clearly reflects changes in the samples.

References

1. Maria D Guillen and Ainhoa Ruiz. Edible oils discrimination by ^{1}H nuclear magnetic resonance. Sci Food Agric 83:338–346 (online: 2003) DOI: 10.1002/jsfa.1317
2. Sinyavsky N.Ya., Mershiev I.G., Kupriyanova G.S. New approaches to identification and quality assessment of oils. Marine intelligent technology. Electronic network (ISSN 2588-0233) and print (ISSN No. 2073-7173) publications. VI International Baltic Marine Forum. 4 (42) T. 3 2018
3. Abene Silva Ribeiro, Liana Ribeiro Gouveia, Carlos Jonnatan Pimentel Barros, Paulo Renato Alves Firmino, Ricardo Oliveira Silva. Discriminating gamma-irradiated soybean seeds by ^{1}H NMR-based metabonomics. Food Control 36 (2014) 266e272
4. Iari-Gabriel Marino, Regularized Inverse Laplace Transform. https://www.mathworks.com/matlabcentral/fileexchange/6523-rilt
5. Nicoleta-Aurelia Chira, Maria-Cristina Todasca, Alina Nicolescu, Aurelia Rosu, Mihaela Nicolae, Sorin-Ioan Rosca. Evaluation of the Computational Methods for Determining Vegetable Oils Composition using ^{1}H NMR Spectroscopy. https://www.researchgate.net/publication/267802323

Peculiarities of microstructure in mixtures SLAS-DTAB-D_2O according to NMR data

Viktoria V. Vasinovich, Maria V. Popova

Department of Nuclear-Physics Research Methods,
198504, St. Petersburg, Uljanovskaja, d. 1, Russia
E-mail: st064748@student.spbu.ru

Introduction

The aggregation and interfacial behavior of aqueous solutions of binary mixtures of anionic (sodium lauroyl sarcosinate, SLAS) and cationic (dodecylammonium bromide, DTAB) surfactants were investigated using ^{1}H and ^{13}C spectroscopy. SLAS possesses unique physical and chemical properties, such as low toxicity, dermatology softness, hydrolysis resistance, high efficiency in hard water, and the fast biodegradability [1].

One of the most important attributes of sarcosinate amphiphiles is their good compatibility with other surfactants. It is well known that in the practical application of surfactants generally amphiphilic mixtures are used. This situation is caused by the lower cost of mixtures compared to individual surfactants.

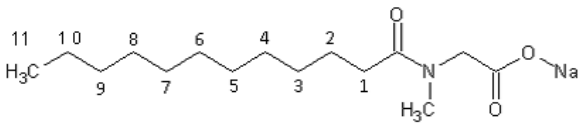

Figure 1(a). The molecular structure of SLAS and the numbering of molecular groups (and spectral lines)

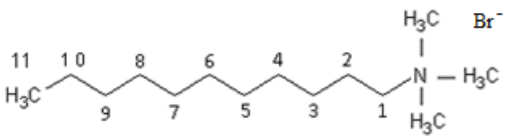

Figure 1(b). The molecular structure of DTAB and the numbering of molecular groups (and spectral lines)

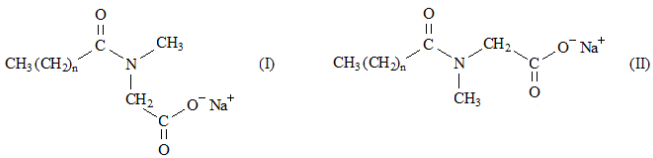

Figure 2. Two conformers of SLS: (I) cis- and (II) trans-configurations

Materials and methods

SLAS and DTAB (see Fig. *1a* and *1b*) were acquired from Sigma-Aldrich and used without additional purification. We studied the NMR parameters of SLAS in mixtures with DTAB at different molar fractions of both surfactants from 0.5 CMC to 2 CMC. 18 samples of solutions SLAS and mixtures SLAS+DTAB in D_2O (99,9 %) in concentration ranges from 4mM/L to 20 mM/L for SLAS and from 3 mM/L to 30 mM/L for DTAB were prepared.

All ^{1}H and ^{13}C NMR experiments were performed using a Bruker AVANCE 500 (in the Center for Magnetic Resonance of St. Petersburg State University) with resonance frequencies 500 MHz for the protons and of 125 MHz for the ^{13}C nuclear spins, respectively.

Results

The examples of the ^{1}H spectra are presented in *Figure 2*.

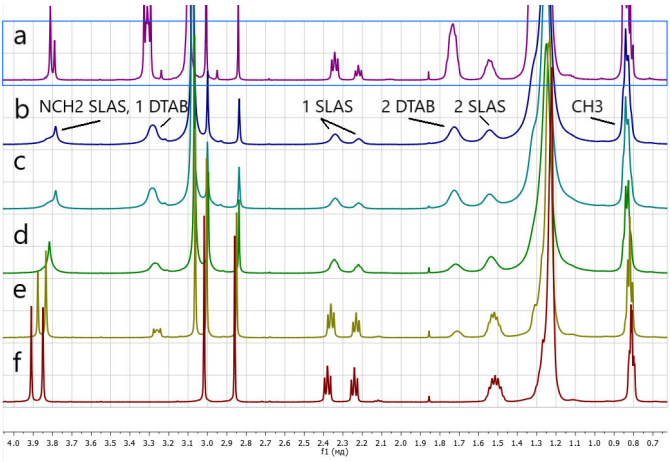

Figure 2. Spectra of the ^{1}H nuclei for the solution SLAS and mixtures SLAS+DTAB (in mM/L): a) 20 SLAS : 30 DTAB, b) 20 SLAS : 20 DTAB, c) 20 SLAS : 15 DTAB, d) 20 SLAS : 8 DTAB, e) 20 SLAS : 4 DTAB, f) 20 SLAS : 0 DTAB

The interpretation of some lines of the spectra is shown in the graph *b*.

We have investigated self-association processes in solutions and binary mixtures in three different concentration ranges under various conditions:

1) The low concentration of amphiphilic molecules up to the critical concentration, when there are monomers, dimers and trimers (no micelle processes).

2) The concentrations of substances amphiphilic in the CMC area, when classical micelles begin to form.

3) The concentrations of substances in the area of 2 CMC and further, when almost all the surfactant substances are in micelles.

In surfactant molecules with the amide bond the energy barrier for the rotation about this bond was sufficiently high (because of the partially double character of the amide bond), and therefore two different relatively stable conformers (cis- and trans-conformers) exist in such molecules (see *Fig. 2*, the lines 1 SLAS). Since the isomerization rate is slow in the NMR time-scale and the N-alkyl groups of the SLAS cis- and trans-molecules are chemically (and magnetically) inequivalent, a splitting of the resonance lines for the N-alkyl groups in the ^{1}H and ^{13}C NMR spectra has been registered [1].

References

1. Popova, M. V., Chernyshev, Y. S., Michel, D. & Chizhik, V. I.,^{1}H and ^{13}C NMR investigation of conformational and aggregation behavior of sodium N-lauroyl sarcosinate, Journal of Molecular Liquids. 280 (2019) 40-48. https://doi.org/10.1016/j.molliq.2019.02.029.

Molecular Dynamics simulation of ethylenediamine-Cu^{2+} complex and copper-II chloride in aqueous solutions

Irina Yefimova, Andrei V. Komolkin, Andrei V. Egorov

Faculty of Physics, Saint Petersburg State University, St. Petersburg, 199034, Russia
E-mail: yefir2000@gmail.com

Introduction

Medical research shows that many anticancer, antiviral and antiseptic agents work by binding to DNA. This can damage the DNA of cancer cells and kill them [1]. The use of metal-based drugs with transition metals, like Cu (II) or Zn (II), presents the most important strategy in the development of new anticancer and antimicrobial agents [2].

Selection of suitable Force Fields for Molecular Dynamics simulation of EDA-Cu^{2+}·$2Cl^-$ and EDA_2-Cu^{2+}·$2Cl^-$ complexes in aqueous solution could be used in further research of anticancer drugs.

Molecular dynamics simulation

The purpose of this work is to model Cu^{2+} ions in aqueous environment by molecular dynamics method with the program AKMD and to choose reasonable parameters of force field so the result of simulation correspond to experiment [3]. The program Jmol was used to visualize the spatial position of molecules.

In this simulation OPLA-AA [4] force field was chosen for ethylenediamine (EDA) molecules and Cl^- ions with SPC/E filed for water molecules. Parameters of Cu^{2+} ion were adapted from Amber-19 force field [5].

Figure 1 shows [EDA_2- Cu^{2+}] planar complex with aqua molecules simulated at 298 K. EDA molecules with this parameters of modeling stay in planar configuration (both of EDA molecules lie in the same plane). Cu^{2+} ion has 6 coordination bonds, which is consistent with simulation by Quantum Chemistry method [6] and other results [7].

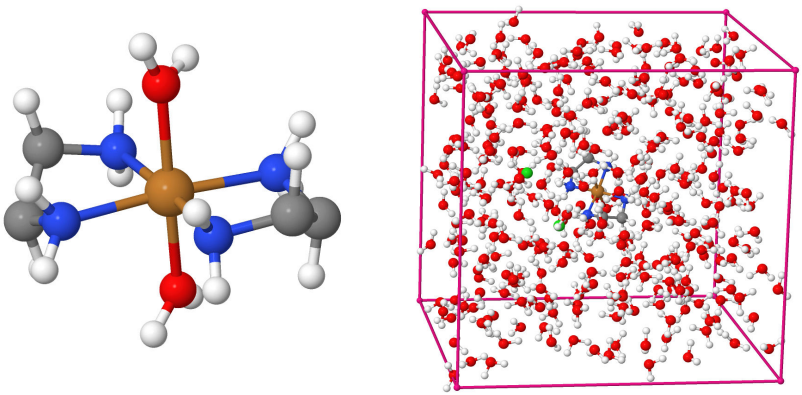

Figure 1. [EDA_2- Cu^{2+}] planar complex with aqua molecules (left) and the simulation cell with [EDA_2-Cu^{2+}]·$2Cl^-$ planar complex in aqueous solution (right)

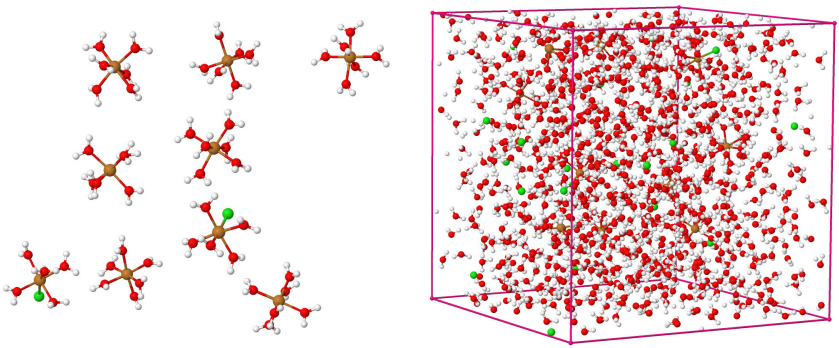

Figure 2. Complex of $Cu^{2+}\cdot 2Cl^-$ with aqua molecules (left), the simulation cell with $Cu^{2+}\cdot 2Cl^-$ in aqueous solution (right)

Figure 2 shows complexes of $Cu^{2+}\cdot 2Cl^-$ with aqua molecules simulated at 298 K. Cu^{2+} ion in this complex has also 6 coordination bonds. It means that chosen Force Field for Cu^{2+} ion is suitable for further modeling. Contact ion pairs $Cu^{2+}\cdot Cl^-$ were observed in the simulation.

Stability of hydration shell of Cu^{2+} ion

To ensure full compliance with experiment, molecules in the solvation shell of Cu^{2+} ion should exchange with bulk water. However, this does not happen at 298 K during the simulation. It may be shown by the radial distribution function of the water oxygen atom from the Cu^{2+} and Cl^- ions (Figure 3).

After the sample is heated to 418 K, one water molecule leaves the hydration shell and replaces by another water molecule during simulation (10 ns). This result means that chosen force field for Cu^{2+} ion allows exchange of water molecules between hydration shell and bulk water.

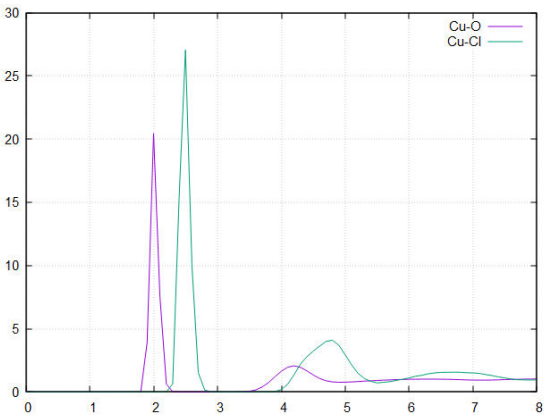

Figure 3. The radial distribution function of the water oxygen atom from the Cu^{2+} and Cl^- ions at 298 K

References

1. N. Raman, A. Selvan, S. Sudharsan. Metallation of ethylenediamine based Schiff base with biologically active Cu(II), Ni(II) and Zn(II) ions: Synthesis, spectroscopic characterization, electrochemical behaviour, DNA binding, photonuclease activity and in vitro antimicrobial efficacy // Spectrochimica Acta Part A: Molecular and Biomolecular Spectroscopy. 2011. V. 79. No 5. P. 873-883.
2. J.G. Liu, B.H. Ye, H. Li, Q.X. Zhen, L.N. Ji, Y.H. Fu. Polypyridyl ruthenium (II) complexes containing intramolecular hydrogen-bond ligand: syntheses, characterization, and DNA-binding properties // J. Inorg. Biochem. 1999. V. 76 No. 3. P. 265–271.
3. E. Selimović, A. V. Komolkin, A. V. Egorov, T. Soldatović. The ligand substitution reactions of [CuCl2(terpy)] and [CuCl2(en)] complexes with bioligands by EPR spectroscopy. // in: Spectroscopy of coordination complexes (Abstracts of XIV International conference. Tuapse, Russia. 24-30 of September, 2017) 2017. P. 136.
4. William L. Jorgensen Research Group — OPLS-AA. URL: http://zarbi.chem.yale.edu/oplsaam.html (accessed 07.05.2020).
5. C. Tian, K. Kasavajhala, K. A. A. Belfon, et al. ff19SB: Amino-Acid-Specific Protein Backbone Parameters Trained against Quantum Mechanics Energy Surfaces in Solution // *Journal of Chemical Theory and Computation*, **2020,** V. 16, No. 1, 528-552, DOI: 10.1021/acs.jctc.9b00591
6. Irina Yefimova, Andrey Egorov, Enisa Selimović, Tanja Soldatović, Andrei V. Komolkin. Structure and dynamics of ethylenediamine-$CuCl_2$ complex investigated by means of Quantum Chemistry and Molecular Dynamics methods. // in: Magnetic Resonance and its Applications (Proceedings 17th International School-Conference, Saint Petersburg, 29.03.2020-03.04..2020). 2020. P. 288-289.
7. Vyacheslav S. Bryantsev, Mamadou S. Diallo, Adri C. T. van Duin, and William A. Goddard III. Hydration of Copper (II): New Insights from Density Functional Theory and the COSMO Solvation Model // J. Phys. Chem. 2008. V. 112. P. 9104–9112.

Poems about School

* * *

Чижик-Spinus, где ты был?
– «Я сигнал за хвост ловил!
Сделал я ему “Фурье” –
Закружилось в голове!»

Цели «Spinus»’а просты:
Дать научные мосты!
Пусть у вас здесь будет шанс
Пообщаться «в резонанс»!

В Школе здесь научат всех
Сочетать с наукой смех,
Дискотеки с Э-Пе-эР,
Я-Ка-эР и Я-эМ-эР!

В Школе много новых лиц,
Будем превращать их в птиц:
Вдруг хотя б одной из ста
Дастся «Нобель-высота»!

2010

* * *

Spinus, Spinus, where you were?
Did you dive in the Resonance world?
– “Yes! I dived with my great joy –
Resonance is a pleasant toy!”

“Spinus” school invited you
To look for a knowledge clue.
We will show the signal birth
In the field of our Earth!

If you wish to have success,
At the School achieve progress!
We will teach you all to fly
In the scientific sky!

We desire you to get
Many victories-побед!
It will be a good surprise
If you catch the Nobel prize!

2010

Author Index

Magnetic Resonance and its Applications

Proceedings

Saint Petersburg State University
March 29 — April 2, 2021

Подписано в печать 24.03.2021. Формат 60 × 84 1/16.
Бумага офсетная. Гарнитура Times. Печать цифровая.
Усл. печ. л. 16,39. Тираж 130 экз. Заказ № 1382.

Отпечатано в Издательстве ВВМ.
198095, Санкт-Петербург, ул. Швецова, 41.